Faculty of Science and Engineering
Department of Applied Geology

Tracking Meteoroids in the Atmosphere: Fireball Trajectory Analysis

Eleanor Kate Sansom

This thesis is presented for the Degree of
Doctor of Philosophy
of
Curtin University

December 2016

DECLARATION OF AUTHORSHIP

I, Eleanor Kate Sansom, declare that to the best of my knowledge and belief that this thesis entitled, ”Tracking Meteoroids in the Atmosphere: Fireball Trajectory Analysis ” contains no material previously published by any other person except where due acknowledgement has been made. This thesis contains no material which has been accepted for the award of any other degree or diploma in any university.

The author acknowledges that copyright of published works contained within this thesis resides with the copyright holder(s) of those works. I warrant that I have obtained, where necessary, permission from the copyright owners to use any third-party copyright material reproduced in the thesis (e.g. questionnaires, artwork, unpublished letters), or to use any of my own published work (e.g. journal articles) in which the copyright is held by another party (e.g. publisher, co-author).

Eleanor Kate Sansom

4 / 12 / 16

Date

ABSTRACT

When meteoroids pass through the Earth's atmosphere they undergo rapid deceleration and can produce fireball phenomena (brighter than Venus). Under the right conditions, this may result in a meteorite falling to Earth. When observed from multiple locations, the atmospheric trajectory and orbit of the meteoroid can be determined. If the associated meteorite is recovered, having this contextual information provides significant insights for Solar System formation and evolution – bridging the gap between meteorites and asteroids.

Dedicated fireball camera networks around the world have been established to observe such phenomena and increase the number of meteorites with orbits. The Desert Fireball Network in Australia is the largest of these, covering a $3 \times 10^6\,\mathrm{km}^2$ multi-station viewing area. The network on average observes ~ 1.8 bright fireballs longer than 3 seconds per night and accumulates over 60 TB of data per month. This requires an automated software pipeline to produce unbiased analyses of the data.

After identifying and calibrating observed positions of the fireball trajectory, modelling the dynamics allows the determination of meteoroid characteristics such as its mass, density and shape. Knowing the terminal mass at the end of the luminous trajectory leads to predictions of possible meteorite fall locations.

Modelling fireball trajectories typically uses a simplistic set of single body aerodynamic equations. Methods have developed over the years to incorporate complexities in fireball modelling, such as fragmentation, but are mostly based on least squares approaches and are not able to rigorously analyse errors.

This thesis improves and develops algorithms for fireball trajectory analysis, generating a technique that is fully automated, provides comprehensive error analysis, and does not impose parameter assumptions in order to provide a routine, unbiased application.

Stochastic estimator algorithms have many applications, including satellite tracking and self driving cars, but have never previously been applied to fireball modelling. They are designed to take a set of potentially noisy observation data and determine the true state of a physical system whilst encapsulating noise and inaccuracies in both models and measurements. This research assesses these statistical tracking methods as viable techniques for meteoroid trajectory analysis.

Various Kalman filters and smoothers, are able to estimate meteoroid states with full error propagation. Incorporating these in an interactive multiple model identifies fragmentation events without the requirement of a light curve. Kalman filters, however, require assumed input parameters. Particle filters can dramatically reduce the assumptions required by other approaches. This iterative Monte Carlo estimator initialises a spread of particles with a range of input parameters, encapsulating prior knowledge of the parameter space to provide an automated, unbiased analysis. To go one step further, removing the need for even triangulated data, the single body aerodynamic equations are defined in 3D and implemented within a particle filter. Incorporating the raw line-of-sight observations directly shows the typical straight-line trajectory assumption to not always be valid. As observations are integral to updating the state estimates of tracking algorithms, using the least manipulated data will provide the most statistically robust analyses, incorporating subtleties in the raw observations.

The single body theory of meteor dynamics is a simplified model to analyse fireball trajectories. Estimator algorithms are adaptable and incorporate the complexities of real world variability through model and observation process noise. Although we only apply dynamic equations in these algorithms at this stage, these techniques are highly versatile and can be applied to any system, allowing future incorporation of such models as brightness and internal heating.

A special thanks to Oli, for marrying me around Chapter 2

The presence of those seeking the truth is to be infinitely preferred to the presence of those who think they've found it.

-Sir Terry Pratchett

ACKNOWLEDGEMENTS

The work presented in this thesis was funded by the Australian Research Council as part of the Australian Laureate Fellowship scheme and carried out at the Department of Applied Geology at Curtin University. I would also like to acknowledge the support and resources provided by the Pawsey Supercomputing Centre with funding from the Australian Government and the Government of Western Australia.

I would like to gratefully acknowledge the guidance and support I have received throughout my research and thank all those without whom this thesis would not have been possible.

- **My principal supervisor Professor Philip Bland** – Thank you for giving me this opportunity to study fireballs in an amazing new country. I would like to express my sincere gratitude for your endless support, patience and motivational chats. Your advice in everything from presentation delivery to getting the story into a paper has dramatically improved how I communicate my research. I have thoroughly enjoyed working with you and have been truly inspired to start my career in academia.
- **My external collaborator Dr. Mark Rutten** – From your first visit to Curtin you have been an invaluable resource. You have opened my eyes to a whole new field of research and the many techniques that can address issues in fireball modelling. Thank you for all the time you have given me in person and over Skype, as well as the countless hours spent in reviewing my code and going over paper revisions. I look forward to working with you in future.

- **My associate supervisors Dr. Jonathan Paxman and Dr. Martin Towner** Thank you both for your continual input into my work and answering my mathematical queries. Jon, I would also like to thank you for introducing me to Kalman Filters, leading directly to my first paper.

- **DFN colleagues** – I have thoroughly enjoyed working with such a fun, enthusiastic and dedicated group of people. From chatting about cameras in the office to around the BBQ on the weekend, I want to thank you for making this more than just a research group, but a group of friends. Without all of you, I would not have had the data to complete this research, so thank you for all your hard work. I would like to especially thank Hadrien Devillepoix for putting up with my ceaseless requests for coding advice and being far superior to any rubber duck.

- **My family and friends** – Although many of you are on the other side of the world, your support and interest in my research and achievements has been never ending. My crew mates at the RPYC, with your ceaseless enthusiasm for my work and, along with my friends at Curtin, have made this experience great fun and given me a home away from home. Rob, Lucy, Luke, Sarah, Hadrien, Jen and Trent: good luck with completing your own theses.

- **My amazing husband, Oli** – I made you move to the opposite side of the world for this opportunity and for that I cannot thank you enough. Not only that, your ceaseless encouragement and love throughout my research, despite my inability to get anywhere on time, has been the greatest support I could have had. I could not have done it without you.

CONTENTS

LIST OF PUBLICATIONS INCLUDED AS PART OF THIS THESIS

This thesis comprises a collection of research papers that were either published or in preparation at the time of writing this document. The objectives and relationship amongst the different papers are described in the introductory chapter. The final chapter summarises the papers and places them into a wider context. All papers have statement of co-authorships in Appendix A, along with reprints of published papers.

The research papers contained within this thesis that are published (or accepted for publication) in peer-reviewed journals are listed below.

PAPER 1 – Sansom, E. K., Bland, P. A, Paxman, J., Towner, M. C. (2015). A novel approach to fireball modeling: The observable and the calculated. *Meteoritics and Planetary Science*, **50**, pp. 1423–1435.

PAPER 2 – Sansom, E. K., Bland, P. A, Rutten, M. G., Paxman, J., Towner, M. C. (2016). Filtering Meteoroid Flights Using Multiple Unscented Kalman Filters. *The Astronomical Journal*, **152**, pp. 148-156.

PAPER 3 – Sansom, E. K., Rutten, M. G., Bland, P. A (2017). Analysing Meteoroid Flights Using Particle Filters. *The Astronomical Journal*, **153**, pp. 87-95.

The formatting of each chapter within this thesis may appear to vary, and may differ to the published form based on the requirements and formatting guidelines of each individual journal and this thesis. Due to the nature of this thesis as a composite of peer-reviewed manuscripts, there is a degree of repetition in the introductory sections of each chapter.

LIST OF ADDITIONAL PUBLICATIONS RELEVANT TO THIS THESIS

Several conference abstracts were published during the research period though were not peer-reviewed and so do not form part of the main thesis. They are listed below, including justification for their inclusion, and may be found in Appendix B.

CONFERENCE ABSTRACT A – Sansom, E. K., Bland, P. A. and Paxman, J. (2014). Automated Dynamic Modelling of Fireballs from the Australian Desert Fireball Network. LPI, Houston, p.1591 (45th Lunar Planetary Science Conference).

Reason for inclusion – This work was presented as a poster at an international conference and outlined the work in paper 1.

CONFERENCE ABSTRACT B – Sansom, E. K., Bland, P.A , Paxman, J. and Towner, M. C. (2014). Characterising Fireballs for Mass Determination: Steps Toward Automating the Australian Desert Fireball Network. 31st URSI General Assembly and Scientific Symposium.

Reason for inclusion – This work was presented as an oral presentation at an international conference and outlined the work in paper 1 as well as the Desert Fireball Network pipeline.

CONFERENCE ABSTRACT C – Sansom, E. K. , Bland, P. A., Towner, M. C., Paxman, J. P., Howie, R. M., Cupak, M., Galloway, M. J., Benedix, G. K. (2015). Initial Results from the Expanded Desert Fireball Network. LPI contributions, p. 5172 (78th Meteoritical Society Meeting).

Reason for inclusion – This work was presented as an oral presentation at an international conference and outlined the first results calculated by the Desert Fireball Network pipeline.

CONFERENCE ABSTRACT D – Sansom, E. K., Bland, P. A., Rutten, M. G. (2016). Exploring Advanced Estimators from Guidance, Navigation and Control in Fireball Modelling. LPI, Houston, p. 1892 (47th Lunar Planetary Science Conference)

Reason for inclusion – This work was presented as an oral presentation at an international conference and outlined the work in paper 2 and paper 3.

CONFERENCE ABSTRACT E – Miljković, K., Sansom, E. K., Daubar, I. J., Karakostas, F., Lognonné, P. (2016). Fate of Meteoroid Impacts on Mars Detectable by the InSight Mission. LPI, Houston, p. 1768 (47th Lunar Planetary Science Conference).

Reason for inclusion – This work was done as part of a collaboration presented as a poster at an international conference. Methods described in paper 1 were used to determine the effect of ablation on meteoroids entering the Martian atmosphere. A description of the work involved in this collaboration is provided in Appendix B.

CONFERENCE ABSTRACT F – Sansom, E. K. , Bland, P. A., Rutten, M. G., Paxman, J., Towner, M. C. (2016). Exploring Uncertainties in Fireball Modelling Using Estimators. Meteoroids 2016

Reason for inclusion – This work was presented as a poster at an international conference and outlined the work in paper 3.

LIST OF FIGURES

LIST OF TABLES

LIST OF SYMBOLS USED IN THIS THESIS

A – Shape parameter - a cross sectional area to volume ratio $A = S\left(\frac{\rho_m}{m}\right)^{2/3}$.

$\hat{\mathbf{a}}_k^{i;n}$ – Apparent line-of sight cartesian unit vector at t_k from any n observatory to any particle i.

$a_\oplus$ – Semi-major axis of the Earth's geoid.

$b_\oplus$ – Semi-minor axis of the Earth's geoid.

c_d – Drag coefficient.

c_h – Heat-transfer coefficient.

$\mathbf{C}$ – Cross-correlation matrix of the state measurement.

$e_\oplus$ – First eccentricity of Earth's geoid.

$ECEF$ – As a subscript, the vector it relates to is in geocentric cartesian coordinates following the Earth Centred, Earth Fixed reference system.

ENU – As a subscript, the vector it relates to is in geocentric cartesian coordinates following the local East, North, Up reference system.

$\mathbf{F}$ – State transition matrix ($\mathrm{m\,s^{-2}}$).

g – Local gravitational acceleration ($\mathrm{m\,s^{-2}}$).

$\mathbf{g}$ – Vector of local gravitational acceleration ($\mathrm{m\,s^{-2}}$).

h_0 – Scale height of the homogeneous atmosphere (m).

H^* – Enthalpy of sublimation ($\mathrm{J\,kg^{-1}}$).

$\mathbf{H}$ – Measurement matrix used to correlate the state to the given observations.

I – Fireball luminosity (Watts).

k — As a subscript, represents that parameter at a given measurement time t_k.

$\mathbf{K}$ — Kalman gain.

k_m — Defined by equation (2.19).

k_v — Defined by equation (2.19).

Kn — Knudsen Number.

l — Meteoroid position along the luminous trajectory (m).

l_0 — Initial meteoroid position (m).

$\mathbf{l}$ — 3D position vector (m; in ECEF coordinates unless otherwise specified).

L — Number of variables in a state matrix.

m — Meteoroid mass (kg).

m_0 — Initial entry mass of meteoroid (kg).

m_f — Terminal mass of the main meteoroid body at the end of the luminous trajectory (kg).

M^i — Model in an IMM.

Ma — Mach number.

N_{obs} — Number of observatories that observed the fireball at time t_k.

N_s — Total number of particles used by a particle filter.

$\mathcal{N}(a; b)$— Notation used to define a Gaussian distribution with a mean a and variance b.

$\mathbf{O}^n$ — The nth observatory's position vector (where $n = 1, ..., N_{obs}$).

$p(a|b)$ — Notation used to represent a probability density function.

$\mathbf{P}$ — Covariance matrix for the state estimate.

$\mathbf{Q}$ — Process noise covariance matrix. Can be either in continuous ($\mathbf{Q}_c$) or discrete ($\mathbf{Q}_k$) time.

$\mathbf{R}$ — Observation/measurement noise covariance matrix.

Re – Reynolds number.

S – Cross sectional area of the body (m^2).

S_0 – Initial cross sectional area of the body (m^2).

$\mathbf{S}$ – Innovation covariance (also known as residual covariance).

t – Time through the luminous trajectory (s).

t_0 – Time of the first observation made of the luminous trajectory.

t_m – Time of first available multi-station observation.

$\mathbf{u}$ – Model process noise. Can be either in continuous ($\mathbf{u}_c$) or discrete ($\mathbf{u}_k$) time.

v – Velocity ($m\,s^{-1}$).

v_0 – Initial entry velocity of the meteoroid ($m\,s^{-1}$).

$\mathbf{v}$ – 3D velocity vector ($m\,s^{-1}$; in ECEF coordinates unless otherwise specified).

$\mathbf{w}$ – Observation/measurement noise.

w^i – Weight calculated for the ith particle in a particle filter.

$\mathbf{x}$ – State vector.

$\hat{\mathbf{x}}$ – Predicted state vector.

$\mathbf{y}$ – Measurement (or innovation) residual.

$\mathbf{z}$ – Observation measurement.

$\hat{\mathbf{z}}$ – Predicted observation extracted from predicted state vector.

$\mathcal{Z}$ – Estimated position for each sample point in an UKF (Equation 3.9).

α – Ballistic Coefficient.

– Also scaling factor used in an UKF (Equation 3.5).

β – Mass loss parameter.

– Also scaling factor used in an UKF (Equation 3.5).

γ – Angle of the meteoroid flight to the horizontal (γ_e is entry angle).

— Also used when describing drag coefficient parameters in Section 2.3, γ refers to the ratio of specific heats.

θ — Angular separation between the line-of-sight observation and the estimated meteoroid position. Used to triangulate trajectories (Equation 5.11).

κ — Shape-density coefficient $\kappa = \frac{Ac_d}{\rho_m^{2/3}}$ $(m^2\,kg^{-2/3})$.

— Also scaling factor used to define λ in an UKF.

λ — Scaling parameter used to determine sample points in an UKF (Equation 3.4).

Λ^i — Likelihood of the predicted measurement for each model in an IMM.

μ — Shape change parameter representing the rotation of a meteoroid body $(0 < \mu < 2/3)$.

— Also the model probability in an IMM.

ρ_a — Atmospheric density $(kg\,m^{-3})$.

ρ_m — Meteoroid bulk density $(kg\,m^{-3})$.

σ — Ablation parameter, $\sigma = \frac{c_h}{H^* c_d}$ $(s^2\,km^{-2})$.

— Also used as the statistical variable for standard deviation (and variance, σ^2) as specified in the text.

τ — Luminous efficiency parameter.

Φ — Transition probability matrix to relate models in an IMM.

χ_i — Weighted sample points used to represent the Gaussian probability distribution of the data in an UKF (Equation 3.4).

$\oplus$ — As a subscript, pertaining to the Earth.

CHAPTER 1

INTRODUCTION

This doctoral thesis describes the development and improvement of algorithms for the analysis of fireball trajectories. Previously there has been progressive, iterative advancement in methods to incorporate nuances in fireball modelling, such as fragmentation and unknown initial and trajectory parameters. This prior work however has not incorporated recent developments outside the field of fireball modelling. Stochastic tracking algorithms can encapsulate noise and measurement uncertainties, as well as generate estimates of unknown parameters, without prior assumptions. The work detailed in this thesis explores these algorithms, including Kalman and particle filters, as approaches to modelling fireball trajectories, up to and including development and implementation in 3D. The aim was a model that could be automated for routine application, without the computational costs of hydrocode modelling, using minimum assumptions regarding input parameters whilst comprehensively propagating all errors and uncertainties. Although the work forms part of the Australian Desert Fireball Network project, and is relevant to the automated data pipeline developed to allow processing of large volume fireball datasets, it is hoped that the work detailed here has relevance beyond this project.

This thesis comprises a collection of research papers that were either published or in preparation at the time of writing this document. The work has been divided into chapters that each address a different evolution of the main aim of the research. This introductory chapter provides the background and rationale for the study, describing the framework within which the series of manuscripts fit. A standard literature review is not presented within this thesis, as individual papers that comprise each chapter incorporate the relevant background literature and place the research in a wider context. Each manuscript includes a discussion of the methods presented with respect to previous studies and cited references. Chapters 2-4 of the main body of research have been published in peer-reviewed journals and Chapter 5 is in preparation for submission. Copies of the published and accepted manuscripts may be found in Appendix A along with statements of co-authorship and reprint permissions from the relevant publishers. Chapter 6 summarises the principal outcomes of this research and readdresses future work to be done.

BACKGROUND

When objects travelling through interplanetary space collide with the Earth's atmosphere at up to $72\,\mathrm{km\,s^{-1}}$, they experience drastic deceleration and frictional heating. The luminous phenomena that results is defined by its overall brightness, ranging from *meteor* to *fireball* to *bolide* (Figure 1.1 after Ceplecha et al. 1998).

The meteoroid objects which generate meteors are generally $0.05\,\mathrm{mm}-20\,\mathrm{cm}$ and mostly burn up high in the atmosphere (Ceplecha et al., 1998). Of the millions that are encountered daily, many are linked to streams of cometary debris that the Earth passes through and can be seen as discrete showers (Jenniskens et al., 2016). Hourly rates can sometimes exceed 1000s per hour (Trigo-

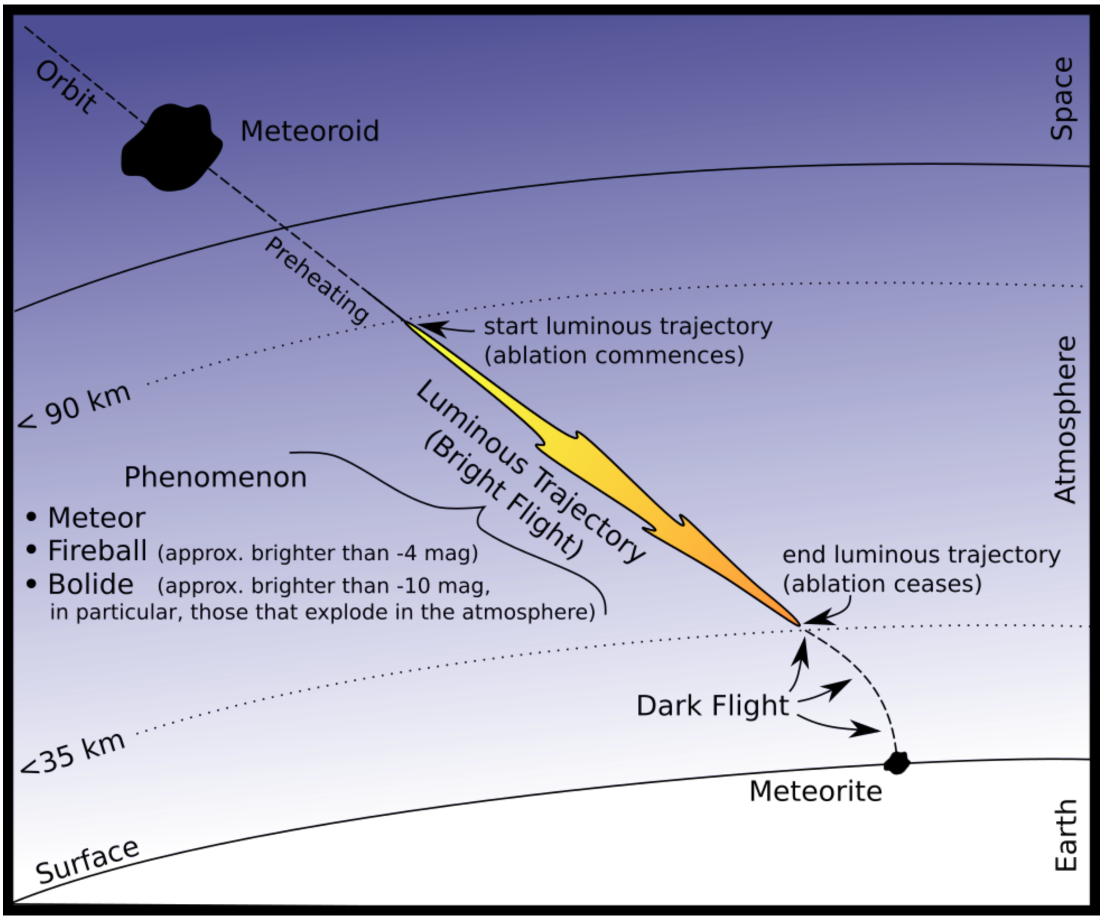

FIGURE 1.1: Illustration of meteoroid definitions after Ceplecha et al. (1998). Altitude at which ablation commences is strongly dependent on velocity and preheating can start as high as 300 km.

Rodríguez et al., 2004). Fireballs and bolides form from larger material and are more likely to survive the luminous trajectory (also referred to as a *bright flight*) as the deceleration is able to compete with ablation in consuming kinetic energy (Ceplecha et al., 1998). If an ablating meteoroid reaches an altitude of $< 35\,\mathrm{km}$ with a terminal velocity of $< 10\,\mathrm{km\,s^{-1}}$, the remaining mass no longer retains enough kinetic energy to sustain ablation and it can be expected to fall to the ground in a *dark flight* (Brown et al., 2013).

THE VALUE OF METEORITES

Meteorites are samples of extra-terrestrial rock that have landed on the Earth's surface. They are remnants of the early Solar System, recording information about its formation around 4.56 billion years ago and its subsequent evolution (e.g. Burbine et al. 2002).

Chondritic meteorites are the most primitive, containing refractory inclusions (the oldest, most primordial solids in the Solar System; MacPherson 2014) and chondrules (spherules formed by localised melting of dust in the protoplanetary disk; Scott and Krot 2003). As the disk collapsed, dust and gasses from the pre-existing interstellar medium were entrained, a study of which provides insights for stellar evolution and nucleosynthesis (Palme and Jones, 2003).

Differentiated meteorites are fragments of planetesimal materials that have undergone various degrees of melting and recrystallisation. They represent the processes of protoplanetary formation and the subsequent geological history of the remnant bodies (e.g. Burbine et al. 2002). Magmatic irons are samples of primitive cores (Bottke et al., 2006) with stony-iron pallasites thought to be examples of core-mantle boundaries (DeMeo et al., 2015). Achondrites, with their typically basaltic composition and low metal content, have a plethora of possible origins; postulated scenarios for the eucrite sub-category alone range from partial melt of chondritic material in a magma ocean (Gupta and Sahijpal, 2010) to partial melting of crustal material above a magma ocean (Barrat et al., 2007).

Meteorites can also provide insights on how the Earth became a habitable planet, namely the origins of organics and water, but also, to a lesser extent, are able to constrain models of giant planet migration (Morbidelli et al., 2012).

Meteorites are therefore valuable time capsules that paint an incredible picture of the compositional diversity of the inner Solar System and the variations in protoplanetary formation throughout the disk over time (DeMeo et al., 2015) (and possibly the outer solar system as well; Gounelle et al. 2008).

WHERE DO METEORITES COME FROM EXACTLY?

For the vast majority of meteorites we have no constraint on their point of origin within the Solar System. Of the $\sim 50,000$ recovered population, only $\sim$ 2% have been observed to fall over the last 300 years (Grady, 2000), and only $\sim$ 2% of these (29 meteorites[1]) have their origin constrained with an orbit. The true potential of the scientific knowledge meteorites can provide cannot be fully exploited without a means for providing spatial context. The value of this context is a primary focus of space agencies around the world, commissioning sample return missions to asteroids (JAXA's Hyabusa1 and Hyabusa2, NASA's OSIRIS-REx ; Mueller et al. 2011) and comets (NASA's Stardust; Brownlee et al. 1997).

Observing the luminous trajectory of a fireball from multiple locations, with high enough precision, enables the pre-atmospheric orbit of the body to be determined (Halliday, 1973; Borovička et al., 2003, 2013). With the growing number of catalogued near Earth objects (NEOs), this even has the increasing potential to identify parent bodies (such as done by Drummond 2000 and Jenniskens et al. 2009) or at the least, source regions within the asteroid belt, and the resonances that sent them toward the Earth. Recovering a corresponding meteorite overlaps with some of the science drivers behind sample return missions. Although the recovered material can never be as pristine, this method, in providing an orbital context, bridges the gap between meteorites and asteroids. Identifying a parent body with certainty can also provide calibration material

---

[1] As of the 1st December 2016. The list provided in Table 1 of Borovička et al. (2015a) has been supplemented by the Annama (Trigo-Rodriguez et al., 2015), Žd'ár nad Sázavou (Spurný et al., 2016), Creston (Meteoritical Society, 2015), Murrili (Bland et al., 2016) and Stubenberg (Spurný et al., 2016) meteorites, along with two further unnamed falls recovered this year (Seckel, 2016; Hunter, 2016).

for telescope spectra.

CAMERA NETWORKS

Deriving precise orbits for meteorites is challenging and requires high quality photographic observations of the bright fireball trails (e.g. Halliday et al. 1978; Spurný et al. 2012). Dedicated camera networks have occasionally been established in different areas around the world to capture fireball and bolide phenomena with the aim of increasing the number of meteorites with orbits (as well as to monitor the flux of impacting material; Halliday et al. 1989). Of the 29 meteorites with orbits to date, 18 have been observed and recovered with the aid of such networks.

The Příbram meteorite was the first to be recovered following high quality photographic observations and also the first meteorite with a known orbit and origin (Ceplecha et al., 1959; Ceplecha, 1961). Příbram was photographed by the precursor to the European Network which has been operating since 1955 (Ceplecha, 1977), introducing all-sky cameras in 1963 (Ceplecha and Rajchl, 1965). The European network today covers a $1 \times 10^6\,\mathrm{km}^2$ viewing area. Two other photographic networks were then initiated: the Prairie Network in the United States, operating for 11 years from 1964 (and covered a $1.1 \times 10^6\,\mathrm{km}^2$ area) (McCrosky and Boeschenstein, 1965), and the Meteorite Observation and Recovery Project in Canada which operated for 14 years from 1971 (and covered $1.3 \times 10^6\,\mathrm{km}^2$) (Halliday et al., 1978).

Although many fireballs were considered as potential meteorite-dropping events over the years, the location of these programs in temperate regions has not been conducive to meteorite recovery.

THE DESERT FIREBALL NETWORK

A SUCCESS STORY FROM THE START — Field searches in desert regions such as the Sahara, Nullarbor (Bland et al., 1996) and Antarctica (Righter et al., 2014) have shown great success in recovering chance *finds* (meteorites whose path through the atmosphere has not been witnessed). The desert environment and lack of vegetation lends itself to ideal searching terrain. Low rainfall favours the recovery of more pristine samples whilst persistent clear skies provide more consistent observations. The Nullarbor Plain in south west Australia was chosen for the initial testing of the Desert Fireball Network (DFN) (Bland et al., 2012, 2009) with the foremost priority to expedite meteorite recovery, and was not selected based on pre-existing observatory locations (as had all previous networks). The trial phase of the network used four large format film cameras, based on the design used by the European Network (Spurný et al., 2006), with heavy modification for the desert environment. Being the first camera network to be situated in the Southern hemisphere, the DFN has a unique perspective on incoming extra-terrestrial material. During this testing period, the DFN recovered two meteorites: Bunburra Rockhole (Spurný et al., 2012) and Mason Gully (Towner et al., 2011), paving the way for a continuation and expansion of the project. The decision was made to move to digital systems which were of significantly lower-cost, but with design features that meant no decrease in instrument precision.

DIGITISING THE NETWORK — The DFN currently has 50 operating autonomous observatories[2] spanning from coast to coast across the southern Australian outback, crossing the Nullarbor Desert and covering a 3×10^6 km^2 viewing area; truly a continental scale instrument (Figure 1.2).

The camera systems in each observatory (Figure 1.3) have been designed

---

[2] With additional observatories on sites awaiting installation. Portable observatories have also been installed in the USA, Canada, Morocco and the UK.

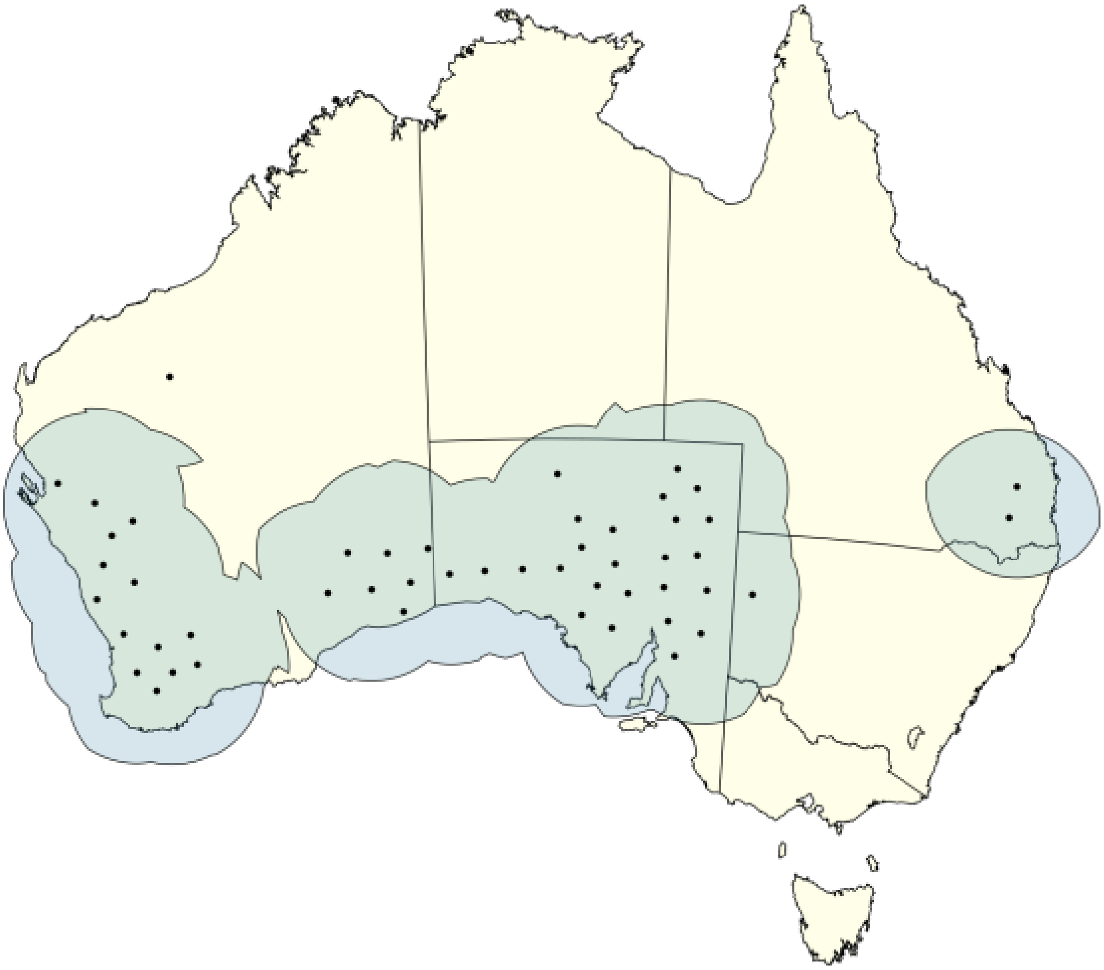

FIGURE 1.2: Current location of Desert Fireball Observatories across Australia.

for easy assembly, installation and maintenance, consisting of predominantly off-the-shelf parts allowing for upgrades as technological advancements in consumer products are made. Each system[3] currently contains a 36 MP DSLR camera with a fish-eye lens allowing a full-sky view from each observatory, a video camera for real-time cloud detection, a minimum of 8 TB of data storage and a liquid crystal (LC) shutter installed within the camera lens. Thirty second-long exposures are taken continuously from local sunset to sunrise when not overcast. Over the entire network, this amounts to approximately 60 TB per month of data from which fireballs need to be identified and analysed, averaging ~ 1.8 fireball observations per night longer than 3 seconds. For events

---

[3] See (Howie et al., 2017) for full description of DFN camera systems.

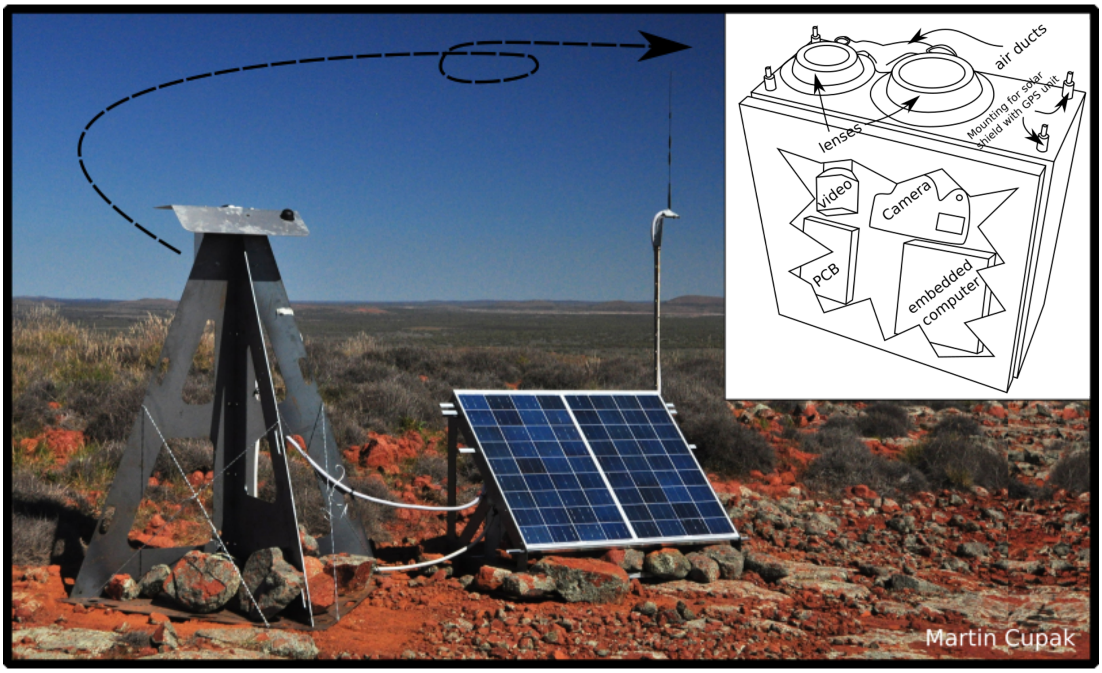

FIGURE 1.3: Installed Desert Fireball Observatory. Inset: simple schematic of basic elements within a camera system (mounted on the reverse side of the stand, and under the solar shield, in the photograph). Air ducts ensure dehumidification of lenses. Aluminium solar shield is mounted flush with the lenses, on which a GPS antenna is mounted. PCB: printed circuit board.

which are determined potential meteorite-droppers, a quick recovery minimises contamination of the rock, increasing its scientific value. In the past, reducing fireball network imagery to generate a trajectory, orbit and fall position (in the case where an object survives to the surface), has required laborious manual data reduction, such that the majority of fireball events go unpublished. To enable a complete, unbiased analysis of the photographic data (not favouring bright events only), and to expedite meteorite recovery, an automated software pipeline had to be compiled.

DATA REDUCTION PIPELINE — On-board the camera systems, the embedded PC runs neural network algorithms to detect fireball events in each image. Remote 3G access to observatories enables a central server to determine if detected events can be correlated between observatories, and instantly download relevant exposures. Each camera image is calibrated using the background star field to determine an observational azimuth and elevation for the fireball trail (Devillepoix and Sokolowski, in prep.). Triangulation of these lines of sight from multiple cameras can give the fireball's trajectory in 3D space.

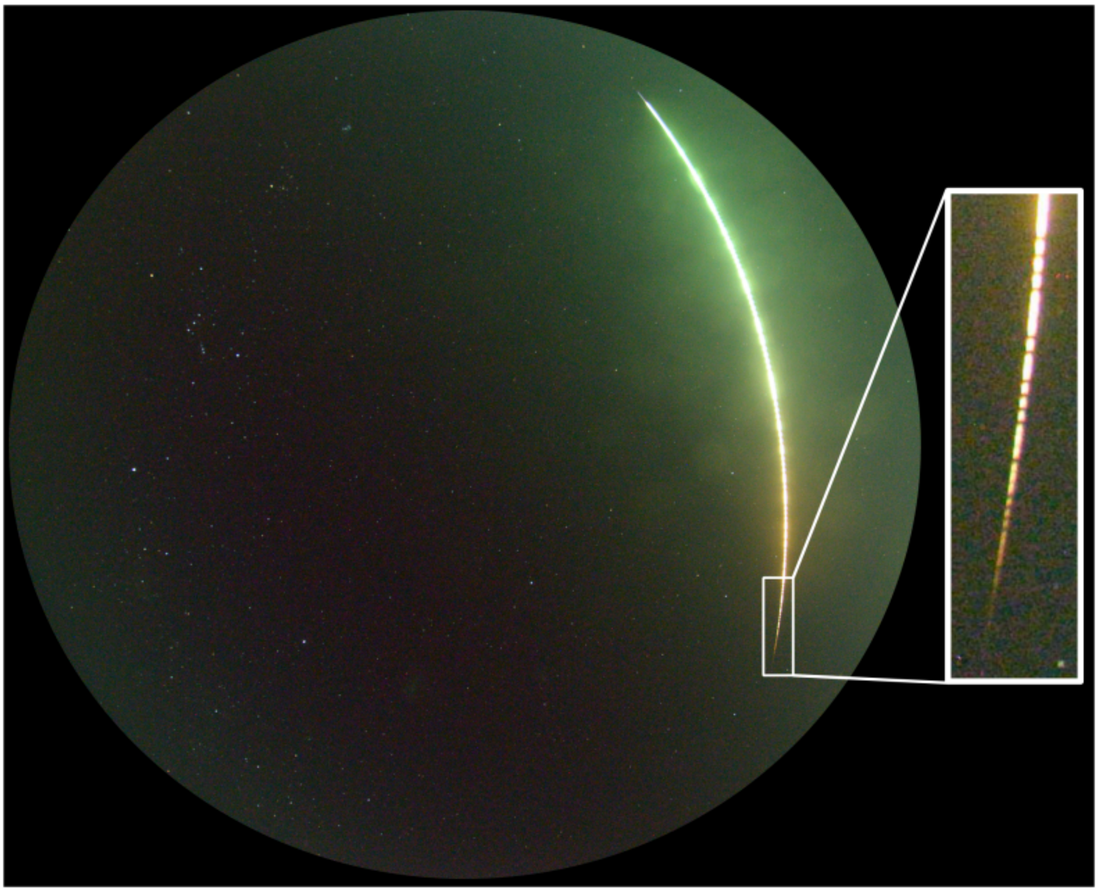

FIGURE 1.4: Fireball DN151212 captured by the Desert Fireball Observatory at Etadunna Station, South Australia. Travelling from North (top) to South (bottom), this fireball lasted over 21 s and is visible across two consecutive images (13.96 seconds represented in this exposure; 1 dash every 0.1 s). Calibration with background stars determines azimuth and elevation of trajectory points.

To know the path of the trajectory in 3D space is not enough to determine orbits however. The exact time the meteoroid entered the atmosphere needs to be known and at what velocity; we need a method to determine the arrival time within each long exposure image. Previous camera networks have included a photomultiplier tube (PMT) in their observatory systems to record the all-sky brightness, synced to a timing device, to determine absolute arrival time of events brighter then −4 magnitude (McCrosky and Boeschenstein, 1965; Halliday et al., 1978; Spurný et al., 2006). Determining fireball velocities has previously involved a rotating (Ceplecha et al., 1959; Ceplecha and Rajchl, 1965) or periodic (McCrosky and Boeschenstein, 1965) shutter occulting the sensor (Jacchia and Whipple, 1956; Ceplecha, 1957) at a known frequency, blocking the light during the long exposure. This enables enough light for stars to be observed for calibration, while chopping fast-moving fireballs into small segments with known relative start and end times.

When designing the digital DFN observatories, a main consideration was for the system to be low-cost so as to build a large number, and to minimise the amount of moving parts that may fail from desert dust. Not only is a PMT an expensive piece of equipment in itself but it also requires additional power supplies which is a limitation in the remote locations of the DFN observatories.

The innovation of Howie et al. (2017) allows any off-the-shelf DSLR camera to be turned into a fireball observatory with the addition of a liquid crystal (LC) shutter. By modulating the shutter following a de Bruijn sequence, the absolute timing of the fireball can be embedded into the long exposure image with an accuracy of $0.4\,\mathrm{ms}$. A one pixel LC display is mounted inside the camera, between the lens and the shutter, keeping the camera sealed to prevent dust penetration.

METEOROID MODELLING

Under the right conditions, including entry velocity, mass, density, strength and flight angle, a meteorite can arrive at the Earth's surface following the observation of a fireball. A key objective of the DFN is to recover meteorites for which the atmospheric trajectory has been observed so as to acquire orbits. To predict whether an event has likely dropped a meteorite, we model the evolution of the meteoroid during its luminous trajectory. Fall positions depend on the resulting terminal bright flight position, velocity and mass, and whether there has been any fragmentation. The outputs from luminous trajectory analyses are used to subsequently initialise dark flight simulations, which use Weather Research and Forecasting (WRF) wind models (Bland et al., 2009), to predict the free fall of meteorites to the ground. Uncertainties in the initial luminous trajectory analyses, introduced by both the underlying models used and the errors in triangulated observations, will also affect the predicted ground search area.

As a meteoroid decelerates through the atmosphere, its motion and ablation can be modelled, assuming no fragmentation, by the single body theory of meteoroid physics (Ceplecha et al., 1993):

$$\frac{dl}{dt} = v \tag{1.1a}$$

$$\frac{dv}{dt} = -\frac{1}{2}\frac{c_d \rho_a v^2 S}{m} + g \sin\gamma_e \tag{1.1b}$$

$$\frac{dm}{dt} = -\frac{1}{2}\frac{c_h \rho_a v^3 S}{H^*} \tag{1.1c}$$

$$I = -\tau\left(\frac{v^2}{2}\frac{dm}{dt} + mv\frac{dv}{dt}\right), \tag{1.1d}$$

where:

l – meteoroid position along the luminous trajectory (m),

t – time throughout the luminous trajectory (s),

v – velocity ($m\,s^{-1}$),

m – meteoroid mass (kg),

c_d – drag coefficient,

ρ_a – atmospheric density ($kg\,m^{-3}$),

S – cross sectional area of the body (m^2),

g – local gravitational acceleration ($m\,s^{-2}$),

γ – angle of the meteoroid trajectory to the horizontal,

H^* – enthalpy of sublimation ($J\,kg^{-1}$),

c_h – heat-transfer coefficient,
I – fireball luminosity (Watts) and
τ – luminous efficiency parameter.

This system of equations requires the knowledge of trajectory parameters that are unique to each event and, although position and velocity, to an extent, can be extracted from the raw data, others are not directly observable. Early research originally assumed values for all fireball characteristics, including the shape and bulk density of the meteoroid (McCrosky et al., 1971; Halliday et al., 1996; Borovička et al., 1998). It was not uncommon to manipulate coefficients to allow models to fit the data (McCrosky et al., 1971).

There are two approaches to finding the terminal bright flight mass, though not mutually exclusive. The *photometric* method uses the amount of radiated energy released from ablation as a proxy for the extent of mass lost through the atmosphere – calculated using Equation (1.1d) (e.g. McCrosky et al. 1971). This method relies on the acquisition of an accurate light curve of the event, although the luminosity of a fireball trajectory is due to kinetic energy loss by both ablated material as well as deceleration of the meteoroid body with no way of separating the contribution of each (Ceplecha et al., 1998; Borovička et al., 1998). Borovička (1993) also determines that 95% of the meteor envelope has an atmospheric origin. The *dynamic* method uses the deceleration of the meteoroid through the atmosphere to determine its changing mass (Whipple, 1952) – calculated using Equations (1.1a)-(1.1c) (e.g. Gritsevich 2008b). In the past, this approach was limited by the accuracy of measurements that could be interpreted from photographic plates (Ceplecha, 1961; McCrosky et al., 1971).

A combination of both approaches is now typically applied, using least squares methodologies (Ceplecha and Revelle, 2005). These methods have undergone iterative developments over the years, but assumptions are still made in some cases (such as for bulk densities (Borovička et al., 2013), shape density coefficients (Ceplecha and Revelle, 2005; Spurný et al., 2012) and ablation parameters (Borovička et al., 2015b)), and coefficients that have been used to fit a single data set are considered constant and uniformly applied across data sets (Ceplecha, 1977).

Work by Stulov et al. (1995), Gritsevich and Stulov (2007) and Gritsevich (2008b,c) has enabled the application of an analytical solution by combining unknown trajectory parameters into two dimensionless constants. This has been applied by Gritsevich (2008a) to data sets resulting in meteorite recoveries. This was the initial method examined by this research and was useful in highlighting the poor quality of existing data sets, and the velocity determinations on which they are based. The data sets used by Gritsevich (2008a) were for the four first significant meteorite falls: Příbram (Ceplecha, 1961), Lost City (McCrosky et al., 1971), Innisfree (Halliday et al., 1978) and Neuschwanstein (Spurný et al., 2003). In the literature, the time, altitude and velocity data are highly averaged and range from 6 data points for Příbram to 18 data points for Innisfree. The extensive fireball data set published by Halliday et al. (1996) for the MORP does not include any events with over 25 data points. When this same method was used on the Bunburra fireball data set (Spurný et al., 2012) with 112 data points, the raw data contained significant noise and a solution was not achieved without prior averaging (Sansom et al., 2015). Although the Bunburra fireball data were derived from images that (at the time) were collected by the most technically sophisticated fireball cameras, this analysis reveals the surprising limitations of that hardware, and data reductions methods; in particular, just how imprecise the current method of velocity determination is. Previous photometric and dynamic methods apply several over-simplifying assumptions such as disregarding the weight of the meteoroid, straight-line trajectories and real changes in atmospheric density (some assume the isothermal atmospheric model).

The accurate determination of a meteorite fall position can lead to the rapid recovery of a meteorite, minimising cross-contamination with the terrestrial environment. The stratospheric winds in dark flight modelling introduce a large uncertainty to fall predictions. Although a well constrained final mass is advantageous, it is impractical without a thorough understanding of the errors involved. Error analysis in least squares methodologies are measured as the standard deviation of the collective residuals between the model values and the observations. There is no differentiation between individual observation errors (introduced by either the measurement, calibration or triangulation processes) nor do they identify uncertainties in the model equations used. The resulting search area will therefore be dependent primarily on the wind model (where the range of projected masses form a fall line), rather than on the modelled meteoroid characteristics (e.g. bulk density, shape, etc.) and their errors. A method was needed that can encapsulate all uncertainties introduced by the model, observations and initial parameters used to provide a realistic search region for the specific dataset. The upper limit of realistically searchable terrain in the Australian outback is approximately $2 - 6\,\mathrm{km}^2$ (Howie et al., 2017). The understanding of the real-world variability on the ground will significantly influence decisions about the feasibility of a remote, ground based search for meteorites, favouring those with greater chances of success.

NEW METHODS FOR MODELLING METEOROIDS

The continental scale deployment of > 50 automated DFN observatories has been possible by the low cost of each system. The innovation of including a de Bruijn-modulated LC shutter enables both absolute and relative timing of fireballs to be encoded into each image, without the need for a separate subsystem such as a PMT. Although this decreases the cost significantly, this means that no light curve is directly measured. Determining the light curve for an event from still images is manually intensive, as is creating the fragmentation input information required by approaches including these data (Ceplecha and Revelle, 2005)

A trajectory analysis approach that is able to determine meteoroid parameters without a light curve, comprehensively include parameter, model and observational uncertainties, whilst being fully automated, will allow an unbiased analysis of all events and provide a more realistic evaluation of errors.

BAYESIAN STATE-SPACE METHODS

Taking a set of potentially noisy observation data and determining the true state of a physical system is known in stochastic processes as filtering (Jazwinski, 1970). Bayesian state-space estimators are statistical algorithms used to address the filtering problem in many fields, particularly that of guidance, navigation and control, where their application ranges from satellite tracking (Ning and Fang, 2007; Mazor et al., 1998) to self driving cars (Thrun et al., 2006). These techniques model a system of equations and determine the statistical likelihood of optimally predicted states based on real measurements. Simply, the *state* describes what a system is 'doing' at any given time; it is a minimum collection of information that allows the future behaviour of the system to be predicted if external inputs are known. For example, a meteoroid's trajectory may be (simply) represented by its position, velocity and mass. Although not all state variables are directly observed, the link between them within the model equations allows the estimation of the other variables. In this case, real time position observations can be made to estimate the meteoroid's velocity and mass through Equations (1.1a) - (1.1c). The knowledge of a system is therefore encapsulated in its state, and associated covariance matrices quantify the errors involved.

KALMAN FILTERS

There are a variety of techniques that recursively solve for Bayes' rule (where $p(a|b)$ notation represents a probability density function),

$$p(\mathbf{x}_k|\mathbf{z}_{1:k}) \quad \propto \quad p(\mathbf{z}_k|\mathbf{x}_k)p(\mathbf{x}_k|\mathbf{z}_{1:k-1}), \tag{1.2}$$

to find the posterior distribution $p(\mathbf{x}_k|\mathbf{z}_{1:k})$ of a model state ($\mathbf{x}$), given a set of observations ($\mathbf{z}$) from time t_1 to t_k, a likelihood function $p(\mathbf{z}_k|\mathbf{x}_k)$, and a prior probability function $p(\mathbf{x}_k|\mathbf{z}_{1:k-1})$ defined through a set of state-space equations. The validity of these methods is dependent on the form of said state-space equations. If they are linear with both noise and prior distributions being Gaussian, an analytical solution can be reached in the form of a Kalman filter (Grewal and Andrews, 1993). For non-linear equations or non-Gaussian distributions, such as the single body equations for meteoroid flight (1.1), an exact solution is not possible and generalisations are required.

An extended Kalman filter (EKF) is an extension to the Kalman filter that statistically optimises estimates of state variables for non-linear dynamic systems (Grewal and Andrews, 1993). The EKF approximates Gaussian noise and prior distributions, and uses a linearised form of Equation (1.1), to estimate the subsequent mean state and covariance. This method is applied to meteoroid trajectories in:

CHAPTER 2 – A NOVEL APPROACH TO FIREBALL MODELLING: THE OBSERVABLE AND THE CALCULATED – *published in Meteoritics and Planetary Science.*

The EKF method successfully models a meteoroid trajectory using only the dynamic single body equations (1.1a)-(1.1c) (no photometry) and rigorously propagates the uncertainties of the model and measurements. A dynamic optimisation is used initially to determine the most favourable trajectory parameters, including initial meteoroid mass, bulk density and shape, using a least squares minimisation. The novelty is the subsequent implementation of these within an extended Kalman filter to explicitly model the errors in triangulated observations and the single body model (1.1a)-(1.1c). As all the data are available at the time of processing, we finally apply a Rauch–Tung–Striebel (RTS) smoothing algorithm (Särkkä, 2008). Smoothers in this field do not refer to any averaging of the data, rather to the process of including both past and future measurement data within a filter.

Initially, the technique of Gritsevich (2008b) was used when exploring possible approaches for this research and the results are also published in this paper (Sansom et al., 2015).

The entry and terminal masses of the Bunburra Rockhole meteoroid estimated by an EKF are consistent with published values determined using both dynamic and photometric methods. This algorithm is however restricted to a single set of input parameters as the state prior which must be predetermined.

The linearisation of the meteoroid state-space equations is suboptimal. An Unscented Kalman Filter (UKF) is an estimator that allows for a more rigorous approach to handling non-linear equations (Julier and Uhlmann, 1997). An UKF still approximates the prior and noise distributions as Gaussian, but uses a method of statistical linearisation (a deterministic sampling technique) to propagate the mean and covariance through measurement and process equations (Särkkä, 2007). This advancement is applied to fireball trajectory modelling in Sansom et al. (2016) (Chapter 3) along with the implementation of interactive multiple models.

INTERACTIVE MULTIPLE MODELS

Meteoroids lose mass as they decelerate through the atmosphere by the processes of ablation and gross fragmentation. Ablation is the loss of mass through vaporisation while gross fragmentation is the sudden extreme loss of mass due to exceeding dynamic pressures (Ceplecha et al., 1998). Ablation is itself challenging to model as the heating parameters are poorly researched, but gross fragmentation is highly unpredictable as the internal properties of the meteoroid are unknown. This significantly challenges the application of a single body theory to observed fireballs (Ceplecha and Revelle, 2005) and, as it significantly influences the mass, it is essential to model.

An interactive multiple model (IMM) is an effective algorithm where the system is not constrained to a single state-space. It performs a weighted output of multiple filters, each implementing different state-space models. This technique is typically used to predict manoeuvres in vehicle tracking, such as an aircraft deviating from a straight line path to perform a turn. Two filters may be simultaneously used to model both a straight line path and a curved path, and an IMM applied after each observation adjusts the relative likelihood of each model (Blom and Bar-Shalom, 1988; Mazor et al., 1998).

Although a meteoroid's state equations will not change during its trajectory, we may still use two Kalman filters to analyse differences in model covariances. An ablating meteoroid is fairly well described by the single body equations and therefore the model noise covariance can be lower. When a gross fragmentation event occurs, the model noise covariance in both mass and velocity will drastically increase due to the unpredictable nature of this phenomenon and its not being taken into account by the single body equations. Combining these two simultaneously within an IMM enables multiple fragmentation events to be predicted automatically without the use of a light curve or manual interpretation, hereto never done. The application of this method along with the progression to an UKF is detailed in:

CHAPTER 3 – **FILTERING METEOROID FLIGHTS USING MULTIPLE UNSCENTED KALMAN FILTERS** – *published in the Astronomical Journal.*

The results of the UKF/IMM on the Bunburra Rockhole fireball data show corresponding features to the published light curve (Spurný et al., 2012), supporting the applicability of this novel technique.

PARTICLE FILTERS

Although the new approaches developed thus far are innovative and show promising results, they require assumptions to be made for the state prior; initial state values must be identified. In order to get a true understanding of final errors, the full parameter space needs to be explored within the statistical estimator. A particle filter is an iterative Monte Carlo approach, representing the posterior by a spread of individual particles rather than a mean and covariance (Arulampalam et al., 2002; Ristic et al., 2004). No limitations are placed on the form of the state-space equations or the distribution of noise (Gordon et al., 1993; Arulampalam et al., 2002). This 'cloud' of initial particles are propagated through the state-space equations and are individually evaluated based on their proximity to the measured observation. The mean state at any time is represented by the weighted average of all particles.

The development and implementation of this method are detailed in:
CHAPTER 4 – ANALYSING METEOROID FLIGHTS USING PARTICLE FILTERS
– *published in the Astronomical Journal.*
This is yet another step closer to fully encapsulating all the uncertainties within this analysis. By initialising a set of $10,000$ particles with a range of initial parameters, this adaptive technique is allowed to explore the parameter space allowing unknown trajectory parameters to be estimated. The particle filter not only incorporates a range of prior possibilities, but also, to some extent, includes fragmentation in the resulting final state. Initial masses however cannot be well constrained without a fragmentation model. Future work will look into combining the output of the IMM with particle filter smoothers (as before, the term smoother is in reference to the stochastic processing technique).

MODELLING IN THREE DIMENSIONS

Traditional modelling of meteoroid trajectories, including applications described above, uses pre-triangulated positions as model observations. Triangulation of observatory lines of sight usually assumes a straight line and performs a least squares fit to the observations. This allows the one dimensional equations (1.1) to model dynamics along the straight line path. This may be an acceptable simplification for some fireballs, but subtleties in the raw observations that may be due to disruptions of the meteoroid body are being removed. As we show in:

CHAPTER 5 – 3D METEOROID TRAJECTORIES *(in preparation for submission)*, the straight line assumption is not always valid and can be $> 1\,\mathrm{km}$ away from the calculated observed point. This distortion of the data also affects velocity and mass estimates through the relationship in the state equations. Modelling fireballs in three dimensions has not previously been computationally viable for routine application with fireball camera network data (Bland and Artemieva, 2006). In this manuscript, we define the single body aerodynamic equations (1.1) in three dimensions and apply them in the particle filter approach to fireball modelling presented by Sansom et al. (2017). This allows the raw line-of-sight observations to be directly incorporated and errors in azimuth and elevation angles, per observatory, to be individually considered. This will provide final state estimates more congruent with observations, and robust final errors propagated from the well quantified azimuth and elevation uncertainties (from astrometric calibration) through to the end of the luminous trajectory. Final particle state estimates may now be directly incorporated within Monte Carlo dark flight models, leading to more realistic meteorite search areas.

From simple least squares based techniques, this thesis advances through a suite of stochastic estimators applied to meteoroid trajectory analyses, with each one contributing a solution to previous restrictions and limitations.

REFERENCES

Arulampalam, M. S., Maskell, S., Gordon, N., and Clapp, T., 2002. A tutorial on particle filters for online nonlinear/non-Gaussian Bayesian tracking. *IEEE Transactions on Signal Processing*, 50(2):174–188. doi: 10.1109/78.978374.

Barrat, J., Yamaguchi, A., Greenwood, R., Bohn, M., Cotten, J., Benoit, M., and Franchi, I., 2007. The stannern trend eucrites: Contamination of main group eucritic magmas by crustal partial melts. *Geochimica et Cosmochimica Acta*, 71 (16):4108–4124.

Bland, P., Smith, T., Jull, A. T., Berry, F., Bevan, A., Cloudt, S., and Pillinger, C., 1996. The flux of meteorites to the earth over the last 50 000 years. *Monthly Notices of the Royal Astronomical Society*, 283(2):551–565.

Bland, P., Spurný, P., Bevan, A., Howard, K., Towner, M., Benedix, G., Greenwood, R., Shrbený, L., Franchi, I., Deacon, G., et al., 2012. The australian desert fireball network: a new era for planetary science. *Australian Journal of Earth Sciences*, 59(2):177–187.

Bland, P. A. and Artemieva, N. A., 2006. The rate of small impacts on earth. *Meteoritics & Planetary Science*, 41(4):607–631. doi: 10.1111/j.1945-5100.2006.tb00485.x.

Bland, P. A., Spurný, P., Towner, M. C., Bevan, A. W. R., Singleton, A. T., Bottke, W. F., Greenwood, R. C., Chesley, S. R., Shrbený, L., Borovička, J., Ceplecha, Z., McClafferty, T. P., Vaughan, D., Benedix, G. K., Deacon, G., Howard, K. T., Franchi, I. a., and Hough, R. M., 2009. An anomalous basaltic meteorite from the innermost main belt. *Science (New York, N.Y.)*, 325(5947):1525–1527. doi: 10.1126/science.1174787.

Bland, P. A., Towner, M. C., Sansom, E. K., Devillepoix, H., Howie, R. M., Paxman, J. P., Cupak, M., Benedix, G. K., Cox, M. A., Jansen-Sturgeon, T., Stuart, D., and Strangway, D., 2016. Fall and Recovery of the Murrili Meteorite, and an Update on the Desert Fireball Network. *LPI Contributions*, 1921:6265.

Blom, H. A. P. and Bar-Shalom, Y., 1988. Interacting multiple model algorithm for systems with Markovian switching coefficients. *IEEE Transactions on Automatic Control*, 33(8):780–783. doi: 10.1109/9.1299.

Borovička, J., 1993. A fireball spectrum analysis. *Astronomy and Astrophysics*, 279:627–645.

Borovička, J., Popova, O., Nemtchinov, I. V., Spurný, P., and Ceplecha, Z., 1998. Bolides produced by impacts of large meteoroids into the Earth's atmosphere: comparison of theory with observations. I. Benesov bolide dynamics and fragmentation. *Astronomy and Astrophysics*, 334:713.

Borovička, J., Spurný, P., Kalenda, P., and Tagliaferri, E., 2003. The Morávka meteorite fall: 1. Description of the events and determination of the fireball trajectory and orbit from video records. *Meteoritics & Planetary Science*, 38(7): 975–987.

Borovička, J., Tóth, J., Igaz, A., Spurný, P., Kalenda, P., Haloda, J., Svoreň, J., Kornoš, L., Silber, E., Brown, P., et al., 2013. The Košice meteorite fall: Atmospheric trajectory, fragmentation, and orbit. *Meteoritics & Planetary Science*, 48(10):1757–1779.

Borovička, J., Spurný, P., and Brown, P., 2015a. Small near-earth asteroids as a source of meteorites. *Asteroids IV*, page 257.

Borovička, J., Spurný, P., Šegon, D., Andreić, Ž., Kac, J., Korlević, K., Atanackov, J., Kladnik, G., Mucke, H., Vida, D., and Novoselnik, F., 2015b. The instrumentally recorded fall of the Kri{ž}evci meteorite, Croatia, February 4, 2011. *Meteoritics & Planetary Science*, 16(7). doi: 10.1111/maps.12469.

Bottke, W. F., Nesvorný, D., Grimm, R. E., Morbidelli, A., and O'Brien, D. P.,

2006. Iron meteorites as remnants of planetesimals formed in the terrestrial planet region. *Nature*, 439(7078):821–824.

Bronshten, V. A., 1983. *Physics of Meteoric Phenomena*. Geophysics and Astrophysics Monographs. Reidel, Dordrecht, Netherlands.

Brown, P., Marchenko, V., Moser, D. E., Weryk, R., and Cooke, W., 2013. Meteorites from meteor showers: A case study of the taurids. *Meteoritics & Planetary Science*, 48(2):270–288.

Brownlee, D. E., Tsou, P., Burnett, D., Clark, B., Hanner, M., Horz, F., Kissel, J., McDonnell, J., Newburn, R., Sandford, S., et al., 1997. The stardust mission: returning comet samples to earth. *Meteoritics and Planetary Science Supplement*, 32.

Burbine, T. H., McCoy, T. J., Meibom, A., Gladman, B., and Keil, K., 2002. Meteoritic parent bodies: Their number and identification. *Asteroids III*, 653.

Ceplecha, Z., 1957. Photographic geminids 1955. *Bulletin of the Astronomical Institutes of Czechoslovakia*, 8:51.

Ceplecha, Z., 1961. Multiple fall of Přibram meteorites photographed. 1. Double-station photographs of the fireball and their relations to the found meteorites. *Bulletin of the Astronomical Institutes of Czechoslovakia*, 12:21–47.

Ceplecha, Z., 1977. Fireballs photographed in central europe. *Bulletin of the Astronomical Institutes of Czechoslovakia*, 28:328–340.

Ceplecha, Z. and Rajchl, J., 1965. Programme of fireball photography in czechoslovakia. *Bulletin of the Astronomical Institutes of Czechoslovakia*, 16: 15.

Ceplecha, Z. and Revelle, D. O., 2005. Fragmentation model of meteoroid motion, mass loss, and radiation in the atmosphere. *Meteoritics & Planetary Science*, 40(1):35–54. doi: 10.1111/j.1945-5100.2005.tb00363.x.

Ceplecha, Z., Rajchl, J., and Sehnal, L., 1959. New czechoslovak meteorite" luhy". *Bulletin of the Astronomical Institutes of Czechoslovakia*, 10:147.

Ceplecha, Z., Spurný, P., Borovička, J., and Keclikova, J., 1993. Atmospheric fragmentation of meteoriods. *Astronomy and Astrophysics*, 279:615–626.

Ceplecha, Z., Borovička, J., Elford, W. G., ReVelle, D. O., Hawkes, R. L., Porubčan, V., and Šimek, M., 1998. Meteor Phenomena and Bodies. *Space Science Reviews*, 84(3):327–471. doi: 10.1023/A:1005069928850.

DeMeo, F., Alexander, C., Walsh, K., Chapman, C., and Binzel, R., 2015. The compositional structure of the asteroid belt. *Asteroids IV*, pages 13–41.

Devillepoix, H. and Sokolowski, M., in prep. Astrometric calibration of all-sky cameras.

Drummond, J. D., 2000. The D discriminant and near-Earth asteroid streams. *Icarus*, 146(2):453–475.

Gordon, N., Salmond, D., and Smith, A., 1993. Novel approach to nonlinear/non-Gaussian Bayesian state estimation. *IEE Proceedings F -Radar and Signal Processing*, 140(2):107. doi: 10.1049/ip-f-2.1993.0015.

Gounelle, M., Morbidelli, A., Bland, P. A., Spurný, P., Young, E. D., and Sephton, M., 2008. Meteorites from the Outer Solar System. *The Solar System Beyond Neptune*, pages 525–541.

Grady, M. M., 2000. *Catalogue of Meteorites*, volume 1. Cambridge University Press, 5 edition.

Grewal, M. S. and Andrews, A. P., 1993. *Kalman filtering: theory and practice*. Prentice-Hall Inc., New Jersey.

Gritsevich, M. I., 2008a. The Pribram, Lost City, Innisfree, and Neuschwanstein falls: An analysis of the atmospheric trajectories. *Solar System Research*, 42(5): 372–390. doi: 10.1134/S003809460805002X.

Gritsevich, M. I., 2008b. Validity of the photometric formula for estimating the mass of a fireball projectile. *Doklady Physics*, 53(2):97–102. doi: 10.1007/s11446-008-2011-x.

Gritsevich, M. I., 2008c. Estimating the terminal mass of large meteoroids. *Doklady Physics*, 53(11):588–594. doi: 10.1134/S1028335808110098.

Gritsevich, M. I. and Stulov, V. P., 2007. Entry mass for bolides of the Canadian network. *Doklady Physics*, 52(4):219–224. doi: 10.1134/S102833580704012X.

Gupta, G. and Sahijpal, S., 2010. Differentiation of vesta and the parent bodies of other achondrites. *Journal of Geophysical Research: Planets (1991–2012)*, 115 (E8). doi: 10.1029/2009JE003525.

Halliday, I., 1973. Photographic fireball networks. *NASA Special Publication*, 319: 1.

Halliday, I., Blackwell, A. T., and Griffin, A. A., 1978. The innisfree meteorite and the canadian camera network. *Journal of the Royal Astronomical Society of Canada*, 72:15–39.

Halliday, I., Blackwell, A. T., and Griffin, A. a., 1989. The flux of meteorites on the earth's surface. *Meteoritics & Planetary Science.*

Halliday, I., Griffin, A. a., and Blackwell, A. T., 1996. Detailed data for 259 fireballs from the Canadian camera network and inferences concerning the influx of large meteoroids. *Meteoritics & Planetary Science*, 31(2):185–217. doi: 10.1111/j.1945-5100.1996.tb02014.x.

Howie, R., Paxman, J., Bland, P., Towner, M., Sansom, E., and Devillepoix, H., 2017. Submillisecond fireball timing using de Bruijn timecodes. *Meteoritic & Planetary Science.*

Howie, R., Paxman, J., Bland, P., Towner, M., Cupak, M., Sansom, E., and Devillepoix, H., 2017. How to build a continental scale fireball camera network. *Experimental Astronomy*, 43237–266.

Hunter, T., 2016. Curtin fireball chasers recover Halloween meteorite from WA farm. *www.fireballsinthesky.com.au, http://news.curtin.edu.au/media-releases/curtin-fireball-chasers-recover-halloween-meteorite-wa-farm*, Accessed: 2016-11-21.

Jacchia, L. G. and Whipple, F. L., 1956. The harvard photographic meteor programme. *Vistas in Astronomy*, 2:982–994.

Jazwinski, A. H., 1970. *Stochastic Processes and Filtering Theory*. Academic Press, New York.

Jenniskens, P., Shaddad, M. H., Numan, D., Elsir, S., Kudoda, A. M., Zolensky, M. E., Le, L., Robinson, G. A., Friedrich, J. M., Rumble, D., Steele, A., Chesley, S. R., Fitzsimmons, A., Duddy, S., Hsieh, H. H., Ramsay, G., Brown, P. G., Edwards, W. N., Tagliaferri, E., Boslough, M. B., Spalding, R. E., Dantowitz, R., Kozubal, M., Pravec, P., Borovička, J., Charvat, Z., Vaubaillon, J., Kuiper, J., Albers, J., Bishop, J. L., Mancinelli, R. L., Sandford, S. A., Milam, S. N., Nuevo, M., and Worden, S. P., 2009. The impact and recovery of asteroid 2008 TC(3). *Nature*, 458(7237):485–488. doi: 10.1038/nature07920.

Jenniskens, P., Nénon, Q., Gural, P., Albers, J., Haberman, B., Johnson, B., Morales, R., Grigsby, B., Samuels, D., and Johannink, C., 2016. Cams newly detected meteor showers and the sporadic background. *Icarus*, 266:384–409.

Julier, S. J. and Uhlmann, J. K., 1997. A New Extension of the Kalman Filter to Nonlinear Systems. *Int Symp AerospaceDefense Sensing Simul and Controls*, 3 (2):26. doi: 10.1117/12.280797.

MacPherson, G. J., 2014. Calcium–Aluminum-Rich Inclusions in Chondritic

Meteorites. In Davis, A. M., editor, *Meteorites and Cosmochemical Processes*, pages 139–179.

Mazor, E., Averbuch, a., Bar-Shalom, Y., and Dayan, J., 1998. Interacting multiple model methods in target tracking: A survey. *IEEE Transactions on Aerospace and Electronic Systems*, 34(1):103–123. doi: 10.1109/7.640267.

McCrosky, R., Posen, A., Schwartz, G., and Shao, C.-Y., 1971. Lost city meteorite - its recovery and a comparison with other fireballs. *Journal of Geophysical Research*, 76(17):4090–4108. doi: 10.1029/JB076i017p04090.

McCrosky, R. E. and Boeschenstein, H., 1965. The prairie meteorite network. *Optical Engineering*, 3(4):304127–304127.

Meteoritical Society, 2015. Creston. volume 104.

Morbidelli, A., Lunine, J. I., O'Brien, D. P., Raymond, S. N., and Walsh, K. J., 2012. Building Terrestrial Planets. *Annual Review of Earth and Planetary Sciences*, 40: 251–275. doi: 10.1146/annurev-earth-042711-105319.

Mueller, M., Delbo, M., Hora, J., Trilling, D. E., Bhattacharya, B., Bottke, W., Chesley, S., Emery, J., Fazio, G., Harris, A., et al., 2011. Exploreneos. iii. physical characterization of 65 potential spacecraft target asteroids. *The Astronomical Journal*, 141(4):109.

Ning, X. and Fang, J., 2007. An autonomous celestial navigation method for leo satellite based on unscented kalman filter and information fusion. *Aerospace Science and Technology*, 11(2):222–228.

Palme, H. and Jones, A., 2003. Solar system abundances of the elements. In Davis, A. M., Holland, H. D., and Turekian, K. K., editors, *Meteorites, Comets and Planets: Treatise on Geochemistry*, volume 1, pages 41–61, Amsterdam, The Netherlands. Elsevier.

Righter, K., Harvey, R., McCoy, T., and Corrigan, C., 2014. *35 Seasons of US Antarctic Meteorites (1976–2010)*. Wiley Online Library.

Ristic, B., Arulampalam, S., and Gordon, N., 2004. *Beyond the Kalman filter: Particle filters for tracking applications*, volume 685. Artech house Boston.

Sansom, E. K., Bland, P. A., Paxman, J., and Towner, M. C., 2015. A novel approach to fireball modeling: The observable and the calculated. *Meteoritics & Planetary Science*, 50(8):1423–1435. doi: 10.1111/maps.12478.

Sansom, E. K., Bland, P. A., Rutten, M. G., Paxman, J., and Towner, M. C., 2016. Filtering meteoroid flights using multiple unscented kalman filters. *The Astronomical Journal*, 152(5):148. doi: 10.3847/0004-6256/152/5/148.

E. Sansom, M. Rutten, and P. Bland. Analyzing meteoroid flights using particle filters. *The Astronomical Journal*, 153(2):87, 2017.

Särkkä, S., 2007. On unscented Kalman filtering for state estimation of continuous-time nonlinear systems. *IEEE Transactions on Automatic Control*, 52(9):1631–1641. doi: 10.1109/TAC.2007.904453.

Särkkä, S., 2008. Unscented Rauch-Tung-Striebel Smoother. *Automatic Control, IEEE Transactions on*, 53(3):845–849.

Scott, E. and Krot, A., 2003. Chondrites and their components. In Davis, A. M., Holland, H. D., and Turekian, K. K., editors, *Meteorites, Comets and Planets: Treatise on Geochemistry*, volume 1, pages 143–200, Amsterdam, The Netherlands. Elsevier.

Seckel, S., 2016. Tracking down the Arizona fireball. *https://asunow.asu.edu/20160628-discoveries-tracking-down-arizona-fireball*, Accessed: 2016-11-21.

Spurný, P., Oberst, J., and Heinlein, D., 2003. Photographic observations of neuschwanstein, a second meteorite from the orbit of the příbram chondrite. *Nature*, 423(6936):151–153.

Spurný, P., Borovička, J., and Shrbený, L., 2006. Automation of the Czech part of the European fireball network: equipment, methods and first results. *Proceedings of the International Astronomical Union*, 2(S236):121. doi: 10.1017/S1743921307003146.

Spurný, P., Bland, P., Shrbený, L., Borovička, J., Ceplecha, Z., Singelton, A., Bevan, A. W. R., Vaughan, D., Towner, M. C., Mcclafferty, T. P., Toumi, R., and Deacon, G., 2012. The Bunburra Rockhole meteorite fall in SW Australia: Fireball trajectory, luminosity, dynamics, orbit, and impact position from photographic and photoelectric records. *Meteoritics & Planetary Science*, 47(2): 163–185. doi: 10.1111/j.1945-5100.2011.01321.x.

Spurný, P., Boroviŭka, J., Haloda, J., and Shrbený, L., 2016. Two Very Precisely Instrumentally Documented Meteorite Falls: Žd'ár nad Sázavou and Stubenburg - Prediction and Reality. In *79th Annual Meteoritical Society Meeting (2016)*, volume 1921, page 6221.

Stulov, V. P., Mirsky, V. N., and Visly, A. I., 1995. Aerodynamics of Bolides. *Nauka*.

Thrun, S., Montemerlo, M., Dahlkamp, H., Stavens, D., Aron, A., Diebel, J., Fong, P., Gale, J., Halpenny, M., Hoffmann, G., Lau, K., Oakley, C., Palatucci, M., Pratt, V., Stang, P., Strohband, S., Dupont, C., Jendrossek, L.-e., Koelen, C., Markey, C., Rummel, C., Niekerk, J. V., Jensen, E., Alessandrini, P., Bradski, G., Davies, B., Ettinger, S., Kaehler, A., Nefian, A., Mahoney, P., van Niekerk, J., Jensen, E., Alessandrini, P., Bradski, G., Davies, B., Ettinger, S., Kaehler, A., Nefian, A., and Mahoney, P., 2006. Stanley: The robot that won the DARPA Grand Challenge. *Journal of Field Robotics*, 23(9):661–692. doi: 10.1002/rob.20147.

Towner, M. C., Bland, P. A., Spurný, P., Benedix, G. K., Dyl, K., Greenwood, R. C., Gibson, J., Franchi, I. A., Shrbený, L., Bevan, A. W. R., and Vaughan, D., 2011. Mason Gully: The Second Meteorite Recovered by the Desert Fireball Network. In *74th Annual Meteoritical Society Meeting (2011)*, volume 74, pages 53124–53124.

Trigo-Rodríguez, J. M., Llorca, J., Lyytinen, E., Ortiz, J. L., Caso, A. S., Pineda, C., and Torrell, S., 2004. 2002 leonid storm fluxes and related orbital elements. *Icarus*, 171(1):219–228.

Trigo-Rodriguez, J. M., Lyytinen, E., Gritsevich, M., Moreno-Ibáñez, M., Bottke, W. F., Williams, I., Lupovka, V., Dmitriev, V., Kohout, T., and Grokhovsky, V., 2015. Orbit and dynamic origin of the recently recovered Annama's H5 chondrite. *Monthly Notices of the Royal Astronomical Society*, 449(2):2119–2127.

Whipple, F. L., 1952. Meteoritic phenomena and meteorites. *Physics and Medicine of the Upper Atmosphere*, 137:149–153.

CHAPTER 2

A NOVEL APPROACH TO FIREBALL MODELING: THE OBSERVABLE AND THE CALCULATED

Eleanor K. Sansom[a], Philip Bland[a], Jonathan Paxman [b], Martin C. Towner[a]

[a]Department of Applied Geology, Curtin University, GPO Box U1987, Bentley, Perth, WA 6845, Australia

[b]Department of Mechanical Engineering, Curtin University, GPO Box U1987, Bentley, Perth, WA 6845, Australia

This article is published in Meteoritics and Planetary Science, 2015, Vol 50, pp. 1423–1435, and reprinted with permission in Appendix A.

ABSTRACT

Estimating the mass of a meteoroid passing through the Earth's atmosphere is essential to determining potential meteorite fall positions. High-resolution fireball images from dedicated camera networks provide the position and timing for fireball bright flight trajectories. There are two established mass determination methods: the photometric and the dynamic. A new approach is proposed, based on the dynamic method. A dynamic optimization initially constrains unknown meteoroid characteristics which are then used in a parametric model for an extended Kalman filter. The extended Kalman filter estimates the position, velocity, and mass of the meteoroid body throughout its flight, and quantitatively models uncertainties. Uncertainties have not previously been modeled so explicitly and are essential for determining fall distributions for potential meteorites. This two-step method aims to automate the process of mass determination for application to any trajectory data set and has been applied to observations of the Bunburra Rockhole fireball. The new method naturally handles noisy raw data. Initial and terminal bright flight mass results are consistent with other works based on the established photometric method and cosmic ray analysis. A full analysis of fragmentation and the variability in the heat-transfer coefficient will be explored in future versions of the model.

INTRODUCTION

The full potential of meteorite analysis for providing valuable insights about protoplanetary disk formation cannot be reached without first constraining their origins in the Solar System. As with terrestrial rocks, without context (outcrop) information, our understanding of the record that meteorites contain will only ever be partial. The recording of fireball phenomena permits the reconstruction of orbits, as well as determines possible meteorite fall locations to enable the recovery of fresh meteorites whose unique geological record can be fully exploited. This objective has been the driver for a number of dedicated fireball camera network projects dating back to the late 1950s (Ceplecha, 1961) and has led to the recovery of multiple meteorites, including two by the Desert Fireball Network (DFN) in Australia during its trial phase (Towner et al., 2011; Spurný et al., 2012).

Over the next few months, the DFN will establish over 50 new Automated Desert Fireball Observatories (ADFOs), with all sky digital cameras, to expand its coverage to an area in excess of 2 million km 2 . This will make it the largest fireball network in history, and with > 100 TB of data being generated per year, automated systems of data analysis will be needed. The calculation of terminal bright flight mass will form part of the DFN's automated work-flow from fireball detection and triangulation through to dark flight and climate modeling for fall calculations.

Once the light of the fireball goes out, there is usually no way of tracking any remaining fragments to the ground. To model this dark flight, and determine any potential fall positions, the terminal bright flight mass must be ascertained. An automated method of analyzing the bright flight data to extract this information is required and previous methods were investigated for suitability. The two previous approaches to analyzing image data for mass determination are: the photometric method and the dynamic method.

The photometric method relates the luminosity of a fireball to the proportion of kinetic energy that is lost due to ablation, as a method for obtaining masses (Ceplecha et al., 1998). It uses the luminosity of the fireball to determine the incoming "photometric" mass, and a corresponding luminous efficiency parameter as a proxy for mass loss. To apply this method, a high- resolution light curve of a fireball needs to be acquired. This can be obtained by the addition of a photoelectric photometer to a fireball observatory (Spurný et al., 2012). Not only is this an expensive piece of equipment in itself but also requires additional power supplies, which are limited in the remote locations of the DFN observatories.

Although advancements have been made to the photometric method, including fragmentation as well as dynamical aspects (Ceplecha and Revelle, 2005), it ultimately still requires qualitative comparisons of trajectories with the light curve and manual inputs of fragmentation information (Ceplecha and Revelle, 2005). These qualitative judgments make this method manually intensive and remove the ability to create fully reproducible data.

The dynamic method uses equations of flight through the atmosphere to calculate mass from deceleration (Whipple, 1952). In the past, this approach was limited by the accuracy of measurements that could be interpreted from photographic plates (Ceplecha, 1961; McCrosky et al., 1971). Ceplecha et al. (1993) used dynamic equations to determine the change in velocity and mass of a meteoroid during its trajectory, along with timings of fragmentation events. However, the authors were unable to calculate initial masses and therefore relied on initial photometric masses. Considering mass loss is relative, this means the terminal mass is based on this photometric entry mass which may be unreliable (Brykina and Stulov, 2012).

Difficulties with the dynamic method are also due to the unknown characteristics of the meteoroid such as density and shape that are required for the dynamic calculation. Work by Stulov et al. (1995) has enabled the application of an analytical solution by combining these unknown parameters into two dimensionless constants. This has been applied by Gritsevich (2008a,b) to the Canadian MORP network data sets, as well as others that have led to meteorite recoveries. This provides good model fits to the data to which it was applied, but assumptions of these same meteoroid characteristics are required to quantify entry mass and subsequently terminal bright flight mass.

Given the limitations of established techniques and improvements to observation technologies, we chose to explore a new approach to the dynamic method. The use of an extended Kalman filter to incorporate the data into the model and provide error estimates was determined to be the most promising approach. An extended Kalman filter is a method of statistically optimizing estimates of an instantaneous state of nonlinear dynamic systems (Grewal and Andrews, 1993). An accompanying covariance matrix allows the uncertainties in the state estimations to be determined and propagated. The Kalman filter estimates the bright flight states (distance traveled, mass, and velocity) based on a two-step process of "predict" and "update." However, this method still requires values for meteoroid parameters to be estimated. To maximize confidence in chosen meteoroid parameters, rather than simply picking values, the Extended Kalman Filter is preceded by a dynamic optimization step. This stage is implemented to constrain the combinations of meteoroid characteristics that will permit a fit to the data. These parameters are then used to initialize a series of extended Kalman filters. To test the new method of mass determination, the data set of the Bunburra Rockhole meteorite fall is used as published by Spurný et al. (2012). This is the most complete fireball data set for which a meteorite has been recovered.

The objective of an automated method of mass determination requires an efficient method that will give sufficiently accurate results to determine a practical search area for likely meteorites. As this new approach is based entirely on the photographic data, this significantly reduces the cost of each ADFO unit as there is no requirement for a photoelectric photometer. The new approach to fireball modeling that we outline here will enable the terminal bright flight mass to be approximated from observable data in a fully automatable method, with uncertainties, to enable rapid recovery of meteorite samples which may provide invaluable data for cosmochemists (particularly when combined with orbital data).

MODELING

In the case of the DFN, ADFOs record high- resolution images throughout the night. Fireball observations made by multiple long-exposure cameras can be used to triangulate the position (latitude, longitude, and altitude) of the meteoroid during its flight. To acquire velocity information, however, requires some specialized modifications. Using a customized shutter within the camera lenses, the light path is interrupted at a known frequency (approximately 20 Hz in the ADFO systems). After calibration to remove the effects of lens distortion and triangulation, we have a series of position observations which underpins the subsequent modeling. Velocity may be calculated based on the change in these positions with time. The accuracy of the position observations determines the accuracy of the velocity values and can cause high scatter in values as seen in the Bunburra Rockhole data set.

All models explored in this work are based on the dynamic equations that characterize the change in mass and velocity of a meteoroid during bright flight through the atmosphere (Baldwin and Sheaffer, 1971):

$$\frac{dv}{dt} = -\frac{1}{2}\frac{c_d \rho_a v^2 S}{m} + g \sin \gamma_e \tag{2.1}$$

$$\frac{dm}{dt} = -\frac{1}{2}\frac{c_h \rho_a v^3 S}{H*} \tag{2.2}$$

where:

m— meteoroid mass (kg),

v— velocity ($\mathrm{m\,s^{-1}}$),

t— time (s),

c_d— drag coefficient,

ρ_a— atmospheric density ($kg\,m^{-3}$),

S— cross sectional area of the body (m^2),

g— local gravitational acceleration ($m\,s^{-2}$),

γ_e— entry angle of the meteoroid to the horizontal,

H^*— enthalpy of sublimation ($J\,kg^{-1}$) and

c_h heat-transfer coefficient.

The position or length along the path of the trajectory, l, is the primary observation extracted from the triangulated images. Its change with time is also included in all models and gives the velocity, i.e., $\frac{dl}{dt} = v$.

A NEW APPROACH

The new approach to determining the terminal masses of meteoroids discussed in this paper is a two- step approach, based on the dynamic Equations (2.1)-(2.2). The initial step is a dynamic optimization which runs a global search for the combination of meteoroid characteristics (model parameters) and unknown initial states (initial mass, m_0 and initial velocity, v_0) that provide a good fit to the observational data. The initial position, l_0 , is also an initial state but as the length along the flight path is relative, we can set it to be $0\,m$ (similar to Ceplecha and Revelle 2005). Errors associated with observational uncertainties in this postulation will be taken into account when the extended Kalman filter is initialized.

The second, main step, runs an extended Kalman filter which uses the unknown initial states and parameters from the dynamic optimization to estimate the states (position, l; mass, m; velocity, v) throughout the entire trajectory, including an explicit uncertainty model.

The cross sectional area, S, in the dynamic Equations (2.1)-(2.2), is dependent on the amount of mass lost due to ablation and may be defined as a function of the mass, meteoroid density, ρ_m, and shape parameter, A (a cross sectional area to volume ratio) (equation 3.5; Bronshten 1983).

$$S = A\left(\frac{m}{\rho_m}\right)^{2/3} \tag{2.3}$$

The change in cross sectional area can be written in terms of the shape change parameter, μ (Equation 2.4) (Bronshten, 1983).

$$S = S_0\left(\frac{m}{m_0}\right)^{\mu} \tag{2.4}$$

S_0 and m_0 are the initial cross sectional area and initial mass respectively. By writing Equation (2.3) in terms of initial parameters only we can combine it with Equation (2.4) to give

$$S = A_0\frac{m_0^{(2/3-\mu)}}{\rho_{m_0}^{2/3}}m^{\mu}. \tag{2.5}$$

Substituting Equation (2.5) into Equations (2.1)-(2.2) allows the dependent variable S to be removed from the dynamic equations. The modeling of meteoroid states during bright flight will therefore be based on the following differential equations

$$\frac{dv}{dt} = -\frac{1}{2}\frac{c_d\rho_a A_0}{\rho_{m_0}^{2/3}}m_0^{(2/3-\mu)}v^2 m^{(\mu-1)} + g\sin\gamma_e \tag{2.6}$$

$$\frac{dm}{dt} = -\frac{1}{2}\frac{c_h\rho_a A_0}{H^*\rho_{m_0}^{2/3}}m_0^{(2/3-\mu)}v^3 m^{\mu} \tag{2.7}$$

CONSTANTS USED IN ALL MODEL STAGES — Although the unknown parameters μ and $\frac{c_h}{H*}$ in Equations (2.6)-(2.7) are variable, they are approximated as constant for both the dynamic optimization and EKF models, along with the remaining unknown initial parameters, m_0 , v_0 , and $\frac{A_0}{\rho_{m_0}^{2/3}}$ (which will hereby be referred to as the shape-density parameter). This has been the typical assumption in previous works also (Bronshten, 1983; Gritsevich, 2008b).

The shape change parameter, μ, has a range from 0, being no rotation, to 2/3, indicating that rotation is rapid enough for uniform ablation to occur across the entire surface area. It is typically assumed that μ has a value of 2/3 (Bronshten, 1983) and as the dynamic equations are highly sensitive to the value of μ, this value is also used in our current model and will not be optimized further at this stage. Note that this removes m_0 as a coefficient from Equations (2.6)-(2.7), although m_0 is still present in the optimization as the initial value for mass.

ATMOSPHERIC PROPERTIES — The NRLMSISE-00 empirical atmosphere model was used to calculate values of atmospheric densities and pressures (Picone et al., 2002). This enables values for temperature, pressure, density, speed of sound, and dynamic viscosity of the atmosphere to be determined as accurately as possible.

DRAG COEFFICIENT — The drag coefficient, c_d, can be calculated throughout the trajectory based on a set of fluid dynamic parameters. ReVelle (1976) discusses the dependence of the Reynolds number and flow regime on the drag coefficient, but does not include a criterion for when the Mach regime is no longer hypersonic. This is unlikely to happen during fireball phenomena but is included here for completeness.

The Knudsen number (Kn) (Equation 2.8) can be used to determine the flow regime of the flight path and is the ratio of the mean free path length to the object length. Kn may be written as a function of the calculable Mach (Ma) and

Reynolds (Re) numbers (Hayes and Probstein, 1959; Truitt, 1959) and the ratio of specific heats γ, which for dry air at atmospheric temperatures is taken to be 1.40).

$$Kn = \frac{Ma}{Re} \times \sqrt{\frac{\gamma\pi}{2}} \tag{2.8}$$

Values of $Kn \geqslant 10$ indicate free molecular flow, $10 < Kn < 0.1$ a transitional flow regime, and $Kn \leqslant 0.1$ continuum flow (ReVelle, 1976). Within the continuum flow regime, the Mach regime defined by the Mach number needs to be taken into consideration. Only when below a Ma of 1.1 is Re used to directly calculate the drag coefficient. For values below the critical Re associated with drag reattachment (Re $\sim$ 2e5) (Schlichting and Gersten, 2000), Equation 11 from Haider and Levenspiel (1989) is used, although it is expected that bright flight values of c_d will remain in the hypersonic regime. Determining the values of c_d for different regimes and turbulence are outlined in Table 2.1.

For the Bunburra Rockhole data set, the meteoroid remains in the hypersonic regime for the duration of bright flight. In this version of the model, for simplicity, we will assume a hypersonic drag coefficient corresponding to that of a circular cylinder.

DYNAMIC OPTIMIZATION

The dynamic optimization based on Equations (2.6)-(2.7) aims to approximate values for $\frac{A_0}{\rho_{m_0}^{2/3}}$ and $\frac{c_h}{H*}$, as well as an entry mass, m_0, and velocity, v_0. This is performed by assigning assumed values to these parameters within given ranges and the constrained optimization then searches millions of combinations to determine the set of parameters that best fit the position data and return the lowest cost. The cost function used is the sum of the squared errors between the modeled and the observed position data. Costs are normalized to the

TABLE 2.1: Calculations used to determine the drag coefficient in various fluid dynamic regimes.

Flow Regime	Knudsen number range	Drag coefficient formulae		
Free molecular flow (f.m.f)	$Kn \geqslant 10$	$c_d = 2.0$		(ReVelle, 1976; Masson et al., 1960)
Transition flow (t.f.)	$0.1 < Kn < 10$	$c_d = c_d^{c.f} + \left(c_d^{f.m.f} - c_d^{c.f.}\right) e^{-0.001 Re^2}$		(Khanukaeva, 2005)
Continuum flow (c.f.)	$Kn \leqslant 0.1$	$Ma \to \infty$ Hypersonic to re-entry	$c_d = 0.92$ for spheres	(Bronshten, 1983; ReVelle, 1976)
			$c_d = 4/3$ for circular cylinders	(Truitt, 1959)
			$c_d = 2.0$ for tiles and bricks	(Zhdan et al., 2007)
		$Ma < 8$	$c_d = \frac{24}{Re}\left[1 + A\,Re^B\right] + \frac{C}{1+\frac{D}{Re}}$	where A, B, C, D are variables based on the sphericity of the object (see Haider and Levenspiel 1989)

TABLE 2.2: Parameter constrains applied during dynamic optimisation.

	Min	Max
m_0	1 kg	1000 kg
v_0	first velocity value $-3000\,\mathrm{m\,s^{-1}}$	first velocity value $+3000\,\mathrm{m\,s^{-1}}$
$\frac{A_0}{\rho_{m_0}^{2/3}}$	$\frac{0.5}{(3500\,\mathrm{kg\,m^{-3}})^{2/3}}$	$\frac{3.5}{(1500\,\mathrm{kg\,m^{-3}})^{2/3}}$
$\frac{c_h}{H*}$	$2.5 \times 10^{-7}\,\mathrm{kg\,J^{-1}}$	$5.0 \times 10^{-11}\,\mathrm{kg\,J^{-1}}$

lowest value, showing 1.0 to be the best fit, to allow comparisons between different parameter sets. As there are multiple unknown parameters, there is a large degree of freedom in the number of plausible combinations. The models that produce cost values > 0.98 (best 2%) are selected for consideration in the following stage of the mass determination method.

The parameter constraints used are shown in Table 2.2. Ranges for $\rho_{m_0}^{2/3}$ are given as assumed preatmospheric meteorite density ranges for typical meteorites. $A_{sphere} = 1.21$ although it is expected that A values should typically be in the range of 2 - 4 (Zhdan et al., 2007). The shape parameter may also be less than that of a sphere depending on which axis is oriented in the direction of the trajectory. The lower and upper bounds for A_0 are chosen as realistic ranges. $\frac{c_h}{H*}$ is given a wide range so that the average value of this variable throughout bright flight is determined.

EXTENDED KALMAN FILTER

An extended Kalman filter (EKF) is a method of statistically optimizing estimates of state variables for nonlinear dynamic systems (Grewal and Andrews, 1993). For bolide bright flight path analysis, the state vector, $\mathbf{x}_k$, is the instantaneous representation of the state at a time k, and is written in terms of the variables' distance along the bright flight path (l), mass (m), and velocity (v)

(Equation 2.9).

$$\mathbf{x}_k = \begin{pmatrix} x_1 \\ x_2 \\ x_3 \end{pmatrix}_k = \begin{pmatrix} l_k \\ m_k \\ v_k \end{pmatrix} \tag{2.9}$$

The state vector at t 0 is initialized as

$$\mathbf{x}_k = \begin{pmatrix} 0 \\ m_0 \\ v_0 \end{pmatrix} \tag{2.10}$$

$\mathbf{x}_k$ can be determined using the nonlinear state equations:

$$\mathbf{x}_k = f(x_{k-1}, k-1) + \mathbf{u}_k \tag{2.11}$$

where $\mathbf{u}_k$ is the process noise with an assumed mean of zero and covariance $\mathbf{Q}_k$ (Equation 2.12).

$$\mathbf{Q}_k = E[\mathbf{u}_k \mathbf{u}_k'] = \begin{bmatrix} \sigma^2_{l_{prc_noise}} & 0 & 0 \\ 0 & \sigma^2_{m_{prc_noise}} & 0 \\ 0 & 0 & \sigma^2_{v_{prc_noise}} \end{bmatrix} \tag{2.12}$$

An extended Kalman filter is an iterative process that involves two repeated processes. The prediction step for the fireball application will use the dynamic Equations (2.6)–(2.7) along with parameters defined by the previous dynamic optimization to estimate a future state based on all preceding observations. The measurement update step accepts a new observation of the state, in this case the distance along the bright flight path only, and calibrates the predicted outcome using an optimal Kalman gain. This process is schematically illustrated in Fig. 2.1.

PREDICTING FUTURE STATES — The prediction step uses all previous data to derive a suitable state estimate, $\hat{\mathbf{x}}_k$:

$$\hat{\mathbf{x}}_{k|k-1} = f(\hat{\mathbf{x}}_{k-1|k-1}, k) \tag{2.13}$$

$$\mathbf{P}_{k|k-1} = \mathbf{F}_k \mathbf{P}_{k-1} \mathbf{F}_k^T + \mathbf{Q}_k \tag{2.14}$$

$\mathbf{F}_k$ is the state transition matrix (Equation 2.15). $\mathbf{P}_k$ is the covariance matrix for the state estimate and is a primary motivation for using an EKF. The diagonal elements can be read to give an indication of the variance for distance, mass, and velocity.

$$\mathbf{F}_k = \left. \begin{bmatrix} \frac{\delta f_1}{\delta l} & \frac{\delta f_1}{\delta m} & \frac{\delta f_1}{\delta v} \\ \frac{\delta f_2}{\delta l} & \frac{\delta f_2}{\delta m} & \frac{\delta f_2}{\delta v} \\ \frac{\delta f_3}{\delta l} & \frac{\delta f_3}{\delta m} & \frac{\delta f_2}{\delta v} \end{bmatrix} \right|_{x=x_k} \tag{2.15}$$

where:

$$\begin{aligned} l_{k+1} = &f_1(l_k, m_k, v_k, t_k) = & l_k + \frac{dl_k}{dt_k}\Delta t = &l_k + v_k \Delta t & (2.16) \\ m_{k+1} = &f_2(l_k, m_k, v_k, t_k) = & m_k + \frac{dm_k}{dt_k}\Delta t = &m_k - (k_m v_k^2 m_k^{(\mu-1)})\Delta t & (2.17) \\ v_{k+1} = &f_3(l_k, m_k, v_k, t_k) = & v_k + \frac{dv_k}{dt_k}\Delta t = &v_k - (k_v v_k^2 m_k^{(\mu-1)} - g \sin\gamma_e)\Delta t & \\ & & & & (2.18) \end{aligned}$$

and

$$\begin{aligned} k_v = &\frac{1}{2} \frac{c_d \rho_a A_0}{\rho_{m_0}^{2/3}} m_0^{(2/3-\mu)} \\ k_m = &\frac{1}{2} \frac{c_h \rho_a A_0}{H^* \rho_{m_0}^{2/3}} m_0^{(2/3-\mu)} \end{aligned} \tag{2.19}$$

MEASUREMENT UPDATES — The measurement update step follows an observation z_k (Equation 2.20), which for ADFO observations is only the distance data $l_k = (x_1)_k$. $\mathbf{H}_k$ provides a relationship between the state of the dynamic system and the measureable observations, simply put, $\mathbf{H}_k\mathbf{x}_k = l_k$. $\mathbf{w}_k$ is the measurement noise with a mean of zero and covariance $\mathbf{R}_k$ (Equation 2.21). $\mathbf{R}_k$, therefore, accounts for errors between measured position and true position due to aspects such as camera calibration, triangulation, camera resolution etc.

$$z_k = \mathbf{H}_k\mathbf{x}_k + \mathbf{w}_k \tag{2.20}$$

$$\mathbf{R}_k = E[\mathbf{w}_k\mathbf{w}_k'] = [\sigma^2_{z_k}] \tag{2.21}$$

The predicted measurement can be made using the output of Equation (2.13)

$$\hat{z}_k = \mathbf{H}_k\hat{\mathbf{x}}_{k|k-1}. \tag{2.22}$$

The residual difference between z_k and $\hat{z}_k$ is y_k (Equation 2.23). $\mathbf{S}_k$ (Equation 2.24) projects the system uncertainty into the measurement space and includes uncertainties in the model up to t_{k-1}, as well as the noise covariance of the current measurement. The optimum Kalman gain, $\mathbf{K}_k$ (Equation 2.25) is used to update the state ($\hat{\mathbf{x}}_k$) and covariance matrices ($\mathbf{P}_k$) (Equations (2.26)–(2.27))

$$y_k = z_k - \hat{z}_k \tag{2.23}$$

$$\mathbf{S}_k = \mathbf{H}_k\mathbf{P}_{k|k-1}\mathbf{H}_k^T + \mathbf{R}_k \tag{2.24}$$

$$\mathbf{K}_k = \mathbf{P}_{k|k-1}\mathbf{H}_k^T\mathbf{S}_k^{-1} \tag{2.25}$$

$$\hat{\mathbf{x}}_k = \hat{\mathbf{x}}_{k|k-1} + \mathbf{K}_k y_k \tag{2.26}$$

$$\mathbf{P}_k = (\mathbf{I} - \mathbf{K}_k\mathbf{H}_k)\mathbf{P}_{k|k-1} \tag{2.27}$$

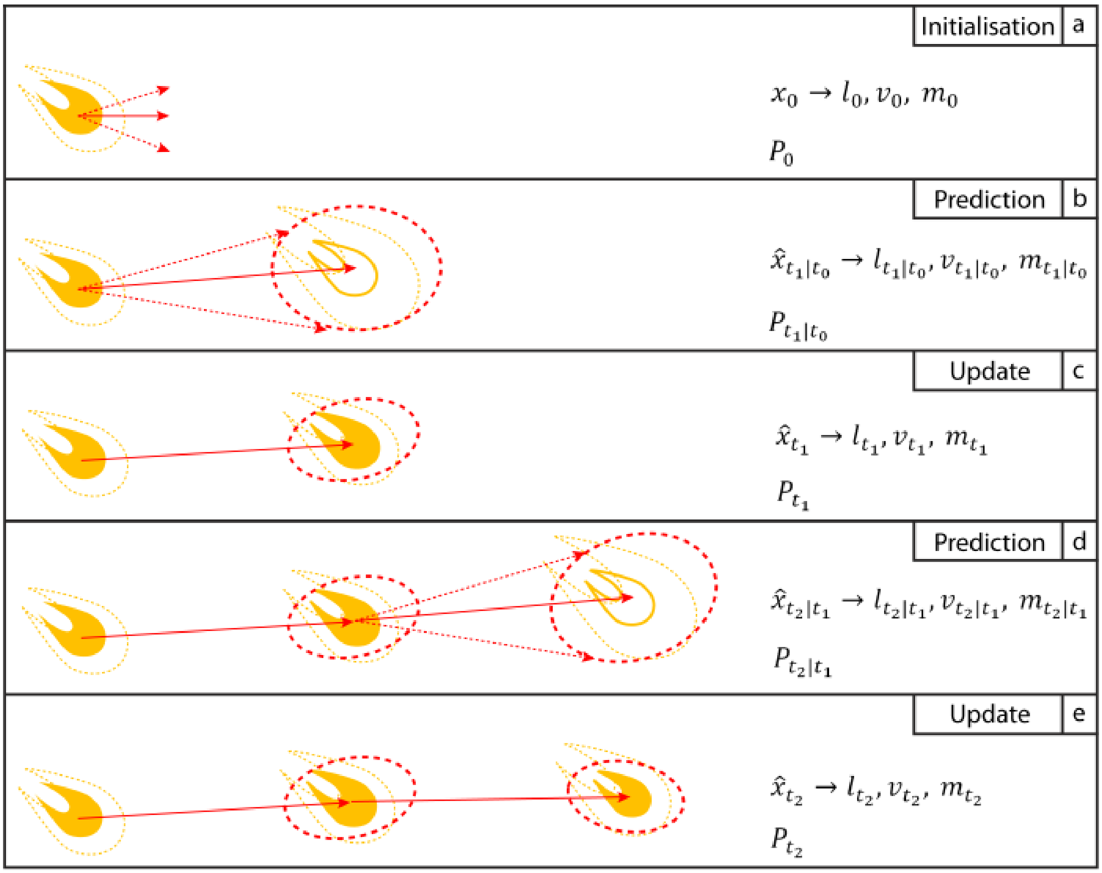

FIGURE 2.1: Illustration of the extended Kalman filter process. (a) initialisation of state. The $\mathbf{P}_0$ matrix defines the initial uncertainties (dashed) in velocity (red arrow) and mass (yellow). (b) a prediction is made and the state matrix, $\hat{\mathbf{x}}_{k|k-1}$, has covariances defined by $\mathbf{P}_{k|k-1}$. Mass uncertainties are initially large, as is position (dashed red). (c) measurement update calibrates the state and uncertainties decrease. (d) prediction step. (e) measurement step. These two processes (d) – (e) repeat to give a final state estimate ($\hat{\mathbf{x}}_f$) and associated covariance matrix($\mathbf{P}_f$).

The square root of the diagonal elements of $\mathbf{P}_k$ is plotted as error bars so that the evolution of state uncertainty with time can be visualized in a meaningful way.

FIREBALL APPLICATIONS — For the nonlinear bolide dynamical equations, $\hat{\mathbf{x}}_{k+1|k}$ is calculated by solving the nonlinear Equations (2.6)–(2.7) between t_{k+1} and t_k. $\mathbf{P}_k$, however, is solved using the linearized state transition matrix, $\mathbf{F}_k$ (Equation 2.28). The linearization of $\mathbf{F}_k$ approximates to:

$$\mathbf{F}_k = \begin{pmatrix} 1 & 0 & \Delta t \\ 0 & 1 - k_m v_0^3 m_0^{\mu} \left(\frac{\mu}{m_0}\right) \Delta t & -k_m v_0^3 m_0^{\mu} \left(\frac{3}{v_0}\right) \Delta t \\ 0 & -k_v v_0^2 m_0^{(\mu-1)} \left(\frac{\mu-1}{m_0}\right) \Delta t & 1 - k_v v_0^2 m_0^{(\mu-1)} \left(\frac{2}{v_0}\right) \Delta t \end{pmatrix} \tag{2.28}$$

The errors associated with this linearization are included in the process covariance matrix, $\mathbf{Q}_k$, along with the uncertainties in the model due to unmodeled factors such atmospheric disturbances and uncertainties in the atmospheric model used. The value of $\mathbf{Q}_k$ encapsulates these model uncertainties and is specific to the individual data set being analyzed.

$\mathbf{P}_0$ is initialized at t_0 as a function of initial data uncertainty (Equation 2.29). As the length along the flight path is relative to the initial point, there is no model error in σ_{l_0} being zero (error in *observation* of positions is accounted for in $\mathbf{R}_k$). The initial mass covariance is given as 0.5 times the initial mass determined by the dynamical optimization. Distance error and timing information give uncertainties of up to $\pm 1500\,\mathrm{m\,s^{-1}}$ for velocity.

$$\mathbf{P}_0 = \begin{bmatrix} \sigma_{l_0}^2 & 0 & 0 \\ 0 & \sigma_{m_0}^2 & 0 \\ 0 & 0 & \sigma_{v_0}^2 \end{bmatrix} = \begin{bmatrix} 0 & 0 & 0 \\ 0 & (m_0 \times 0.5\,\mathrm{kg})^2 & 0 \\ 0 & 0 & (1500\,\mathrm{km\,s^{-1}})^2 \end{bmatrix} \tag{2.29}$$

The initial errors are large but $\mathbf{P}_k$ is updated throughout the iterative estimation, giving a concrete representation of the evolution of the confidence of the state estimate, incorporating the uncertainties defined by the process noise covariance, $\mathbf{Q}_k$ (Equation 2.12), and the measurement noise covariance, $\mathbf{R}_k$ (Equation 2.21). The measurement noise covariance for the bolide problem is set to be $(100\,\mathrm{m})^2$ and is dependent on camera resolution, the angle of the fireball with respect to the camera, and calibration of lens distortion.

SMOOTHING PROBLEM — More generally, we can apply a smoothing estimator to our fireball data sets, as we will always have the observations from the entire trajectory available when the estimation is performed. A *filtering* estimator, such as described above, uses only past data (and hence is suitable for real-time estimation), whereas a *smoothing* estimator uses all data (future and past) to generate an optimal state estimate. The Rauch–Tung–Striebel (RTS) smoothing algorithm is implemented using the method described by Särkkä (2008). The resulting state estimate values for the trajectory are improved, along with their uncertainties.

RESULTS

The most complete data set available to test this method is that of Bunburra Rockhole, published by Spurný et al. (2012), which contains 113 data points with time, length of segment, and altitude information. As this data resulted in a recovered meteorite, constraints are available on final mass (Spurný et al., 2012), and cosmic ray exposure rates (Welten et al., 2012) provide an estimate of initial body diameter.

DYNAMIC OPTIMISATION

The dynamic optimization method described earlier, is applied to the data set using the constraints on parameters given in Table 2.2. Five parameter sets produce a fit with cost values > 0.98 (Table 2.3). The initial masses range from 27.65 to $30.12\,\mathrm{kg}$ (Fig. 2.2) but the final masses converge to values of $\sim 2.4\,\mathrm{kg}$.

Figure 2.2 allows a visual comparison of these model outputs to the raw data. The parameter sets defined in Table 2.3 are used to initialize a set of Kalman filters that will take the data itself into consideration to determine a final mass.

TABLE 2.3: Top five best fit parameter sets resulting from dynamical optimisation.

Normalised sum of square differences to position	m_0 (kg)	v_0 ($\mathrm{m\,s^{-1}}$)	$\frac{A_0}{\rho {m_0}^{2/3}}$ ($\mathrm{(kg\,m^{-3})^{-2/3}}$)	$\frac{c_h}{H^*}$ ($\times 10^{-8}\,\mathrm{J kg^{-1}}$)	l_f (m)	m_f (kg)	v_f ($\mathrm{m\,s^{-1}}$)
1.00000	30.12	13198	0.009511	4.82	60071.8	2.36	6109
0.99859	30.95	13203	0.009689	4.76	60042.4	2.50	6100
0.98862	29.82	13203	0.009545	4.68	60061.8	2.51	6124
0.98544	28.64	13204	0.009466	4.66	60057.6	2.44	6125
0.98108	27.65	13205	0.009394	4.64	60052.7	2.38	6126

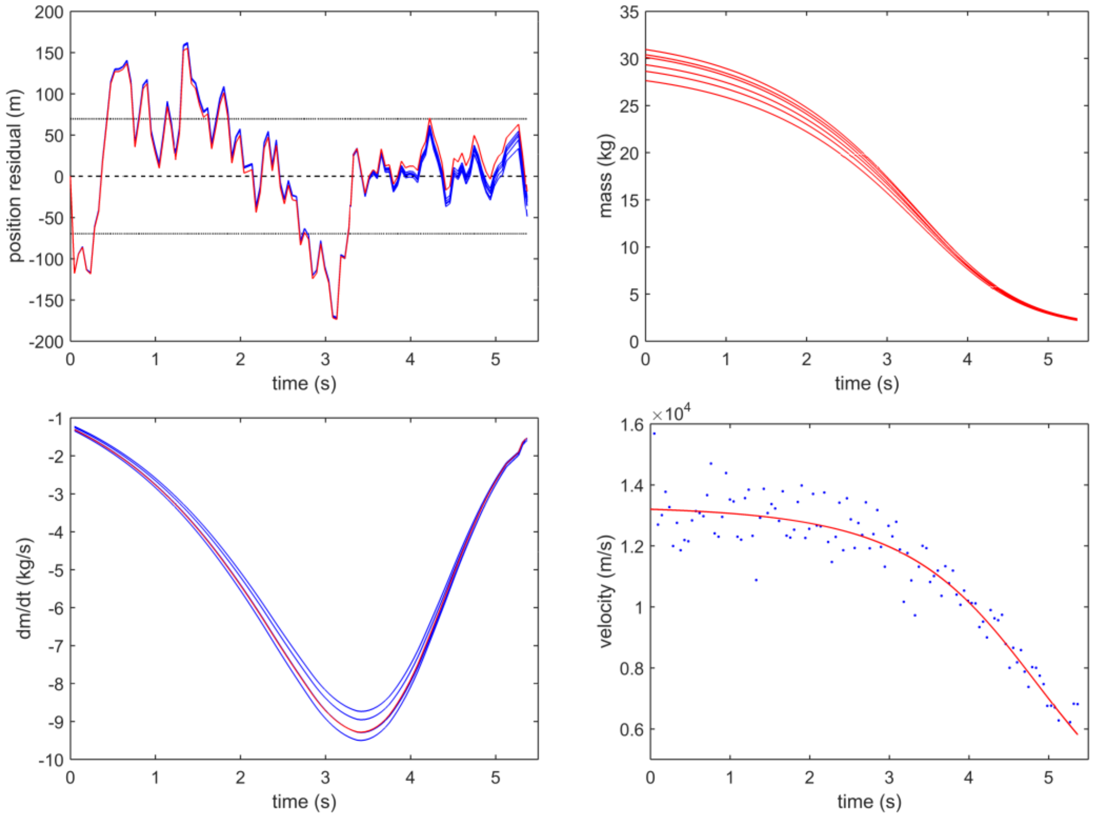

FIGURE 2.2: Top left: position data subtracted from modelled position for models with parameters given in Table 2.3. Red curve is model that gives the lowest normalised sum of square differences (initial mass of 30.12 kg). Dotted line is one standard deviation (70.14 m). Top right: shows associated change in mass for corresponding model parameters with costs > 0.98. Bottom left: derivative of mass with time for models. Bottom right: comparison of models (red curves) to calculated velocity (blue points).

KALMAN FILTER

The Extended Kalman Filter runs separately on each set of parameters resulting from the dynamical optimization stage. The final states of each model setup are given in Table 2.4.

TABLE 2.4: Final states (x_f , m_f , v_f) for parameter sets from dynamic optimisation corresponding to the following initial masses.

m_0 (kg)	x_f (m)	m_f (kg)	v_f ($\mathrm{m\,s^{-1}}$)
30.12	60032 ± 62	2.30 ± 1.63	6052 ± 241
30.95	60032 ± 62	2.47 ± 1.67	6057 ± 236
29.82	60033 ± 62	2.40 ± 1.67	6061 ± 238
28.64	60033 ± 62	2.35 ± 1.66	6062 ± 240
27.65	60033 ± 62	2.29 ± 1.64	6062 ± 242

The change in state values during the iterative EKF process are graphed against time with covariance plotted as approximate error bars (Fig. 2.3). The uncertainties are high initially. Mass uncertainties are only constrained by the data through the link to velocity with the dynamic equations and therefore remain high while the iterative process determines a value.

After running the forward EKF, the Rauch–Tung– Striebel smoothing algorithm is run (Fig. 2.4). The outcome of smoothing produces an initial entry mass of 30.20 ± 6.53 kg.

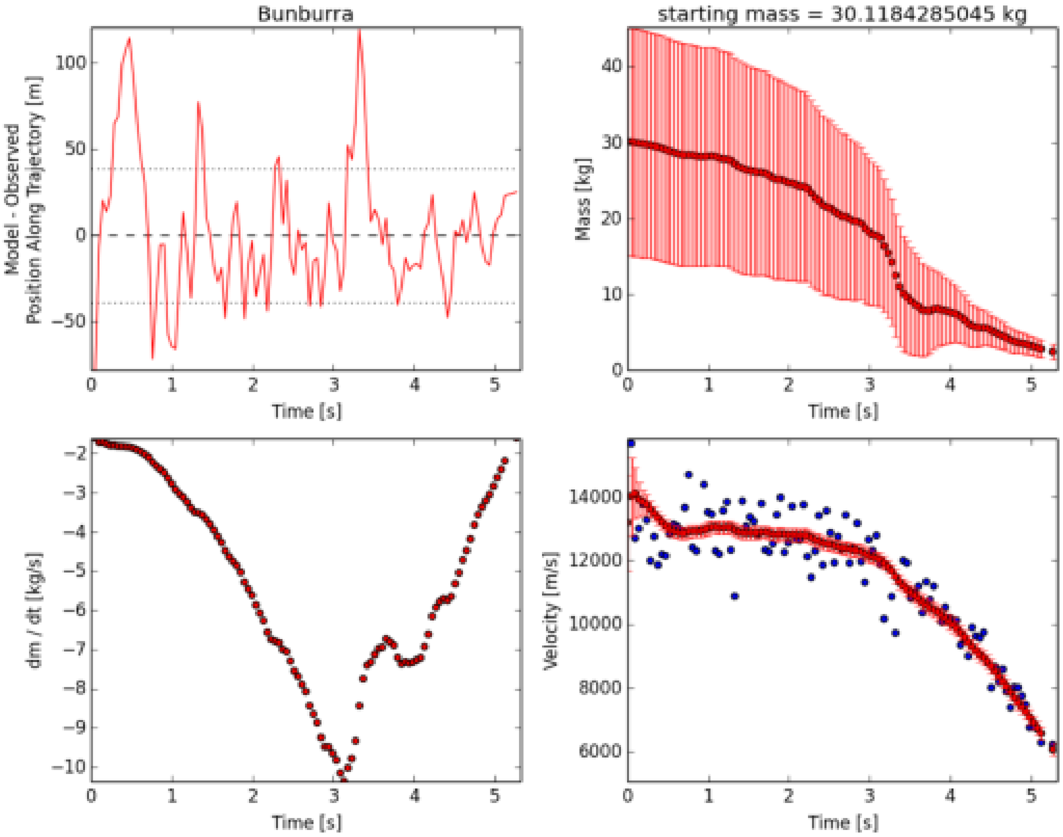

FIGURE 2.3: Extended Kalman Filter results for initial mass of 30.12 kg. Top left: residual plot of position data subtracted from EKF position estimate. Dotted lines represent one standard deviation (38.83 m). Top right: mass error bars are extracted from the constantly updating P matrix. Bottom left: derivative of mass with time, showing relative mass loss predicted for each time step. Bottom right: blue points represent calculated velocity values. Red points are EKF estimates of velocity given only past data from each time step. Although mass and velocity will never realistically increase, as the EKF is provided with new data at each time step, it corrects the values of previous estimates.

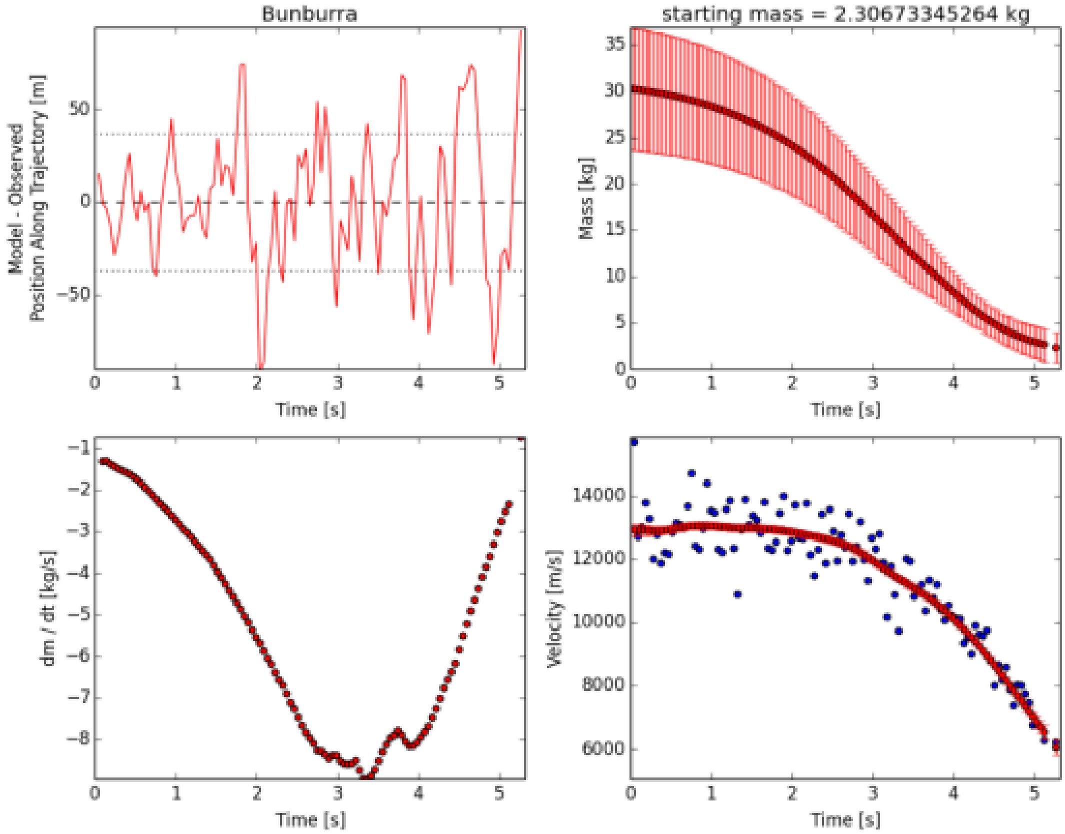

FIGURE 2.4: RTS smoothing filter results for the best fit parameter set. Top left: residual plot of position data subtracted from RTS position estimate. Dotted lines represent one standard deviation (36.73 m). Top right: predicted mass along trajectory. Bottom left: derivative of mass with time, showing relative mass loss predicted for each time step. Bottom right: blue points represent calculated velocity values. Red points are RTS estimates of velocity given both past and future state estimates.

CHECKING RESULTS USING THE DIMENSIONLESS COEFFICIENT METHOD

As a comparison, we also analyzed the Bunburra Rockhole data set using the approach based on Stulov et al. (1995) and applied by Gritsevich (2008b). In this method, the dynamic Equations 2.1–2.2 are modified by normalizing the values of mass, velocity, and altitude (h) to the entry mass, entry velocity, and the scale height of the homogeneous atmosphere ($h_0 = 7160\,m$), respectively. A set of dimensionless parameters (ballistic coefficient, α (2.30), and mass loss parameter, β (2.31)) are substituted to remove the need of unknown individual variables.

$$\alpha = \frac{c_d \rho_0 h_0 A_0 m_0^{-1/3}}{2\rho_{m_0}^{2/3} \sin\gamma} \tag{2.30}$$

$$\beta = (1-\mu)\frac{c_h v_0^2}{2c_d H^*} \tag{2.31}$$

where ρ_0 is the atmospheric density near the surface and γ is the trajectory entry angle.

The Q_4 method of least-squares minimization defined by Gritsevich (2008b) is used to create a fit of the Kulakov and Stulov (1992) Equation (2.32) to the Bunburra Rockhole data set.

$$y = \ln\alpha - \ln(-\ln V) + 0.83\beta(1-V) \tag{2.32}$$

where $y = \frac{h}{h_0}$ and $V = \frac{v}{v_0}$.

The isothermal atmosphere approximation is used to derive Equation (2.32): $\rho_a = e^{-y}$, making it difficult to implement a more accurate atmosphere model.

Although this method has proved successful on previous fireball data sets (Gritsevich, 2008a), these are limited to fewer than 20 velocity points with an average based smoothing applied (Ceplecha, 1961). The value of v_0 that is used to normalize all velocity values is simply the initial velocity. For the Bunburra Rockhole data set, the 113 data points show high scatter and the velocity range within the first half a second has a range of over $3500\,\mathrm{m\,s^{-1}}$. It was found that the noise in the raw data could not be accommodated by this method without pretreating the data, making it rather unsuitable for use in an automated data pipeline where large noisy data sets need to be processed.

Smoothing the data using a five-point moving average, and using the average initial velocity from Table 2.3, $13,200\,\mathrm{m\,s^{-1}}$, and a value of 2/3 for the shape change parameter allows a result to be calculated as a comparison to the new method. This gives $\alpha = 25.23$ and $\beta = 1.53$ (Fig. 2.5). The equation for the ballistic coefficient (Equation 2.30) allows an initial mass to be calculated. By assuming values of the shape-density parameter from the dynamic optimization, and a constant drag coefficient of 1.3, an approximate value for m_0 is determined to be $84.92\,\mathrm{kg}$. When used in the following Equation (2.33), along with a value of 2/3 for rotation, a final mass of $1.90\,\mathrm{kg}$ results.

$$m_f = m_0 e^{\left(-\beta \frac{1-V_f^2}{1-\mu}\right)} \quad \text{(equation 6 [Gritsevich 2008b])} \tag{2.33}$$

It is difficult to assess the error in this case, and the ranges in initial and final masses are harder to obtain. The amount of scatter in the velocity data is significant and a change in initial velocity used by 1% can result in initial masses varying by $\pm 30\,\mathrm{kg}$ and final masses to be $\pm 2\,\mathrm{kg}$.

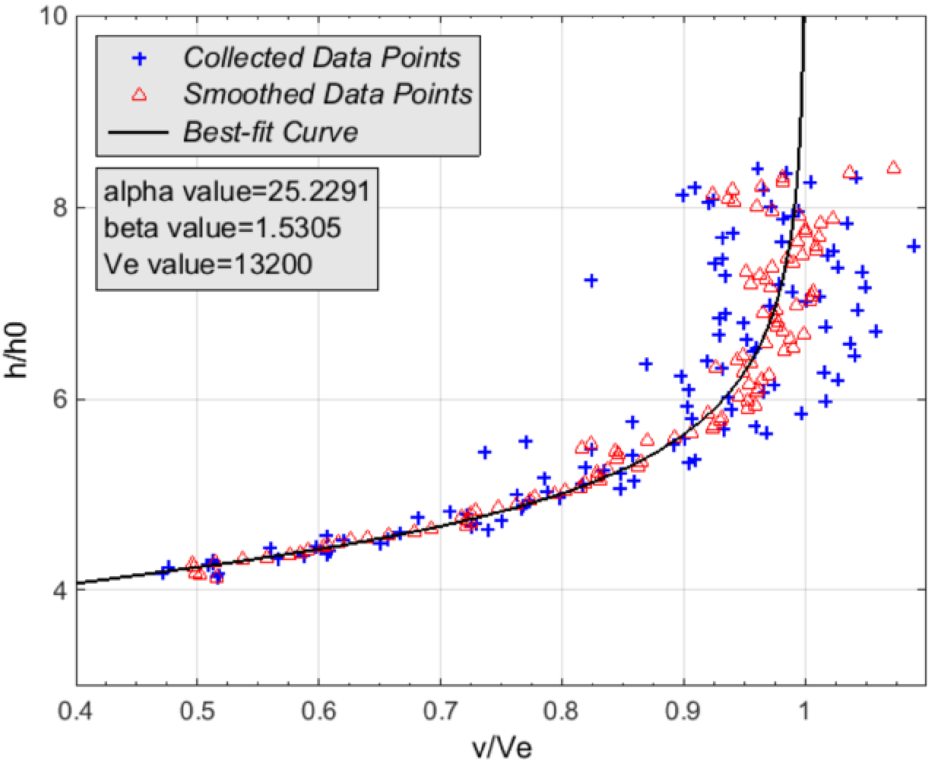

FIGURE 2.5: Raw (+) and smoothed (Δ) Bunburra Rockhole velocities normalised to an entry velocity of 13200 m s^{-1} vs. normalised altitude, y. Best fit for Equation (2.32) is shown which is produced using $\alpha = 25.23$ and $\beta = 1.53$.

DISCUSSION

DETERMINING MODEL PARAMETERS

The dynamical optimization of the Bunburra Rockhole data set returned a large number of parameter sets with cost values > 0.9, although only five with > 0.98, all of which show relatively similar starting masses. The ranged (27.65 - 31.12 kg) initial masses converge (Fig. 2.2) to give very similar final mass values (Table 2.3). As the final masses are needed for determining any potential fall positions, it is more important that these values be limited. It should be remembered that the dynamic optimization is estimating appropriate meteoroid parameters to use as inputs in our main model (EKF step) based on this specific fireball data set. Previous works have assumed "typical," or average meteoroid parameter values, without the link to the data from the event in question (e.g., densities by Borovička et al. (1998, 2013) and McCrosky et al. (1971); shape density coefficient used by Ceplecha and Revelle (2005) and Spurný et al. (2012)). We believe that this is an advantage of our approach. This step gives us greater confidence in the estimates to be used in the EKF step, especially considering the similarities in meteoroid characteristics of the top results (Table 2.3).

The shape parameter and preatmospheric meteoroid density cannot be uniquely identified in this model. The values of $\frac{A_0}{\rho_{m_0}^{2/3}}$ in Table 2.3 could correspond to a spherical object ($A_0 = 1.21$) with a preatmospheric meteoroid density of $\sim 1400\,\mathrm{kg\,m^{-3}}$, a circular cylinder with a cross sectional diameter to length ratio of roughly 1:1 and $\rho_{m_0} \sim 2700\,\mathrm{kg\,m^{-3}}$, or even a 3:2:1 triaxial ellipsoid (as suggested by Zhdan et al. (2007) with $\rho_{m_0} \sim 3500\,\mathrm{kg\,m^{-3}}$. A unique solution is not needed for finding any potential meteorites and any fragments found will be able to resolve these two parameters.

Knowing the Bunburra Rockhole bulk meteorite density to be $2700\,\mathrm{kg\,m^{-3}}$ (Spurný et al., 2012) enables us to approximate the meteoroid shape, $A \sim 1.85$. This corresponds to a circular cylinder with a cross sectional diameter to length ratio of roughly 1:1, or a 3:2:1.5 axial ellipsoid. If the value of A and ρ_m were to remain constant, these values of A_0 and ρ_{m_0} with the given initial mass corresponds approximately to a cross sectional area of $0.092\,\mathrm{m^2}$. Figure 7.2 in Stulov et al. (1995) shows a distribution of values of H^* for bolides, resulting in an overwhelming majority with entry masses $> 1\,\mathrm{kg}$, having values close to $2 \times 10^6\,\mathrm{J\,kg^{-1}}$. If this value is assumed for H^*, values for c_h can be approximated (Table 2.5). It may be useful as a comparison to give also the ablation coefficient, $\sigma = \frac{c_h}{c_d H^*}$ (Table 2.5), given a drag coefficient of 1.3. σ values are very similar to the apparent ablation coefficient values determined by Spurný et al. (2012). This is to be expected as fragmentation is currently not incorporated to allow intrinsic values of σ to be determined by the dynamic optimization.

TABLE 2.5: Values of $\frac{c_h}{H^*}$ determined by the dynamical optimization stage (Table 2.3) and the subsequent approximate values of c_h. σ values are given for a drag coefficient of 1.3.

$\frac{c_h}{H^*}$ $(\times 10^{-8}\,\mathrm{J\,kg^{-1}})$	c_h given $H^* = 2 \times 10^6\,\mathrm{J\,kg^{-1}}$	σ $(\times 10^{-6}\,\mathrm{s^2\,m^{-2}})$
4.820	0.0964	0.0371
4.755	0.0951	0.0366
4.684	0.0937	0.0360
4.662	0.0932	0.0359
4.644	0.0929	0.0357

THE MODEL SOLUTION

The initial 3 s of the Bunburra Rockhole velocity data is rather noisy, varying by around $\pm 2000\,\mathrm{m\,s^{-1}}$. However, it is handled coherently by our EKF approach without the inclusion of an arbitrary smoothing step. The EKF optimizes the state of the bolide at each individual time-step. Each point on the graphs of Fig. 2.3 are the instantaneous representation of the state at a given time given only the past data. The values are variable within their error ranges as the data are not perfect. It is not a simple least squares, it does not aim to reduce the covariance, rather it “learns” from the data and predicts where it should be and carries the errors forward. The covariance incorporates both measurement uncertainty and scatter to give a comprehensive understanding of the errors associated with each state. Where previous works have used best fit modeling, primarily least squares fits (Ceplecha and Revelle, 2005), by taking this intelligent “predict” and “update” approach, the EKF method is likely to come closer to approximating the real position of the object at any given time. This is reflected in the lower standard deviation of the residual plots (38.83 m for EKF versus 70.14 m for dynamical optimization).

Despite the variation in parameter sets provided by the dynamical optimization, the final masses which are most important for finding any potential fall positions (and therefore the primary solution of this modeling), are very similar and their range constrains the final bright flight mass. The best estimate of final mass is $2.30 \pm 1.63\,\mathrm{kg}$ and is close to the published value of $1.1\,\mathrm{kg}$ by Spurný et al. (2012).

The initial mass determined by Spurný et al. (2012) using both the methods described by both Ceplecha et al. (1998) and Ceplecha and Revelle (2005) is $22.0 \pm 1.3\,\mathrm{kg}$. Cosmic ray exposure rates were analyzed for the Bunburra Rockhole meteorite; however, the pre- entry radius was determined to be larger than a radius corresponding to a mass of $22\,\mathrm{kg}$ (Welten et al., 2012). By performing a reverse extended Kalman filter, the entry mass is determined to be closer to $30.20 \pm 6.53\,\mathrm{kg}$. This corresponds to a pre-entry radius of around $17.1\,\mathrm{cm}$. This is close to the 13 - 17 cm range determined by Welten et al. (2012).

Although fragmentation is not yet explicitly handled using this method, the data reflects both effects of ablation and fragmentation. The process noise $\mathbf{Q}_k$ in the EKF model handles some degree of unexpected mass change, allowing these variations to be incorporated in the final mass estimates.

Furthermore, sudden increases in the magnitude of the state variance matrix $\mathbf{P}_k$ can give an indication that a fragmentation event may have occurred, along with examining the change in mass with time (Figs. 2.3 and 2.4). It is noticeable from both Figs. 2.3 and 2.4 that there are peaks of maximum mass loss at around 3.133 and 3.845 s as well as at 4.415 s in Fig. 2.3. It is likely that these correspond to fragmentation events. These times correspond to altitudes of 41.31, 37.16, and $34.18\,\mathrm{km}$, respectively, allowing a comparison to fig. 13 in Spurný et al. (2012) which shows significant changes of mass at 37.8 and $35.85\,\mathrm{km}$ altitude. The significant mass loss event seen in fig. 13 in Spurný et al. (2012) at $54.9\,\mathrm{km}$ (corresponding to 1.0 s) is not evident, although it is well within the large error bracket given at this time. Future work will aim to capture this fragmentation information in a coherent and consistent way.

The scatter in the Bunburra Rockhole data set presented difficulties when initially attempting to use the method outlined by Gritsevich (2008a). After smoothing the data and using the initial parameters determined by the dynamic optimization, final values are similar to those determined using this new method. The dependence on an initial velocity for normalization makes it very sensitive to initial scatter and there is no constraint on the errors this or the smoothing may cause. The EKF method avoids these dependences.

CONCLUSION

The method outlined here provides a consistent and detailed approach to characterizing meteoroids without the need for brightness data as they pass through the atmosphere. In addition, it provides a rigorous way of propagating uncertainties in trajectory states (position, mass, and velocity), something that previous approaches have not explicitly described. A dynamic optimization determines the optimum parameters for the meteoroid flight such as the shape-density parameter and initial mass. An extended Kalman filter then includes observation and dynamic uncertainty models, which are valuable in understanding the errors in the model states, and which can adapt to fragmentation events or other unexpected dynamic changes. The initial (30.20 ± 6.53 kg) and final masses (2.30 ± 1.63 kg) calculated for the Bunburra Rockhole data set is within the range of previously published values by Spurný et al. (2012) (22.0 ± 1.3 and 1.1 kg, respectively) and corresponds with cosmic ray exposure studies (Welten et al., 2012) to constrain preatmospheric radius and mass. Although the method used by Gritsevich (2008b) was re-created using the meteoroid characteristics determined by dynamic optimization, the sensitivity of this method to (widely varying) data for initial entry velocity translates to a range of estimates for entry and terminal masses. As the errors are not quantified, the confidence in mass calculations using this method—crucial for automating our data flow and constraining search areas—cannot be constrained. The two-step approach outlined in this paper is an automated method which will allow the DFN to reduce data for every observed fireball, rather than only selecting high value or unusual cases. For the subset that involve a meteorite fall, this approach will calculate multiple fall positions with comprehensive error values to allow for efficient recovery searches. Work still needs to be carried out on integrating the variability in the heat-transfer coefficient. The assumption in this method that it remains constant throughout the trajectory is a simplification. The identification and analysis of fragmentation events also needs to be incorporated in a more coherent and consistent manner.

ACKNOWLEDGMENTS

This work was funded by the Australian Research Council as part of the Australian Laureate Fellowship scheme. The authors thank N. Artemieva, J. Borovicka, and O. Popova for constructive comments and reviews that significantly improved the quality of the final manuscript.

REFERENCES

Baldwin, B. and Sheaffer, Y., 1971. Ablation and breakup of large meteoroids during atmospheric entry. *Journal of Geophysical Research*, 76(19):4653–4668.

Borovička, J., Popova, O., Nemtchinov, I. V., Spurný, P., and Ceplecha, Z., 1998. Bolides produced by impacts of large meteoroids into the Earth's atmosphere: comparison of theory with observations. I. Benesov bolide dynamics and fragmentation. *Astronomy and Astrophysics*, 334:713.

Borovička, J., Tóth, J., Igaz, A., Spurný, P., Kalenda, P., Haloda, J., Svoreň, J., Kornoš, L., Silber, E., Brown, P., et al., 2013. The Košice meteorite fall: Atmospheric trajectory, fragmentation, and orbit. *Meteoritics & Planetary Science*, 48(10):1757–1779.

Bronshten, V. A., 1983. *Physics of Meteoric Phenomena*. Geophysics and Astrophysics Monographs. Reidel, Dordrecht, Netherlands.

Brykina, I. G. and Stulov, V. P., 2012. The reciprocal role of convective and radiant heat exchange in the meteor-parameter range. *Doklady Physics*, 57(4): 164–165. doi: 10.1134/S1028335812040039.

Ceplecha, Z., 1961. Multiple fall of Přibram meteorites photographed. 1. Double-station photographs of the fireball and their relations to the found meteorites. *Bulletin of the Astronomical Institutes of Czechoslovakia*, 12:21–47.

Ceplecha, Z. and Revelle, D. O., 2005. Fragmentation model of meteoroid motion, mass loss, and radiation in the atmosphere. *Meteoritics & Planetary Science*, 40(1):35–54. doi: 10.1111/j.1945-5100.2005.tb00363.x.

Ceplecha, Z., Spurný, P., Borovička, J., and Keclikova, J., 1993. Atmospheric fragmentation of meteoriods. *Astronomy and Astrophysics*, 279:615–626.

Ceplecha, Z., Borovička, J., Elford, W. G., ReVelle, D. O., Hawkes, R. L., Porubčan, V., and Šimek, M., 1998. Meteor Phenomena and Bodies. *Space Science Reviews*, 84(3):327–471. doi: 10.1023/A:1005069928850.

Grewal, M. S. and Andrews, A. P., 1993. *Kalman filtering: theory and practice*. Prentice-Hall Inc., New Jersey.

Gritsevich, M. I., 2008a. The Pribram, Lost City, Innisfree, and Neuschwanstein falls: An analysis of the atmospheric trajectories. *Solar System Research*, 42(5): 372–390. doi: 10.1134/S003809460805002X.

Gritsevich, M. I., 2008b. Validity of the photometric formula for estimating the mass of a fireball projectile. *Doklady Physics*, 53(2):97–102. doi: 10.1007/s11446-008-2011-x.

Haider, A. and Levenspiel, O., 1989. Drag coefficient and terminal velocity of spherical and nonspherical particles. *Powder Technology*, 58(1):63–70. doi: 10.1016/0032-5910(89)80008-7.

Hayes, W. D. and Probstein, R. F., 1959. *Hypersonic Flow Theory*. Academic Press, New York.

Khanukaeva, D. Y., 2005. Calculation of variable drag and heat-transfer coefficients in meteoric physics equations. In *Modern Meteor Science An Interdisciplinary View*, pages 433–439. Springer.

Kulakov, A. and Stulov, V., 1992. Determination of meteor body parameters from observational data. *Astronomicheskii Vestnik*, 26:67–75.

Masson, D. J., Morris, D. N., and Bloxsom, D. E., 1960. *Measurements of Sphere Drag From Hypersonic Continuum to Free-Molecular Flow*. Rand Corporation, Santa Monica, CA.

McCrosky, R., Posen, A., Schwartz, G., and Shao, C.-Y., 1971. Lost city meteorite - its recovery and a comparison with other fireballs. *Journal of Geophysical Research*, 76(17):4090–4108. doi: 10.1029/JB076i017p04090.

Picone, J. M., Hedin, A. E., Drob, D. P., and Aikin, A. C., 2002. NRLMSISE-00 empirical model of the atmosphere: Statistical comparisons and scientific issues. *Journal of Geophysical Research: Space Physics (1978–2012)*, 107(A12): 1468.

ReVelle, D. O., 1976. *Dynamics and thermodynamics of large meteor entry: a quasi-simple ablation model*. Herzberg Institute of Astrophysics, National Research Council Canada.

Särkkä, S., 2008. Unscented Rauch-Tung-Striebel Smoother. *Automatic Control, IEEE Transactions on*, 53(3):845–849.

Schlichting, H. and Gersten, K., 2000. *Boundary Layer Theory*. Springer, New York, 8th edition.

Spurný, P., Bland, P., Shrbený, L., Borovička, J., Ceplecha, Z., Singelton, A., Bevan, A. W. R., Vaughan, D., Towner, M. C., Mcclafferty, T. P., Toumi, R., and Deacon, G., 2012. The Bunburra Rockhole meteorite fall in SW Australia: Fireball trajectory, luminosity, dynamics, orbit, and impact position from photographic and photoelectric records. *Meteoritics & Planetary Science*, 47(2): 163–185. doi: 10.1111/j.1945-5100.2011.01321.x.

Stulov, V. P., Mirsky, V. N., and Visly, A. I., 1995. Aerodynamics of Bolides. *Nauka*.

Towner, M. C., Bland, P. A., Spurný, P., Benedix, G. K., Dyl, K., Greenwood, R. C., Gibson, J., Franchi, I. A., Shrbený, L., Bevan, A. W. R., and Vaughan, D., 2011. Mason Gully: The Second Meteorite Recovered by the Desert Fireball Network. In *74th Annual Meteoritical Society Meeting (2011)*, volume 74, pages 53124–53124.

Truitt, R. W., 1959. *Hypersonic aerodynamics*. Ronald Press, New York.

Welten, K. C., Meier, M. M. M., Caffee, M. W., Laubenstein, M., Nishizumi, K., Wieler, R., Bland, P. a., Towner, M. C., and Spurný, P., 2012. Cosmic-ray exposure age and preatmospheric size of the Bunburra Rockhole achondrite. *Meteoritics & Planetary Science*, 47(2):186–196. doi: 10.1111/j.1945-5100.2011.01262.x.

Whipple, F. L., 1952. Meteoritic phenomena and meteorites. *Physics and Medicine of the Upper Atmosphere*, 137:149–153.

Zhdan, I. A., Stulov, V. P., Stulov, P. V., and Turchak, L. I., 2007. Drag coefficients for bodies of meteorite-like shapes. *Solar System Research*, 41(6):505–508. doi: 10.1134/S0038094607060068.

CHAPTER 3

FILTERING METEOROID FLIGHTS USING MULTIPLE UNSCENTED KALMAN FILTERS

Eleanor K. Sansom[a], Philip Bland[a], Mark G. Rutten[b], Jonathan Paxman [c], Martin C. Towner[a]

[a]Department of Applied Geology, Curtin University, GPO Box U1987, Bentley, Perth, WA 6845, Australia

[b]Defence Science and Technology Group, Edinburgh, SA 5111, Australia

[c]Department of Mechanical Engineering, Curtin University, GPO Box U1987, Bentley, Perth, WA 6845, Australia

This article is published in The Astronomical Journal, 2016, Vol. 152, pp. 148–156, and reprinted with permission in Appendix A.

ABSTRACT

Estimator algorithms are immensely versatile and powerful tools that can be applied to any problem where a dynamic system can be modeled by a set of equations and where observations are available. A well designed estimator enables system states to be optimally predicted and errors to be rigorously quantified. Unscented Kalman filters (UKFs) and interactive multiple models can be found in methods from satellite tracking (Ning and Fang, 2007; Mazor et al., 1998) to self-driving cars (Thrun et al., 2006). The luminous trajectory of the Bunburra Rockhole fireball was observed by the Desert Fireball Network in mid- 2007 (Spurný et al., 2012). The recorded data set is used in this paper to examine the application of these two techniques as a viable approach to characterizing fireball dynamics. The non-linear, single-body system of equations, used to model meteoroid entry through the atmosphere, is challenged by gross fragmentation events that may occur. The incorporation of the UKF within an interactive multiple model smoother provides a likely solution for when fragmentation events may occur as well as providing a statistical analysis of the state uncertainties. In addition to these benefits, another advantage of this approach is its automatability for use within an image processing pipeline to facilitate large fireball data analyses and meteorite recoveries.

INTRODUCTION

Fireballs are the visible phenomena that are observed when a meteoroid penetrates the Earth's atmosphere (Ceplecha et al., 1998). Dedicated fireball networks (e.g. the Desert Fireball Network in Australia; Bland et al. 2012) record the luminous paths of fireball phenomena at discrete increments, from multiple viewpoints, allowing the triangulated trajectory to be determined as a function of time. With good timing and position information recorded during flight, the final position, velocity, and mass may lead to the recovery of a meteorite. Few meteorites discovered have known orbits, and giving contextual information for these primitive objects gives valuable insights into solar system formation. As a meteoroid decelerates through the atmosphere, it loses mass by both ablation and gross fragmentation, which can be modeled by the single-body theory of meteoroid physics (Ceplecha et al., 1993). This system of equations requires the knowledge of trajectory parameters that are unique to each event and not directly observable. Modeling how a meteoroid's mass changes has typically been based on comparing positions observed along a fireball trajectory with model-computed distances, using the method of least-squares (Ceplecha et al., 1993; Ceplecha and Revelle, 2005). The main complication to fireball modeling is the incorporation of gross fragmentation. Fragmentation is a phenomenon that significantly challenges the application of a single-body theory to observed fireballs (Ceplecha and Revelle, 2005)

The least-squares method has undergone an iterative development over the years. Ceplecha et al. (1993) used it to solve for four free parameters in single-body dynamic equations, and introduced two additional parameters with the inclusion of a single gross fragmentation event. The standard deviation of least-squares residuals is used as a measure of model error. To determine the timing of a gross fragmentation event, Ceplecha et al. (1993) use a brute force approach. Each observation is tested as a potential gross fragmentation point and a solution that yields the minimum standard deviation case is considered as a possible point of gross fragmentation. This method, when applied to Prairie Network bolides greater than -10 mag, resulted in an average standard deviation for the position residuals equal to ± 30 m (Ceplecha et al., 1996) which is comparable to the ± 20 m typical precision in the observed position. Ceplecha and Revelle (2005) added to this method further by incorporating the computation of meteoroid light intensity. This is also part of the single-body equation system for a meteoroid, but to be able to compare to observations, the light curve of the fireball must be known. This is typically acquired using a high-cost photoelectric photometer tube attached to each observation station. As well as being strongly dependent on an accurate light curve for luminosity values, Ceplecha and Revelle (2005) assume that flares on a meteor light curve represent gross fragmentation events. These are amassed to create an assumed 'fragmentation pattern,' prior to model computation, with further assumptions on the amount of mass released from the main body and changes to model parameters that occur during these events. This is manually intensive, especially when different flare forms are associated with various types of fragmentation (e.g. a spike in the light curve is linked to the release of dust and a smooth 'hump' is associated with an eroding fragment; Borovička et al. 2013). This can lead to a trial-and-error fit of the fragmentation pattern to reproduce major features on a light curve (Borovička et al., 2013).

The majority of fireball trajectories are also limited to fewer than 25 discreet positional observations (Halliday et al., 1996) and due to low sample rates, and in many cases averaging of multiple observations during processing (Ceplecha, 1961; McCrosky and Posen, 1968), there is little scatter in the data. This has led to issues when the typical approach is confronted with a highly scattered data set such as that of the Bunburra Rockhole fireball. Of the 113 observations measured by Spurný et al. (2012), only 87 were used for their modeling. The majority of the discarded points were during significant periods of deceleration and are acknowledged by the authors to be caused by large fragmentation events.

The least-squares approach has become increasingly complex as it has evolved, from no fragmentation to the manually intense modeling of a full suite of fragments based on a trial-and-error approach to fitting the light curve. Final errors are determined based on the residual fit to observations; this does not offer a rigorous analysis of the errors introduced by the assumed parameters, the single-body theory model used, or complete error propagation of uncertainties in the observations.

Sansom et al. (2015) proposed a two-step process for assessing meteoroid entry using position dynamics alone. Their method includes an extended Kalman filter (EKF) to rigorously examine errors in meteoroid modeling. An EKF is an estimator that uses linearized models to predict the state of an object with nonlinear system equations and provides a comprehensive understanding of the errors involved based on the observational data set. A major benefit of this approach is that it can be automated; the least-squares method requires some manual input, meaning the majority of data collected by a fireball network does not undergo a full trajectory analysis. In the case of large dedicated camera networks (e.g. the Desert Fireball Network in Australia; Bland et al. 2012), the ability to integrate fireball modeling into a complete automated data reduction pipeline is a significant advantage. Data volumes are such that traditional (manually intensive) approaches would only allow a very small fraction of events to be analyzed. Software that has been developed for this pipeline includes event detection, calibration of coordinates, triangulation, mass determination, orbital calculations, wind modeling and the prediction of a fall line for potential surviving masses. Although the EKF introduced by Sansom et al. (2015) is a step forward in terms of error analysis, the use of an EKF algorithm does require the single-body dynamic equations to be linearized and does not explicitly handle fragmentation.

Here we propose the use of another estimator used in the field of guidance, navigation and control: the unscented Kalman filter (UKF) as well as the interacting multiple model (IMM) to address the linearization and fragmentation shortcomings of the EKF. An UKF allows a more rigorous approach to handling the nonlinear model equations, and an IMM enables an analysis of when gross fragmentation is likely to occur. Once again the trajectory data set for Bunburra Rockhole (Spurný et al., 2012) will be used to test the model as well as compare results with the EKF.

METEOROID FLIGHT USING FILTERS

The application of filtering and estimation to the problem of meteoroid flight was first used by Sansom et al. (2015) with the use of an EKF. The filtering process allows the prediction and evaluation of the state, $\mathbf{x}_k$ = (position (l), mass (m) and velocity (v)), of the meteoroid based on the observations $\mathbf{z}_k$ of its position at each time step k during flight. The flight of a meteoroid through the atmosphere as a function of time t may be modeled using the dynamic single-body aerodynamic Equation (3.1). These are the three state equations used by the filtering process:

$$\frac{dl}{dt} = v \tag{3.1a}$$

$$\frac{dm}{dt} = -\frac{1}{2}\sigma\kappa\rho_a v^3 m^{\mu} \tag{3.1b}$$

$$\frac{dv}{dt} = -\frac{1}{2}\kappa\rho_a v^2 m^{(\mu-1)} + g\sin\gamma_e \tag{3.1c}$$

where ρ_a, g and γ_e are the local atmospheric density ($\mathrm{kg\,m^{-3}}$), gravity ($\mathrm{m\,s^{-2}}$) and flight angle from horizontal respectively and the shape density coefficient $\kappa = \frac{c_d A_0}{\rho_m^{2/3}}$ (c_d being the drag coefficient and A_0 the shape parameter as described by Bronshten (1983) and the ablation coefficient σ ($\mathrm{s^2\,km^{-2}}$) $= \frac{c_h}{H^* c_d}$ (c_h is the coefficient of heat and H^* the enthalpy of vaporization). For all our models, the atmospheric properties are acquired using the NRLMSISE-00 atmospheric model (Picone et al., 2002).

With an EKF, the mean state $\bar{\mathbf{x}}_k$ of the meteoroid may be predicted from the propagation of a previous mean through a linearized form of the state Equations

(3.2). This may then be evaluated based on a given observation, $\mathbf{z}_k$ (3.3), at each time step. The observations made by the autonomous Desert Fireball Observatories (DFOs) are the triangulated position only, but are inherently linked to the other states through the state equations:

$$\mathbf{x}_k = F(\bar{\mathbf{x}}_{k-1}, k) + \mathbf{u}_k \qquad \mathbf{u}_k \sim \mathcal{N}(0, \mathbf{Q}_k) \tag{3.2}$$

$$\mathbf{z}_k = H(\bar{\mathbf{x}}_k) + \mathbf{w}_k \qquad \mathbf{w}_k \sim \mathcal{N}(0, \mathbf{R}_k). \tag{3.3}$$

Incorporating both discrete process noise, $\mathbf{u}_k$, and observation noise, $\mathbf{w}_k$, enables a statistical analysis of the state and corresponding uncertainties. The process noise accounts for uncertainties that are introduced by the dynamic model. This not only includes the approximations introduced by using the single-body dynamic Equations (3.1) but the imprecision in the atmospheric density model used, variables that are held constant, and of course fragmentation phenomena etc. These uncertainties associated with the modeling process and the incorporation of observation errors had not been explored previous to Sansom et al. (2015). $\mathbf{u}_k$ and $\mathbf{w}_k$, can be approximated as Gaussian noise with means of zero and discrete covariance $\mathbf{Q}_k$ and $\mathbf{R}_k$ respectively (Särkkä and Sarmavuori, 2013). While $\mathbf{R}_k$ is linked to the error associated with individual measurements, $\mathbf{Q}_k$ can be derived from the continuous process noise covariance $\mathbf{Q}_c$ as described by Grewal and Andrews (1993).

THE UNSCENTED KALMAN FILTER

The linearization of the state equations in an EKF is a suboptimal approximation of the meteoroid trajectory. An UKF allows a more rigorous approach to estimating systems with non linear dynamics (Julier and Uhlmann, 1997, 2004; Wan and Merwe, 2000). Rather than estimating the transformation of the mean, $\bar{\mathbf{x}}_k$ (with a number of states equal to L), and covariance ($\mathbf{P}_k$), a UKF uses a set of $2L + 1$ weighted sample points (χ_i) that together represent the Gaussian probability distribution of the data (after Wan and Merwe 2000):

$$\begin{aligned}
&\chi_0 = \bar{\mathbf{x}}_{k-1|k-1} \\
&\chi_i = \bar{\mathbf{x}}_{k-1|k-1} + (\sqrt{(L+\lambda)\mathbf{P}_k})_i \qquad i = 1, ..., L \\
&\chi_i = \bar{\mathbf{x}}_{k-1|k-1} - (\sqrt{(L+\lambda)\mathbf{P}_k})_{i-L} \quad i = L+1, ..., 2L
\end{aligned} \tag{3.4}$$

where the sample mean and covariance weightings are calculated by

$$\begin{aligned}
&W_0^{(m)} = \lambda/(L+\lambda) \\
&W_0^{(c)} = \lambda/(L+\lambda) + (1 - \alpha^2 + \beta) \\
&W_i^{(m)} = W_i^{(c)} = 1/\{2(L+\lambda)\} \qquad i = 1, ..., 2L.
\end{aligned} \tag{3.5}$$

The scaling parameter, $\lambda = \alpha^2(L + \kappa) - L$. The scaling factor, α, controls the weighting of sample points as well as their spread around the mean and is typically given a value $1 \times 10^{-4} \leqslant \alpha \leqslant 1$ (Wan and Merwe, 2001). Small α values result in a smaller spread from the mean (Julier, 2002). κ, in this equation only, refers to the secondary scaling parameter described by Wan and Merwe (2001). It is generally set to $\kappa = 0$ or $3 - L$. The β parameter incorporates prior knowledge of the mean distribution and a value of $\beta = 2$ is used to represent a Gaussian distribution (Wan and Merwe, 2000). To determine the matrix root of $\mathbf{P}_k$, a lower triangular matrix in a Cholesky factorization is used (Särkkä, 2007). As with an EKF there is a prediction and a measurement update step.

PREDICTION — These sample points are individually propagated through the nonlinear state equations:.

$$\chi_{i,k|k-1} = f(\chi_{i,k-1|k-1}, \mathbf{u}_k, k) \qquad i = 0, ..., 2L. \tag{3.6}$$

The estimate of the incremented mean and covariance are then recalculated using (3.5) and (3.6) to give:

$$\hat{\mathbf{x}}_{k|k-1} \approx \sum_{i=0}^{2L} W_k^{(m)} \chi_{i,k|k-1} \tag{3.7}$$

$$\mathbf{P}_{k|k-1} \approx \sum_{i=0}^{2L} W_k^{(c)} \{\chi_{i,k|k-1} - \hat{\mathbf{x}}_{k|k-1}\}\{\chi_{i,k|k-1} - \hat{\mathbf{x}}_{k|k-1}\}^{T} + \mathbf{Q}_k. \tag{3.8}$$

UPDATE – The estimated position for each sample point may be extracted from each of their state matrices using (3.9). The mean predicted position can therefore be calculated (Equation 3.10) as well as the measurement covariance of the prediction (Equation 3.11). The observation noise covariance, $\mathbf{R}_k$, is independent of the innovation covariance, $\mathbf{S}_k$, and is therefore additive (Julier and Uhlmann, 1997):

$$\mathcal{Z}_{i,k|k-1} = h(\chi_{i,k|k-1}, k) \tag{3.9}$$

$$\hat{\mathbf{z}}_{k|k-1} \approx \sum_{i=0}^{2L} W_k^{(m)} \mathcal{Z}_{i,k|k-1} \tag{3.10}$$

$$\mathbf{S}_k = \sum_{i=0}^{2L} W_k^{(c)} \{\mathcal{Z}_{i,k|k-1} - \hat{\mathbf{z}}_{k|k-1}\}\{\mathcal{Z}_{i,k|k-1} - \hat{\mathbf{z}}_{k|k-1}\}^{T} + \mathbf{R}_k \tag{3.11}$$

$$\mathbf{C}_k = \sum_{i=0}^{2L} W_k^{(c)} \{\chi_{i,k|k-1} - \hat{\mathbf{x}}_{k|k-1}\}\{\mathcal{Z}_{i,k|k-1} - \hat{\mathbf{z}}_{k|k-1}\}^{T}. \tag{3.12}$$

The measurement covariance (Equation 3.11) and the cross-correlation matrix of the state and measurement (Equation 3.12) are used to calculate the Kalman gain, $\mathbf{K}_k$ (Equation 3.13), which controls the weighting of the predicted state vs. the observed measurement. These are used along with Equations (3.7) and (3.8) to perform the final measurement update of the state and covariance (Hartikainen and Särkkä, 2007).

$$\mathbf{K}_k = \mathbf{C}_k \mathbf{S}_k^{-1} \tag{3.13}$$

$$\hat{\mathbf{x}}_{k|k} = \hat{\mathbf{x}}_{k|k-1} + \mathbf{K}_k \left[z_k - \hat{\mathbf{z}}_{k|k-1} \right] \tag{3.14}$$

$$\mathbf{P}_{k|k} = \mathbf{P}_{k|k-1} - \mathbf{K}_k \mathbf{S}_k \mathbf{K}_k^T. \tag{3.15}$$

MODELING A METEOROID TRAJECTORY USING AN UKF

UKF parameters used here are the same as those used by Sansom et al. (2015) to allow a comparison of the methodologies. Values used in the process noise covariance matrix $\mathbf{Q}_c$ (3.16) reflect the uncertainties introduced by the dynamic model being used. For example, uncertainty in position and velocity is introduced through noise in acceleration. The changes in mass and velocity as a function of time are also dependent on unmodeled factors such as fragmentation and variations in assumed constants and are influenced by the precision of atmospheric densities:

$$\mathbf{Q}_c = \begin{pmatrix} (3.75\,\mathrm{m\,s^{-1}})^2 & 0 & 0 \\ 0 & \left(0.2\,\mathrm{kg\,s^{-1}}\right)^2 & 0 \\ 0 & 0 & \left(75\,\mathrm{m\,s^{-2}}\right)^2 \end{pmatrix}. \tag{3.16}$$

All observed positions of the meteoroid are assigned the same covariance $\mathbf{R}_k$ in this simulation:

$$\mathbf{R}_k = (100\,\mathrm{m})^2. \tag{3.17}$$

As for the scaling parameters required for Equations (3.4) and (3.5), given that there are three states used in the meteoroid problem, $L = 3$. To ensure a reasonable spread of sample points, $\kappa = 0$ and $\alpha = 1$ is used, following Särkkä and Sarmavuori (2013).

RESULTS OF THE UKF

Once again the Bunburra-Rockhole data set is used to test the model. Observation measurements are taken from Table 2 of Spurný et al. (2012) and include all values after the first recorded dash. As the constants σ and κ in (Equation 3.1) are unknown, a prior assumption of their values, along with the initial state values, must be made. As with the EKF presented by Sansom et al. (2015), we must precede this estimator with the dynamic optimization step described in that paper. To allow a direct comparison between the two filters, we will use the same initial conditions as determined by these authors for the Bunburra Rockhole fireball: $m_0 = 30.12\,\mathrm{kg}$, $v_0 = 13198\,\mathrm{m\,s^{-1}}$, $\kappa\,(SI) = 0.0124$ and $\sigma = 0.0371\,\mathrm{s^2\,km^{-2}}$. A drag coefficient of 1 is used. The state values after each measurement update step are represented in Figure 3.1. This appears similar to Figure 3 in Sansom et al. (2015); however standard deviation values are lower and the final mass and velocity estimates using this more robust form of filtering are $m_f = 2.88 \pm 1.04\,\mathrm{kg}$ and $v_f = 6095 \pm 203\,\mathrm{m\,s^{-1}}$.

The lower error values here show that the use of a UKF gives us an improved state estimate compared to an EKF (see the summary Table 3.1).

The incorporation of sudden significant mass loss, however, is still not fully represented. Fragmentation events that occur within the error ranges are allowed to be incorporated due to the observation update but the timing of their occurrence is not directly examinable. As discussed by Sansom et al. (2015), the minima in the dm/dt plot (Figure 3.1) may indicate fragmentation event locations. A more robust way of modeling fragmentation events and fully incorporating them may be achieved with an IMM.

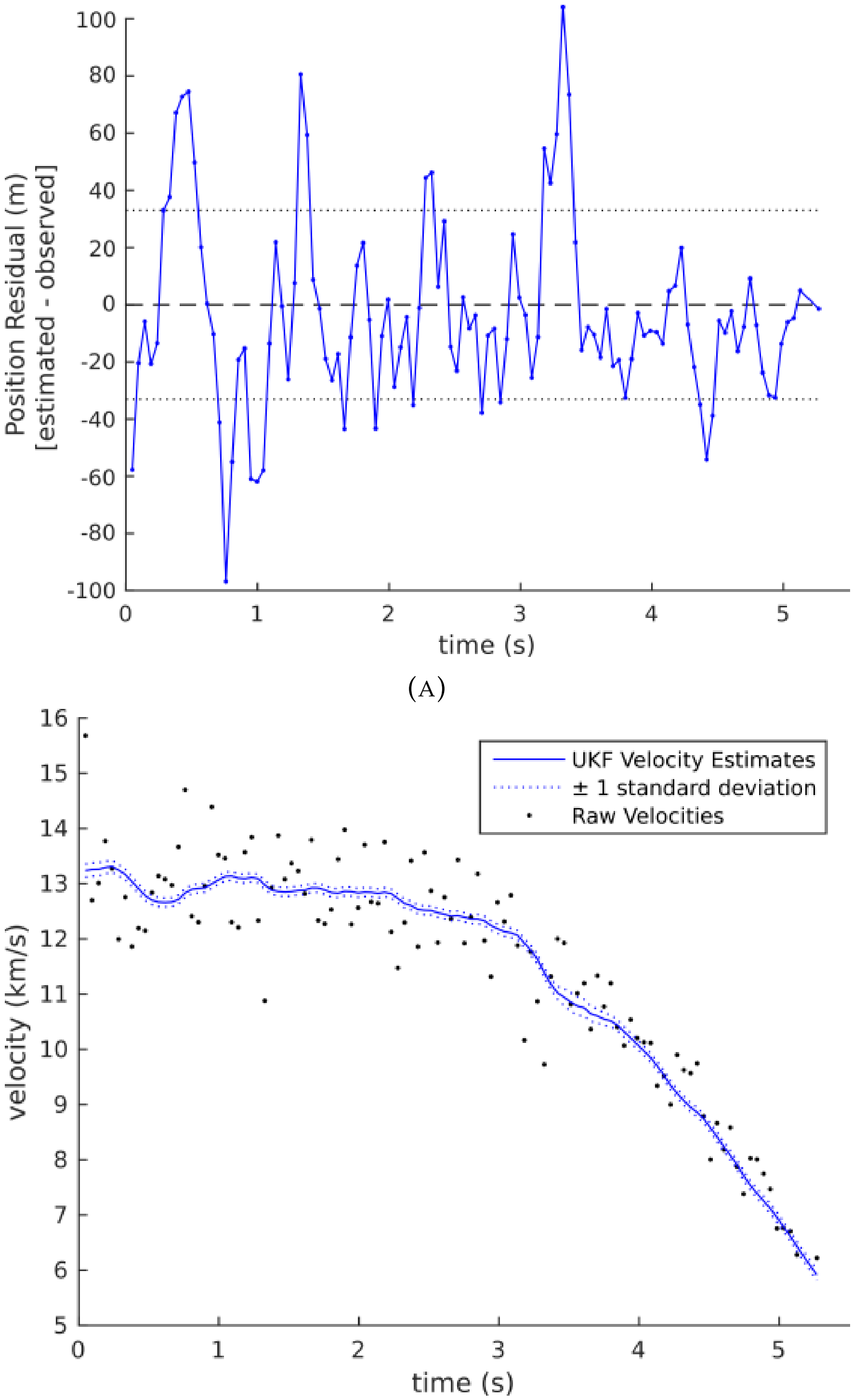

(A)

(B)

FIGURE 3.1: Unscented Kalman filter results for an initial mass of 30.12 kg. (a) Residual plot of observed position data subtracted from the UKF position estimate. Dotted lines represent one standard deviation (33.05 m). (b) The blue curve shows UKF velocity estimates with blue dotted curves representing ± one standard deviation, calculated from the $\mathbf{P}_k$ matrix. Black points represent velocity values calculated from observations using $v = \mathrm{d}l/\mathrm{d}t$.

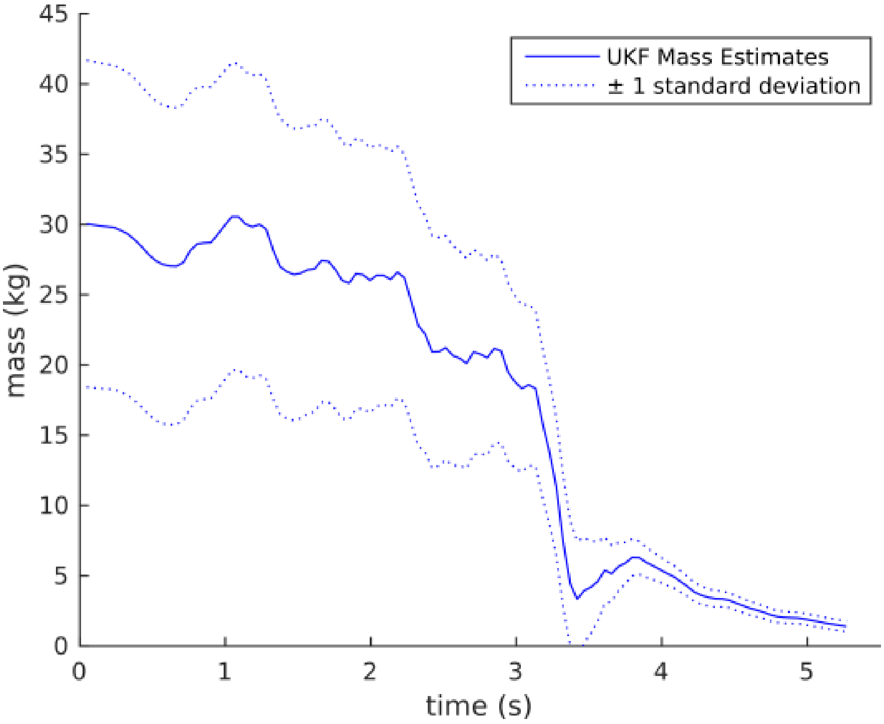

(C)

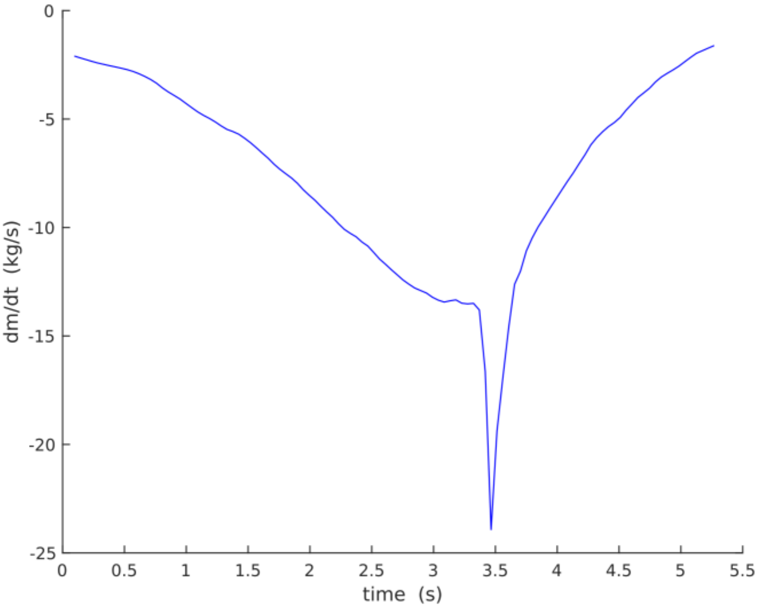

(D)

FIGURE 3.1 *(contd.)*: (c) UKF mass estimates with the dotted curve representing ± one standard deviation, taken from $\mathbf{P}_k$ matrix. Slight increases in velocity and mass are within error ranges and are due to the constant updating as part of the filtering process. (d) Rate of mass loss calculated by change in state mass estimates over the difference in observation times.

INTERACTING MULTIPLE MODEL

The IMM algorithm is an effective and efficient hybrid model for state estimation (Blom and Bar-Shalom, 1988; Mazor et al., 1998). The adaptive approach of an IMM enables the inclusion of discrete changes to the meteoroid flight model that would be difficult to handle in a single UKF. Model changes such as instantaneous gross fragmentation may therefore be explicitly included. This is achieved by running two UKFs simultaneously with different values for mass uncertainty within the process noise covariance, Q_c. Equation 3.18(a) allows typical error ranges for ablation. Equation 3.18(b) has larger errors in order to include gross fragmentation events:

$$\mathbf{Q}_c^1 = \begin{pmatrix} \left(3.75\,\mathrm{m\,s^{-1}}\right)^2 & 0 & 0 \\ 0 & \left(0.05\,\mathrm{kg\,s^{-1}}\right)^2 & 0 \\ 0 & 0 & \left(75\,\mathrm{m\,s^{-2}}\right)^2 \end{pmatrix} \tag{3.18a}$$

$$\mathbf{Q}_c^2 = \begin{pmatrix} \left(3.75\,\mathrm{m\,s^{-1}}\right)^2 & 0 & 0 \\ 0 & \left(2\,\mathrm{kg\,s^{-1}}\right)^2 & 0 \\ 0 & 0 & \left(75\,\mathrm{m\,s^{-2}}\right)^2 \end{pmatrix}. \tag{3.18b}$$

Different initial uncertainties in mass are also set to vary by model, allowing the confidence in the initial mass value to also be tested:

$$\mathbf{P}_0^1 = \begin{pmatrix} (10\,\mathrm{m})^2 & 0 & 0 \\ 0 & (2\,\mathrm{kg})^2 & 0 \\ 0 & 0 & \left(1500\,\mathrm{m\,s^{-1}}\right)^2 \end{pmatrix} \tag{3.19a}$$

$$\mathbf{P}_0^2 = \begin{pmatrix} (10\,\mathrm{m})^2 & 0 & 0 \\ 0 & (5\,\mathrm{kg})^2 & 0 \\ 0 & 0 & \left(1500\,\mathrm{m\,s^{-1}}\right)^2 \end{pmatrix}. \tag{3.19b}$$

For each model, M^i, we assign a prior probability,

$$\mu_0 = \left[P\{M_0^1\} \quad P\{M_0^2\}\right] = \left[\mu_0^1 \quad \mu_0^2\right]. \tag{3.20}$$

For the meteoroid problem, an equal weighting is given to both models initially; $\mu_0 = [0.5 \quad 0.5]$.

The probability of changing between model j from time $k-1$ to model i at time k is written as $p_{ij} = P\{M_k^i | M_{k-1}^j\}$ (Hartikainen and Särkkä, 2007). These can be combined into a two-model transition probability matrix

$$\Phi = \begin{bmatrix} P\{M_k^1|M_{k-1}^1\} & P\{M_k^1|M_{k-1}^2\} \\ P\{M_k^2|M_{k-1}^1\} & P\{M_k^2|M_{k-1}^2\} \end{bmatrix}. \tag{3.21}$$

Here we assume an 80% probability that an ablating meteoroid will not suddenly fragment at any point in time, and a body that is in the process of fragmenting is 40% likely to carry on doing so (Equation 3.22). These likelihood values are based on the results of this analysis with the Bunburra Rockhole fireball. Further examination will be required to determine the general suitability of these values for other fireball events:

$$\Phi = \begin{bmatrix} 0.8 & 0.2 \\ 0.6 & 0.4 \end{bmatrix}. \tag{3.22}$$

Three stages of the IMM filter are performed at each time step (Mazor et al. (1998); Hartikainen and Särkkä (2007); equations described in these stages are after these works). First, an interaction between all the model states based on the mixing probabilities, $\mu_k^{i|j}$; then filtering using an UKF on each model; finally a recombination of states, based on the weightings of each model estimates, to produce a final state and covariance estimate.

INTERACTION

The mixing probability for each model with a prior probability μ_{k-1}^{i} is calculated using a normalization factor, c_j:

$$\mu_k^{i|j} = \frac{1}{c_j} p_{ij} \mu_{k-1}^{i} \tag{3.23a}$$

$$c_j = \sum_i p_{ij} \mu_{k-1}^{i}. \tag{3.23b}$$

The 'mixed' mean and covariance that will be used as the a priori inputs to the filtering step are calculated as

$$\hat{\mathbf{x}}_{k-1|k-1}^{0i} = \sum_i \mu_k^{i|j} \hat{\mathbf{x}}_{k-1|k-1}^{i} \tag{3.24a}$$

$$\mathbf{P}_{k-1|k-1} = \sum_i \mu_k^{i|j} \times \left(\mathbf{P}_{k-1|k-1}^{i} + \left[\hat{\mathbf{x}}_{k-1|k-1}^{i} - \hat{\mathbf{x}}_{k-1|k-1}^{0j} \right] \left[\hat{\mathbf{x}}_{k-1|k-1}^{i} - \hat{\mathbf{x}}_{k-1|k-1}^{0j} \right]^{T} \right). \tag{3.24b}$$

APPLYING THE FILTER

The filtering step uses the UKF as described in section 3.2.1. Both the prediction and measurement update of the mean and covariance are calculated for each model. The likelihood, Λ_k^i, of the predicted position measurement is calculated for each model as the Gaussian probability of the position residual with zero mean and covariance $\mathbf{S}_k$ (from (3.11)) (Equation 3.25). This is then used to determine the overall probability of that model (Equation 3.27), where c is another normalization factor:

$$\Lambda_k^i \approx \mathcal{N}\left(\left[z_k - \hat{\mathbf{z}}_{k|k-1}\right]; 0, \mathbf{S}_\mathbf{k}\right) \tag{3.25}$$

$$c = \sum_i \Lambda_k^i c_i \tag{3.26}$$

$$\mu_k^i = \frac{1}{c} \Lambda_k^i c_i. \tag{3.27}$$

COMBINATION

Finally, to calculate a single state and covariance estimate, the updated estimates, Equations (3.14) and (3.15), from each model are weighted using the probabilities from Equation (3.27):

$$\hat{\mathbf{x}}_{k|k} = \sum_i \mu_k^i \hat{\mathbf{x}}_{k|k}^i \tag{3.28}$$

$$\mathbf{P}_{k|k} = \sum_i \mu_k^i \times \left(\mathbf{P}_{k|k}^i + \left[\hat{\mathbf{x}}_{k|k} - \hat{\mathbf{x}}_k\right]\left[\hat{\mathbf{x}}_{k|k} - \hat{\mathbf{x}}_k\right]^T\right). \tag{3.29}$$

The state estimates at each time step are continuously updated based on the past data; future observations are not included. This means only the state estimate for the end of the trajectory is the result of processing all observations. This is how any filter works and is necessary if data are acquired in real time. If the full data set is available, however, it is more logical to include all the known data (both past and future) by the process known in this field as smoothing. To incorporate all the data, we can apply an IMM smoother to the data.

IMM SMOOTHER

In the context of filtering, smoothing does not relate to any form of averaging, rather to the method of determining estimates based on all (past and future) measurements (Särkkä, 2008). An IMM smoother will therefore incorporate all the observations of the fireball data set into each estimate. To do so, the IMM filter is run forwards as described in Section 3.3, then subsequently in reverse. A backwards (b) filtering probability, $\mu_k^{i\,(b)}$ is calculated, along with the mixed backwards mean and covariance ($\hat{\mathbf{x}}_k^{(b)}$ and $\hat{\mathbf{P}}_k^{(b)}$). Together with the forward probabilities and estimates, the smoothed estimates for each time step can be determined. The smoothed state and covariance estimates are calculated following the equations outlined in Hartikainen and Särkkä (2007) where the smoothed model probabilities are calculated by

$$\mu_k^{i(s)} = \frac{1}{d}\mu_k^i \mathbf{d}_j \tag{3.30}$$

where

$$\mathbf{d}_j = \sum_i p_{ij} \Lambda_k^{i(s)} \tag{3.31}$$

$$d = \sum_i d_j \mu_k^i \tag{3.32}$$

and for our two-model problem, the smoothed likelihoods of each model, $\Lambda_k^{i(s)}$, are calculated as a Gaussian distribution and can be written as

$$\Lambda_k^{i(s)} = \begin{bmatrix} \mathcal{N}\left(\hat{\hat{\mathbf{x}}}_k^{1(b)} - \hat{\hat{\mathbf{x}}}_k^{1} \,|\, 0, \mathbf{P}_k^{1(b)} - \mathbf{P}_k^{1}\right) & \mathcal{N}\left(\hat{\hat{\mathbf{x}}}_k^{2(b)} - \hat{\hat{\mathbf{x}}}_k^{1} \,|\, 0, \mathbf{P}_k^{2(b)} - \mathbf{P}_k^{1}\right) \\ \mathcal{N}\left(\hat{\hat{\mathbf{x}}}_k^{1(b)} - \hat{\hat{\mathbf{x}}}_k^{2} \,|\, 0, \mathbf{P}_k^{1(b)} - \mathbf{P}_k^{2}\right) & \mathcal{N}\left(\hat{\hat{\mathbf{x}}}_k^{2(b)} - \hat{\hat{\mathbf{x}}}_k^{2} \,|\, 0, \mathbf{P}_k^{2(b)} - \mathbf{P}_k^{2}\right) \end{bmatrix}. \quad (3.33)$$

By taking into account the entire data set at each observation time, this allows for a full analysis of the trajectory based on all observations, and a comprehensive understanding of all the errors throughout the bright flight.

RESULTS OF THE IMM AND SMOOTHER

The same initial parameters as used in Section 3.2.3 are used for both UKF models. The mixed state mean estimates for the forward IMM are shown in Figure 3.2 and represent the estimates based on prior data only and therefore display an overall higher covariance. The smoothed estimates in Figure 3.2 use all data available and are a truer representation of the overall covariance at each time step. Any over-estimation in the change in a state parameter by the forward model is corrected by the subsequent smoother to produce a comprehensively consistent result (such as can be seen in Figure 3.2(b)-(c) at ~ 3.4 seconds).

The smoothed model probabilities (Equation 3.30) are shown in Figure 3.3(a). Likely fragmentation events may be attributed to periods when the higher mass covariance allocated to model 2 is of greater probability.

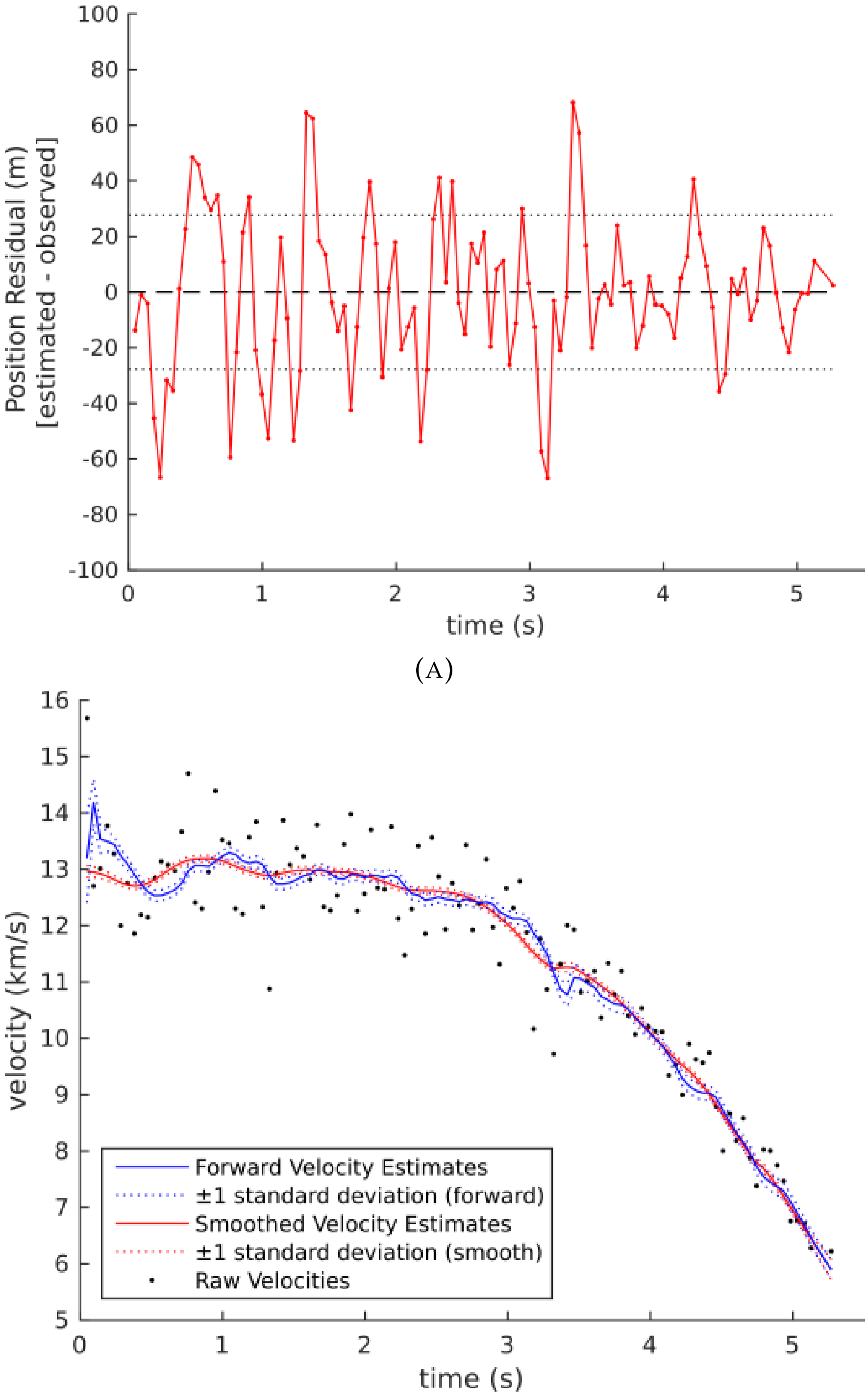

(A)

(B)

FIGURE 3.2: UKF IMM results for forward pass (blue) and smoother (red). (a) Residual plot of position data subtracted from IMM smoother position estimate - dotted lines represent one standard deviation (28 m). (b) Velocity estimates with standard deviation values taken from $\mathbf{P}_k$ matrix. Black points represent velocity values calculated from observations using $v = dl/dt$.

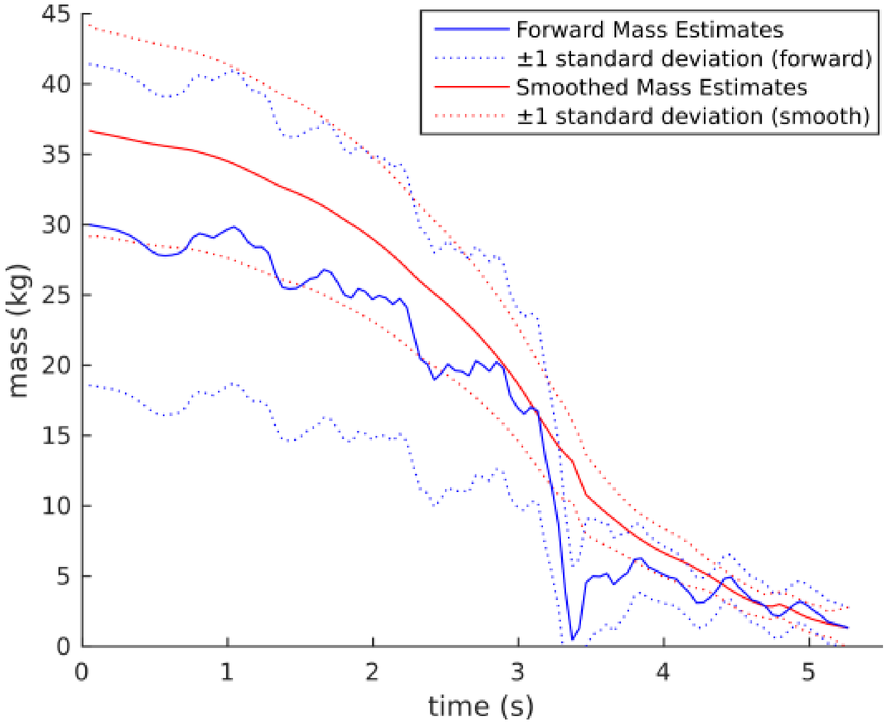

(C)

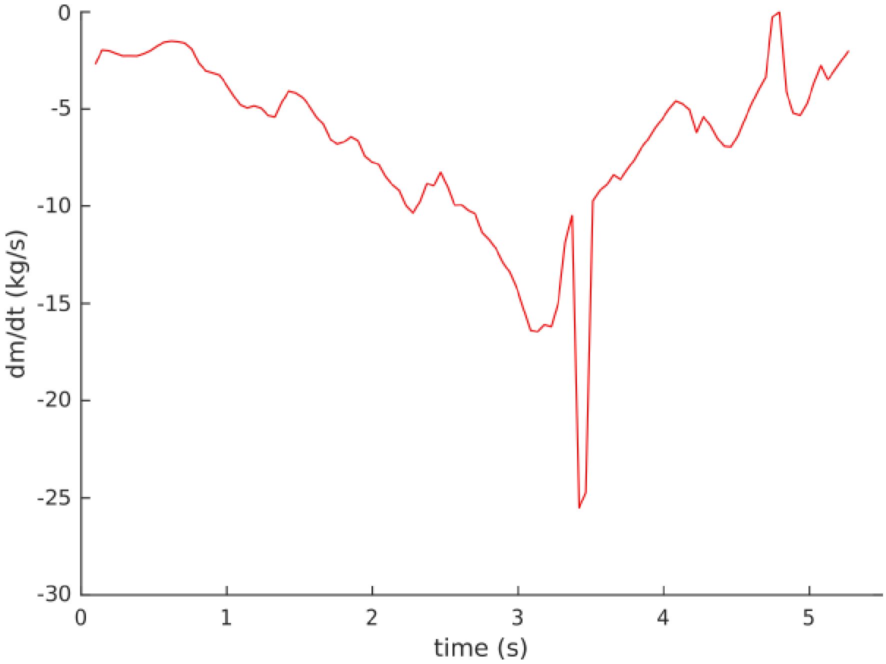

(D)

FIGURE 3.2 *(contd.)*: (c) Mass estimates with standard deviation values taken from $\mathbf{P}_k$ matrix. (d) Rate of mass loss calculated by change in state mass estimates of the IMM smoother over difference in observation times.

TABLE 3.1: Comparison of final state values using different filtering methods.

	Final Position Estimate With Error ($\sqrt{\sigma_l^2}$)	Final Mass Estimate With Error ($\sqrt{\sigma_m^2}$)	Final Velocity Estimate With Error ($\sqrt{\sigma_v^2}$)
EKF[1]	$60032 \pm 62\,\mathrm{m}$	$2.30 \pm 1.63\,\mathrm{kg}$	$6052 \pm 241\,\mathrm{m\,s^{-1}}$
UKF	$60040 \pm 58\,\mathrm{m}$	$2.88 \pm 1.04\,\mathrm{kg}$	$6095 \pm 203\,\mathrm{m\,s^{-1}}$
IMM	$60011 \pm 7\,\mathrm{m}$	$1.32 \pm 0.49\,\mathrm{kg}$	$5896 \pm 59\,\mathrm{m\,s^{-1}}$

The incorporation of fragmentation by way of the IMM significantly decreases the errors attributed to the final state estimates as seen in Table 3.1.

Using a Rauch-Tung-Striebel smoother with the EKF, Sansom et al. (2015) estimated the initial mass to be $30.20 \pm 6.53\,\mathrm{kg}$. The use of the UKF IMM smoother allows for a better estimate of the initial states resulting in lower covariance values; $m_0 = 36.68 \pm 3.81$ kg and $v_0 = 12963 \pm 35\,\mathrm{m\,s^{-1}}$.

DISCUSSION

In our model, we use all measurements from the second recorded dash onward of the Bunburra Rockhole fireball (published in Table 2 of Spurný et al. 2012) and therefore $t_0 = 0.1899$s. All model time values are therefore shifted by 0.1899 s from those published in Spurný et al. (2012). Comparisons will therefore be made in altitude. The same filter parameters ($\mathbf{P_0}, \mathbf{Q_c}, \mathbf{R_k}$) used by Sansom et al. (2015) for the EKF were used here in the UKF. From Table 3.1, there is small overall decrease in the errors of the state estimates for the UKF in comparison to the EKF results of Sansom et al. (2015). This shows that the nonlinear dynamics of fireball trajectories are better estimated by the Gaussian distribution of sample points of the UKF. The application of this estimator in an IMM allows the possibility of sudden large changes in mass that would not be allowable within the normal error range of simple ablation dynamics modeled by a single EKF or UKF. The similarity in the final covariance values

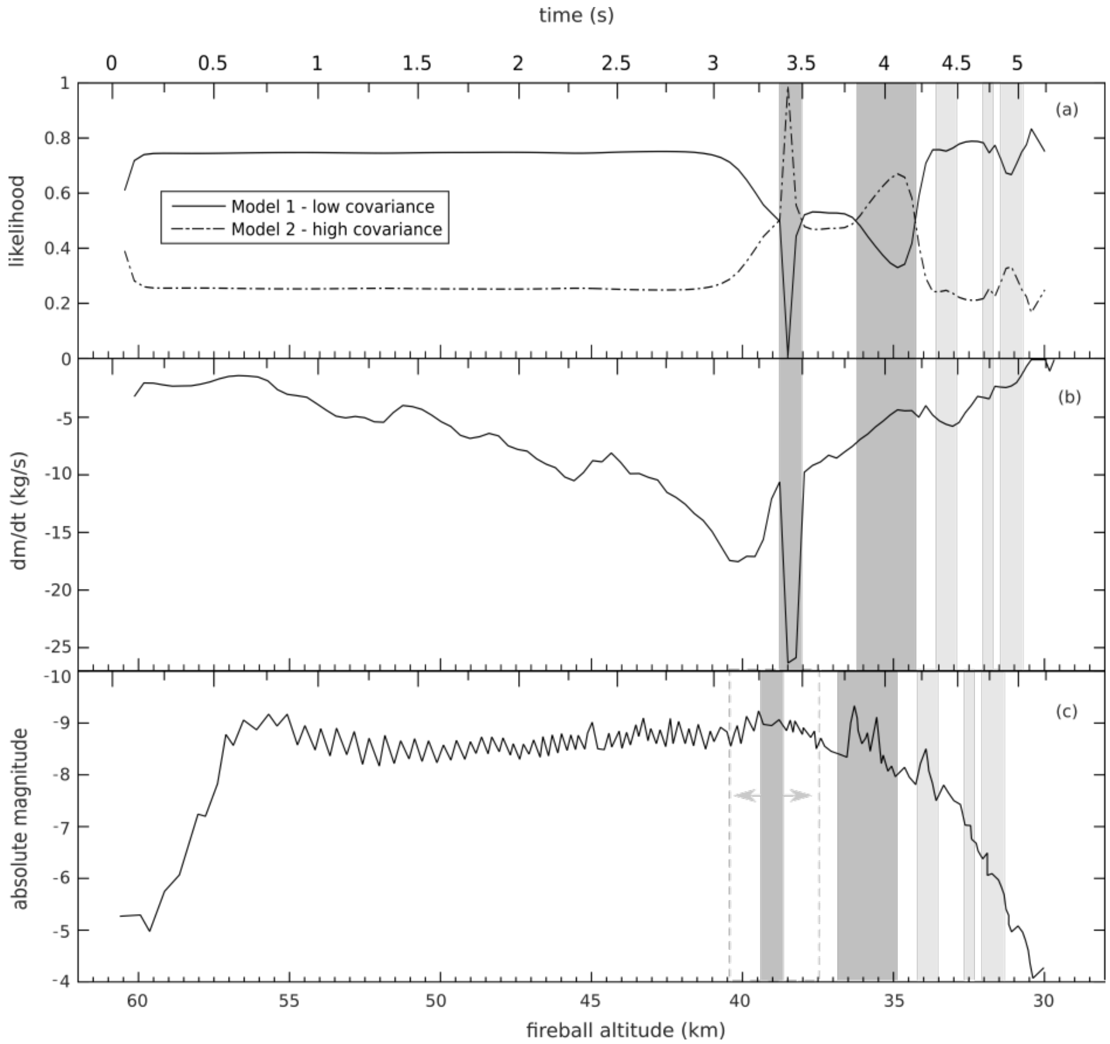

FIGURE 3.3: The primary x-axis displays altitude in kilometres (below). The secondary x-axis displays time in seconds from the start of the second measured dash (above) - note the nonlinearity of the secondary axis. (a) Smoothed model probabilities. Model 1 (solid) has a low mass covariance and mass loss is dominated by ablation. Model 2 (dashed) has a high mass covariance and likely indicates fragmentation events when likelihood increases. Dark gray areas show where $\mu_k^{M2(s)} > \mu_k^{M1(s)}$ and light gray areas show where there are local maxima in $\mu_k^{M2(s)}$. (b) Rate of mass loss calculated by change in state mass estimates of the IMM smoother over difference in observation times. (c) Light curve for the Bunburra Rockhole fireball replicated from Spurný et al. (2012). Highlighted areas are duplicated from (a) but offset by 530 m altitude. Dashes outline the extent of a 'hump' in the light curve.

of all estimators used (Table 3.1) shows that the final state estimates remain consistent with the observed positions.

The IMM smoothed model probabilities plotted in Figure 3.3a show the relative likelihoods of a given model compared to the observation data. When low error ranges are able to fit the data (Model 1 (M1)- (3.18a)) mass loss is most likely via steady ablation. When higher error ranges are needed to produce a good fit to the data, Model 2 (M2)- (3.18b) is more probable and gross fragmentation is likely contributing to a sudden increase in mass loss. Figure 3.3(a) highlights two regions where M2 has a higher likelihood than M1: from 38.8 to $38.0\,\mathrm{km}$ and from 36.2 to $34.2\,\mathrm{km}$. There are also features highlighted at $\sim$ 33.2, $\sim$ 31.9, $\sim 31.1\,\mathrm{km}$ where the probability of M2 shows a slight increase. Figure 3.3(c) is a reproduction of the corrected radiometric light curve for Bunburra Rockhole produced by Spurný et al. (2012). The highlighted regions from Figure 3.3(a) have been replicated on the light curve (Figure 3.3(c)) with an offset of $530\,\mathrm{m}$. The initial spike in Figure 3.3(a) at $38.8 - 38.0\,\mathrm{km}$ appears at the centre of a hump in the light curve (width of 'hump' outlined in 3.3(c)). A hump in the light curve according to Borovička et al. (2013) is caused by an eroding fragment; a larger chunk that itself holds together and ablates gradually. This coincides well with the large decrease in mass loss at this time (Figure 3.3b). The sharper spike in the light curve seen from 36.5 to $35.4\,\mathrm{km}$ on the other hand would correspond to release of dust (Borovička et al., 2013) and not necessarily to a large mass loss, which indeed is not a feature in Figure 3.3(b). The other three lightly highlighted features in Figure 3.3(a) also appear to correspond to relative spikes in the light curve (Figure 3.3(c)) as well as roughly correlating with local minima in the rate of mass loss (Figure 3.3(b)).

As the IMM smoothed model probabilities include all the observed data, the offset between Figures 3.3(a) and (c) is not due to any lag in model response time. A $530\,\mathrm{m}$ offset in altitude at the end of the trajectory roughly corresponds to $2 - 3$ shutter iterations ($2 - 3$ observations). This offset could be due to a physical delay between the emission of light recorded by the light curve and the time taken for the meteoroid to decelerate. It is also possible that it is a ramification of the light curve processing itself. In order to convert the highly accurate photometric light curve into a function of altitude (no calibrated light curve with time published), it is compared to the photographic record and errors in the fit may introduce uncertainties in altitude values.

The first half of the changing mass profile seen in Figure 3.2(c) does not resemble that given in Figure 13 of Spurný et al. (2012). This is likely due to Spurný et al. (2012) excluding all points between 62.4 and 58.2 km; 51.9 and 51.6 km; and 42.8 to 39.1 km altitude. Spurný et al. (2012) acknowledge that the points around 40 km altitude are most likely caused by large fragments 'forming the head.' This corresponds to our analysis of an eroding fragment, albeit modeled to begin at 38.8 km; however, Spurný et al. (2012) also do not illustrate any significant mass loss in their Figure 13 at an altitude of 40 km. The large amount of fragmentation surmized by Spurný et al. (2012) to cause the anomalies at the start of the trajectory (altitude above 58.2 km) cannot be substantiated. The scatter within the first 0.38 s (altitude above 58.2 km) is not dissimilar to that of the first 2.5 s (altitude above 44 km). The UKF/IMM smoother constrains the error of the state for the full trajectory by including all observation errors and issues caused by the single-body Equation (3.1) simplifying the fireball process. There is no need for a drastic change in initial mass for the model to fit the observed data. The final decreases in mass in Figure 13 of Spurný et al. (2012) are at approximately 38 km and 36 km, as well as smaller steps at 34.6, 33.6, 32.3, 31.2, corresponding well to the shaded regions in Figure 3.3(a).

The incorporation of the UKF within an IMM smoother provides likely occurrences of fragmentation as well as providing a statistical analysis of the state uncertainties. This is a fully automated method of obtaining a likely fragmentation pattern of a meteoroid trajectory from position observations alone.

CONCLUSION

The use of an unscented Kalman filter within an interactive multiple model smoother allows a set of dynamic equations alone to model a fireball trajectory. An UKF enables an estimation of the state using a more robust approach to the nonlinear equations for the dynamics of this system. The application of this estimator in an IMM smoother allows the incorporation of gross fragmentation events and identifies their approximate time of occurrence. Different shapes in the light curve can also be said to correspond to local minima in the rate of mass loss. This method can handle highly noisy data in the Bunburra Rockhole example, indicating that the method is robust enough to be applied to other raw fireball data sets, including all observations with no need for prior smoothing. The use of an UKF/IMM filter, however, still requires assumptions to be made for the initial entry parameters and unknown equation constants. The initial state covariance matrix allows for flexibility in the initial state values, and some uncertainty in the unknown constants will be included in the model noise covariance, although it must be remembered that the state estimates and their covariance remain dependent on the initial assumptions used. To remove this dependency, a statistical analysis should be made for the selection of these parameters.

ACKNOWLEDGEMENTS

The authors would like to thank the reviewer for their outstanding and thorough review of this paper. This work was funded by the Australian Research Council as part of the Australian Laureate Fellowship scheme.

REFERENCES

Bland, P., Spurný, P., Bevan, A., Howard, K., Towner, M., Benedix, G., Greenwood, R., Shrbený, L., Franchi, I., Deacon, G., et al., 2012. The australian desert fireball network: a new era for planetary science. *Australian Journal of Earth Sciences*, 59(2):177–187.

Blom, H. A. P. and Bar-Shalom, Y., 1988. Interacting multiple model algorithm for systems with Markovian switching coefficients. *IEEE Transactions on Automatic Control*, 33(8):780–783. doi: 10.1109/9.1299.

Borovička, J., Tóth, J., Igaz, A., Spurný, P., Kalenda, P., Haloda, J., Svoreň, J., Kornoš, L., Silber, E., Brown, P., et al., 2013. The Košice meteorite fall: Atmospheric trajectory, fragmentation, and orbit. *Meteoritics & Planetary Science*, 48(10):1757–1779.

Bronshten, V. A., 1983. *Physics of Meteoric Phenomena*. Geophysics and Astrophysics Monographs. Reidel, Dordrecht, Netherlands.

Ceplecha, Z., 1961. Multiple fall of Přibram meteorites photographed. 1. Double-station photographs of the fireball and their relations to the found meteorites. *Bulletin of the Astronomical Institutes of Czechoslovakia*, 12:21–47.

Ceplecha, Z. and Revelle, D. O., 2005. Fragmentation model of meteoroid motion, mass loss, and radiation in the atmosphere. *Meteoritics & Planetary Science*, 40(1):35–54. doi: 10.1111/j.1945-5100.2005.tb00363.x.

Ceplecha, Z., Spurný, P., Borovička, J., and Keclikova, J., 1993. Atmospheric fragmentation of meteoriods. *Astronomy and Astrophysics*, 279:615–626.

Ceplecha, Z., Spalding, R. E., Jacobs, C. F., and Tagliaferri, E., 1996. Luminous efficiencies of bolides. In *SPIE's 1996 International Symposium on Optical Science, Engineering, and Instrumentation*, volume 2813, pages 46–56. International Society for Optics and Photonics. doi: 10.1117/12.256072.

Ceplecha, Z., Borovička, J., Elford, W. G., ReVelle, D. O., Hawkes, R. L., Porubčan, V., and Šimek, M., 1998. Meteor Phenomena and Bodies. *Space Science Reviews*, 84(3):327–471. doi: 10.1023/A:1005069928850.

Grewal, M. S. and Andrews, A. P., 1993. *Kalman filtering: theory and practice*. Prentice-Hall Inc., New Jersey.

Halliday, I., Griffin, A. a., and Blackwell, A. T., 1996. Detailed data for 259 fireballs from the Canadian camera network and inferences concerning the influx of large meteoroids. *Meteoritics & Planetary Science*, 31(2):185–217. doi: 10.1111/j.1945-5100.1996.tb02014.x.

Hartikainen, J. and Särkkä, S., 2007. Optimal filtering with Kalman filters and smoothers a Manual for Matlab toolbox EKF / UKF. *Journal of Interprofessional Care*, 25:1–57. doi: 10.3109/13561820.2010.500445.

Julier, S. J., 2002. The scaled unscented transformation. *Proceedings of the 2002 American Control Conference (IEEE Cat. No.CH37301)*, 6(2):4555–4559. doi: 10.1109/ACC.2002.1025369.

Julier, S. J. and Uhlmann, J. K., 1997. A New Extension of the Kalman Filter to Nonlinear Systems. *Int Symp AerospaceDefense Sensing Simul and Controls*, 3 (2):26. doi: 10.1117/12.280797.

Julier, S. J. and Uhlmann, J. K., 2004. Unscented filtering and nonlinear estimation. *Proceedings of the IEEE*, 92(3):401–422. doi: 10.1109/JPROC.2003.823141.

Mazor, E., Averbuch, a., Bar-Shalom, Y., and Dayan, J., 1998. Interacting multiple model methods in target tracking: A survey. *IEEE Transactions on Aerospace and Electronic Systems*, 34(1):103–123. doi: 10.1109/7.640267.

McCrosky, R. E. and Posen, A., 1968. Special Data-Reduction Procedures for Prairie Network Meteor Photographs. *SAO Special Report*, 273.

Ning, X. and Fang, J., 2007. An autonomous celestial navigation method for leo satellite based on unscented kalman filter and information fusion. *Aerospace Science and Technology*, 11(2):222–228.

Picone, J. M., Hedin, A. E., Drob, D. P., and Aikin, A. C., 2002. NRLMSISE-00 empirical model of the atmosphere: Statistical comparisons and scientific issues. *Journal of Geophysical Research: Space Physics (1978–2012)*, 107(A12): 1468.

Sansom, E. K., Bland, P. A., Paxman, J., and Towner, M. C., 2015. A novel approach to fireball modeling: The observable and the calculated. *Meteoritics & Planetary Science*, 50(8):1423–1435. doi: 10.1111/maps.12478.

Särkkä, S., 2007. On unscented Kalman filtering for state estimation of continuous-time nonlinear systems. *IEEE Transactions on Automatic Control*, 52(9):1631–1641. doi: 10.1109/TAC.2007.904453.

Särkkä, S., 2008. Unscented Rauch-Tung-Striebel Smoother. *Automatic Control, IEEE Transactions on*, 53(3):845–849.

Särkkä, S. and Sarmavuori, J., 2013. Gaussian filtering and smoothing for continuous-discrete dynamic systems. *Signal Processing*, 93(2):500–510. doi: 10.1016/j.sigpro.2012.09.002.

Spurný, P., Bland, P., Shrbený, L., Borovička, J., Ceplecha, Z., Singelton, A., Bevan, A. W. R., Vaughan, D., Towner, M. C., Mcclafferty, T. P., Toumi, R., and Deacon, G., 2012. The Bunburra Rockhole meteorite fall in SW Australia: Fireball trajectory, luminosity, dynamics, orbit, and impact position from photographic and photoelectric records. *Meteoritics & Planetary Science*, 47(2): 163–185. doi: 10.1111/j.1945-5100.2011.01321.x.

Thrun, S., Montemerlo, M., Dahlkamp, H., Stavens, D., Aron, A., Diebel, J., Fong, P., Gale, J., Halpenny, M., Hoffmann, G., Lau, K., Oakley, C., Palatucci, M., Pratt, V., Stang, P., Strohband, S., Dupont, C., Jendrossek, L.-e., Koelen, C., Markey, C., Rummel, C., Niekerk, J. V., Jensen, E., Alessandrini, P., Bradski, G., Davies, B., Ettinger, S., Kaehler, A., Nefian, A., Mahoney, P., van Niekerk, J., Jensen, E., Alessandrini, P., Bradski, G., Davies, B., Ettinger, S., Kaehler, A., Nefian, A., and Mahoney, P., 2006. Stanley: The robot that won the DARPA Grand Challenge. *Journal of Field Robotics*, 23(9):661–692. doi: 10.1002/rob.20147.

Wan, E. A. and Merwe, R. V. D., 2000. The unscented kalman filter for nonlinear estimation. In *Adaptive Systems for Signal Processing, Communications, and Control Symposium 2000. AS-SPCC. The IEEE 2000*, pages 153–158. doi: 10.1109/ASSPCC.2000.882463.

Wan, E. A. and Merwe, R. V. D., 2001. The Unscented Kalman Filter. In Hayki, S., editor, *Kalman Filtering and Neural Networks*, chapter Chapter 7, page 62 pages. Wiley Publishing.

CHAPTER 4

ANALYSING METEOROID FLIGHTS USING PARTICLE FILTERS

Eleanor K. Sansom[a],Mark G. Rutten[b], Philip Bland[a]

[a]Department of Applied Geology, Curtin University, GPO Box U1987, Bentley, Perth, WA 6845, Australia

[b]Defence Science and Technology Group, Edinburgh, SA 5111, Australia

This article is published in The Astronomical Journal, 2017, Vol. 153, pp. 87-95, and reprinted with permission in Appendix A.

ABSTRACT

Fireball observations from camera networks provide position and time information along the trajectory of a meteoroid that is transiting our atmosphere. The complete dynamical state of the meteoroid at each measured time can be estimated using Bayesian filtering techniques. A particle filter is a novel approach to modelling the uncertainty in meteoroid trajectories and incorporates errors in initial parameters, the dynamical model used and observed position measurements. Unlike other stochastic approaches, a particle filter does not require predefined values for initial conditions or unobservable trajectory parameters. The Bunburra Rockhole fireball (Spurný et al., 2012), observed by the Australian Desert Fireball Network (DFN) in 2007, is used to determine the effectiveness of a particle filter for use in fireball trajectory modelling. The final mass is determined to be $2.16 \pm 1.33\,\mathrm{kg}$ with a final velocity of $6030 \pm 216\,\mathrm{m\,s^{-1}}$, similar to previously calculated values. The full automatability of this approach will allow an unbiased evaluation of all events observed by the DFN and lead to a better understanding of the dynamical state and size frequency distribution of asteroid and cometary debris in the inner solar system.

INTRODUCTION

A meteoroid is a small object moving in interplanetary space. When one enters the Earth's atmosphere, it creates a bright phenomenon called a meteor, fireball or bolide (depending on brightness). The interaction of this material with our atmosphere provides us with an opportunity to observe and study a portion of interplanetary material that would otherwise be inaccessible to us. Telescopes cannot image mm-m sized objects, and discoveries of 10's m sized asteroids constitute a tiny fraction of the predicted population (Harris, 2012). Determining the physical state of this material in our atmosphere – its strength and mass distribution, and its velocity frequency distribution, provides a unique window on cometary and asteroidal material in the inner solar system. In order to derive that data, we need to model the meteoroid-atmosphere interaction.

A set of idealised equations govern how a single meteoroid body will respond in terms of velocity and mass loss. The amount of deceleration experienced by a meteoroid is related to its shape and bulk density via a *shape-density parameter*, $\kappa = \frac{c_d A}{2\rho_m^{2/3}}$, where c_d is the aerodynamic drag coefficient [1], A the shape parameter as described by Bronshten (1983) and the bulk density of the meteoroid- ρ_m. Both ablation and gross fragmentation of the meteoroid is responsible for loss of mass. Gross fragmentation is hard to predict and is linked to the strength of the object. Ablation can be quantified through the *ablation parameter* - σ, which is defined as $\sigma = \frac{c_h}{H^* c_d}$ [1] (where c_h is the coefficient of heat and H^* the enthalpy of vaporisation).

If the meteoroid survives this luminous trajectory or *bright flight*, there is the possibility of recovering a meteorite on the ground. Dedicated fireball camera networks such as the Desert Fireball Network (DFN) in Australia (Bland et al., 2012) allow triangulated trajectories of larger meteoroid bodies to be observed. Special shutters are used (in the case of the DFN, a liquid crystal shutter using modulated sequences; Howie et al. 2017) to encode timing throughout the trajectory. Being able to predict the final state of the meteoroid is paramount to determining if there is any recoverable material, and is a necessary input to so-called *dark flight* modelling (the process by which data from the luminous trajectory is converted into a fall line on the ground using atmospheric wind models), enabling likely search areas to be defined (Ceplecha, 1987). Accurately calculating a trajectory also allows the orbit for that body to be determined. Meteorites with orbits are rare; less than 0.05 % of all meteorites. Knowing a

---

[1] Γ is referred to as the drag factor in many meteoroid trajectory works, including (Ceplecha and Revelle, 2005). The aerodynamic drag coefficient, $c_d = 2\Gamma$ (Bronshten, 1983; Borovička et al., 2015).

meteorite's pre-atmospheric orbit gives contextual information to the picture they provide on early Solar System formation. Over time, the statistical analysis of calculated orbits may also assist in planetary defence of asteroidal debris streams.

Determining the state of a physical system based on a set of noisy measurements is known as filtering. The *state* describes what a system is 'doing' at any given time. The flight path of an aircraft for example may be represented by its position, velocity and heading; position observations can be made in real time to estimate the velocity and heading of the aircraft. Bayesian state-space estimation methods, such as the Kalman filter and its variants, address the filtering problem with the aim of estimating the true state of a system. The adaptive approach predicts future states through a model of system equations and updates with respect to an observation. Links between state variables defined in model equations allows unobserved state values to also be updated.

This stochastic filtering approach suits the modelling of meteoroid trajectories using noisy and uncertain measurements. Typical meteoroid models mostly rely on measurements of the meteor/fireball brightness (Kikwaya et al., 2011; Murray et al., 2000; Ceplecha and Revelle, 2005), though light curves tend to be variable and do not represent typical values predicted by single-body ablation models (Campbell-Brown and Koschny, 2004). The meteoroid problem is complicated not only by unpredictable gross fragmentation in the atmosphere, but the majority of initial state parameters are entirely unknown (m_0, σ, κ). Multiple approaches have been taken to handle these unknowns in fireball trajectory analysis. The manually intensive method of Revelle (2007) is based on the brute force least squares approach of Ceplecha and Revelle (2005). It does include the luminosity of the fireball (derived from manual interpretation of a light curve) as a proxy for mass loss and solves for fragmentation as well as σ and κ. As it is still based on a least squares optimisation, model and observation errors are not rigorously examined, rather overall errors are given as the standard deviation of residuals. The amount of manual input required also limits the number of fireballs that may be analysed. The DFN observed over 300 fireball events in 2015 over its 2.5 million km^2 double station viewing area. This continental scale deployment of > 50 automated observatories has been possible by the low cost of each system. At this time, there is no expensive, high voltage photomultiplier tube to measure fireball brightnesses. A trajectory analysis approach that is able to determine meteoroid parameters without a light curve, and which can be automated, will allow an unbiased evaluation of all events.

Very few models exist that enable the reduction of fireball data without a light curve, a photometrically determined mass or assumptions of key trajectory parameters. The method of Gritsevich (2009) solves for two dimensionless parameters rather than multiple unknown trajectory parameters. This still requires an initial accurate velocity and struggles with highly scattered datasets (Sansom et al., 2015). The various Kalman filtering methods used by Sansom et al. (2015) and Sansom et al. (2016) are fully automated techniques of determining the statistical likelihood of meteoroid state throughout bright flight, and allow a robust analysis of observation and model errors. As with previous dynamical approaches to fireball modelling, these require a pre-determined initial parameter set, withholding a general solution. To remove this limitation and fully analyse the statistical likelihood of the final state of a meteoroid given a range of likely initial states, we can use a method that combines a Monte Carlo (MC) approach to the filtering problem- a particle filter (Gordon et al., 1993). Simply, a ’cloud’ of particles are initiated with state values determined by a probability function. The ’cloud’ will be denser where probabilities are higher. Particles are propagated forward in time according to the state equations and weighted according to an observation. A new generation of particles are *resampled* from the existing pool, based on their weighting, and particles that are of low probability are preferentially removed.

The Bunburra Rockhole fireball was observed over the Australian outback by the DFN in 2007, and produced the network's first recovered meteorite (Spurný et al., 2012). An extended Kalman filter (Sansom et al., 2015) and an unscented Kalman filter (Sansom et al., 2016) have been used to model the Bunburra Rockhole fireball given a set of starting parameters. Neither filters explicitly include gross fragmentation, however Sansom et al. (2016) applied two Unscented Kalman filters in an Interactive Multiple Model to determine likely periods of fragmentation. Here we will examine the suitability of this sequential Monte Carlo technique for modelling fireball meteoroid trajectories using the Bunburra Rockhole fireball dataset.

BAYESIAN STATE-SPACE ESTIMATION

The technique used in this paper for estimating meteoroid parameters is one of a broader class of techniques known as Bayesian state-space methods. These methods involve encapsulating the knowledge of a system based on its *state*, given by the vector $\mathbf{x}$. The state of an object could be its position and velocity, for example. The probability of the object being in state $\mathbf{x}$ at time instant t_k is represented as the conditional probability density function

$$p(\mathbf{x}_k|\mathbf{z}_{1:k}), \tag{4.1}$$

where $\mathbf{z}_k$ is the observation of the system made at time t_k and $\mathbf{z}_{1:k}$ is the history of all observations up until time t_k.

The calculation of (4.1) is achieved recursively through the application of Bayes' rule

$$p(\mathbf{x}_k|\mathbf{z}_{1:k}) = \frac{p(\mathbf{z}_k|\mathbf{x}_k)p(\mathbf{x}_k|\mathbf{z}_{1:k-1})}{p(\mathbf{z}_k|\mathbf{z}_{1:k-1})}. \tag{4.2}$$

The terms in the numerator of (4.2) are defined through the *state-space equations*, while the denominator can simply be considered as a normalising constant.

There are three state-space equations. The state *prior* initialises the recursion and encapsulates all prior information about the state of the system

$$p(\mathbf{x}_0). \tag{4.3}$$

The *measurement equation* relates the observations (e.g. position) to the state of the system (e.g. position and velocity)

$$\mathbf{z}_k = h(\mathbf{x}_k, \mathbf{w}_k), \tag{4.4}$$

where $\mathbf{w}_k$ is a stochastic noise process with known distribution. Equation (4.4) defines the *likelihood function*, $p(\mathbf{z}_k|\mathbf{x}_k)$, which is the first term in the numerator of (4.2). The *process equation* models how the state evolves in discrete time

$$\mathbf{x}_{k+1} = f(\mathbf{x}_k, \mathbf{u}_k), \tag{4.5}$$

where $\mathbf{u}_k$ is another noise process with known distribution. Equation (4.5) defines the transition density $p(\mathbf{x}_{k+1}|\mathbf{x}_k)$, which is incorporated into the second term in the numerator of (4.2) through the Chapman-Kolmogorov equation (Jazwinski, 1970)

$$p(\mathbf{x}_k|\mathbf{z}_{1:k-1}) = \int p(\mathbf{x}_k|\mathbf{x}_{k-1})p(\mathbf{x}_{k-1}|\mathbf{z}_{1:k-1})d\mathbf{x}_{k-1}. \tag{4.6}$$

METEOROID STATE-SPACE EQUATIONS

This section outlines the state-space equations chosen to model the motion and measurement of a meteoroid process for the purposes of this paper. The specific parameters used in the model to estimate the trajectory characteristics of the Bunburra Rockhole data-set are given in Section 4.5.

The state that defines the meteoroid system includes the physical parameters of motion, as well as trajectory parameters σ and κ;

$$\mathbf{x}_k = \left[\begin{array}{c|l} l_k & \text{position} \\ v_k & \text{velocity} \\ m_k & \text{mass} \\ \sigma_k & \text{ablation parameter} \\ \kappa_k & \text{shape-density parameter,} \end{array}\right. \tag{4.7}$$

where the position is measured along a pre-defined path produced by triangulating observations from several imaging sensors.

The measurement equation (4.4) is given by

$$\mathbf{z}_k = H\mathbf{x}_k + \mathbf{w}_k, \tag{4.8}$$

where the measurement matrix is

$$H = \begin{bmatrix} 1 & 0 & 0 & 0 & 0 \end{bmatrix} \tag{4.9}$$

and the measurement noise process, $\mathbf{w}_k$, is Gaussian with zero mean and variance R_k.

As a meteoroid passes through the atmosphere, its behaviour can be modelled by the aerodynamic equations from the single body theory of meteoroid entry (Hoppe, 1937; Baldwin and Sheaffer, 1971) (4.11), which uses atmospheric densities, ρ_a, acquired using the NRLMSISE-00 atmospheric model (Picone et al., 2002), local acceleration due to gravity, g, and entry angle from horizontal, γ_e. It is natural to model the change of meteoroid state as a continuous-time differential equation

$$\dot{\mathbf{x}} = f_c(\mathbf{x}) + \mathbf{u}_c, \tag{4.10}$$

where $f_c(\mathbf{x})$ is defined using

$$\frac{dl}{dt} = v \tag{4.11a}$$

$$\frac{dv}{dt} = -\frac{1}{2}\frac{c_d A \rho_a}{\rho_m^{2/3}} v^2 m^{(\mu-1)} + g \sin\gamma_e \qquad = -\kappa\rho_a v^2 m^{(\mu-1)} + g\sin\gamma_e \tag{4.11b}$$

$$\frac{dm}{dt} = -\frac{1}{2}\frac{c_h A \rho_a}{H^*} v^3 m^{\mu} \qquad = -\sigma\kappa\rho_a v^3 m^{\mu} \tag{4.11c}$$

$$\frac{d\sigma}{dt} = 0 \tag{4.11d}$$

$$\frac{d\kappa}{dt} = 0, \tag{4.11e}$$

and the continuous-time process noise, $\mathbf{u}_c$, is Gaussian with zero mean and covariance $\mathbf{Q}_c$. Time integration of (4.10) is needed to arrive at the form required by the filtering state-space equation (4.5). In this case

$$\mathbf{x}_{k+1} = \int_{t_k}^{t_{k+1}} f_c(\mathbf{x})\, dt + \mathbf{u}_k. \tag{4.12}$$

Due to the non-linearities of (4.11) the discrete-time process noise, $\mathbf{u}_k$, is not Gaussian, but can be closely approximated by Gaussian noise with zero mean and covariance

$$\mathbf{Q}_k = \int_{t_k}^{t_{k+1}} e^{Ft}\, \mathbf{Q}_c\, e^{F^T t}\, dt \tag{4.13}$$

(Grewal and Andrews, 1993), where the matrix F is the linearised form of the process equation

$$F = \frac{\partial f_c(\mathbf{x})}{\partial \mathbf{x}}. \tag{4.14}$$

Due to the form of the nonlinear functions (4.11), the integrations required by (4.12) and (4.13) cannot be found analytically. Numerical methods are used to calculate the integrals.

PARTICLE FILTER

There are a range of methods for finding the distribution of $\mathbf{x}_k$ by solving (4.2). The applicability of the method depends on the form of the state-space equations. If the measurement function and process function are linear and all the noise and prior distributions are Gaussian, then the solution to (4.2) can be found analytically. This solution is known as the Kalman Filter (Grewal and Andrews, 1993). In the case where the equations are non-linear or the distributions are non-Gaussian, such as the single body equations for modelling meteoroid trajectory (4.11), there are no exact solutions and approximations are required.

The Extended Kalman Filter (EKF) (Sansom et al., 2015) approximates the noise distributions as Gaussian and finds a linear approximation to the process equations. The Unscented Kalman Filter (Sansom et al., 2016) approximates the posterior distribution as a Gaussian, but avoids approximating the measurement or process equations through a method of statistical linearisation (Särkkä, 2007).

A particle filter does not require any assumptions about the form of the state equations or have any limitations on the noise distributions. This flexibility is achieved by representing the posterior density (4.2) as a set of N_s weighted particles, which are simply points in the state-space (Gordon et al., 1993; Arulampalam et al., 2002). The ith random particle at time t_k is represented by its state, $\mathbf{x}_k^i$, and weight, w_k^i

$$\{\mathbf{x}_k^i, w_k^i\} \quad i = 1, ..., N_s. \tag{4.15}$$

Weights are normalised so that

$$\sum_{i}^{N_s} w_k^i = 1. \tag{4.16}$$

The probability distribution of the state is approximated by this set of weighted particles

$$p(\mathbf{x}_k|\mathbf{z}_{1:k}) \approx \sum_{i}^{N_s} \delta(\mathbf{x}_k - \mathbf{x}_k^i) w_k^i, \tag{4.17}$$

where $\delta(\mathbf{y})$ is the Dirac delta function, defined such that

$$\delta(\mathbf{y}) = \begin{cases} 1 & \mathbf{y} = 0 \\ 0 & \text{otherwise.} \end{cases} \tag{4.18}$$

Statistics can be computed on this set of particles, for example the mean of the distribution at any time t_k is approximated by

$$\hat{\mathbf{x}}_k = \sum_{i}^{N_s} w_k^i \mathbf{x}_k^i, \tag{4.19}$$

with the state covariance calculated as

$$Cov(\mathbf{x}_k) = \sum_{i}^{N_s} w_k^i (\mathbf{x}_k^i - \hat{\mathbf{x}}_k)(\mathbf{x}_k^i - \hat{\mathbf{x}}_k)^T. \tag{4.20}$$

There are strong similarities between the implementation of a particle filter and the simpler Kalman filter. Both follow the three steps

1. Initialisation: start the filter with a known prior distribution, $p(\mathbf{x}_0)$
2. Prediction: propagate the distribution from time $k-1$ to time k using the process equation (4.5)

3. Update: use the measurement equation (4.4) to update the predicted distribution with the measurement information, producing the posterior distribution at time k, $p(\mathbf{x}_k|\mathbf{z}_{1:k})$

The Kalman filter achieves these steps by exact analytic equations which manipulate the mean and covariance of the distribution at each step. On the other hand the particle filter proceeds through calculation on each of the particles individually.

To initialise the particle filter, a set of particles are randomly sampled from the prior distribution, $p(\mathbf{x}_0)$, and weighted equally as $w_0^i = \frac{1}{N_s}$.

In the prediction step each particle is propagated forward in time via the process equation (4.12). To incorporate the uncertainty of the system, a sample from the process noise, u_k, is randomly generated for each particle. Using the process equation to propagate the particles results in the simplest form of the filter. The particle filter literature generalises this through importance sampling, where an arbitrary proposal distribution can be used, instead of the process equation (Arulampalam et al., 2002). Sophisticated proposal distributions can make a particle filter implementation more efficient (require fewer particles), but they have not been investigated for this application.

The update step adjusts the weight of each particle. The weight is obtained by evaluating the likelihood function for each particle

$$\tilde{w}_k^i = p(\mathbf{z}_k|\mathbf{x}_k^i)w_{k-1}^i. \tag{4.21}$$

The weights are then normalised to satisfy (4.16)

$$w_k^i = \frac{\tilde{w}_k^i}{\sum_i^{N_s} \tilde{w}_k^i}. \tag{4.22}$$

Over time the particle weights can transfer to a few select particles, thereby updating insignificant particles at the expense of computing power (Arulampalam et al., 2002). This is known as the degeneracy problem and equation (4.23) gives an approximate measure of particle effectiveness that can be used to assess the severity of the issue (Arulampalam et al., 2002).

$$\hat{N}_{\text{eff}} = \left(\sum_{i}^{N_s} (w_k^i)^2 \right)^{-1} \tag{4.23}$$

The degeneracy problem can be addressed by resampling the data after weights have been calculated. A new population of particles are generated from the current sample pool based on given weightings; the objective being to preferentially remove samples of lower weights. The probability of resampling any given particle i is w_k^i. The optional resampling step is taken if the number of effective particles drops below some threshold. After resampling all of the particle weights are set to $1/N_s$.

PARTICLE FILTER PARAMETERS FOR A METEOROID TRAJECTORY

Dedicated fireball networks, such as the DFN, capture fireball events from multiple locations, providing triangulated position observations with time. This also enables a rough calculation of velocities throughout the trajectory.

INITIALISATION

When initialising the state prior for the set of N_s particles at the start of the luminous trajectory (t_0), the initial position and, to an extent, the initial veloc-

TABLE 4.1: Describes the method used by the particle filter to initialise state parameters for each particle. A random selection is made for each value using either a Gaussian probability density function (PDF) (mean and standard deviation given), a uniform PDF within a given value range or a multi-modal distribution in the case of bulk density.

parameter to be initiated	**method used**
l_0	random choice based on Gaussian $\mathcal{N}(0, 10\,\mathrm{m})$ (from triangulation errors)
v_0	random choice based on Gaussian $\mathcal{N}(v_0, 500\,\mathrm{m\,s^{-1}})$ (from triangulation errors)
m_0	random choice from 0 to m_0^{max} (kg)
σ	random choice between 0.001 to 0.05 $\mathrm{s^2\,km^{-2}}$ (from Ceplecha et al. (1998) for asteroidal material)
κ	c_d - random choice based on Gaussian $\mathcal{N}(1.3, 0.3)$ (based on aerodynamic drag values from Zhdan et al. 2007) A - random choice based on Gaussian $\mathcal{N}(1.4, 0.33)$ (close to spherical values) ρ_m - the PDF representing meteorite bulk densities is multi-modal. To fully represent this distribution, initialisation is performed in two stages. First, a random choice of meteorite type is made based on recovered percentages (80 % chondrites, 11 % achondrites, 2 % stony-iron, 5 % iron, 2% cometary; Grady 2000). Second, a random choice of bulk density is made based on the Gaussian PDF representing chosen meteorite type; chondrites - $\mathcal{N}(2700, 420)$[1]; achondrites - $\mathcal{N}(3100, 133)$[1]; stony-iron - $\mathcal{N}(4500, 133)$[1]; iron - $\mathcal{N}(7500, 167)$[2]; cometary - $\mathcal{N}(850, 117)$ [3].

---

[1] after Britt and Consolmagno (2003)

[2] after Consolmagno S.J. and Britt (1998)

[3] after Weissman and Lowry (2008)

ity[2] can be reasonably well constrained. The other state parameters, m, σ, κ, however are not directly observable. To explore the data space and determine likely values for m_0, as well as constants σ and κ, each particle is initiated with a random value within a given range. The state prior for each particle is initialised according to Table 4.1, with m_0^{min} in all cases set to 0.5 kg.

PREDICTION

At every observation time, t_k, the state of each particle is evaluated using the system model (4.10). $\mathbf{Q}_c$ values used here to represent the continuous process noise in the given model for meteoroid trajectories are given by (4.24). The diagonal elements of $\mathbf{Q}_c$ in (4.24) are the variance values for dl/dt, dv/dt, dm/dt, $d\sigma/dt$, $d\kappa/dt$ respectively. The uncertainty in position and velocity are introduced through noise in the acceleration model 4.11b, and the variance for dl/dt for this process model is therefore set to $0\,m\,s^{-1}$. The other model equations however are not able to represent the system in its entirety; complications, such as fragmentation, affect all other state process models. At this stage, we assume that the shape density and ablation parameters will not change dramatically over the meteoroid flight and are attributed small process noise values. There is a high uncertainty in the mass loss for the single-body ablation model 4.11c and so a large range of masses are allowed to be explored by the particles. The process noise in mass is a multiple of the mass in order to keep it within a consistent order of magnitude. The discrete process noise, $\mathbf{Q}_k$, is calculated at every time step following (4.13). To improve compute time of this method, the non-linear integration (4.12) of all N_s particles, and their associated $\mathbf{Q}_k$, is

---

[2] Determining v_{inf} - or the velocity with which a body entered the Earth's atmosphere, as opposed to the 'initial' velocity that it has when its luminous trajectory is first observed, can be determined using reverse integration methods from the start of the luminous trajectory back to beyond the Earth's sphere of influence (e.g. Trigo-Rodriguez et al. 2015). This is done by the DFN data reduction process as part of orbital modelling. For the larger objects that generate fireballs (and that are the focus of this work) the difference between v_{inf} and v_0 is likely to be small, however a detailed discussion is outside the scope of this paper as the method described in this work (in accordance with others in the literature) model meteoroid bright flight only.

performed simultaneously using parallel multiprocessing.

$$\mathbf{Q}_c = \begin{bmatrix} (0\,\mathrm{m\,s^{-1}})^2 & 0 & 0 & 0 & 0 \\ 0 & (75\,\mathrm{m\,s^{-2}})^2 & 0 & 0 & 0 \\ 0 & 0 & (0.2 \times m_k\ \mathrm{kg\,s^{-1}})^2 & 0 & 0 \\ 0 & 0 & 0 & (10^{-4}\ \mathrm{s\,km^{-2}})^2 & 0 \\ 0 & 0 & 0 & 0 & (10^{-5}\ \mathrm{m^2\,kg^{-2/3}\,s^{-1}})^2 \end{bmatrix} \tag{4.24}$$

UPDATE

The triangulated position of the meteoroid along the trajectory at time k is the observation measurement $\mathbf{z}_k$. The weight $(\tilde{w}_k^i)$ for each particle, $\mathbf{x}_k^i$ is calculated using a one dimension Gaussian probability distribution function

$$p(\mathbf{z}_k|\mathbf{x}_k^i) = \frac{1}{\sqrt{2R_k\pi}} e^{-\frac{(\mathbf{z}_k - \mathbf{H}\mathbf{x}_k^i)^2}{2R_k}} \tag{4.25}$$

in (4.21), with the observation noise having a variance $R_k = (100\,\mathrm{m})^2$. This is based on errors in timing and triangulated position, reflecting the accuracy of the data set being used.

In order to avoid degeneracy in the particle set, we have use the stratified resampling method described by Arulampalam et al. (2002) after each update step.

USING A PARTICLE FILTER TO PREDICT A METEOROID TRAJECTORY

The data acquired by Spurný et al. (2012) for the Bunburra Rockhole fireball is used to test the suitability of the particle filter in estimating the state of a meteoroid during atmospheric entry. The Bunburra Rockhole dataset consists of 113 published observations of position with time along the trajectory. Note that no observation data were published between $t = 0.0$ s and $t = 0.1899$ s or from $t = 5.3165$ s to $t = 5.4589$ s. Our modelling will use times relative to $t_0 = 0.1899$ s along the trajectory. A particle filter is run using set of 10,000 particles ($N_s = 10,000$). Particles are initiated according to Table 4.1 with m_0^{max} set to 2,000 kg.

Figure 4.1 shows all the resulting particle masses with weights > 0 from t_0 to t_{end}. The range of σ and κ values used to initiate each particle results in a variety of predicted trajectory 'paths'.

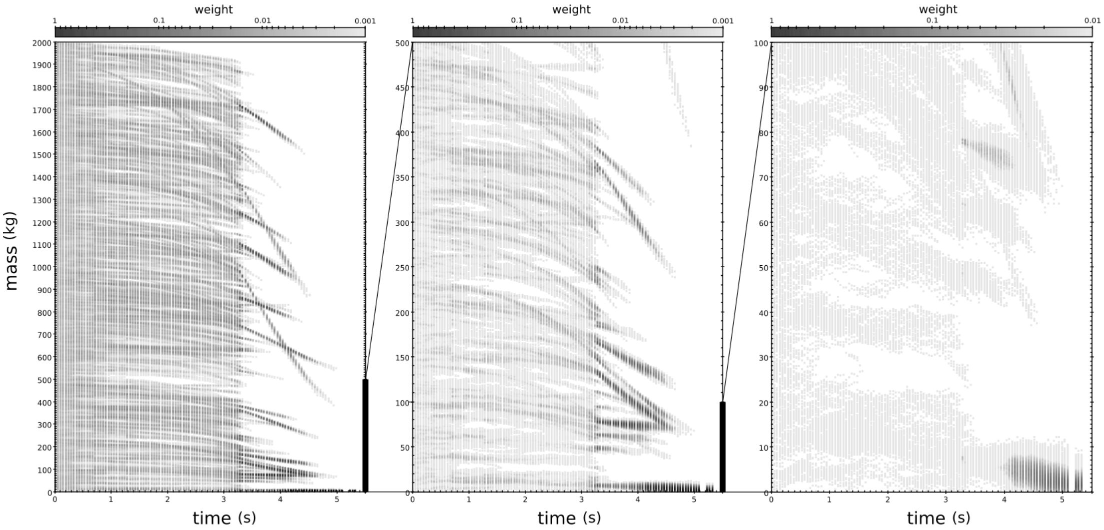

FIGURE 4.1: Mass estimates for particles, with $w_k^i > 0$, produced by the particle filter where $N_s = 10,000$, $m_0^{max} = 2000$ kg were used and $\mathbf{Q}_c$ given by (4.24). Colour scale is additive; weights of particles plotted in the same location are summed. Note the change in colour scale in the third frame to highlight t_{end} weightings. At $t = 4.9$ s all particles with a weight greater than zero have a mass of 11 kg or lower. Times correspond to the seconds since the 2nd recorded dash of the Bunburra Rockhole fireball; $t_0 = 0.1899$ s into the trajectory. It is noticeable at $t_k = 3.32$ s that there is a drastic reduction in the number of particle 'paths' that fit the observational data. The parameter space after this time is much more constrained.

To aid in understanding the different trajectories predicted by the particle filter, five particles at t_0 have been selected to discuss ($\mathbf{x}_0^j$ given in Table 4.2). Figure 4.2 highlights these particles, $\mathbf{x}_0^{a-e}$, along with all particles that are generated from them at later time steps (either by propagation from t_{k-1} or resampling at t_k).

TABLE 4.2: The state of five particles at t_0 are shown. All future particles resampled from these are highlighted in Figure 4.2 according to the colour given here.

$\mathbf{x}_0^j$	l_0 (m)	v_0 ($\mathrm{km\,s^{-1}}$)	m_0 (kg)	σ_0 ($\mathrm{s^2\,km^{-2}}$)	κ_0 (SI)	reference colour in Figure 4.2
$\mathbf{x}_0^a$	-1.57	12.80	10.1	0.022	0.0083	blue
$\mathbf{x}_0^b$	-18.60	12.88	14.3	0.020	0.0058	green
$\mathbf{x}_0^c$	5.00	12.48	176.2	0.021	0.0039	red
$\mathbf{x}_0^d$	-17.19	12.96	212.1	0.037	0.0083	dark orange
$\mathbf{x}_0^e$	12.41	13.10	234.0	0.041	0.0133	light orange

The variation in σ (Figure 4.2b) and κ (Figure 4.2c) values with time is due to the addition of process noise, $\mathbf{u}_k$, in (4.10). As this noise is random Gaussian, it allows small variations between identical resampled particles that would have originally shared equal values. Areas of greater particle density are characteristic of higher probability states.

Orange particles in Figure 4.2 originate from $\mathbf{x}_0^e$. The steep change in mass with time (Figure 4.2(a) is due to the high σ (Figure 4.2(b)) and κ (Figure 4.2(c) values with which they were initiated. Particles that no longer fit the observed data are preferentially removed by the resampling process and their 'path' discontinues in Figure 4.2. Although particles originating from $\mathbf{x}_0^{c-e}$ were initiated with diverse σ (Figure 4.2b) and κ (Figure 4.2c) values, they, along with all other particles with $m_0^i > 27\,\mathrm{kg}$ have insignificant weight past 5.0 seconds. A visual comparison of predicted particle velocities with velocities calculated from position measurements is shown in Figure 4.2d. The 'survival' of $\mathbf{x}_0^{a,b}$ to t_{end} is due to their higher w_k^i values indicating superior fits to the observations (and visually noticeable in Figure 4.2d).

The final trajectory parameters of the Bunburra Rockhole meteoroid have been previously determined by Spurný et al. (2012) using the dynamic gross

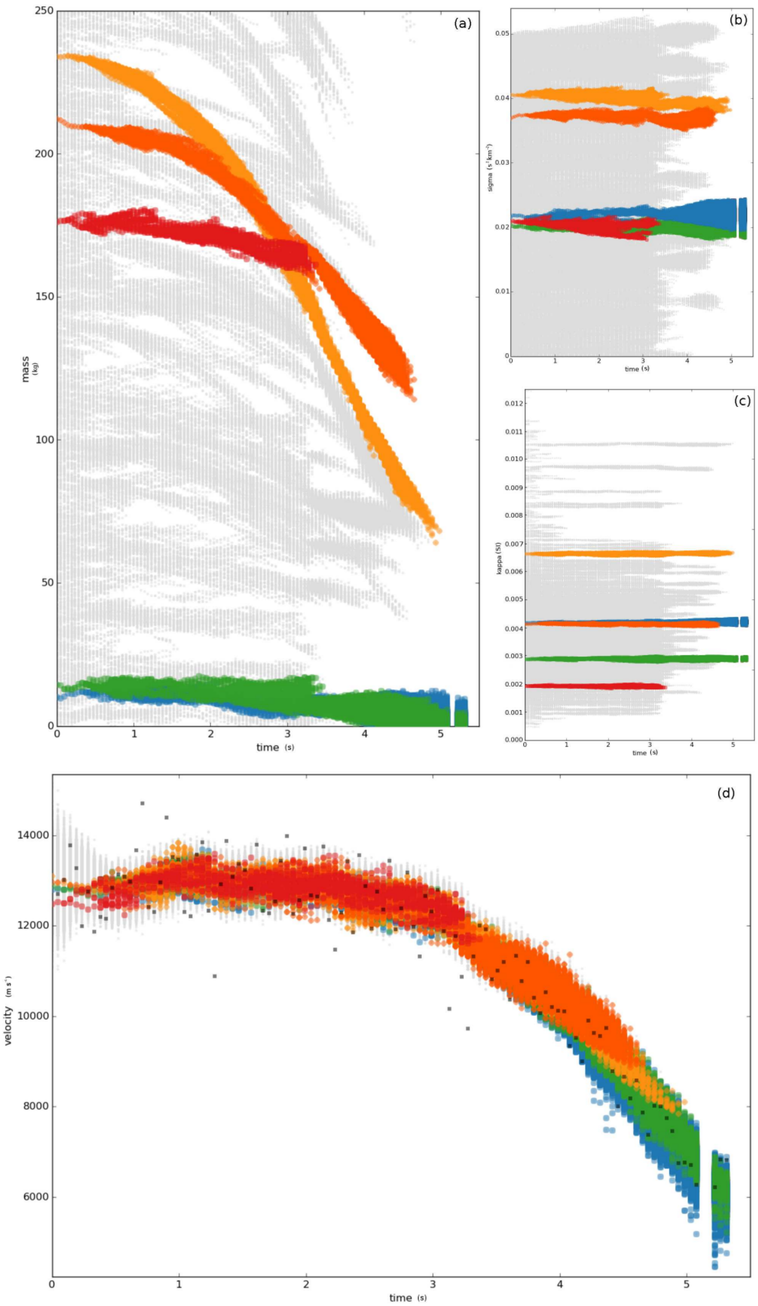

FIGURE 4.2: Particle states estimated by the particle filter. (a) Predicted mass with time. (b) Predicted ablation parameter,σ with time. (c) Predicted shape density, κ, with time. (d) Predicted velocity with time. Particles originating from $\mathbf{x}_0^{a-e}$ (Table 4.2) are highlighted with reference colours given in Table 4.2). Note times correspond to seconds since the 2nd recorded dash of the Bunburra Rockhole fireball; $t_0 = 0.1899$ s into the trajectory. It is noticeable at $t_k = 3.32$ s that there is a drastic reduction in the number of particle 'paths' that fit the observational data. The parameter space after this time is much more constrained.

fragmentation model (GFM) of Ceplecha et al. (1993) and the meteoroid fragmentation model (MFM) of Ceplecha and Revelle (2005) which integrates fireball brightness with the dynamics (Table 4.3). Both the GFM and MFM depend upon model assumptions. The later not only requires an initial entry mass, but also a manually pre-defined fragmentation pattern based on the light curve (Ceplecha and Revelle, 2005). Errors given by these models relate to the standard deviation of the residuals between modelled and measured observations; observational uncertainties, assumptions made in the model and model parameters are not propagated.

The Kalman filter methods applied by Sansom et al. (2015) and Sansom et al. (2016) to meteoroid trajectory modelling perform a comprehensive analysis of the errors of both model and observations but share the limitations of previous models in requiring a single set of initial entry parameters to be pre-determined.

The statistical approach of the particle filter is not limited to any one set of input parameters. It encapsulates all prior knowledge of the parameter space by exploring the full range of plausible parameter values to produce an unbiased analysis. Given that model and observation uncertainties are incorporated and propagated, this method provides a statistically robust final state estimate which is no longer dependent on any single set of assumed input parameters, providing a more realistic understanding of real-world variability. The independence of the particle filter and lack of manual input enables full automation of this method. The spread of final particle states at t_{end} can be summarised by the weighted mean (4.19) in Table 4.3. Errors are calculated as the square root of the covariance diagonal elements given by Equation (4.20). The ablation parameter is an interesting result. Although the particle filter does not explicitly model fragmentation, Q_c allows for a certain amount of variation in state parameters due to un-modelled processes and inherently includes fragmentation to some extent, without the need for a pre-defined fragmentation pattern (required by MFM; Ceplecha and Revelle 2005). As discussed by Ceplecha and

TABLE 4.3: Mean final state values estimated by the particle filter (4.19), alongside published values. Errors given by all previous methods reflect only model errors within the given initial input assumptions given. The GFM and MFM methods do not consider observation uncertainties (Ceplecha and Revelle, 2005). The particle filter errors are calculated as $\sqrt{Var(\hat{x}_k)}$ given by (4.20), and alone gives a fully inclusive analysis of trajectory model and observation uncertainties to provide a more realistic understanding of real-world variability.

	l_{end} (km)	v_{end} (km s^{-1})	m_{end} (kg)	σ_{end} (s^2 km^{-2})	κ_{end} (SI)
GFM [1]			1.5 ±0.2	0.0331 ±0.0007 (apparent)	
MFM [1]		5.77 ±0.04	1.1	0.002 ±0.001/0.004 (intrinsic)	0.0035
Dynamic [2] optimisation	60.07	6.109	2.36	0.0371 (apparent)	0.0062
EKF [2]	60.03 ±0.062	6.05 ±0.24	2.30 ±1.63		
UKF [3]	60.04 ±0.058	6.10 ±0.20	2.88 ±1.04		
IMM [3]	60.01 ±0.007	5.90 ±0.06	1.32 ±0.49		
Particle filter	59.89 ±0.038	6.03 ±0.22	2.16 ±1.33	0.02 ±0.001 (apparent)	0.0042 ±0.0005

Revelle (2005), the intrinsic value of the ablation parameter remains constant throughout the trajectory regardless of fragmentation. When fragmentation is not modelled explicitly, variations in the ablation parameter appear to occur and must therefore be expressed as the *apparent* ablation parameter. The GFM produces an *apparent* σ whereas the MFM, as it incorporates the light curve, is able to define the *intrinsic* σ. The value determined using the particle filter is slightly lower than the apparent σ of the GFM and it is therefore plausible that we can use this difference to quantify the extent to which fragmentation is included in the final state estimate.

Using a particle filter the state estimates at each time step are iteratively updated based on the past data; future observations are not included. The final states alone result from processing all observations. As a predicted particle becomes inconsistent with the observations, it becomes an unlikely scenario for future times but it does not mean this original path can be discounted. It is noticeable at $t_k = 3.32\,\mathrm{s}$ that there is a drastic reduction in the number of particle 'paths' that fit the observational data. The parameter space after this time is much more constrained. All particles at t_{end} originate from particles with $\mathbf{x}_0 < 27\,\mathrm{kg}$; these particles are consistent with both parts of the trajectory displaying no dramatic change in mass. It is possible that particles of initially higher mass are discontinued in favour of lower mass scenarios as a result of gross fragmentation reflected in the observation data. Without including all the data at every time-step, the most likely state 'path' for the entire trajectory cannot be constrained; we cannot distinguish the full particle history.

In order to distinguish likely initial masses, we need to be able to explore drastic changes in mass. The interactive multiple model (IMM) smoother as described by Sansom et al. (2016) has this capability and uses all observational data at each time step. It however requires a single pre-defined set of initial parameters. This is a well suited complementary method to our current implementation of a particle filter. The particle filter framework however is flexible enough to incorporate dynamic models that explicitly capture gross fragmentation events. Future work will explore more sophisticated dynamic models as well as particle filter smoothing to reconstruct the full meteoroid trajectory.

Including brightness as a state in trajectory modelling would also provide an additional observation with which to weight particles. As brightness is linked to mass, its addition would not only improve state estimates, but would inherently include information on fragmentation.

CONCLUSION

The use of a particle filter to approximate fireball trajectories provides a statistical analysis of the meteoroid state, including unobservable trajectory parameters. This is the first approach of its kind in this field. Other non-linear filtering algorithms such as the Extended Kalman filter (Sansom et al., 2015) and the Unscented Kalman filter (Sansom et al., 2016), as well as other least-squares approaches (Ceplecha et al., 1993; Ceplecha and Revelle, 2005), require a pre-determined set of initial parameters to statistically analyse the trajectory of a meteoroid. The iterative Monte Carlo simulations of a particle filter is not only capable of automating the analysis of fireball trajectories, but is able to do so without the need for limiting input parameters to single assumed values, rather it encapsulates all prior knowledge of the parameter space, to produce an unbiased analysis. The adaptive filter approach uses the observations of the meteoroid's position as it travels through the Earth's atmosphere to update state estimates. Predicted positions similar to those observed are given a higher weighting and are preferentially resampled at the next time step. This gives a final state estimate (Table 4.3) with robust error propagation of uncertainties in the initial parameters, observations and the dynamic model (e.g. unpredictable gross fragmentation events). Even though trajectory parameters σ and κ are not currently set to vary systematically with time (noise is added to create diversity between resampled particles to avoid degeneracy only), a stochastic approach to their determination has not previously been conducted. Incorporating brightness as an additional state will provide supplementary data and improve estimates. This method currently allows an automated dynamic analysis of fireball trajectories.

ACKNOWLEDGEMENTS

This work was funded by the Australian Research Council as part of the Australian Laureate Fellowship scheme.

REFERENCES

Arulampalam, M. S., Maskell, S., Gordon, N., and Clapp, T., 2002. A tutorial on particle filters for online nonlinear/non-Gaussian Bayesian tracking. *IEEE Transactions on Signal Processing*, 50(2):174–188. doi: 10.1109/78.978374.

Baldwin, B. and Sheaffer, Y., 1971. Ablation and breakup of large meteoroids during atmospheric entry. *Journal of Geophysical Research*, 76(19):4653–4668.

Bland, P., Spurný, P., Bevan, A., Howard, K., Towner, M., Benedix, G., Greenwood, R., Shrbený, L., Franchi, I., Deacon, G., et al., 2012. The australian desert fireball network: a new era for planetary science. *Australian Journal of Earth Sciences*, 59(2):177–187.

Borovička, J., Spurný, P., and Brown, P., 2015. Small near-earth asteroids as a source of meteorites. *Asteroids IV*, page 257.

Britt, D. and Consolmagno, G., 2003. Stony meteorite porosities and densities: A review of the data through 2001. *Meteoritics & Planetary Science*, 38(8): 1161–1180. doi: 10.1111/j.1945-5100.2003.tb00305.x.

Bronshten, V. A., 1983. *Physics of Meteoric Phenomena*. Geophysics and Astrophysics Monographs. Reidel, Dordrecht, Netherlands.

Campbell-Brown, M. D. and Koschny, D., 2004. Model of the ablation of faint meteors. *Astronomy and Astrophysics*, 418(2):751–758. doi: 10.1051/0004-6361:20041001-1.

Ceplecha, Z., 1987. Geometric, dynamic, orbital and photometric data on meteoroids from photographic fireball networks. *Bulletin of the Astronomical Institutes of Czechoslovakia*, 38:222–234.

Ceplecha, Z. and Revelle, D. O., 2005. Fragmentation model of meteoroid motion, mass loss, and radiation in the atmosphere. *Meteoritics & Planetary Science*, 40(1):35–54. doi: 10.1111/j.1945-5100.2005.tb00363.x.

Ceplecha, Z., Spurný, P., Borovička, J., and Keclikova, J., 1993. Atmospheric fragmentation of meteoriods. *Astronomy and Astrophysics*, 279:615–626.

Ceplecha, Z., Borovička, J., Elford, W. G., ReVelle, D. O., Hawkes, R. L., Porubčan, V., and Šimek, M., 1998. Meteor Phenomena and Bodies. *Space Science Reviews*, 84(3):327–471. doi: 10.1023/A:1005069928850.

Consolmagno S.J., G. J. and Britt, D. T., 1998. The density and porosity of meteorites from the vatican collection. *Meteoritics & Planetary Science*, 33(6): 1231–1241. doi: 10.1111/j.1945-5100.1998.tb01308.x.

Gordon, N., Salmond, D., and Smith, A., 1993. Novel approach to nonlinear/non-Gaussian Bayesian state estimation. *IEE Proceedings F -Radar and Signal Processing*, 140(2):107. doi: 10.1049/ip-f-2.1993.0015.

Grady, M. M., 2000. *Catalogue of Meteorites*, volume 1. Cambridge University Press, 5 edition.

Grewal, M. S. and Andrews, A. P., 1993. *Kalman filtering: theory and practice.* Prentice-Hall Inc., New Jersey.

Gritsevich, M. I., 2009. Determination of parameters of meteor bodies based on flight observational data. *Advances in Space Research*, 44(3):323–334. doi: 10.1016/j.asr.2009.03.030.

Harris, A. W., 2012. The value of enhanced neo surveys. In *AAS/Division for Planetary Sciences Meeting Abstracts*, volume 44.

Hoppe, J., 1937. Die physikalischen Vorgänge beim Eindringen meteoritischer Körper in die Erdatmosphäre. *Astronomische Nachrichten*, 262(10):169–198.

Howie, R., Paxman, J., Bland, P., Towner, M., Sansom, E., and Devillepoix, H., 2017. Submillisecond fireball timing using de Bruijn timecodes. *Meteoritic & Planetary Science.*

Howie, R., Paxman, J., Bland, P., Towner, M., Cupak, M., Sansom, E., and Devillepoix, H., 2017. How to build a continental scale fireball camera network. *Experimental Astronomy*, 43237–266.

Jazwinski, A. H., 1970. *Stochastic Processes and Filtering Theory.* Academic Press, New York.

Kikwaya, J.-B., Campbell-Brown, M. D., and Brown, P. G., 2011. Bulk density of small meteoroids. *Astronomy & Astrophysics*, 530:A113. doi: 10.1051/0004-6361/201116431.

Murray, I. S., Beech, M., Taylor, M. J., Jenniskens, P., and Hawkes, R. L., 2000. Comparison of 1998 and 1999 leonid light curve morphology and meteoroid structure. *Earth, Moon, and Planets*, 82(0):351–367. doi: 10.1023/A:1017003019448.

Picone, J. M., Hedin, A. E., Drob, D. P., and Aikin, A. C., 2002. NRLMSISE-00 empirical model of the atmosphere: Statistical comparisons and scientific issues. *Journal of Geophysical Research: Space Physics (1978–2012)*, 107(A12): 1468.

Revelle, D. O., 2007. NEO fireball diversity: energetics-based entry modeling and analysis techniques. In Milani, A., Valsecchi, G. B., and Vokrouhlicky, D., editors, *Near Earth Objects, Our Celestial Neighbors: Opportunity and Risk*, Proceedings of the International Astronomical Union S236, pages 95–106. Cambridge University Press.

Sansom, E. K., Bland, P. A., Paxman, J., and Towner, M. C., 2015. A novel approach to fireball modeling: The observable and the calculated. *Meteoritics & Planetary Science*, 50(8):1423–1435. doi: 10.1111/maps.12478.

Sansom, E. K., Bland, P. A., Rutten, M. G., Paxman, J., and Towner, M. C., 2016. Filtering meteoroid flights using multiple unscented kalman filters. *The Astronomical Journal*, 152(5):148. doi: 10.3847/0004-6256/152/5/148.

Särkkä, S., 2007. On unscented Kalman filtering for state estimation of continuous-time nonlinear systems. *IEEE Transactions on Automatic Control*, 52(9):1631–1641. doi: 10.1109/TAC.2007.904453.

Spurný, P., Bland, P., Shrbený, L., Borovička, J., Ceplecha, Z., Singelton, A., Bevan, A. W. R., Vaughan, D., Towner, M. C., Mcclafferty, T. P., Toumi, R., and Deacon, G., 2012. The Bunburra Rockhole meteorite fall in SW Australia: Fireball trajectory, luminosity, dynamics, orbit, and impact position from photographic and photoelectric records. *Meteoritics & Planetary Science*, 47(2): 163–185. doi: 10.1111/j.1945-5100.2011.01321.x.

Trigo-Rodriguez, J. M., Lyytinen, E., Gritsevich, M., Moreno-Ibáñez, M., Bottke, W. F., Williams, I., Lupovka, V., Dmitriev, V., Kohout, T., and Grokhovsky, V., 2015. Orbit and dynamic origin of the recently recovered Annama's H5 chondrite. *Monthly Notices of the Royal Astronomical Society*, 449(2):2119–2127.

Weissman, P. R. and Lowry, S. C., 2008. Structure and density of cometary nuclei. *Meteoritics & Planetary Science*, 43(6):1033–1047. doi: 10.1111/j.1945-5100.2008.tb00691.x.

Zhdan, I. A., Stulov, V. P., Stulov, P. V., and Turchak, L. I., 2007. Drag coefficients for bodies of meteorite-like shapes. *Solar System Research*, 41(6):505–508. doi: 10.1134/S0038094607060068.

CHAPTER 5

3D METEOROID TRAJECTORIES

Eleanor K. Sansom[a], Trent Jansen-Sturgeon[a], Mark G. Rutten[b]

[a]Department of Applied Geology, Curtin University, GPO Box U1987, Bentley, Perth, WA 6845, Australia

[b]Defence Science and Technology Group, Edinburgh, SA 5111, Australia

This chapter is laid out as a manuscript to be submitted to Icarus

ABSTRACT

Meteoroid modelling of fireball data typically uses a one dimensional model along a straight-line triangulated trajectory. The assumption of a straight-line trajectory has been considered an acceptable simplification for fireballs, given that gravitational forces are significantly smaller than drag forces, but it has not been rigorously tested. Here we show that it is not valid for the 21 second long fireball captured by the Desert Fireball Network in Australia (event name DN151212). To model this event reliably, the line-of-sight observations need to be incorporated directly. To improve meteoroid modelling and remove the need for a pre-triangulated data set, we define the single body aerodynamic equations in three dimensions and use them in the particle filter approach to fireball modelling presented by Sansom et al. (2017). Modelling fireball camera network data in three dimensions has not previously been attempted. A three dimensional particle filter uses the azimuth and elevation observations of fireball network observatories to update the state of a meteoroid in geocentric cartesian coordinates. In analysing DN151212, the triangulated positions based on a straight-line assumption result in the meteoroid diverging up to $1.3\,\mathrm{km}$ from the calculated observed point. The position estimates of the 3D particle filter are mostly less than $270\,\mathrm{m}$ different (with the maximum mean deviation of $482\,\mathrm{m}$). To put this in context, typically quoted model residuals for a well observed bright fireball are in the range of 20-30m (Spurný et al., 2012). This automated approach adapts to the raw observations, allowing subtleties in the data to be incorporated, while providing a more robust analysis of errors.

INTRODUCTION

When meteoroids pass through the Earth's atmosphere they undergo rapid deceleration. The bright phenomena produced can be characterised by its brightness, from meteor to fireball to bolide (Ceplecha et al., 1998). Dedicated camera networks have been established to observe these phenomenon. Fireballs in particular are significant as they are frequent enough for such networks to capture regularly whilst still having the potential to survive entry and drop meteorites to Earth.

The Desert Fireball Network in Australia observes ~ 1.8 fireballs per night (greater than 3 seconds) over its $2.5 \times 10^6\,\mathrm{km}^2$, double-station viewing area (Howie et al., 2017). This is the largest network to date and the only one in the Southern Hemisphere. Thirty second-long exposures are taken continuously from local sunset to sunrise producing roughly 60 TB of data per month. Reducing this data requires an automated software pipeline. Determining the potential of a fireball to produce a meteorite involves a trajectory analysis of each individual event. The relative position and time of a fireball recorded from multiple locations can be used to triangulate the trajectory of the meteoroid. The object can then be modelled based on the single body theory of meteoroid dynamics – a set of continuous differential equations representing the evolution of a meteoroid's behaviour as it passes through the atmosphere (Hoppe, 1937; Baldwin and Sheaffer, 1971; Stulov et al., 1995):

$$\frac{dl}{dt} = v \tag{5.1a}$$

$$\frac{dv}{dt} = -\kappa \rho_a v^2 m^{(\mu-1)} + g \sin \gamma_e \tag{5.1b}$$

$$\frac{dm}{dt} = -\kappa \sigma \rho_a v^3 m^{\mu}, \tag{5.1c}$$

with trajectory parameters

$$\kappa = \frac{1}{2}\frac{c_d A}{\rho_m^{2/3}} \qquad \text{and} \qquad \sigma = \frac{c_h}{c_d H^*},$$

where the position and velocity along the path of the meteoroid trajectory are l and v respectively and m is the meteoroid mass, γ_e the flight angle from local horizontal, g the local acceleration of gravity, A the shape parameter as described by Bronshten (1983), ρ_m the bulk density of the meteoroid, H^* the enthalpy of sublimation, and c_d and c_h the drag and heat coefficients respectively. μ is the shape change parameter, representing the rotation of the body, here assumed to be 2/3, representing spin rapid enough for ablation to be uniform across the entire surface (Bronshten, 1983). Atmospheric densities, ρ_a, can be calculated using the NRLMSISE-00 atmospheric model (Picone et al., 2002).

This is, however, a simplified theory and does not explicitly include any large disruptions to the body. Furthermore, many of the trajectory parameters are unknown and assumptions must be made, or models used, to determine their values.

Models such as those used by Ceplecha and Revelle (2005) and (Kikwaya et al., 2011) apply a least squares methodology to determine the characteristics of a meteoroid during its flight based on positional observations and light curves. A least squares approach however does not rigorously examine the uncertainties in observations, or the limitations posed by the single body model applied, when evaluating errors.

Even though meteor ablation models (Campbell-Brown and Koschny, 2004; Kikwaya et al., 2011) expand on the single body equations for ablation (5.1) by including thermal fragmentation mechanisms, their application is limited to small meteors (10^{-12} to 4×10^{-5} kg / $10\mu m$ to $2mm$; Campbell-Brown and Koschny 2004). Hydrodynamic numerical models (such as SOVA (Shuvalov, 1999) and the model of Shuvalov and Artemieva (2002)) focus on external processes for modelling the interaction and propagation of shock waves through the atmosphere caused by hypersonic flight of bolides (Artemieva and Shuvalov, 2016). They do not use raw observational data and are computationally expensive procedures (Artemieva and Pierazzo, 2009).

For this reason a simplified approach, such as used by Sansom et al. (2017) (after Ristic et al. 2004), is favourable to model meteoroid atmospheric entry of large fireball network data sets. Although the particle filter technique of Sansom et al. (2017) applies the single body equations as a model, the adaptive approach uses appropriate covariances with observations to incorporate, to some extent, unmodelled processes such as gross fragmentation. The iterative Monte Carlo technique of the particle filter also explores the parameter space, allowing unknown trajectory parameters to be estimated.

When a fireball is captured by multiple Desert Fireball Network remote observatories, each camera image is calibrated using the background star field to determine an astrometric azimuth and elevation for positions along the fireball trail (Devillepoix and Sokolowski, in prep.). This method of calibration accounts well for any effects of atmospheric refraction. Triangulation of these lines-of-sight can give the fireball's trajectory in 3D space. Up to this point, models for characterising meteoroids from fireball network data have been limited to a single dimension along the path of the trajectory. The raw line-of-sight observations from camera observatories are triangulated assuming a straight line (for example McCrosky and Boeschenstein 1965; Spurný et al. 2012; Brown et al. 1994; Hildebrand et al. 2006). Historically, there have been two predominant meteoroid triangulation methods; the method of planes (Ceplecha, 1987) and the straight-line least squares method (Borovička, 1990). The method of planes involves finding the best fit, 2D plane for each observatory that contains both the observatory location and the line-of-sight meteoroid observations. The intersection of multiple planes defines the trajectory; in the case of more than two observatories, this will result in multiple trajectories. The straight-line least squares method on the other hand determines a best fit straight-line radiant for the trajectory from all the raw observations at once. This is done by minimising the angular difference between the observed lines of sight and the closest corresponding point along the radiant trajectory line.

By assuming a straight-line trajectory, this effectively destroys any subtleties in the data by forcing it to fit an oversimplified model. Notably changes due to disruption of the body and to a lesser extent, the effects of gravity, are being disregarded, as well as other unmodelled factors. Gravitational forces act at a greater angle to the trajectory of shallow fireballs, though are significantly smaller than drag forces. The straight-line assumption may be an acceptable simplification for some fireballs, but as we show here, is not always valid and represents an oversimplification that prohibits the model reliably recreating the flight path.

Here we will define the single body equations in three dimensions for the first time and apply them to the particle filter methodology described by Sansom et al. (2017). In doing this, the observations used by the filter to update the state matrix are permitted to be in the form of the raw line-of-sight observations in azimuth and elevation. This drops the simplifying assumption of a straight-line trajectory as particles will be modelled in three dimensional space. Error propagation will be thorough as the filter will consider the different uncertainties in each azimuth and elevation individually as well as consider model process limitations.

The better understanding we have of the final state of a meteoroid, and the uncertainties throughout the modelling phase, the more reliable our predicted fall region will be. This will significantly influence decisions about the feasibility of a ground based search for meteorites.

PARTICLE FILTER MODELLING USING THREE DIMENSIONAL METEOROID FLIGHT

Bayesian state-space methodologies use a vector, $\mathbf{x}$, to represent the *state* of a system. In meteoroid trajectory analysis this includes the motion parameters (position and velocity) as well as trajectory parameters in Equation (5.1).

To use a three dimensional model for flight, we will be dividing positions and velocities into their x, y, z components in Earth centred, Earth fixed (ECEF), geocentric coordinates. The state vector is therefore represented as Equation (5.2) and encapsulates the knowledge of the meteoroid system at a given time t_k.

$$\mathbf{x}_k = \begin{bmatrix} l_{x;k} \\ l_{y;k} \\ l_{z;k} \\ v_{x;k} \\ v_{y;k} \\ v_{z;k} \\ m_k \\ \kappa_k \\ \sigma_k \end{bmatrix} \begin{array}{l} \text{position in X} \\ \text{position in Y} \\ \text{position in Z} \\ \text{velocity in X} \\ \text{velocity in Y} \\ \text{velocity in Z} \\ \text{mass} \\ \text{shape-density parameter} \\ \text{ablation parameter} \end{array} \tag{5.2}$$

This state is determined by assessing the conditional probability density function $p(\mathbf{x}_k|\mathbf{z}_{1:k})$ given an observation $\mathbf{z}_k$ of the system at t_k ($\mathbf{z}_{1:k}$ therefore being the history of all observations from $t_1 : t_k$).

This is achieved through the three state-space equations:

(i) The state prior, $$p(\mathbf{x}_0), \tag{5.3}$$

encapsulates prior knowledge of the state of the system and initialises the recursion.

(ii) The process equation, $$\mathbf{x}_{k+1} = f(\mathbf{x}_k) + \mathbf{u}_k, \tag{5.4}$$

defines the evolution of the state in discrete time, with process noise $\mathbf{u}_k$.

(iii) The measurement equation, $$\mathbf{z}_k = h(\mathbf{x}_k) + \mathbf{w}_k, \tag{5.5}$$

uses the measurement function $h(\mathbf{x}_k)$ to correlate the state of the meteoroid to the given azimuth and elevation measurements from camera observatories. Observation noise, $\mathbf{w}_k$, is assumed to be Gaussian with a mean of zero and covariance $\mathbf{R}_k$ in degrees. Further explanation of the measurement function are detailed in Section 5.2.1.

Although fireball observations are made in discrete time, modelling the meteoroid dynamics is more appropriate using continuous model equations such as (5.1). Continuous-time differential state equations $(f_c(\mathbf{x}))$ may be integrated in order to attain the form needed for the process equation (5.4):

$$\mathbf{x}_{k+1} = \int_{t_k}^{t_{k+1}} f_c(\mathbf{x})\, dt + \mathbf{u}_k. \tag{5.6}$$

Although $f_c(\mathbf{x})$, using the single body equations, is non-linear, the discrete-time process noise, $\mathbf{u}_k$, can be closely approximated by Gaussian noise with zero mean and covariance $\mathbf{Q}_k$. A particle filter is very flexible and requires no constraints on the linearity of state equations, nor the noise distributions (Ristic et al., 2004). This is due to there being no single representation of the state prior, rather a set of N_s weighted particles are used to represent the distribution, similar to a Monte Carlo method.

Each ith particle can be represented at any time t_k by its state, $\mathbf{x}_k^i$, and weight, w_k^i as:

$$\{\mathbf{x}_k^i, w_k^i\} \quad i = 1, ..., N_s, \tag{5.7}$$

with weights normalised as:

$$\sum_i^{N_s} w_k^i = 1. \tag{5.8}$$

The weighted mean of the distribution can be approximated at any time t_k as:

$$\hat{\mathbf{x}}_k = \sum_i^{N_s} w_k^i \mathbf{x}_k^i, \tag{5.9}$$

with covariance

$$\mathrm{Cov}(\mathbf{x}_k) = \sum_i^{N_s} w_k^i (\mathbf{x}_k^i - \hat{\mathbf{x}}_k)(\mathbf{x}_k^i - \hat{\mathbf{x}}_k)^T. \tag{5.10}$$

There are three steps in running a particle filter, similar to other Baysian filtering methods: *initialisation, prediction, update*. A detailed description of applying particle filters to meteoroid trajectories is presented in Sansom et al. (2017). Here we will outline the variations required to allow a particle filter to be performed in three dimensions.

INITIALISATION IN GEOCENTRIC, CARTESIAN COORDINATES

An initial set of particles is required that best represents the state prior (5.3) of the meteoroid system; initialisation in 3D requires an approximate start location. Possible original values for mass, κ and σ can be randomised within theoretical bounds (see Sansom et al. 2017). As the full data set is available at the time of executing the particle filter, the initial position and velocity components may be more accurately estimated from a straight-line least squares triangulation

(Borovička, 1990) of the first handful of multi-station observations. This is achieved by minimising the angular separation, θ, between the observed line-of-sight unit vector from each observatory, $\mathbf{z}^n$, and the line-of-sight to the estimated meteoroid position, $\mathbf{l}$, from the corresponding observatory, $\mathbf{O}^n$ (where $\mathbf{z}^n$, $\mathbf{l}$ and $\mathbf{O}^n$ are in ECEF geocentric coordinate system).

$$\theta = \sqrt{\sum_n \left[\arccos \left(\frac{\mathbf{l} - \mathbf{O}^n}{||\mathbf{l} - \mathbf{O}^n||} \bullet \mathbf{z}^n \right) \right]^2} \tag{5.11}$$

Following this point-wise triangulation, the velocities can be determined by simply taking the difference in position with time: $\mathbf{v}_k = \dfrac{d\mathbf{l}_{k:k+1}}{dt_{k:k+1}}$. Due to the inherent scatter in the initial determined positions and therefore velocities, v_0 may be reasonably well approximated by assuming constant deceleration between the first few multi-station observations and t_0:

$$\mathbf{v}_0 = \mathbf{v}_m - \frac{d\mathbf{v}}{dt} \times t_m, \tag{5.12}$$

where t_m is the time of the first available multi-station observations and the value of $\mathbf{v}_m$ and $\dfrac{d\mathbf{v}}{dt}$ are determined by a linear least squares fit to the scattered velocities.

An initial position may then be roughly approximated by rearranging and integrating (5.12) with respect to time:

$$\mathbf{l}_0 = \mathbf{l}_m - \mathbf{v}_0 t_m - \frac{1}{2} \frac{d\mathbf{v}}{dt} \times {t_m}^2. \tag{5.13}$$

The initialisation of particle state parameters for position and velocity at t_0 is then drawn from a Gaussian distribution shown by

$$\mathbf{l}_0^i = \mathcal{N}(\mathbf{l}_0; \mathbf{P}_{\mathbf{l};0}) \qquad \mathbf{v}_0^i = \mathcal{N}(\mathbf{v}_0; \mathbf{P}_{\mathbf{v};0}) \qquad i = 1, ..., N_s \tag{5.14}$$

where mean values of the $\mathbf{l}_0$ and $\mathbf{v}_0$ vectors are calculated as described above, and covariance values, $\mathbf{P}_0$, are determined by the uncertainty in this least squares fit and may vary for each directional component.

The mass, ablation and shape-density parameters are initialised as given in Table 1 of Sansom et al. (2017) and range typical values. All particles are initially weighted equally as $w_0^i = \frac{1}{N_s}$.

FILTER PREDICTION USING THREE DIMENSIONAL STATE EQUATIONS

Recursion commences after initialisation, beginning with a forward prediction of particles from t_k to t_{k+1} by the process equation (5.4).

The change in trajectory parameters κ and σ with time is not well known and at this stage is assumed to be nil:

$$\frac{d\kappa}{dt} = \frac{d\sigma}{dt} = 0. \tag{5.15}$$

In order to analyse the full trajectory in 3D, the differential equations of motion (5.1a, 5.1b) must be split into their vector components:

$$\frac{d\mathbf{l}}{dt} = \mathbf{v} \tag{5.16a}$$

$$\frac{d\mathbf{v}}{dt} = -\kappa \rho_a m^{(\mu-1)} ||\mathbf{v}|| \mathbf{v} + \mathbf{g} \tag{5.16b}$$

$$\frac{dm}{dt} = -\kappa \sigma \rho_a m^{2/3} ||\mathbf{v}||^3, \tag{5.16c}$$

where **l** and **v** are the position and velocity vectors and $||\mathbf{v}||$ is its magnitude.

This gives the continuous-time state equation for a meteoroid travelling through the atmosphere in 3D as:

$$f_c(\mathbf{x}) = \left[\frac{dl_x}{dt}, \frac{dl_y}{dt}, \frac{dl_z}{dt}, \frac{dv_x}{dt}, \frac{dv_y}{dt}, \frac{dv_z}{dt}, \frac{dm}{dt}, \frac{d\kappa}{dt}, \frac{d\sigma}{dt} \right]. \tag{5.17}$$

with the continuous-time Gaussian process noise $\mathbf{u}_c$ of zero mean and covariance $\mathbf{Q}_c$. The discrete-time process noise covariance, $\mathbf{Q}_k$ can be approximated as

$$\mathbf{Q}_k = \int_{t_k}^{t_{k+1}} e^{Ft}\, \mathbf{Q}_c\, e^{F^T t}\, dt \tag{5.18}$$

using the linearised form of the process equation, $F = \dfrac{\partial f_c(\mathbf{x})}{\partial \mathbf{x}}$ (Grewal and Andrews, 1993). In the 3D filter, we use

$$\begin{aligned} \mathbf{Q}_c = \mathrm{diag}[&(0\,{\scriptstyle \mathrm{m\,s^{-1}}}), (0\,{\scriptstyle \mathrm{m\,s^{-1}}}), (0\,{\scriptstyle \mathrm{m\,s^{-1}}}), \\ &(75\,{\scriptstyle \mathrm{m\,s^{-2}}}), (75\,{\scriptstyle \mathrm{m\,s^{-2}}}), (75\,{\scriptstyle \mathrm{m\,s^{-2}}}), \\ &(0.8 \times m_k\,{\scriptstyle \mathrm{kg\,s^{-1}}}), (10^{-3}\,{\scriptstyle \mathrm{m^2\,kg^{-2/3}\,s^{-1}}}), (10^{-4}\,{\scriptstyle \mathrm{s\,km^{-2}}})]^2, \end{aligned} \tag{5.19}$$

where each element along this square matrix diagonal represents the uncertainty of each differential model equation in (5.17). That is, the uncertainty in position and velocity components are introduced through noise in the acceleration model (5.16b), allowing the variance of $d\mathbf{l}/dt = 0\,\mathrm{m\,s^{-1}}$. The process model for dm/dt

is not able to fully represent the change of mass due to gross fragmentation; the process noise is therefore set as a relatively high percentage of the existing mass. Although the trajectory parameters κ and σ are currently assumed to be constant (5.15), this is not entirely true, therefore process noise is attributed to allow small variations to these parameters throughout the trajectory.

The discrete process noise, $\mathbf{Q}_k$, is then calculated at every time step from Equation (5.18).

LINE-OF-SIGHT MEASUREMENT UPDATE

Images taken by each observatory show a discontinuous streak across a star background. The Desert Fireball Network uses the modulation of a liquid crystal shutter within the lens of each camera to encode a unique time sequence into the fireball's path (Howie et al., 2017). By comparing the position of the start and end of each fireball segment with the background stars, the azimuth and elevation of each encoded time can be determined (Devillepoix and Sokolowski, in prep.).

Since the ground-based observations of the fireball path are azimuth and elevations, $\mathbf{z}_k$ in the measurement equation (5.5) is a series of angular observations. The measurement function in Equation (5.5) extracts the state components (position vector) which are to be compared to these observations and, as $\mathbf{l}_k^i$ is in ECEF, performs the coordinate transformation required. Within this function, $\mathbf{l}_k^i$ is converted from ECEF to the apparent line-of-sight azimuth and elevation values with respect to each observatory. An n number of conversions are required for N_{obs} number of observatories that made an observation at t_k.

Each observatory's position is recorded in spherical latitude, longitude and height (LLH) coordinates (O^n_{lat}, O^n_{lon}, O^n_{height}). The conversion from LLH to ECEF coordinates ($\mathbf{O}^n_{ECEF}$) is performed using the transform (Hofmann-

Wellenhof et al., 2012).

$$\mathbf{O}^{n}_{\mathsf{ECEF}} = \begin{bmatrix} O^{n}_{x} \\ O^{n}_{y} \\ O^{n}_{z} \end{bmatrix} = \begin{bmatrix} (N + O^{n}_{\mathtt{height}}) \times \cos(O^{n}_{\mathtt{lat}}) \cos(O^{n}_{\mathtt{lon}}) \\ (N + O^{n}_{\mathtt{height}}) \times \cos(O^{n}_{\mathtt{lat}}) \sin(O^{n}_{\mathtt{lon}}) \\ \left(\frac{a^{2}_{\oplus}}{b^{2}_{\oplus}} N + O^{n}_{\mathtt{height}} \right) \times \sin(O^{n}_{\mathtt{lat}}) \end{bmatrix}, \tag{5.20}$$

where:

$$N = \frac{a_{\oplus}}{\sqrt{a^{2}_{\oplus} \cos^{2} O^{n}_{\mathtt{lat}} + b^{2}_{\oplus} \sin^{2} O^{n}_{\mathtt{lat}}}} \quad ,$$

$a_{\oplus} = 6,378,137\,\mathrm{m}$ is the semi-major axis[1] of the Earth's geoid and

$b_{\oplus} = 6,356,752\,\mathrm{m}$ is the semi-minor axis[2] of the Earth's geoid.

The apparent line-of-sight cartesian unit vector for any n observatory (located at $\mathbf{O}^{n}_{\mathsf{ECEF}}$) to any particle i is given by

$$\left[\hat{\mathbf{a}}^{i;n}_{k}\right]_{\mathsf{ECEF}} = \frac{\mathbf{l}^{i}_{k;\mathsf{ECEF}} - \mathbf{O}^{n}_{\mathsf{ECEF}}}{||\mathbf{l}^{i}_{k;\mathsf{ECEF}} - \mathbf{O}^{n}_{\mathsf{ECEF}}||}. \tag{5.21}$$

This is then rotated into local observatory-centred coordinates (East, North, Up) by taking the dot product of the ECEF to ENU transformation matrix with $\left[\hat{\mathbf{a}}^{i;n}_{k}\right]_{\mathsf{ECEF}}$ (Hofmann-Wellenhof et al., 2012):

$$\left[\hat{\mathbf{a}}^{i;n}_{k}\right]_{\mathsf{ENU}} = \begin{bmatrix} -\sin(\mathbf{O}^{n}_{\mathtt{lon}}) & \cos(\mathbf{O}^{n}_{\mathtt{lon}}) & 0 \\ -\sin(\mathbf{O}^{n}_{\mathtt{lat}})\cos(\mathbf{O}^{n}_{\mathtt{lon}}) & -\sin(\mathbf{O}^{n}_{\mathtt{lat}})\sin(\mathbf{O}^{n}_{\mathtt{lon}}) & \cos(\mathbf{O}^{n}_{\mathtt{lat}}) \\ \cos(\mathbf{O}^{n}_{\mathtt{lat}})\cos(\mathbf{O}^{n}_{\mathtt{lon}}) & \cos(\mathbf{O}^{n}_{\mathtt{lat}})\sin(\mathbf{O}^{n}_{\mathtt{lon}}) & \sin(\mathbf{O}^{n}_{\mathtt{lat}}) \end{bmatrix} \bullet \left[\hat{\mathbf{a}}^{i;n}_{k}\right]_{\mathsf{ECEF}}. \tag{5.22}$$

---

[1] WGS84 value for semi-major axis of the Earth's geoid (Decker, 1986).

[2] WGS84 value for earth flattening (Decker, 1986) used to calculate semi-major axis of the Earth's geoid.

$\left[\hat{\mathbf{a}}_k^{i;n}\right]_{ENU}$ is then converted to azimuth and elevation in the local observatory's coordinate system as (Hofmann-Wellenhof et al., 2012):

$$az_k^{i;n} = \arctan 2\left(\left[\hat{\mathbf{a}}_k^{i;n}\right]_E\ ,\ \left[\hat{\mathbf{a}}_k^{i;n}\right]_N\right) \qquad (\mathrm{mod}\, 2\pi) \tag{5.23}$$

$$el_k^{i;n} = \arcsin\left(\left[\hat{\mathbf{a}}_k^{i;n}\right]_U\right). \tag{5.24}$$

As an azimuth value of 2π radians is congruent to a value of 0 radians, a modulo operation is included in (5.23) .

The result of the measurement function, $\hat{\mathbf{z}}_k^i$, is the predicted line-of-sight unit vectors for a given particle i in azimuth and elevation from all n observatories and can be summarised by

$$\hat{\mathbf{z}}_k^i = \left[az_k^{i;n}, el_k^{i;n}, ..., az_k^{i;N_{obs}}, el_k^{i;N_{obs}}\right] \qquad n = 1, ..., N_{obs} \tag{5.25}$$

A multivariate Gaussian probability is then used to calculate the weighting of a particle:

$$w_k^i = \left(2\pi^{\frac{N_s}{2}} |\mathbf{R}_k|^{\frac{1}{2}}\right)^{-1} e^{-\frac{1}{2}[\hat{\mathbf{z}}_k - \mathbf{z}_k]^T \mathbf{R}_k^{-1} \left[\hat{\mathbf{z}}_k^i - \mathbf{z}_k\right]}, \tag{5.26}$$

where $|\mathbf{R}_k|$ is the determinant of the observation noise covariance matrix containing azimuth and elevation errors pertaining to each observatory:

$$\mathbf{R}_k = diag[Var(az^n), Var(el^n), .., Var(az^{N_{obs}}), Var(el^{N_{obs}})]. \tag{5.27}$$

The observational uncertainties in both azimuth and elevation are linked to the accuracy of picking the start and end points of modulated segments in the fireball image, their calibration and the shutter response time. For all-sky images captured using fish eye lenses, the accuracy in azimuth is much greater than in elevation.

As described by Sansom et al. (2017) (after Arulampalam et al. 2002), the number of effective particles are monitored, though resampling is performed after every iteration.

ANALYSING A FIREBALL

On the 12th of December 2015, at 11:36:22.60 UTC, a $>$ 21 second long fireball over South Australia was captured by five DFN observatories (hereafter referred to as event DN151212). As DFN exposures are initiated on the minute and at 30 seconds, the fireball appears on two consecutive images. The second picture taken by the closest camera is shown in Figure 5.1. The modulation of the liquid crystal shutter can be seen as long and short dashes along the trajectory. Here we will analyse the latter half of the trajectory from where deceleration begins to have an affect (the final 13 seconds).

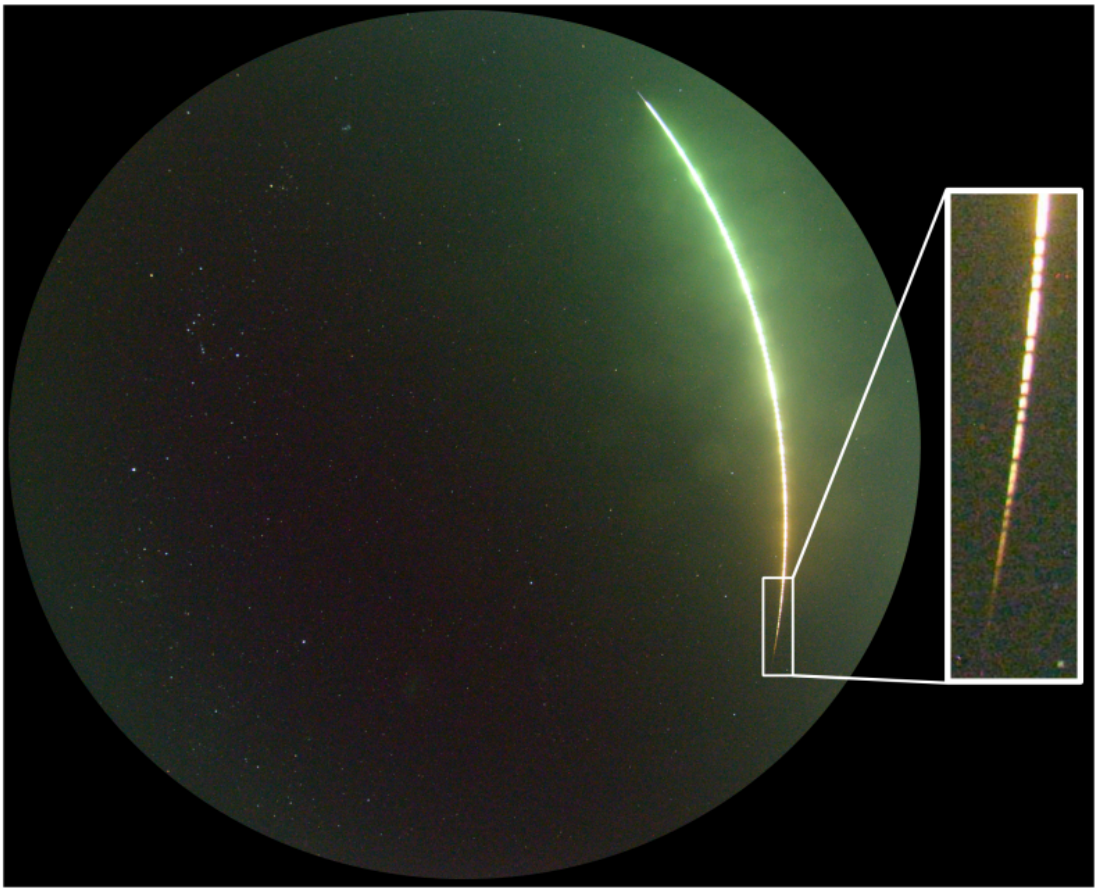

FIGURE 5.1: DN151212 fireball as seen from Etadunna Station, South Australia, travelling from North (top) to South (bottom) with a final recorded point at 11:36:43.96 UTC. Calibration with background stars determines azimuth and elevation of trajectory points.

A straight-line least squares method of triangulation following Borovička (1990) was initially used to determine the position of the meteoroid along its entire trajectory for use with a one dimensional model based particle filter (as performed by Sansom et al. 2017). It became apparent that this was not appropriate when comparing the resulting positions to the full suite of observations (Figure 5.2).

The unique method used by DFN camera systems to encode timing provides absolute synchronisation of observations between observatories. This allows a rough estimate of the meteoroid position, at every time-step with multi-station observations, to be individually triangulated (following the point-wise triangulation described in Section 5.2.1).

The divergence of the straight-line least squares positions from these individually triangulated points are shown in Figure 5.3 (red). A 3D particle filter was performed on the same data. The normal distance between the individually triangulated points and all predicted particle positions are also shown in Figure 5.3 with their weightings. The weighted mean residuals, as calculated by Equation (5.9), are marked in black. It is clear from Figure 5.3 that the 3D particle filter predicts meteoroid positions truer to the observations than the straight-line approach. The maximum the weighted mean deviates from the calculated observed position is $482\,\mathrm{m}$, with $> 98\%$ below $270\,\mathrm{m}$. The two outliers at 6.12 and 6.22 seconds could be indicative of a disruption to the body or other unmodelled cause that resulted in the predicted particles becoming unsuitable thereby forcing the filter to adapt. Gaps in Figure 5.3 are where the fireball was observed by a single station only and therefore no reference is available. Plotting all these data in Google Earth provides a more visual perception of the differences (Figure 5.2).

The geometrical precision of the Prairie Network according to Ceplecha et al. (1996) was ± 10 to $\pm 40\,\mathrm{m}$. More recent modelling of fireball data shows detailed analyses of the deviation of observations from a straight line (standard deviation of $58\,\mathrm{m}$ for Jesenice, $\gamma_e = 59^\circ$, Spurný et al. 2010; $65\,\mathrm{m}$ for Križevci, $\gamma_e = 65^\circ$, Borovička et al. 2015; the lower deviations calculated for these two cases may be due to their relatively steep trajectories). However, model residuals of typically less than $30\,\mathrm{m}$ (Spurný et al., 2012) are taken as trajectory errors, or no model errors are given.

The effect of this straight-line assumption will not only affect the position estimates, but via the link through the state equations (5.1), will influence the other state parameters: velocity and mass. As the particle filter is an adaptive approach that uses observations to update state estimates, using

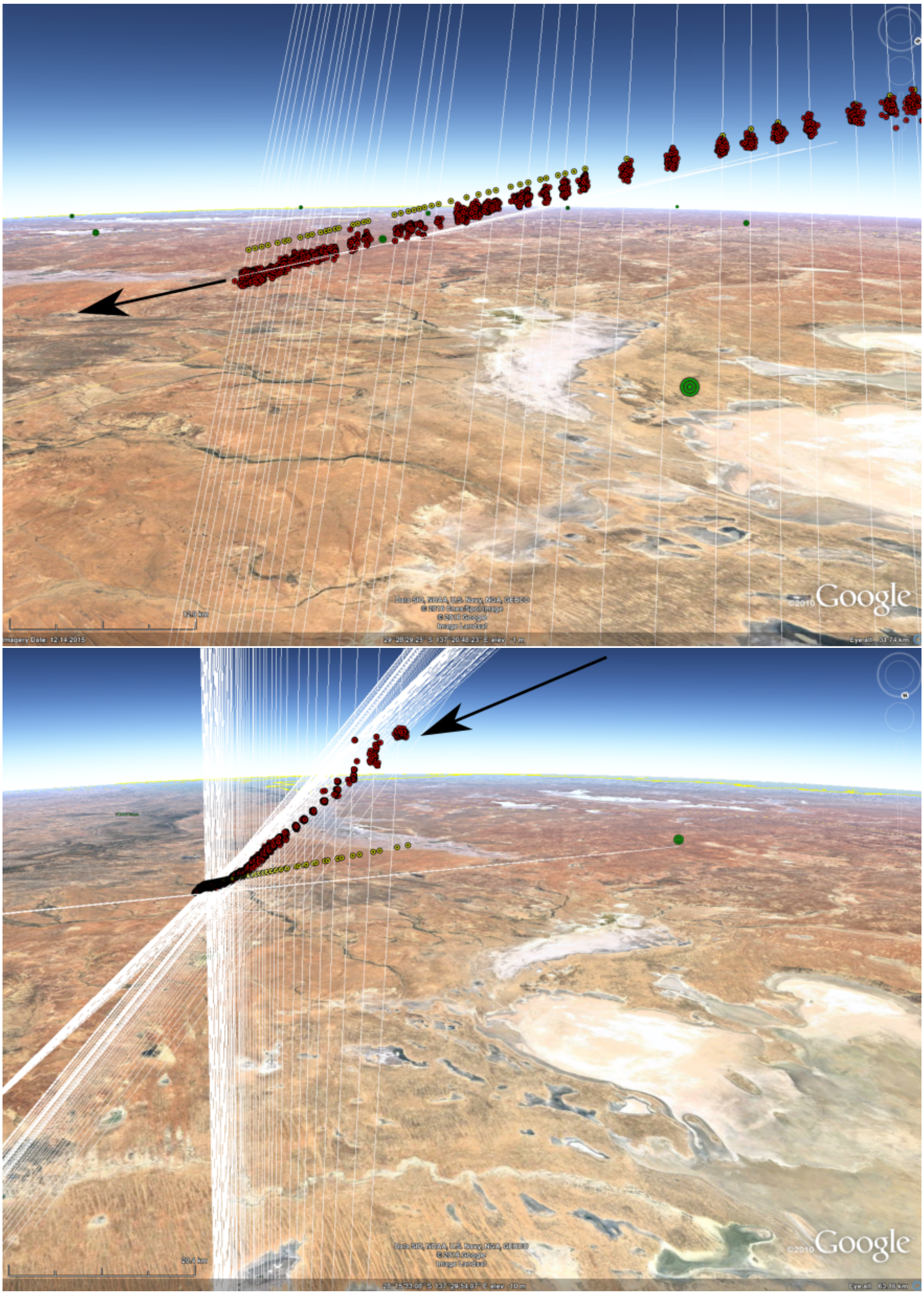

FIGURE 5.2: Google Earth visualisation; white rays are line-of-sight observations from 4 different DFN observatories (green ground stations), yellow points show straight-line least squares estimate of meteoroid position, red points show position of individual particles predicted using a 3D particle filter. Black arrows show rough direction of meteoroid flight

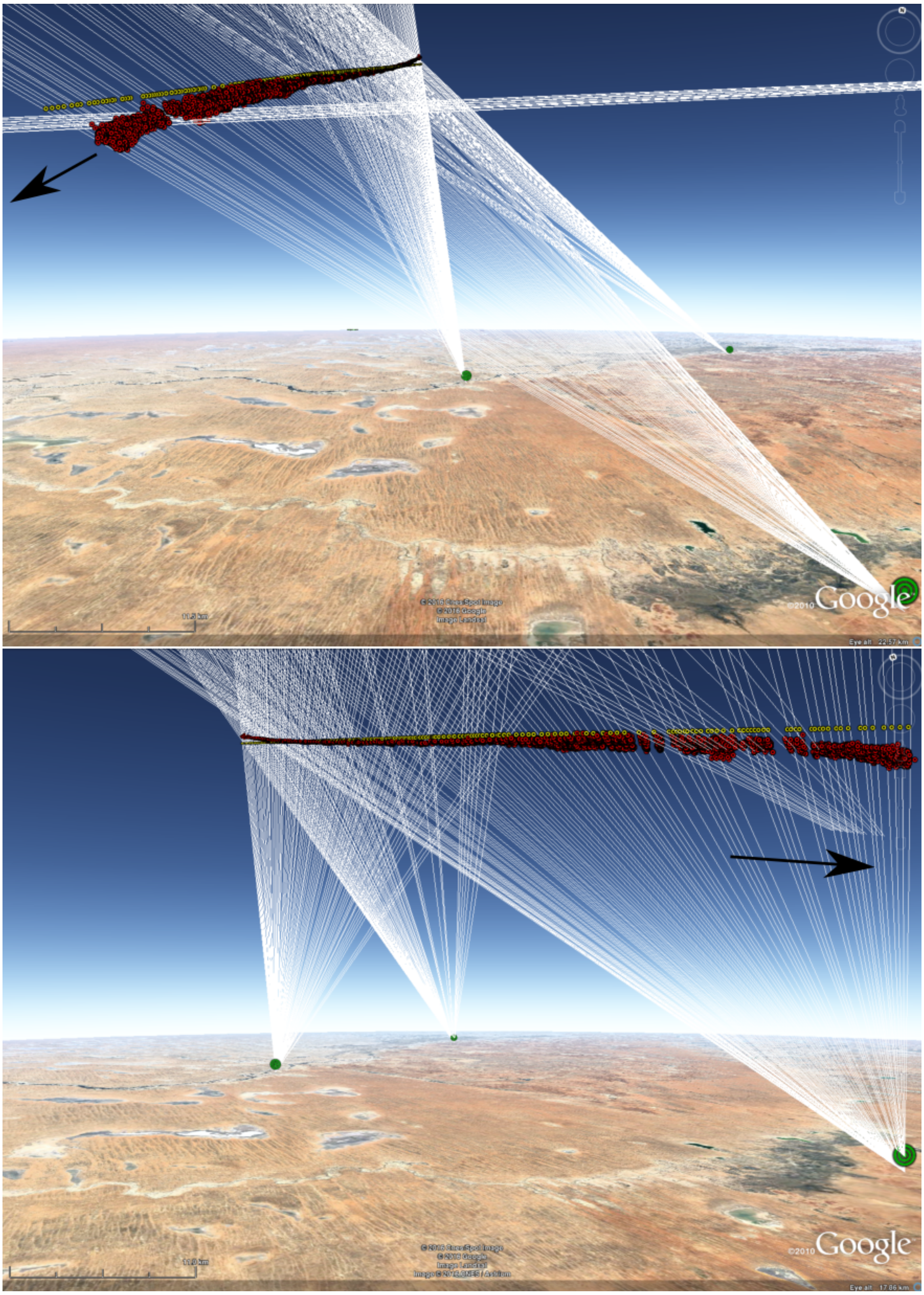

FIGURE 5.2 *(contd.)*

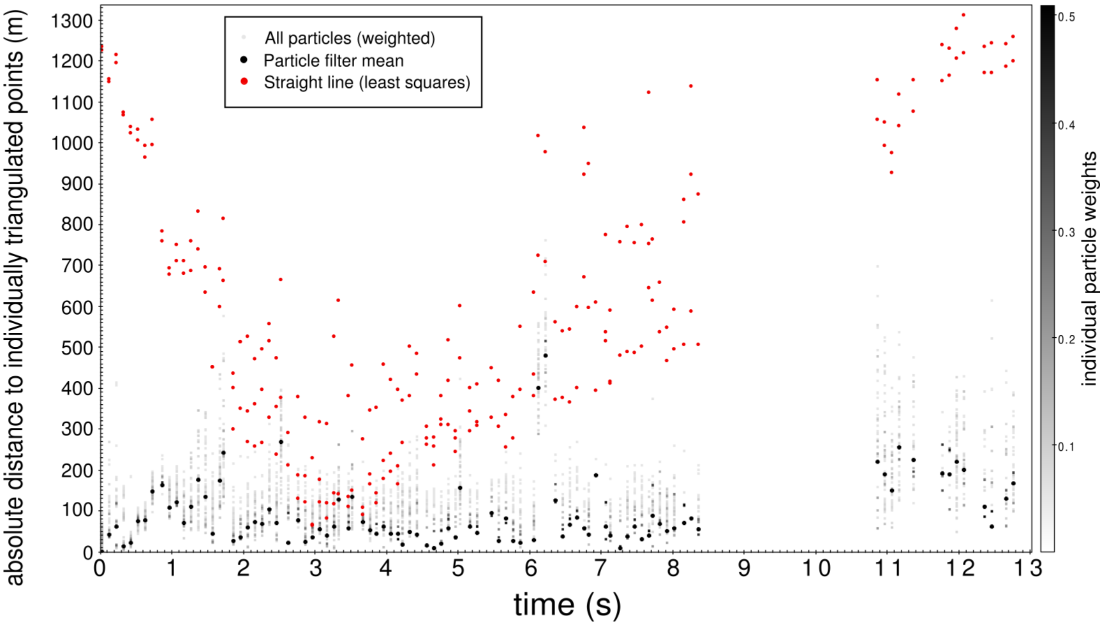

FIGURE 5.3: The absolute distance between individually triangulated observations (y=0) and the estimated position of a meteoroid using the straight-line least squares approximation (red) and a 3D particle filter (means shown in black, individually weighted particles shown in greyscale).

the most unprocessed measurements will permit subtleties in the data the opportunity to influence the predicted state. This will also provide a more robust error analysis as uncertainties are propagated comprehensively from well constrained azimuth and elevation errors (from astrometric calibration) through to the end of the luminous trajectory where remaining particles at t_{end} can be used as a direct input to Monte Carlo dark flight simulations. Calculating a search region on the ground that represents the real world variability of possible fragmentation spread is of great importance. Field searches in remote areas of outback Australia have an upper limit of approximately $2 - 6\,\mathrm{km}^2$ (Howie et al., 2017). Identifying events with greater chances of a successful find will significantly influence decisions about the feasibility of a remote, ground based search for meteorites. Shallow events in particular, such as DN151212 ($\gamma_e = 15.8°$) tend to produce extended fall lines 10s of km long from small fragments to main body masses. Well constrained final states in these cases are essential. For this event, the mean final state estimate resulted in a final mass of

723.55 ± 14.1 g, along with a shape density coefficient $\kappa = 0.0069 \pm 5.8 \times 10^{-6}$ (SI), and an ablation coefficient $\sigma = 0.04 \pm 5.4 \times 10^{-5}\,\mathrm{s}^2\,\mathrm{km}^{-2}$.

CONCLUSION

Modelling fireball camera network data in three dimensions has not previously been attempted. Executing a particle filter on fireball data in three dimensions allows the raw line-of-sight (azimuth and elevation) measurements as seen by each observatory to be incorporated directly into the estimation of a meteoroid state. This removes the need for a complete pre-triangulated data set. Triangulating data using a straight-line assumption eliminates subtleties in the data that may be indicative of unmodelled processes for example gross fragmentation. Long, shallow fireballs will be more strongly influenced by gravitational effects, such as the > 21 second long DN151212. Other shape related effects could also cause a meteoroid to deviate from a straight-line trajectory. When analysing the flight of the DN151212 meteoroid, the straight-line approximation puts meteoroid positions up to $1.3\,\mathrm{km}$ away from the calculated observed point. A 3D particle filter estimates positions mostly within $270\,\mathrm{m}$. This misrepresentation of the data not only affects position estimates, but additionally influences the velocity and mass values through the relationship in the state equations (5.1).

By incorporating the raw observations, errors in each azimuth and elevation can be accounted for and propagated individually. This results in a final state estimate with fully comprehensive errors, leading to more realistic meteorite search areas. Adapting the self-contained particle filter approach of Sansom et al. (2017) for a three dimensional dynamic model has significantly improved meteoroid state estimates and will allow an automated, systematic evaluation of trajectories observed by multiple station camera networks.

ACKNOWLEDGEMENTS

We would like to thank the other members of the Desert Fireball Network team, in particular Hadrien Devillepoix and Morgan Cox for their involvement in generating the data required for this work. This work was funded by the Australian Research Council as part of the Australian Laureate Fellowship scheme, and supported by resources provided by the Pawsey Supercomputing Centre with funding from the Australian Government and the Government of Western Australia.

REFERENCES

Artemieva, N. and Pierazzo, E., 2009. The canyon diablo impact event: Projectile motion through the atmosphere. *Meteoritics & Planetary Science*, 44(1):25–42. doi: 10.1111/j.1945-5100.2009.tb00715.x.

Artemieva, N. A. and Shuvalov, V. V., 2016. From Tunguska to Chelyabinsk via Jupiter. *Annual Review of Earth and Planetary Sciences*, 44:37–56. doi: 10.1146/annurev-earth-060115-012218.

Arulampalam, M. S., Maskell, S., Gordon, N., and Clapp, T., 2002. A tutorial on particle filters for online nonlinear/non-Gaussian Bayesian tracking. *IEEE Transactions on Signal Processing*, 50(2):174–188. doi: 10.1109/78.978374.

Baldwin, B. and Sheaffer, Y., 1971. Ablation and breakup of large meteoroids during atmospheric entry. *Journal of Geophysical Research*, 76(19):4653–4668.

Bland, P. A. and Artemieva, N. A., 2006. The rate of small impacts on earth. *Meteoritics & Planetary Science*, 41(4):607–631. doi: 10.1111/j.1945-5100.2006.tb00485.x.

Borovička, J., 1990. The comparison of two methods of determining meteor trajectories from photographs. *Bulletin of the Astronomical Institutes of Czechoslovakia*, 41:391–396.

Borovička, J., Spurný, P., Šegon, D., Andreić, Ž., Kac, J., Korlević, K., Atanackov, J., Kladnik, G., Mucke, H., Vida, D., and Novoselnik, F., 2015. The instrumentally recorded fall of the Kri{ž}evci meteorite, Croatia, February 4, 2011. *Meteoritics & Planetary Science*, 16(7). doi: 10.1111/maps.12469.

Bronshten, V. A., 1983. *Physics of Meteoric Phenomena*. Geophysics and Astrophysics Monographs. Reidel, Dordrecht, Netherlands.

Brown, P. G., Ceplecha, Z., Hawkes, R. L., Wetherill, G., Beech, M., and Mossman, K., 1994. The orbit and atmospheric trajectory of the Peekskill meteorite from video records. *Nature*, 367(6464):624–626. doi: 10.1038/367624a0.

Campbell-Brown, M. D. and Koschny, D., 2004. Model of the ablation of faint meteors. *Astronomy and Astrophysics*, 418(2):751–758. doi: 10.1051/0004-6361:20041001-1.

Ceplecha, Z., 1987. Geometric, dynamic, orbital and photometric data on meteoroids from photographic fireball networks. *Bulletin of the Astronomical Institutes of Czechoslovakia*, 38:222–234.

Ceplecha, Z. and Revelle, D. O., 2005. Fragmentation model of meteoroid motion, mass loss, and radiation in the atmosphere. *Meteoritics & Planetary Science*, 40(1):35–54. doi: 10.1111/j.1945-5100.2005.tb00363.x.

Ceplecha, Z., Spalding, R. E., Jacobs, C. F., and Tagliaferri, E., 1996. Luminous efficiencies of bolides. In *SPIE's 1996 International Symposium on Optical Science, Engineering, and Instrumentation*, volume 2813, pages 46–56. International Society for Optics and Photonics. doi: 10.1117/12.256072.

Ceplecha, Z., Borovička, J., Elford, W. G., ReVelle, D. O., Hawkes, R. L., Porubčan, V., and Šimek, M., 1998. Meteor Phenomena and Bodies. *Space Science Reviews*, 84(3):327–471. doi: 10.1023/A:1005069928850.

Decker, B. L., 1986. World geodetic system 1984. Technical report, DTIC Document.

Devillepoix, H. and Sokolowski, M., in prep. Astrometric calibration of all-sky cameras.

Grewal, M. S. and Andrews, A. P., 1993. *Kalman filtering: theory and practice*. Prentice-Hall Inc., New Jersey.

Hildebrand, A. R., McCausland, P. J. A., Brown, P. G., Longstaffe, F. J., Russell, S. D. J., Tagliaferri, E., Wacker, J. F., and Mazur, M. J., 2006. The fall and recovery of the tagish lake meteorite. *Meteoritics & Planetary Science*, 41(3):407–431. doi: 10.1111/j.1945-5100.2006.tb00471.x.

Hofmann-Wellenhof, B., Lichtenegger, H., and Collins, J., 2012. *Global positioning system: theory and practice*. Springer Science & Business Media.

Hoppe, J., 1937. Die physikalischen Vorgänge beim Eindringen meteoritischer Körper in die Erdatmosphäre. *Astronomische Nachrichten*, 262(10):169–198.

Howie, R., Paxman, J., Bland, P., Towner, M., Sansom, E., and Devillepoix, H., 2017. Submillisecond fireball timing using de Bruijn timecodes. *Meteoritic & Planetary Science*.

Howie, R., Paxman, J., Bland, P., Towner, M., Cupak, M., Sansom, E., and Devillepoix, H., 2017. How to build a continental scale fireball camera network. *Experimental Astronomy*, 43237–266.

Kikwaya, J.-B., Campbell-Brown, M. D., and Brown, P. G., 2011. Bulk density of small meteoroids. *Astronomy & Astrophysics*, 530:A113. doi: 10.1051/0004-6361/201116431.

McCrosky, R. E. and Boeschenstein, H., 1965. The prairie meteorite network. *Optical Engineering*, 3(4):304127–304127.

Picone, J. M., Hedin, A. E., Drob, D. P., and Aikin, A. C., 2002. NRLMSISE-00 empirical model of the atmosphere: Statistical comparisons and scientific issues. *Journal of Geophysical Research: Space Physics (1978–2012)*, 107(A12): 1468.

Ray, S. and Fröhlich, J., 2015. An analytic solution to the equations of the motion of a point mass with quadratic resistance and generalizations. *Archive of Applied Mechanics*, 85(4):395–414.

Ristic, B., Arulampalam, S., and Gordon, N., 2004. *Beyond the Kalman filter: Particle filters for tracking applications*, volume 685. Artech house Boston.

E. Sansom, M. Rutten, and P. Bland. Analyzing meteoroid flights using particle filters. *The Astronomical Journal*, 153(2):87, 2017.

Shuvalov, V., 1999. Multi-dimensional hydrodynamic code sova for interfacial flows: Application to the thermal layer effect. *Shock Waves*, 9(6):381–390. doi: 10.1007/s001930050168.

Shuvalov, V. V. and Artemieva, N. a., 2002. Numerical modeling of Tunguska-like impacts. *Planetary and Space Science*, 50(2):181–192. doi: 10.1016/S0032-0633(01)00079-4.

Spurný, P., Borovička, J., Kac, J., Kalenda, P., Atanackov, J., Kladnik, G., Heinlein, D., and Grau, T., 2010. Analysis of instrumental observations of the jesenice meteorite fall on april 9, 2009. *Meteoritics & Planetary Science*, 45(8):1392–1407. doi: 10.1111/j.1945-5100.2010.01121.x.

Spurný, P., Bland, P., Shrbený, L., Borovička, J., Ceplecha, Z., Singelton, A., Bevan, A. W. R., Vaughan, D., Towner, M. C., Mcclafferty, T. P., Toumi, R., and Deacon, G., 2012. The Bunburra Rockhole meteorite fall in SW Australia:

Fireball trajectory, luminosity, dynamics, orbit, and impact position from photographic and photoelectric records. *Meteoritics & Planetary Science*, 47(2): 163–185. doi: 10.1111/j.1945-5100.2011.01321.x.

Stulov, V. P., Mirsky, V. N., and Visly, A. I., 1995. Aerodynamics of Bolides. *Nauka*.

CHAPTER 6

THESIS CONCLUSIONS AND FUTURE WORK

The goal of this doctoral thesis was to improve and develop algorithms for fireball trajectory analysis.

Existing methods of modelling meteoroid trajectories using precise, distributed-station observations, have undergone iterative developments over the years, but are still based on least squares methodologies. Model errors are measured as the standard deviation of the collective least-squares residuals and assumptions are made for parameters that are not measurable. The light curve of the fireball is typically integral to the modelling process for quantifying mass loss and requires manual interpretation.

The intention of this work was to explore methods outside of these established techniques to see if we could not only automate meteoroid trajectory analyses without a light curve, or imposing parameter assumptions, but also comprehensively include parameter, model and observational uncertainties. This will provide a means to routinely analyse large fireball data sets, such as is being acquired by the Desert Fireball Network in Australia, without bias.

The results and conclusions described within each individual chapter of this thesis have documented the progressive advancement in statistical algorithms to address this objective. The first method implements an extended Kalman filter and a Rauch-Tung-Striebel smoother (Chapter 2). This relatively simple approach provides a detailed way of characterising meteoroids along their luminous trajectories without the need for brightness data. It also propagates uncertainties in trajectory states in a way that previous approaches had not been able to. An upgrade to this was implementing an unscented Kalman filter (Chapter 3). Combining two unscented Kalman filters in an interactive multiple model (IMM) delivers the additional ability to identify possible fragmentation events from the dynamic data alone, rendering this previous advantage of a light curve unnecessary. Outstanding issues with these Kalman filter based approaches (as with previous models in the literature) is the need to assume input parameters. As this research aimed to avoid such assumptions, the next logical advance was to implement a particle filter (Chapter 4). This iterative Monte Carlo estimator allows a 'cloud' of particles to be initialised with a range of input parameters, encapsulating prior knowledge of the parameter space, resulting in an unbiased analysis.

Up to this point all estimators were executed using the one dimensional single body theory of meteoroid aerodynamics (Equation 1.1) as system equations, in accordance with the majority of previous fireball trajectory models. These equations define the change in position, velocity and mass along the 1D path of a meteoroid's trajectory. Measurements used to update estimated model states are the pre-triangulated data - the positions along the straight-line that collectively best fits all the raw observations. This straight-line assumption has been considered an acceptable simplification of a meteoroid trajectory, given that gravitational forces are significantly smaller than drag forces. This has not been rigorously tested however and we found that for some cases, a straight-line meteoroid trajectory represents an oversimplification and is not valid for the long, shallow fireball trajectory analysed. The adaptive particle filter approach is fully capable of removing the need for a pre-triangulated data set; the raw line-of-sight observations can be used directly when three dimensional state-space equations are implemented instead. As observations are integral to updating the state estimates of tracking algorithms, using the least processed data will provide the most statistically robust analysis, incorporating subtleties in the raw observations that would otherwise have been removed by the straight-line approximation.

Errors in meteoroid position at the end of the luminous trajectory will strongly affect the search region on the ground in the case of a meteorite fall. Being able to rigorously encapsulate all uncertainties introduced by the model, observations and initial parameters used, provides an understanding of the real-world variability when propagated to the ground during subsequent dark flight simulations. This will help inform decisions regarding the feasibility of remote, ground based searches and favour events with greater chances of success.

Using estimator algorithms has provided the adaptability needed for modelling fireballs using the simplified single body theory of meteor dynamics, allowing additional complexities to be incorporated through the model process noise. Although we have shown these algorithms applying dynamic equations only, the methods are highly flexible and can be applied to other underlying system models. This includes the ability to add the luminosity relationship (Equation 1.1d) as a state equation to better constrain initial masses. Incorporating brightness is the next logical advancement and will provide supplementary data to improve both mass and velocity estimates.

Future work will also include combining the results of the interactive multiple model with the particle filter. As the IMM is able to identify the timing of potential fragmentation events without the need for a light curve or any manual input, a powerful tool comes from incorporating its results into a particle filter. Once timing of disruption events are identified, a particle filter can be run where model noise covariance is set to increase at these times.

By improving the statistical algorithms for meteoroid trajectory analyses, this not only influences luminous trajectory models and fall positions, but will also lead to improved orbit determination with statistical smoothers providing reliable initial velocity vectors. Accurately determining orbits for meteorite falls will provide the missing contextual information, leading to a greater understanding of asteroid parent bodies, the composition of the main asteroid belt, its resonances and eventually the compositional stratification of the protoplanetary disk. These are some of the main objectives of fireball camera networks and overlap to some degree with sample return missions in that we can derive context information for meteorites, bridging the gap between meteorites and asteroids. Knowing more about the formation of our own Solar System will help our understanding of planetary formation and provide constraints on models of exoplanet formation and composition.

Another aim of fireball networks is to constrain the flux of incoming extra terrestrial material. The DFN data set is rapidly growing and already surpasses the largest single compilation of fireball data presented by Halliday et al., 1996. By contributing to the automation of the Desert Fireball Network and data reduction, this research will increase the efficiency of the DFN and allow an unbiased analysis of fireball data.

APPENDIX A

FIRST AUTHOR JOURNAL PUBLICATION REPRINTS

PAPER 1 – A NOVEL APPROACH TO FIREBALL MODELING: THE OBSERVABLE AND THE CALCULATED

Meteoritics and Planetary Science (2015), Volume 50, Issue 8, pp. 1423–1435

Sansom, E. K., Bland, P. A, Paxman, J., Towner, M. C.

STATEMENT OF AUTHORSHIP

TITLE OF PAPER: A novel approach to fireball modeling: The observable and the calculated.

PUBLICATION STATUS: Published

AUTHOR CONTRIBUTIONS

By signing the Statement of Authorship, each author certifies that their stated contribution to the publication is accurate and that permission is granted for the publication to be included in the candidate's thesis.

Name of Principal Author: Eleanor K. Sansom

Contribution to the Paper: Led all aspects of this research, drafted and revised the manuscript for this publication.

Overall Percentage: 83%

Signature: ***Date:*** 01 / 12 / 16

Name of Co-Author: Phillip A. Bland

Contribution to the Paper: Assisted with editing and revision of the manuscript.

Overall Percentage: 5%

Signature: Philip Bland ***Date:*** 4 / 12 / 16

Name of Co-Author: Jonathan Paxman

Contribution to the Paper: Helped with MATLAB coding of dynamic optimisation step and assisted with editing and revision of the manuscript.

Overall Percentage: 10%

Signature: J. Pa ***Date:*** 5/12/16

Name of Co-Author: Martin C. Towner

Contribution to the Paper: Helped in the final review of the manuscript.

Overall Percentage: 2%

Signature: M Town ***Date:*** 05/12/16

The Meteoritical Society

Meteoritics & Planetary Science 50, Nr 8, 1423–1435 (2015)
doi: 10.1111/maps.12478

A novel approach to fireball modeling: The observable and the calculated

Eleanor Kate SANSOM[1*], Philip BLAND[1], Jonathan PAXMAN[2], and Martin TOWNER[1]

[1]Department of Applied Geology, Curtin University, GPO Box U1987, Perth, Western Australia 6845, Australia
[2]Department of Mechanical Engineering, Curtin University, GPO Box U1987, Perth, Western Australia 6845, Australia
[*]Corresponding author. E-mail: eleanor.sansom@postgrad.curtin.edu.au

(Received 16 September 2014; revision accepted 14 May 2015)

Abstract–Estimating the mass of a meteoroid passing through the Earth's atmosphere is essential to determining potential meteorite fall positions. High-resolution fireball images from dedicated camera networks provide the position and timing for fireball bright flight trajectories. There are two established mass determination methods: the photometric and the dynamic. A new approach is proposed, based on the dynamic method. A dynamic optimization initially constrains unknown meteoroid characteristics which are then used in a parametric model for an extended Kalman filter. The extended Kalman filter estimates the position, velocity, and mass of the meteoroid body throughout its flight, and quantitatively models uncertainties. Uncertainties have not previously been modeled so explicitly and are essential for determining fall distributions for potential meteorites. This two-step method aims to automate the process of mass determination for application to any trajectory data set and has been applied to observations of the Bunburra Rockhole fireball. The new method naturally handles noisy raw data. Initial and terminal bright flight mass results are consistent with other works based on the established photometric method and cosmic ray analysis. A full analysis of fragmentation and the variability in the heat-transfer coefficient will be explored in future versions of the model.

INTRODUCTION

The full potential of meteorite analysis for providing valuable insights about protoplanetary disk formation cannot be reached without first constraining their origins in the solar system. As with terrestrial rocks, without context (outcrop) information, our understanding of the record that meteorites contain will only ever be partial. The recording of fireball phenomena permits the reconstruction of orbits, as well as determines possible meteorite fall locations to enable the recovery of fresh meteorites whose unique geological record can be fully exploited. This objective has been the driver for a number of dedicated fireball camera network projects dating back to the late 1950s (Ceplecha 1961) and has led to the recovery of multiple meteorites, including two by the Desert Fireball Network (DFN) in Australia during its trial phase (Towner et al. 2011; Spurný et al. 2012).

Over the next few months, the DFN will establish over 50 new Automated Desert Fireball Observatories (ADFOs), with all sky digital cameras, to expand its coverage to an area in excess of 2 million km^2. This will make it the largest fireball network in history, and with >100 TB of data being generated per year, automated systems of data analysis will be needed. The calculation of terminal bright flight mass will form part of the DFN's automated work-flow from fireball detection and triangulation through to dark flight and climate modeling for fall calculations.

Once the light of the fireball goes out, there is usually no way of tracking any remaining fragments to the ground. To model this dark flight, and determine any potential fall positions, the terminal bright flight mass must be ascertained. An automated method of analyzing the bright flight data to extract this information is required and previous methods were investigated for suitability. The two previous approaches to analyzing image data for mass determination are: the photometric method and the dynamic method.

The photometric method relates the luminosity of a fireball to the proportion of kinetic energy that is lost due to ablation, as a method for obtaining masses (Ceplecha et al. 1998). It uses the luminosity of the fireball to determine the incoming "photometric" mass, and a corresponding luminous efficiency parameter as a proxy for mass loss. To apply this method, a high-resolution light curve of a fireball needs to be acquired. This can be obtained by the addition of a photoelectric photometer to a fireball observatory (Spurný et al. 2012). Not only is this an expensive piece of equipment in itself but also requires additional power supplies, which are limited in the remote locations of the DFN observatories.

Although advancements have been made to the photometric method, including fragmentation as well as dynamical aspects (Ceplecha and ReVelle 2005), it ultimately still requires qualitative comparisons of trajectories with the light curve and manual inputs of fragmentation information (Ceplecha and ReVelle 2005). These qualitative judgments make this method manually intensive and remove the ability to create fully reproducible data.

The dynamic method uses equations of flight through the atmosphere to calculate mass from deceleration (Whipple 1952). In the past, this approach was limited by the accuracy of measurements that could be interpreted from photographic plates (Ceplecha 1961; McCrosky et al. 1971). Ceplecha et al. (1993) used dynamic equations to determine the change in velocity and mass of a meteoroid during its trajectory, along with timings of single fragmentation events. However, the authors were unable to calculate initial masses and therefore relied on initial photometric masses. Considering mass loss is relative, this means the terminal mass is based on this photometric entry mass which may be unreliable (Brykina and Stulov 2012).

Difficulties with the dynamic method are also due to the unknown characteristics of the meteoroid such as density and shape that are required for the dynamic calculation. Work by Stulov et al. (1995) has enabled the application of an analytical solution by combining these unknown parameters into two dimensionless constants. This has been applied by Gritsevich (2008a, 2008b) to the Canadian MORP network data sets, as well as others that have led to meteorite recoveries. This provides good model fits to the data to which it was applied, but assumptions of these same meteoroid characteristics are required to quantify entry mass and subsequently terminal bright flight mass.

Given the limitations of established techniques and improvements to observation technologies, we chose to explore a new approach to the dynamic method. The use of an extended Kalman filter to incorporate the data into the model and provide error estimates was determined to be the most promising approach. An extended Kalman filter is a method of statistically optimizing estimates of an instantaneous state of nonlinear dynamic systems (Grewal and Andrews 1993). An accompanying covariance matrix allows the uncertainties in the state estimations to be determined and propagated. The Kalman filter estimates the bright flight states (distance traveled, mass, and velocity) based on a two-step process of "predict" and "update." However, this method still requires values for meteoroid parameters to be estimated. To maximize confidence in chosen meteoroid parameters, rather than simply picking values, the Extended Kalman Filter is preceded by a dynamic optimization step. This stage is implemented to constrain the combinations of meteoroid characteristics that will permit a fit to the data. These parameters are then used to initialize a series of extended Kalman filters. To test the new method of mass determination, the data set of the Bunburra Rockhole meteorite fall is used as published by Spurný et al. (2012). This is the most complete fireball data set for which a meteorite has been recovered.

The objective of an automated method of mass determination requires an efficient method that will give sufficiently accurate results to determine a practical search area for likely meteorites. As this new approach is based entirely on the photographic data, this significantly reduces the cost of each ADFO unit as there is no requirement for a photoelectric photometer. The new approach to fireball modeling that we outline here will enable the terminal bright flight mass to be approximated from observable data in a fully automatable method, with uncertainties, to enable rapid recovery of meteorite samples which may provide invaluable data for cosmochemists (particularly when combined with orbital data).

MODELING

In the case of the DFN, ADFOs record high-resolution images throughout the night. Fireball observations made by multiple long-exposure cameras can be used to triangulate the position (latitude, longitude, and altitude) of the meteoroid during its flight. To acquire velocity information, however, requires some specialized modifications. Using a customized shutter within the camera lenses, the light path is interrupted at a known frequency (approximately 20 Hz in the ADFO systems). After calibration to remove the effects of lens distortion and triangulation, we have a series of position observations which underpins the subsequent modeling. Velocity may be calculated based on the change in these positions with time. The accuracy of the position observations determines the accuracy of the velocity values and can cause high scatter in values as seen in the Bunburra Rockhole data set.

All models explored in this work are based on the dynamic equations that characterize the change in mass and velocity of a meteoroid during bright flight through the atmosphere (Baldwin and Sheaffer 1971):

$$\frac{\mathrm{d}v}{\mathrm{d}t} = -\frac{1}{2}\frac{c_\mathrm{d}\rho_\mathrm{a}v^2S}{m} + g\sin\gamma_\mathrm{e} \tag{1}$$

$$\frac{\mathrm{d}m}{\mathrm{d}t} = -\frac{1}{2}\frac{c_\mathrm{h}\rho_\mathrm{a}v^3S}{H^*} \tag{2}$$

where m is the meteoroid mass (kg), v is the velocity (m s^{-1}), t is the time (s), c_d is the drag coefficient, ρ_a is the atmospheric density (kg m^{-3}), S is the cross sectional area of the body (m^2), g is the gravitational constant (m s^{-1}), γ_e is the entry angle of the meteoroid to the horizontal, H^* is the enthalpy of sublimation (J kg^{-1}), and c_h is the heat-transfer coefficient.

The position or length along the path of the trajectory, l, is the primary observation extracted from the triangulated images. Its change with time is also included in all models and gives the velocity, i.e., $\frac{\mathrm{d}l}{\mathrm{d}t} = v$.

A New Approach

The new approach to determining the terminal masses of meteoroids discussed in this paper is a two-step approach, based on the dynamic Equations 1–2. The initial step is a dynamic optimization which runs a global search for the combination of meteoroid characteristics (model parameters) and unknown initial states (initial mass, m_0 and initial velocity, v_0) that provide a good fit to the observational data. The initial position, l_0, is also an initial state but as the length along the flight path is relative, we can set it to be 0 m (similar to Ceplecha and ReVelle 2005). Errors associated with observational uncertainties in this postulation will be taken into account when the extended Kalman filter is initialized.

The second, main step, runs an extended Kalman filter which uses the unknown initial states and parameters from the dynamic optimization to estimate the states (position, l; mass, m; velocity, v) throughout the entire trajectory, including an explicit uncertainty model.

The cross sectional area, S, in the dynamic Equations 1–2, is dependent on the amount of mass lost due to ablation and may be defined as a function of the mass, meteoroid density, ρ_m, and shape parameter, A (a cross sectional area to volume ratio) (equation 3.5; Bronshten 1983)

$$S = A\left(\frac{m}{\rho_\mathrm{m}}\right)^{\frac{2}{3}} \tag{3}$$

The change in cross sectional area can be written in terms of the shape change parameter, μ (Equation 4) (Bronshten 1983).

$$S = S_0\left(\frac{m}{m_0}\right)^{\mu} \tag{4}$$

S_0 and m_0 are the initial cross sectional area and initial mass respectively.

By writing Equation 3 in terms of initial parameters only we can combine it with Equation 4 to give

$$S = A_0\frac{m_0^{2/3-\mu}}{\rho_{\mathrm{m}_0}^{2/3}}m^{\mu} \tag{5}$$

Substituting Equation 5 into Equations 1–2 allows the dependent variable S to be removed from the dynamic equations. The modeling of meteoroid states during bright flight will therefore be based on the following differential equations.

$$\frac{\mathrm{d}v}{\mathrm{d}t} = -\frac{1}{2}\frac{c_\mathrm{d}\rho_\mathrm{a}A_0}{\rho_{\mathrm{m}_0}^{2/3}}m_0^{\left(2/3-\mu\right)}v^2m^{(\mu-1)} + g\sin\gamma_\mathrm{e} \tag{6}$$

$$\frac{\mathrm{d}m}{\mathrm{d}t} = -\frac{1}{2}\frac{c_\mathrm{h}\rho_\mathrm{a}A_0}{H^*\rho_{\mathrm{m}_0}^{2/3}}m_0^{\left(2/3-\mu\right)}v^3m^{\mu} \tag{7}$$

Constants Used in All Model Stages

Although the unknown parameters μ and $\frac{c_\mathrm{h}}{H^*}$ in Equations 6–7 are variable, they are approximated as constant for both the dynamic optimization and EKF models, along with the remaining unknown initial parameters, m_0, v_0, and $\frac{A_0}{\rho_{\mathrm{m}_0}^{2/3}}$ (which will hereby be referred to as the shape-density parameter). This has been the typical assumption in previous works also (Bronshten 1983; Gritsevich 2008b).

The shape change parameter, μ, has a range from 0, being no rotation, to 2/3, indicating that rotation is rapid enough for uniform ablation to occur across the entire surface area. It is typically assumed that μ has a value of 2/3 (Bronshten 1983) and as the dynamic equations are highly sensitive to the value of μ, this value is also used in our current model and will not be optimized further at this stage. Note that this removes m_0 as a coefficient from Equations 6–7, although m_0 is still present in the optimization as the initial value for mass.

Atmospheric Properties

The NRLMSISE-00 empirical atmosphere model was used to calculate values of atmospheric densities and pressures (Picone et al. 2002). This enables values for temperature, pressure, density, speed of sound, and dynamic viscosity of the atmosphere to be determined as accurately as possible.

Drag Coefficient

The drag coefficient, c_d, can be calculated throughout the trajectory based on a set of fluid dynamic parameters. ReVelle (1976) discusses the dependence of the Reynolds number and flow regime on the drag coefficient, but does not include a criterion for when the Mach regime is no longer hypersonic. This is unlikely to happen during fireball phenomena but is included here for completeness.

The Knudsen number (*Kn*) (Equation 8) can be used to determine the flow regime of the flight path and is the ratio of the mean free path length to the object length. *Kn* may be written as a function of the calculable Mach (*Ma*) and Reynolds (*Re*) numbers (Hayes and Probstein 1959; Truitt 1959) and the ratio of specific heats γ, which for dry air at atmospheric temperatures is taken to be 1.40).

$$Kn = \frac{Ma}{Re} \times \sqrt{\frac{\gamma\pi}{2}} \tag{8}$$

Values of $Kn \geq 10$ indicate free molecular flow, $10 < Kn < 0.1$ a transitional flow regime, and $Kn \leq 0.1$ continuum flow (ReVelle 1976). Within the continuum flow regime, the Mach regime defined by the Mach number needs to be taken into consideration. Only when below a *Ma* of 1.1 is *Re* used to directly calculate the drag coefficient. For values below the critical *Re* associated with drag reattachment (*Re* ~ 2e5) (Schlichting et al. 2000), Equation 11 from Haider and Levenspiel (1989) is used, although it is expected that bright flight values of c_d will remain in the hypersonic regime. Determining the values of c_d for different regimes and turbulence are outlined in Table 1.

For the Bunburra Rockhole data set, the meteoroid remains in the hypersonic regime for the duration of bright flight. In this version of the model, for simplicity, we will assume a hypersonic drag coefficient corresponding to that of a circular cylinder.

Dynamic Optimization

The dynamic optimization based on Equations 6–7 aims to approximate values for $\frac{A_0}{{\rho_{\mathrm{m}_0}}^{2/3}}$ and $\frac{c_\mathrm{h}}{H^*}$, as well as an entry mass, m_0, and velocity, v_0. This is performed by assigning assumed values to these parameters within given ranges and the constrained optimization then searches millions of combinations to determine the set of parameters that best fit the position data and return the lowest cost. The cost function used is the sum of the squared errors between the modeled and the observed position data. Costs are normalized to the lowest value, showing 1.0 to be the best fit, to allow comparisons between different parameter sets. As there are multiple unknown parameters, there is a large degree of freedom in the number of plausible combinations. The models that produce cost values >0.98 (best 2%) are selected for consideration in the following stage of the mass determination method.

The parameter constraints used are shown in Table 2. Ranges for ρ_{m_0} are given as assumed preatmospheric meteorite density ranges for typical meteorites. $A_\mathrm{sphere} = 1.21$ although it is expected that A values should typically be in the range of 2–4 (Zhdan et al. 2007). The shape parameter may also be less than that of a sphere depending on which axis is oriented in the direction of the trajectory. The lower and upper bounds for A_0 are chosen as realistic ranges. $\frac{c_\mathrm{h}}{H^*}$ is given a wide range so that the average value of this variable throughout bright flight is determined.

Extended Kalman Filter

An extended Kalman filter (EKF) is a method of statistically optimizing estimates of state variables for nonlinear dynamic systems (Grewal and Andrews 1993). For bolide bright flight path analysis, the state vector, x_k, is the instantaneous representation of the state at a time k, and is written in terms of the variables' distance along the bright flight path (l), mass (m), and velocity (v) (Equation 9).

$$x_k = \begin{pmatrix} x_1 \\ x_2 \\ x_3 \end{pmatrix}_k = \begin{pmatrix} l_k \\ m_k \\ v_k \end{pmatrix} \tag{9}$$

The state vector at t_0 is initialized as

$$x_0 = \begin{pmatrix} 0 \\ m_0 \\ v_0 \end{pmatrix} \tag{10}$$

x_k can be determined using the nonlinear state equations:

Table 1. Calculations used to determine the drag coefficient in various fluid dynamic regimes.

Flow regime	Knudsen number range	Mach number range	Drag coefficient formulae
Free molecular flow	$Kn \geq 10$		$c_d = 2.0$ (ReVelle 1976; Masson et al. 1960)
Transition flow regime	$0.1 < Kn < 10$		$c_d = c_d^{\text{cont.}} + \left(c_d^{\text{f.m.}} - c_d^{\text{cont.}}\right) e^{-0.001 Re^2}$ (Khanukaeva 2005)
Continuum flow regime	$Kn \leq 0.1$	$Ma \rightarrow \infty$ *Hypersonic to re-entry*	$c_d = 0.92$ for spheres (Bronshten 1983; ReVelle 1976; Masson et al. 1960) $c_d = 4/3$ for circular cylinders (Truitt 1959) $c_d = 2.0$ for tiles and bricks (Zhdan et al. 2007)
		$Ma < 8$	$c_d = \frac{24}{Re}[1 + A Re^B] + \frac{C}{1 + \frac{D}{Re}}$ where A, B, C, D are variables based on the sphericity of the object (see Haider and Levenspiel 1989)

Table 2. Parameter constraints applied during dynamic optimization.

	Min	Max
m_0	1 kg	1000 kg
v_0	(First velocity value) -3000 m s^{-1}	(First velocity value) $+3000$ m s^{-1}
$\frac{A_0}{\rho_{m_0}{}^{2/3}}$	$\frac{0.5}{(3500 \text{ kg m}^{-3})^{2/3}}$	$\frac{3.5}{(1500 \text{ kg m}^{-3})^{2/3}}$
$\frac{c_h}{H^*}$	2.5×10^{-7} kg J^{-1}	5.0×10^{-11} kg J^{-1}

$$x_k = f(x_{k-1}, k-1) + w_k \tag{11}$$

where w_k is the process noise with an assumed mean of zero and covariance Q_k (Equation 12).

$$Q_k = E[w_k w_k'] = \begin{bmatrix} \sigma_{l_{prs\ noise}}{}^2 & 0 & 0 \\ 0 & \sigma_{m_{prs\ noise}}{}^2 & 0 \\ 0 & 0 & \sigma_{v_{prs\ noise}}{}^2 \end{bmatrix} \tag{12}$$

An extended Kalman filter is an iterative process that involves two repeated processes. The prediction step for the fireball application will use the dynamic Equations 6–7 along with parameters defined by the previous dynamic optimization to estimate a future state based on all preceding observations. The measurement update step accepts a new observation of the state, in this case the distance along the bright flight path only, and calibrates the predicted outcome using an optimal Kalman gain. This process is schematically illustrated in Fig. 1.

Predicting Future States

The prediction step uses all previous data to derive a suitable state estimate, $\hat{x}_k$:

$$\hat{x}_{k|k-1} = f\left(\hat{x}_{k-1|k-1}, k\right) \tag{13}$$

$$P_{k|k-1} = F_k P_{k-1} F_k^T + Q_k \tag{14}$$

F_k is the state transition matrix (Equation 15). P_k is the covariance matrix for the state estimate and is a primary motivation for using an EKF. The diagonal elements can be read to give an indication of the variance for distance, mass, and velocity.

$$F_k = \left.\begin{bmatrix} \frac{\partial f_1}{\partial l} & \frac{\partial f_1}{\partial m} & \frac{\partial f_1}{\partial v} \\ \frac{\partial f_2}{\partial l} & \frac{\partial f_2}{\partial m} & \frac{\partial f_2}{\partial v} \\ \frac{\partial f_3}{\partial l} & \frac{\partial f_3}{\partial m} & \frac{\partial f_3}{\partial v} \end{bmatrix}\right|_{x=x_k} \tag{15}$$

where:

$$l_{k+1} = f_1(l_k, m_k, v_k, t_k) = l_k + \frac{\mathrm{d}l_k}{\mathrm{d}t_k}\Delta t = l_k + v_k \Delta t \tag{16}$$

$$\begin{aligned} m_{k+1} &= f_2(l_k, m_k, v_k, t_k) = m_k + \frac{\mathrm{d}m_k}{\mathrm{d}t_k}\Delta t \\ &= m_k - (k_m v_k^2 m_k^{\mu})\Delta t \end{aligned} \tag{17}$$

$$\begin{aligned} v_{k+1} &= f_3(l_k, m_k, v_k, t_k) = v_k + \frac{\mathrm{d}v_k}{\mathrm{d}t_k}\Delta t \\ &= v_k - (k_v v_k^2 m_k^{(\mu-1)} - g \sin \gamma_e)\Delta t \end{aligned} \tag{18}$$

And:

$$k_v = \frac{1}{2} \frac{c_d \rho_a A_0}{\rho_{m_0}{}^{2/3}} m_0^{\left(2/3 - \mu\right)}, k_m = \frac{1}{2} \frac{c_h \rho_a A_0}{H^* \rho_{m_0}{}^{2/3}} m_0^{\left(2/3 - \mu\right)}. \tag{19}$$

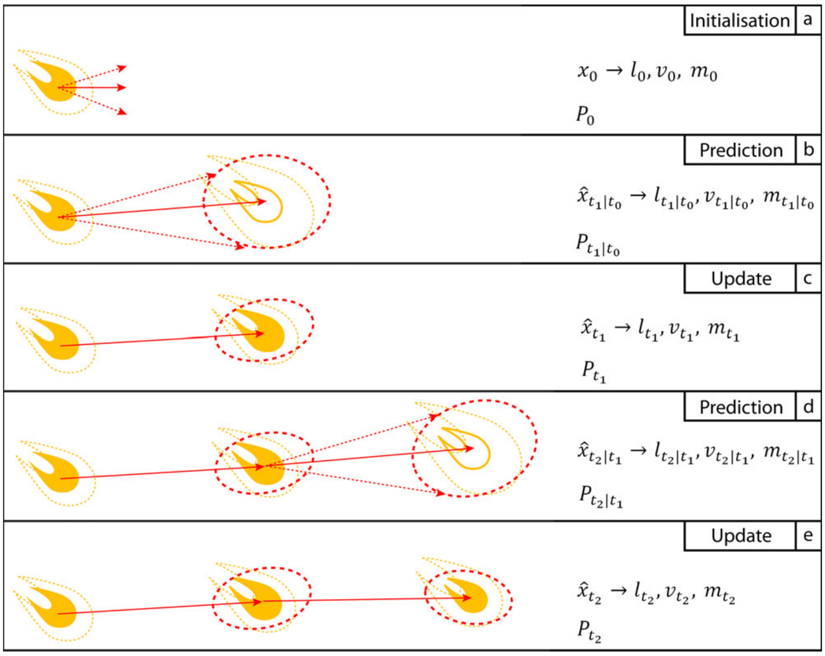

Fig. 1. Illustration of the extended Kalman filter process. a) Initialization of state. The P_0 matrix defines the initial uncertainties (dashed) in velocity (red arrow) and mass (yellow). b) A prediction is made and the state matrix, $\hat{x}_{k|k-1}$, has covariances defined by $P_{k|k-1}$. Mass uncertainties are initially large, as is position (dashed red). (c) Measurement update calibrates the state and uncertainties decrease (d) prediction step (e) measurement step. These two processes (d–e) repeat to give a final state estimate ($\hat{x}_f$) and associated covariance matrix (P_f).

Measurement Updates

The measurement update step follows an observation z_k (Equation 20), which for ADFO observations is only the distance data $l_k = (x_1)_k$. H_k provides a relationship between the state of the dynamic system and the measureable observations, simply put, $H_k x_k = l_k$. n_k is the measurement noise with a mean of zero and covariance R_k (Equation 21). R_k, therefore, accounts for errors between measured position and true position due to aspects such as camera calibration, triangulation, camera resolution etc.

$$z_k = H_k x_k + n_k \tag{20}$$

$$R_k = E[n_k n_k'] = \left[{\sigma_{z_k}}^2\right] \tag{21}$$

The predicted measurement can be made using the output of Equation 13

$$\hat{z}_k = H_k \hat{x}_{k|k-1} \tag{22}$$

The residual difference between z_k and $\hat{z}_k$ is y_k (Equation 23). S_k (Equation 24) projects the system uncertainty into the measurement space and includes uncertainties in the model up to t_{k-1}, as well as the noise covariance of the current measurement. The optimum Kalman gain, K_k (Equation 25) is used to update the state ($\hat{x}_k$) and covariance matrices (P_k) (Equations 26–27)

$$y_k = z_k - \hat{z}_k \tag{23}$$

$$S_k = H_k P_{k|k-1} H_k^T + R_k \tag{24}$$

$$K_k = P_{k|k-1} H_k^T S_k^{-1} \tag{25}$$

$$\hat{x}_k = \hat{x}_{k|k-1} + K_k y_k \tag{26}$$

$$P_k = (I - K_k H_k) P_{k|k-1} \tag{27}$$

The square root of the diagonal elements of P_k is plotted as error bars so that the evolution of state uncertainty with time can be visualized in a meaningful way.

Fireball Applications

For the nonlinear bolide dynamical equations, $\hat{x}_{k+1|k}$ is calculated by solving the nonlinear

Equations 6–7 between t_{k+1} and t_k. P_k, however, is solved using the linearized state transition matrix, F_k (Equation 28). The linearization of F_k approximates to:

$$F_k = \begin{pmatrix} 1 & 0 & \Delta t \\ 0 & 1 - k_m v_0^3 m_0^{\mu}\left(\frac{\mu}{m_0}\right)\Delta t & -k_m v_0^3 m_0^{\mu}\left(\frac{3}{v_0}\right)\Delta t \\ 0 & -k_v v_0^2 m_0^{(\mu-1)}\left(\frac{(\mu-1)}{m_0}\right)\Delta t & 1 - k_v v_0^2 m_0^{(\mu-1)}\left(\frac{2}{v_0}\right)\Delta t \end{pmatrix} \tag{28}$$

The errors associated with this linearization are included in the process covariance matrix, Q_k, along with the uncertainties in the model due to unmodeled factors such atmospheric disturbances and uncertainties in the atmospheric model used. The value of Q_k encapsulates these model uncertainties and is specific to the individual data set being analyzed.

P_0 is initialized at t_0 as a function of initial data uncertainty (Equation 29). As the length along the flight path is relative to the initial point, there is no model error in σ_{l_0} being zero (error in *observation* of positions is accounted for in R_k). The initial mass covariance is given as 0.5 times the initial mass determined by the dynamical optimization. Distance error and timing information give uncertainties of up to ±1500 m s^{-1} for velocity.

$$P_0 = \begin{bmatrix} \sigma_{l_0}^2 & 0 & 0 \\ 0 & \sigma_{m_0}^2 & 0 \\ 0 & 0 & \sigma_{v_0}^2 \end{bmatrix} = \begin{bmatrix} 0 & 0 & 0 \\ 0 & \left(m_0 \times 0.5\,\mathrm{kg}\right)^2 & 0 \\ 0 & 0 & \left(1500\,\mathrm{km\,s^{-1}}\right)^2 \end{bmatrix} \tag{29}$$

The initial errors are large but P_k is updated throughout the iterative estimation, giving a concrete representation of the evolution of the confidence of the state estimate, incorporating the uncertainties defined by the process noise covariance, Q_k (Equation 12), and the measurement noise covariance, R_k (Equation 21). The measurement noise covariance for the bolide problem is set to be $(100\ \mathrm{m})^2$ and is dependent on camera resolution, the angle of the fireball with respect to the camera, and calibration of lens distortion.

Smoothing Problem

More generally, we can apply a smoothing estimator to our fireball data sets, as we will always have the observations from the entire trajectory available when the estimation is performed. A *filtering* estimator, such as described above, uses only past data (and hence is suitable for real-time estimation), whereas a *smoothing* estimator uses all data (future and past) to generate an optimal state estimate. The Rauch–Tung–Striebel (RTS) smoothing algorithm is implemented using the method described by Sarkka (2008). The resulting state estimate values for the trajectory are improved, along with their uncertainties.

RESULTS

The most complete data set available to test this method is that of Bunburra Rockhole, published by Spurný et al. (2012), which contains 113 data points with time, length of segment, and altitude information. As this data resulted in a recovered meteorite, constraints are available on final mass (Spurný et al. 2012), and cosmic ray exposure rates (Welten et al. 2012) provide an estimate of initial body diameter.

Dynamic Optimization

The dynamic optimization method described earlier, is applied to the data set using the constraints on parameters given in Table 2. Five parameter sets produce a fit with cost values >0.98 (Table 3). The initial masses range from 27.65 to 30.12 kg (Fig. 2) but the final masses converge to values of ~2.4 kg.

Figure 2 allows a visual comparison of these model outputs to the raw data. The parameter sets defined in Table 3 are used to initialize a set of Kalman filters that will take the data itself into consideration to determine a final mass.

Kalman Filter

The Extended Kalman Filter runs separately on each set of parameters resulting from the dynamical optimization stage. The final states of each model setup are given in Table 4.

The change in state values during the iterative EKF process are graphed against time with covariance plotted as approximate error bars (Fig. 3). The uncertainties are high initially. Mass uncertainties are only constrained by the data through the link to velocity with the dynamic equations and therefore remain high while the iterative process determines a value.

After running the forward EKF, the Rauch–Tung–Striebel smoothing algorithm is run (Fig. 4). The outcome of smoothing produces an initial entry mass of 30.20 ± 6.53 kg.

Checking Results Using the Dimensionless Coefficient Method

As a comparison, we also analyzed the Bunburra Rockhole data set using the approach based on Stulov et al. (1995) and applied by Gritsevich (2008b). In this

Table 3. Top five best fit parameter sets resulting from dynamical optimization.

Normalized sum of square differences to position	m_0 (kg)	v_0 (m s^{-1})	$\frac{A_0}{{\rho_{m_0}}^{2/3}}$ (kg m^{-3})$^{-2/3}$	$\frac{c_h}{H^*}$ ($\times 10^{-8}$ J kg^{-1})	l_f (m)	m_f (kg)	v_f (m s^{-1})
1.00000	30.12	13198	0.009511	4.82	60071.8	2.36	6109
0.99859	30.95	13203	0.009689	4.76	60042.4	2.50	6100
0.98862	29.82	13203	0.009545	4.68	60061.8	2.51	6124
0.98544	28.64	13204	0.009466	4.66	60057.6	2.44	6125
0.98108	27.65	13205	0.009394	4.64	60052.7	2.38	6126

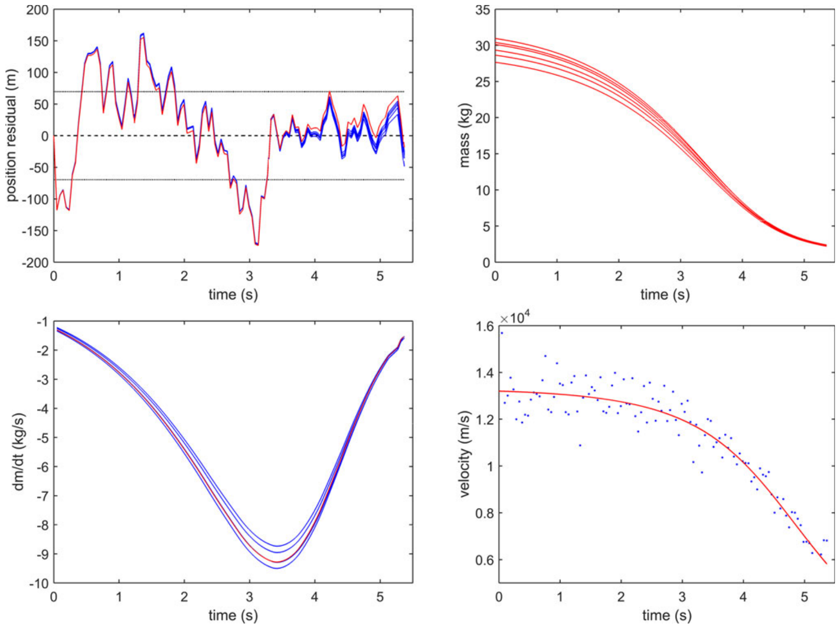

Fig. 2. Top left: position data subtracted from modeled position for models with parameters given in Table 3. Red curve is model that gives the lowest normalized sum of square differences (initial mass of 30.12). Dotted line is one standard deviation (70.14 m). Top right: shows associated change in mass for corresponding model parameters with costs >0.98. Bottom left: derivative of mass with time for models. Bottom right: comparison of models (red curves) to calculated velocity (blue points).

Table 4. Final states (x_f, m_f, v_f) for parameter sets from dynamic optimization corresponding to the following initial masses.

m_0 (kg)	x_f (m)	m_f (kg)	v_f (m s^{-1})
30.12	60032 ± 62	2.30 ± 1.63	6052 ± 241
30.95	60032 ± 62	2.47 ± 1.67	6057 ± 236
29.82	60033 ± 62	2.40 ± 1.67	6061 ± 238
28.64	60033 ± 62	2.35 ± 1.66	6062 ± 240
27.65	60033 ± 62	2.29 ± 1.64	6062 ± 242

method, the dynamic Equations 1–2 are modified by normalizing the values of mass, velocity, and altitude (h) to the entry mass, entry velocity, and the scale height of the homogeneous atmosphere (h_0 = 7160 m), respectively. A set of dimensionless parameters (ballistic coefficient, α [26], and mass loss parameter, β [31]) are substituted to remove the need of unknown individual variables.

$$\alpha = \frac{c_d \rho_0 h_0 A_0 {m_0}^{-1/3}}{2{\rho_{m_0}}^{2/3} \sin\gamma} \tag{30}$$

$$\beta = (1-\mu)\frac{c_h v_0^2}{2 c_d H^*} \tag{31}$$

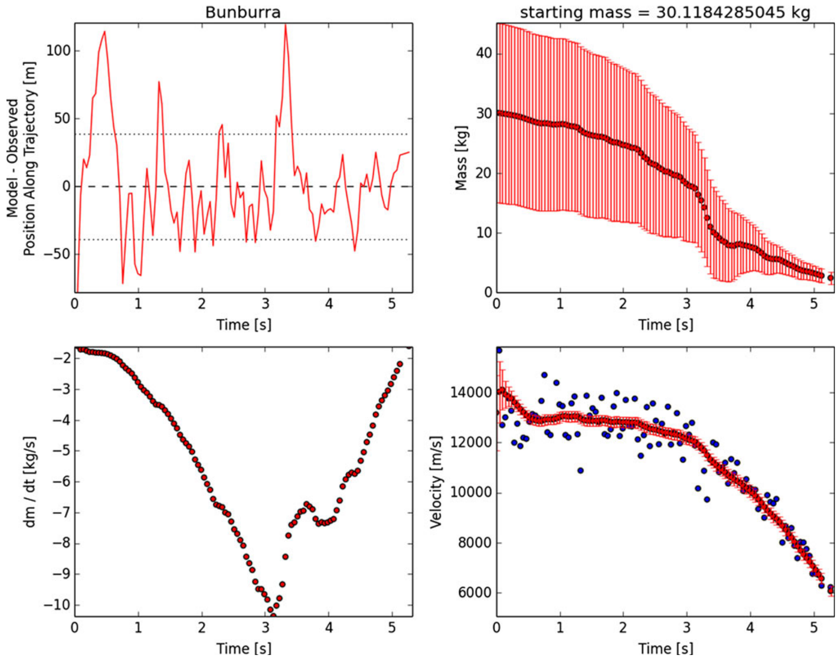

Fig. 3. Extended Kalman Filter results for initial mass of 30.12 kg. Top left: residual plot of position data subtracted from EKF position estimate. Dotted lines represent one standard deviation (38.83 m). Top right: mass error bars are extracted from the constantly updating P matrix. Bottom left: derivative of mass with time, showing relative mass loss predicted for each time step. Bottom right: blue points represent calculated velocity values. Red points are EKF estimates of velocity given only past data from each time step. Although mass and velocity will never realistically increase, as the EKF is provided with new data at each time step, it corrects the values of previous estimates.

where ρ_0 is the atmospheric density near the surface and γ is the trajectory entry angle.

The Q_4 method of least-squares minimization defined by Gritsevich (2008b) is used to create a fit of the Kulakov and Stulov (1992) Equation 32 to the Bunburra Rockhole data set.

$$y = \ln\alpha - \ln(-\ln V) + 0.83\beta(1 - V) \tag{32}$$

where $y = \frac{h}{h_0}$ and $V = \frac{v}{v_0}$.

The isothermal atmosphere approximation is used to derive Equation 32: $\rho_a = e^{-y}$, making it difficult to implement a more accurate atmosphere model.

Although this method has proved successful on previous fireball data sets (Gritsevich 2008a), these are limited to fewer than 20 velocity points with an average based smoothing applied (Ceplecha 1961). The value of v_0 that is used to normalize all velocity values is simply the initial velocity. For the Bunburra Rockhole data set, the 113 data points show high scatter and the velocity range within the first half a second has a range of over 3500 m s^{-1}. It was found that the noise in the raw data could not be accommodated by this method without pretreating the data, making it rather unsuitable for use in an automated data pipeline where large noisy data sets need to be processed.

Smoothing the data using a five-point moving average, and using the average initial velocity from Table 3, 13,200 m s^{-1}, and a value of 2/3 for the shape change parameter allows a result to be calculated as a comparison to the new method. This gives $\alpha = 25.23$ and $\beta = 1.53$ (Fig. 5). The equation for the ballistic coefficient (Equation 30) allows an initial mass to be calculated. By assuming values of the shape-density parameter from the dynamic optimization, and a constant drag coefficient of 1.3, an approximate value for m_0 is determined to be 84.92 kg.

When used in the following Equation 33, along with a value of 2/3 for rotation, a final mass of 1.90 kg results.

$$m_f = m_0 e^{\left(-\beta\frac{1-V_f^2}{1-\mu}\right)} \tag{33}$$

(equation 6 [Gritsevich 2008b])

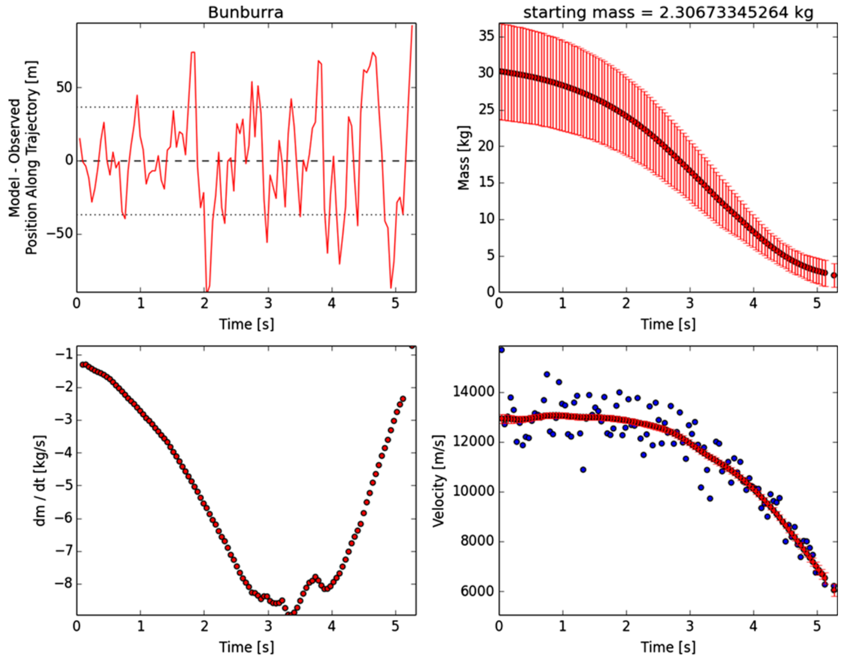

Fig. 4. RTS smoothing filter results for the best fit parameter set. Top left: residual plot of position data subtracted from RTS position estimate. Dotted lines represent one standard deviation (36.73 m). Top right: predicted mass along trajectory. Bottom left: derivative of mass with time, showing relative mass loss predicted for each time step. Bottom right: blue points represent calculated velocity values. Red points are RTS estimates of velocity given both past and future state estimates.

It is difficult to assess the error in this case, and the ranges in initial and final masses are harder to obtain. The amount of scatter in the velocity data is significant and a change in initial velocity used by 1% can result in initial masses varying by ±30 kg and final masses to be ±2 kg.

DISCUSSION

Determining Model Parameters

The dynamical optimization of the Bunburra Rockhole data set returned a large number of parameter sets with cost values >0.9, although only five with >0.98, all of which show relatively similar starting masses. The ranged (27.65–31.12 kg) initial masses converge (Fig. 2) to give very similar final mass values (Table 3). As the final masses are needed for determining any potential fall positions, it is more important that these values be limited. It should be remembered that the dynamic optimization is estimating appropriate meteoroid parameters to use as inputs in our main model (EKF step) based on this specific fireball data set. Previous works have assumed "typical," or average meteoroid parameter values, without the link to the data from the event in question (e.g., densities by Borovička et al. [1998, 2013] and McCrosky et al. [1971]; shape density coefficient used by Ceplecha and ReVelle [2005] and Spurný et al. [2012]). We believe that this is an advantage of our approach. This step gives us greater confidence in the estimates to be used in the EKF step, especially considering the similarities in meteoroid characteristics of the top results (Table 3).

The shape parameter and preatmospheric meteoroid density cannot be uniquely identified in this model. The values of $\frac{A_0}{\rho_{m_0}^{2/3}}$ in Table 3 could correspond to a spherical object ($A_0 = 1.21$) with a preatmospheric meteoroid density of ~1400 kg m^{-3}, a circular cylinder with a cross sectional diameter to length ratio of roughly 1:1 and ρ_{m_0} ~2700 kg m^{-3}, or even a 3:2:1 triaxial ellipsoid (as suggested by Zhdan et al. 2007) with ρ_{m_0} ~3500 kg m^{-3}. A unique solution is not needed for finding any potential meteorites and any fragments found will be able to resolve these two parameters.

Knowing the Bunburra Rockhole bulk meteorite density to be 2700 kg m^{-3} (Spurný et al. 2012) enables us to approximate the meteoroid shape, A ~1.85. This corresponds to a circular cylinder with a cross sectional

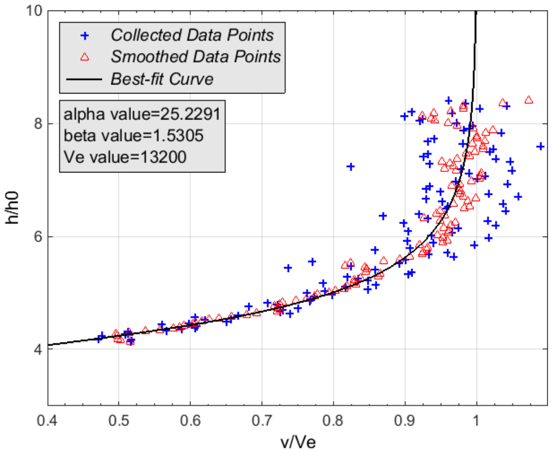

Fig. 5. Raw (+) and smoothed (Δ) Bunburra Rockhole velocities normalized to an entry velocity of 13,200 m s^{-1} versus normalized altitude, *y*. Best fit for Equation 32 is shown which is produced using α = 25.23 and β = 1.53.

Table 5. Values of $\frac{c_h}{H^*}$ determined by the dynamical optimization stage (Table 3) and the subsequent approximate values of c_h. σ values are given for a drag coefficient of 1.3.

$\frac{c_h}{H^*}$ ($\times 10^{-8}$ J kg^{-1})	c_h given H* = 2 × 10^6 J kg^{-1}	σ ($\times 10^{-6}$ s^2 m^{-2})
4.820	0.0964	0.0371
4.755	0.0951	0.0366
4.684	0.0937	0.0360
4.662	0.0932	0.0359
4.644	0.0929	0.0357

diameter to length ratio of roughly 1:1, or a 3:2:1.5 axial ellipsoid. If the value of *A* and ρ_m were to remain constant, these values of A_0 and ρ_{m_0} with the given initial mass corresponds approximately to a cross sectional area of 0.092 m^2. Figure 7.2 in Stulov et al. (1995) shows a distribution of values of *H** for bolides, resulting in an overwhelming majority with entry masses >1 kg, having values close to 2 × 10^6 J kg^{-1}. If this value is assumed for *H**, values for c_h can be approximated (Table 5). It may be useful as a comparison to give also the ablation coefficient, $\sigma = \frac{c_h}{c_d H^*}$ (Table 5), given a drag coefficient of 1.3. σ values are very similar to the apparent ablation coefficient values determined by Spurný et al. (2012). This is to be expected as fragmentation is currently not incorporated to allow intrinsic values of σ to be determined by the dynamic optimization.

The Model Solution

The initial 3 s of the Bunburra Rockhole velocity data is rather noisy, varying by around ±2000 m s^{-1}. However, it is handled coherently by our EKF approach without the inclusion of an arbitrary smoothing step. The EKF optimizes the state of the bolide at each individual time-step. Each point on the graphs of Fig. 3 are the instantaneous representation of the state at a given time given only the past data. The values are variable within their error ranges as the data are not perfect. It is not a simple least squares, it does not aim to reduce the covariance, rather it "learns" from the data and predicts where it should be and carries the errors forward. The covariance incorporates both measurement uncertainty and scatter to give a comprehensive understanding of the errors associated with each state. Where previous works have used best fit modeling, primarily least squares fits (Ceplecha and ReVelle 2005), by taking this intelligent "predict" and "update" approach, the EKF method is likely to come closer to approximating the real position of the object at any given time. This is reflected in the lower standard deviation of the residual plots (38.83 m for EKF versus 70.14 m for dynamical optimization)

Despite the variation in parameter sets provided by the dynamical optimization, the final masses which are most important for finding any potential fall positions (and therefore the primary solution of this modeling), are very similar and their range constrains the final bright flight mass. The best estimate of final mass is 2.30 ± 1.63 kg and is close to the published value of 1.1 kg by Spurný et al. (2012).

The initial mass determined by Spurný et al. (2012) using both the methods described by both Ceplecha et al. (1998) and Ceplecha and ReVelle (2005) is 22.0 ± 1.3 kg. Cosmic ray exposure rates were analyzed for the Bunburra Rockhole meteorite; however, the pre-entry radius was determined to be larger than a radius corresponding to a mass of 22 kg (Welten et al. 2012). By performing a reverse extended Kalman filter, the entry mass is determined to be closer to 30.20 ± 6.53 kg. This corresponds to a pre-entry radius of around 17.1 cm. This is close to the 13–17 cm range determined by (Welten et al. 2012).

Although fragmentation is not yet explicitly handled using this method, the data reflects both effects of ablation and fragmentation. The process noise Q_k in the EKF model handles some degree of unexpected mass change, allowing these variations to be incorporated in the final mass estimates.

Furthermore, sudden increases in the magnitude of the state variance matrix P_k can give an indication that a fragmentation event may have occurred, along with examining the change in mass with time (Figs. 3 and 4). It is noticeable from both Figs. 3 and 4 that there are peaks of maximum mass loss at around 3.133 and 3.845 s as well as at 4.415 s in Fig. 3. It is likely that these correspond to fragmentation events. These times correspond to altitudes of 41.31, 37.16, and 34.18 km, respectively, allowing a comparison to fig. 13 in Spurný et al. (2012) which shows significant changes of mass at 37.8 and 35.85 km altitude. The significant mass loss event seen in fig. 13 in Spurný et al. (2012) at 54.9 km (corresponding to 1.0 s) is not evident, although it is well within the large error bracket given at this time. Future work will aim to capture this fragmentation information in a coherent and consistent way.

The scatter in the Bunburra Rockhole data set presented difficulties when initially attempting to use the method outlined by Gritsevich (2008a). After smoothing the data and using the initial parameters determined by the dynamic optimization, final values are similar to those determined using this new method. The dependence on an initial velocity for normalization makes it very sensitive to initial scatter and there is no constraint on the errors this or the smoothing may cause. The EKF method avoids these dependences.

CONCLUSION

The method outlined here provides a consistent and detailed approach to characterizing meteoroids without the need for brightness data as they pass through the atmosphere. In addition, it provides a rigorous way of propagating uncertainties in trajectory states (position, mass, and velocity), something that previous approaches have not explicitly described.

A dynamic optimization determines the optimum parameters for the meteoroid flight such as the shape-density parameter and initial mass. An extended Kalman filter then includes observation and dynamic uncertainty models, which are valuable in understanding the errors in the model states, and which can adapt to fragmentation events or other unexpected dynamic changes. The initial (30.20 ± 6.53 kg) and final masses (2.30 ± 1.63 kg) calculated for the Bunburra Rockhole data set is within the range of previously published values by Spurný et al. (2012) (22.0 ± 1.3 and 1.1 kg, respectively) and corresponds with cosmic ray exposure studies (Welten et al. 2012) to constrain preatmospheric radius and mass. Although the method used by Gritsevich (2008b) was re-created using the meteoroid characteristics determined by dynamic optimization, the sensitivity of this method to (widely varying) data for initial entry velocity translates to a range of estimates for entry and terminal masses. As the errors are not quantified, the confidence in mass calculations using this method—crucial for automating our data flow and constraining search areas—cannot be constrained.

The two-step approach outlined in this paper is an automated method which will allow the DFN to reduce data for every observed fireball, rather than only selecting high value or unusual cases. For the subset that involve a meteorite fall, this approach will calculate multiple fall positions with comprehensive error values to allow for efficient recovery searches. Work still needs to be carried out on integrating the variability in the heat-transfer coefficient. The assumption in this method that it remains constant throughout the trajectory is a simplification. The identification and analysis of fragmentation events also needs to be incorporated in a more coherent and consistent manner.

Acknowledgments—This work was funded by the Australian Research Council as part of the Australian Laureate Fellowship scheme. The authors thank N. Artemieva, J. Borovička, and O. Popova for constructive comments and reviews that significantly improved the quality of the final manuscript.

Editorial Handling—Dr. Natalia Artemieva

REFERENCES

Baldwin B. and Sheaffer Y. 1971. Ablation and breakup of large meteoroids during atmospheric entry. *Journal of Geophysical Research* 76:4653–4668.

Borovička J., Popova O., Nemtchinov I., Spurný P., and Ceplecha Z. 1998. Bolides produced by impacts of large meteoroids into the Earth's atmosphere: Comparison of theory with observations. I. Benesov bolide dynamics and fragmentation. *Astronomy & Astrophysics* 334:713–728.

Borovička J., Tóth J., Igaz A., Spurný P., Kalenda P., Haloda J., Svoreň J., Kornoš L., Silber E., Brown P., and Husárik M. 2013. The Košice meteorite fall: Atmospheric trajectory, fragmentation, and orbit. *Meteoritics & Planetary Science* 48:1757–1779.

Bronshten V. A. 1983. *Physics of meteoric phenomena. Fizika meteornykh iavlenii, Moscow, Izdatel'stvo Nauka, 1981.* Dordrecht: D. Reidel Publishing Co. 372 p.

Brykina I. and Stulov V. 2012. The reciprocal role of convective and radiant heat exchange in the meteor-parameter range. *Doklady Physics* 57:164–165.

Ceplecha Z. 1961. Multiple fall of Příbram meteorites photographed. 1. Double-station photographs of the fireball and their relations to the found meteorites. *Bulletin of the Astronomical Institutes of Czechoslovakia* 12:21.

Ceplecha Z. and ReVelle D. O. 2005. Fragmentation model of meteoroid motion, mass loss, and radiation in the atmosphere. *Meteoritics & Planetary Science* 40:35–54.

Ceplecha Z., Spurny P., Borovička J., and Keclikova J. 1993. Atmospheric fragmentation of meteoriods. *Astronomy & Astrophysics* 279:615–626.

Ceplecha Z., Borovička J., Elford W. G., ReVelle D. O., Hawkes R. L., Porubčan V., and Šimek M. 1998. Meteor phenomena and bodies. *Space Science Reviews* 84:327–471.

Grewal M. and Andrews A. P. 1993. *Kalman filtering: Theory and practice*. Upper Saddle River, NJ: Pearson Prentice Hall.

Gritsevich M. 2008a. The Příbram, Lost City, Innisfree, and Neuschwanstein falls: An analysis of the atmospheric trajectories. *Solar System Research* 42:372–390.

Gritsevich M. 2008b. Validity of the photometric formula for estimating the mass of a fireball projectile. *Doklady Physics* 53:97–102.

Haider A. and Levenspiel O. 1989. Drag coefficient and terminal velocity of spherical and nonspherical particles. *Powder Technology* 58:63–70.

Hayes W. D. and Probstein R. F. 1959. *Hypersonic flow theory*. New York: Academic Press.

Khanukaeva D. Y. 2005. Calculation of variable drag and heat-transfer coefficients in meteoritic physics equations. In *Modern meteor science: An interdisciplinary view*, edited by Hawkes R. L., Mann I., and Brown P. G. Dordrecht, the Netherlands: Springer. pp. 433–439.

Kulakov A. and Stulov V. 1992. Determination of meteor body parameters from observational data. *Astronomicheskii Vestnik* 26:67–75.

Masson D. J., Morris D. N., and Bloxsom D. E. 1960. *Measurements of sphere drag from hypersonic continuum to free-molecule flow*. Santa Monica, California: RAND Corporation.

McCrosky R., Posen A., Schwartz G., and Shao C.-Y. 1971. Lost City meteorite—Its recovery and a comparison with other fireballs. *Journal of Geophysical Research* 76:4090–4108.

Picone J., Hedin A., Drob D. P., and Aikin A. 2002. NRLMSISE-00 empirical model of the atmosphere: Statistical comparisons and scientific issues. *Journal of Geophysical Research: Space Physics (1978–2012)* 107:1468.

ReVelle D. O. 1976. *Dynamics and thermodynamics of large meteor entry: A quasi-simple ablation model*. Ottawa, Canada: Herzberg Institute of Astrophysics, National Research Council Canada.

Sarkka S. 2008. Unscented Rauch-Tung-Striebel Smoother. *Automatic Control, IEEE Transactions on* 53:845–849.

Schlichting H., Gersten K., and Gersten K. 2000. *Boundary-layer theory*. New York: Springer.

Spurný P., Bland P. A., Borovicka J., Shrbený L., McClafferty T., Singelton A., Bevan A. W. R., Vaughan D., Towner M. C., and Deacon G. 2012. The Bunburra Rockhole meteorite fall in SW Australia: Fireball trajectory, luminosity, dynamics, orbit, and impact position from photographic and photoelectric records. *Meteoritics & Planetary Science* 47:163–185.

Stulov V., Mirskii V., and Vislyi A. 1995. *Aerodynamics of bolides*. Moscow: Science. Fizmatlit.

Towner M., Towner M. C., Bland P. A., Spurný P., Benedix G. K., Dyl K., Greenwood R. C., Gibson J., Franchi I. A., Shrbený L., Bevan A. W. R., and Vaughan D. 2011. Mason Gully: The second meteorite recovered by the Desert Fireball Network. *Meteoritics & Planetary Science Supplement* 74:5124.

Truitt R. W. 1959. *Hypersonic aerodynamics*. New York: Ronald Press Co.

Welten K. C., Meier M. M., Caffee M. W., Laubenstein M., Nishizumi K., Wieler R., Bland P. A., Towner M. C., and Spurný P. 2012. Cosmic-ray exposure age and preatmospheric size of the Bunburra Rockhole achondrite. *Meteoritics & Planetary Science* 47:186–196.

Whipple F. L. 1952. Meteoritic phenomena and meteorites. *Physics and Medicine of the Upper Atmosphere* 137:149–153.

Zhdan I., Stulov V., Stulov P., and Turchak L. 2007. Drag coefficients for bodies of meteorite-like shapes. *Solar System Research* 41:505–508.

PAPER 2 – FILTERING METEOROID FLIGHT USING MULTIPLE UNSCENTED KALMAN FILTERS

The Astronomical Journal (2016), Volume 152, Issue 5, pp. 148–156

Sansom, E. K., Rutten, M. G., Bland, P. A, Paxman, J., Towner, M. C.

STATEMENT OF AUTHORSHIP

TITLE OF PAPER: Filtering Meteoroid Flight Using Multiple Unscented Kalman Filters

PUBLICATION STATUS: Published

AUTHOR CONTRIBUTIONS

By signing the Statement of Authorship, each author certifies that their stated contribution to the publication is accurate and that permission is granted for the publication to be included in the candidate's thesis.

Name of Principal Author: Eleanor K. Sansom

Contribution to the Paper: Led all aspects of this research, drafted and revise the manuscript for this publication.

Overall Percentage: 85%

Signature: *Date:* 01 / 12 / 16

Name of Co-Author: Mark G. Rutten

Contribution to the Paper: Helped with MATLAB coding and integration of smoother within the interacting multiple model as well as editing and revision of the manuscript.

Overall Percentage: 10%

Signature: *Date:* 5 / 12 / 16

Name of Co-Author: Phillip A. Bland

Contribution to the Paper: Assisted with editing and revision of the manuscript.

Overall Percentage: 3%

Signature: Philip Bland *Date:* 4 / 12 / 16

Name of Co-Author: Jonathan Paxman

Contribution to the Paper: Helped in the final review of the manuscript.

Overall Percentage: 1%

Signature: *Date:* 5/12/16

Name of Co-Author: Martin C. Towner

Contribution to the Paper: Helped in the final review of the manuscript.

Overall Percentage: 1%

Signature: M Tow *Date:* 05/12/16

THE ASTRONOMICAL JOURNAL, 152:148 (8pp), 2016 November
doi:10.3847/0004-6256/152/5/148

FILTERING METEOROID FLIGHTS USING MULTIPLE UNSCENTED KALMAN FILTERS

E. K. SANSOM[1], P. A. BLAND[1], M. G. RUTTEN[2], J. PAXMAN[3], AND M. C. TOWNER[1]
[1] Department of Applied Geology, Curtin University, GPO Box U1987, Perth, WA 6845, Australia
[2] Defence Science and Technology Group, Edinburgh, SA 5111, Australia
[3] Department of Mechanical Engineering, Curtin University, GPO Box U1987, Perth, WA 6845, Australia
Received 2016 April 27; revised 2016 August 17; accepted 2016 August 31; published 2016 October 31

ABSTRACT

Estimator algorithms are immensely versatile and powerful tools that can be applied to any problem where a dynamic system can be modeled by a set of equations and where observations are available. A well designed estimator enables system states to be optimally predicted and errors to be rigorously quantified. Unscented Kalman filters (UKFs) and interactive multiple models can be found in methods from satellite tracking to self-driving cars. The luminous trajectory of the Bunburra Rockhole fireball was observed by the Desert Fireball Network in mid-2007. The recorded data set is used in this paper to examine the application of these two techniques as a viable approach to characterizing fireball dynamics. The nonlinear, single-body system of equations, used to model meteoroid entry through the atmosphere, is challenged by gross fragmentation events that may occur. The incorporation of the UKF within an interactive multiple model smoother provides a likely solution for when fragmentation events may occur as well as providing a statistical analysis of the state uncertainties. In addition to these benefits, another advantage of this approach is its automatability for use within an image processing pipeline to facilitate large fireball data analyses and meteorite recoveries.

Key words: meteorites, meteors, meteoroids – methods: observational – methods: statistical

1. INTRODUCTION

Fireballs are the visible phenomena that are observed when a meteoroid penetrates the Earth's atmosphere (Ceplecha et al. 1998). Dedicated fireball networks (e.g., the Desert Fireball Network in Australia; Bland et al. 2012) record the luminous paths of fireball phenomena at discrete increments, from multiple viewpoints, allowing the triangulated trajectory to be determined as a function of time. With good timing and position information recorded during flight, the final position, velocity, and mass may lead to the recovery of a meteorite. Few meteorites discovered have known orbits, and giving contextual information for these primitive objects gives valuable insights into solar system formation. As a meteoroid decelerates through the atmosphere, it loses mass by both ablation and gross fragmentation, which can be modeled by the single-body theory of meteoroid physics (Ceplecha et al. 1993). This system of equations requires the knowledge of trajectory parameters that are unique to each event and not directly observable. Modeling how a meteoroid's mass changes has typically been based on comparing positions observed along a fireball trajectory with model-computed distances, using the method of least squares (Ceplecha et al. 1993; Ceplecha & Revelle 2005). The main complication to fireball modeling is the incorporation of gross fragmentation. Fragmentation is a phenomenon that significantly challenges the application of a single-body theory to observed fireballs (Ceplecha & Revelle 2005).

The least-squares method has undergone an iterative development over the years. Ceplecha et al. (1993) used it to solve for four free parameters in single-body dynamic equations, and introduced two additional parameters with the inclusion of a single gross fragmentation event. The standard deviation of least-squares residuals is used as a measure of model error. To determine the timing of a gross fragmentation event, Ceplecha et al. (1993) use a brute force approach. Each observation is tested as a potential gross fragmentation point and a solution that yields the minimum standard deviation case is considered as a possible point of gross fragmentation. This method, when applied to Prairie Network bolides greater than −10 mag, resulted in an average standard deviation for the position residuals equal to ±30 m (Ceplecha et al. 1996) which is comparable to the ±20 m typical precision in the observed position. Ceplecha & Revelle (2005) added to this method by incorporating the computation of meteoroid light intensity. This is also part of the single-body equation system for a meteoroid, but to be able to compare to observations, the light curve of the fireball must be known. This is typically acquired using a high-cost photoelectric photometer tube attached to each observation station. As well as being strongly dependent on an accurate light curve for luminosity values, Ceplecha & Revelle (2005) assume that flares on a meteor light curve represent gross fragmentation events. These are amassed to create an assumed "fragmentation pattern," prior to model computation, with further assumptions on the amount of mass released from the main body and changes to model parameters that occur during these events. This is manually intensive, especially when different flare forms are associated with various types of fragmentation (e.g., a spike in the light curve is linked to the release of dust and a smooth "hump" is associated with an eroding fragment; Borovička et al. 2013). This can lead to a trial-and-error fit of the fragmentation pattern to reproduce major features on a light curve (Borovička et al. 2013).

The majority of fireball trajectories are also limited to fewer than 25 discreet positional observations (Halliday et al. 1996) and due to low sample rates, and in many cases averaging of multiple observations during processing (Cep; McCrosky & Posen 1968), there is little scatter in the data. This has led to issues when the typical approach is confronted with a highly scattered data set such as that of the Bunburra Rockhole fireball. Of the 113 observations measured by Spurný et al. (2012), only 87 were used for their modeling. The majority of the discarded points were during significant periods of deceleration and are acknowledged by the authors to be caused by large fragmentation events.

The least-squares approach has become increasingly complex as it has evolved, from no fragmentation to the manually intense modeling of a full suite of fragments based on a trial-and-error approach to fitting the light curve. Final errors are determined based on the residual fit to observations; this does not offer a rigorous analysis of the errors introduced by the assumed parameters, the single-body theory model used, or complete error propagation of uncertainties in the observations.

Sansom et al. (2015) proposed a two-step process for assessing meteoroid entry using position dynamics alone. Their method includes an extended Kalman filter (EKF) to rigorously examine errors in meteoroid modeling. An EKF is an estimator that uses linearized models to predict the state of an object with nonlinear system equations and provides a comprehensive understanding of the errors involved based on the observational data set. A major benefit of this approach is that it can be automated; the least-squares method requires some manual input, meaning the majority of data collected by a fireball network does not undergo a full trajectory analysis. In the case of large dedicated camera networks (e.g., the Desert Fireball Network in Australia; Bland et al. 2012), the ability to integrate fireball modeling into a complete automated data reduction pipeline is a significant advantage. Data volumes are such that traditional (manually intensive) approaches would only allow a very small fraction of events to be analyzed. Software that has been developed for this pipeline includes event detection, calibration of coordinates, triangulation, mass determination, orbital calculations, wind modeling, and the prediction of a fall line for potential surviving masses. Although the EKF introduced by Sansom et al. (2015) is a step forward in terms of error analysis, the use of an EKF algorithm does require the single-body dynamic equations to be linearized and does not explicitly handle fragmentation.

Here we propose the use of another estimator used in the field of guidance, navigation and control: the unscented Kalman filter (UKF) as well as the interacting multiple model (IMM) to address the linearization and fragmentation shortcomings of the EKF. A UKF allows a more rigorous approach to handling the nonlinear model equations, and an IMM enables an analysis of when gross fragmentation is likely to occur. Once again the trajectory data set for Bunburra Rockhole (Spurný et al. 2012) will be used to test the model as well as compare results with the EKF.

2. METEOROID FLIGHT USING FILTERS

The application of filtering and estimation to the problem of meteoroid flight was first used by Sansom et al. (2015) with the use of an EKF. The filtering process allows the prediction and evaluation of the state, $\boldsymbol{x}_k = $ (position (l), mass (m) and velocity (v)), of the meteoroid based on the observations z_k of its position at each time step k during flight. The flight of a meteoroid through the atmosphere as a function of time t may be modeled using the dynamic single-body aerodynamic Equation (1). These are the three state equations used by the filtering process:

$$\frac{dl}{dt} = v \tag{1a}$$

$$\frac{dm}{dt} = -\frac{1}{2}\sigma\kappa\rho_a v^3 m^{\mu} \tag{1b}$$

$$\frac{dv}{dt} = -\frac{1}{2}\kappa\rho_a v^2 m^{(\mu-1)} + g\sin\gamma_e \tag{1c}$$

where ρ_a, g and γ_e are the local atmospheric density (kg m^{-3}), gravity (m s^{-2}) and flight angle from horizontal respectively and the shape density coefficient $\kappa = \frac{c_d A_0}{\rho_m^{2/3}}$ (c_d being the drag coefficient and A_0 the shape parameter as described by Bronshten 1983) and the ablation coefficient σ (s^2 km^{-2}) $= \frac{c_h}{H^* c_d}$ (c_h is the coefficient of heat and H^* the enthalpy of vaporization). For all our models, the atmospheric properties are acquired using the NRLMSISE-00 atmospheric model (Picone et al. 2002).

With an EKF, the mean state $\bar{\boldsymbol{x}}_k$ of the meteoroid may be predicted from the propagation of a previous mean through a linearized form of the state Equations (2). This may then be evaluated based on a given observation, z_k (3), at each time step. The observations made by the autonomous Desert Fireball Observatories are the triangulated position only, but are inherently linked to the other states through the state equations:

$$\boldsymbol{x}_k = F(\bar{\boldsymbol{x}}_{k-1}, k) + \boldsymbol{u}_k \quad \boldsymbol{u}_k \sim \mathcal{N}(0, \boldsymbol{Q}_k) \tag{2}$$

$$z_k = H(\bar{\boldsymbol{x}}_k) + \boldsymbol{w}_k \quad \boldsymbol{w}_k \sim \mathcal{N}(0, \boldsymbol{R}_k). \tag{3}$$

Incorporating both discrete process noise, $\boldsymbol{u}_k$, and observation noise, $\boldsymbol{w}_k$, enables a statistical analysis of the state and corresponding uncertainties. The process noise accounts for uncertainties that are introduced by the dynamic model. This not only includes the approximations introduced by using the single-body dynamic Equations (1) but the imprecision in the atmospheric density model used, variables that are held constant, and of course fragmentation phenomena etc. These uncertainties associated with the modeling process and the incorporation of observation errors had not been explored previous to Sansom et al. (2015). $\boldsymbol{u}_k$ and $\boldsymbol{w}_k$, can be approximated as Gaussian noise with means of zero and discrete covariance $\boldsymbol{Q}_k$ and $\boldsymbol{R}_k$ respectively (Särkkä & Sarmavuori 2013). While $\boldsymbol{R}_k$ is linked to the error associated with individual measurements, $\boldsymbol{Q}_k$ can be derived from the continuous process noise covariance $\boldsymbol{Q}_c$ as described by Grewal & Andrews (1993).

2.1. *The Unscented Kalman Filter*

The linearization of the state equations in an EKF is a suboptimal approximation of the meteoroid trajectory. A UKF allows a more rigorous approach to estimating systems with nonlinear dynamics (Julier & Uhlmann 1997, 2004; Wan & Merwe 2000). Rather than estimating the transformation of the mean, $\bar{\boldsymbol{x}}_k$ (with a number of states equal to L), and covariance ($\boldsymbol{P}_k$), a UKF uses a set of $2L + 1$ weighted sample points (χ_i) that together represent the Gaussian probability distribution of the data (after Wan & Merwe 2000):

$$\begin{aligned}
&\chi_0 = \bar{\boldsymbol{x}}_{k-1|k-1} \\
&\chi_i = \bar{\boldsymbol{x}}_{k-1|k-1} + (\sqrt{(L+\lambda)\boldsymbol{P}_k})_i \quad i = 1, \ldots, L \\
&\chi_i = \bar{\boldsymbol{x}}_{k-1|k-1} - (\sqrt{(L+\lambda)\boldsymbol{P}_k})_{i-L} \quad i = L+1, \ldots, 2L
\end{aligned} \tag{4}$$

where the sample mean and covariance weightings are calculated by

$$
\begin{aligned}
W_0^{(m)} &= \lambda/(L+\lambda)\\
W_0^{(c)} &= \lambda/(L+\lambda) + (1-\alpha^2+\beta)\\
W_i^{(m)} &= W_i^{(c)} = 1\big/\{2(L+\lambda)\} \quad i = 1,\ \ldots, 2L.
\end{aligned} \tag{5}
$$

The scaling parameter, $\lambda = \alpha^2(L+\kappa) - L$. The scaling factor, α, controls the weighting of sample points as well as their spread around the mean and is typically given a value $1 \times 10^{-4} \leqslant \alpha \leqslant 1$ (Wan & Merwe 2001). Small α values result in a smaller spread from the mean (Julier 2002). κ, in this equation only, refers to the secondary scaling parameter described by Wan & Merwe (2001). It is generally set to $\kappa = 0$ or $3 - L$. The β parameter incorporates prior knowledge of the mean distribution and a value of $\beta = 2$ is used to represent a Gaussian distribution (Wan & Merwe 2000). To determine the matrix root of $\boldsymbol{P}_k$, a lower triangular matrix in a Cholesky factorization is used (Särkkä 2007). As with an EKF there is a prediction and a measurement update step.

2.1.1. Prediction

These sample points are individually propagated through the nonlinear state equations:

$$\chi_{i,k|k-1} = f(\chi_{i,k-1|k-1}, \boldsymbol{u}_k, k) \qquad i = 0,\ \ldots, 2L. \tag{6}$$

The estimate of the incremented mean and covariance are then recalculated using (5) and (6) to give:

$$\hat{\boldsymbol{x}}_{k|k-1} \approx \sum_{i=0}^{2L} W_k^{(m)} \chi_{i,k|k-1} \tag{7}$$

$$\boldsymbol{P}_{k|k-1} \approx \sum_{i=0}^{2L} W_k^{(c)} \{\chi_{i,k|k-1} - \hat{\boldsymbol{x}}_{k|k-1}\}\{\chi_{i,k|k-1} - \hat{\boldsymbol{x}}_{k|k-1}\}^T + \boldsymbol{Q}_k. \tag{8}$$

2.1.2. Update

The estimated position for each sample point may be extracted from each of their state matrices using (9). The mean predicted position can therefore be calculated (Equation (10)) as well as the measurement covariance of the prediction (Equation (11)). The observation noise covariance, $\boldsymbol{R}_k$, is independent of the innovation covariance, $\boldsymbol{S}_k$, and is therefore additive (Julier & Uhlmann 1997):

$$\boldsymbol{\mathcal{Z}}_{i,k|k-1} = h(\chi_{i,k|k-1}, k) \tag{9}$$

$$\hat{z}_{k|k-1} \approx \sum_{i=0}^{2L} W_k^{(m)} \boldsymbol{\mathcal{Z}}_{i,k|k-1} \tag{10}$$

$$\boldsymbol{S}_k = \sum_{i=0}^{2L} W_k^{(c)} \{\boldsymbol{\mathcal{Z}}_{i,k|k-1} - \hat{z}_{k|k-1}\}\{\boldsymbol{\mathcal{Z}}_{i,k|k-1} - \hat{z}_{k|k-1}\}^T + \boldsymbol{R}_k \tag{11}$$

$$\boldsymbol{C}_k = \sum_{i=0}^{2L} W_k^{(c)} \{\chi_{i,k|k-1} - \hat{\boldsymbol{x}}_{k|k-1}\}\{\boldsymbol{\mathcal{Z}}_{i,k|k-1} - \hat{z}_{k|k-1}\}^T. \tag{12}$$

The measurement covariance (Equation (11)) and the cross-correlation matrix of the state and measurement (Equation (12)) are used to calculate the Kalman gain, $\boldsymbol{K}_k$ (Equation (13)), which controls the weighting of the predicted state versus the observed measurement. These are used along with Equations (7) and (8) to perform the final measurement update of the state and covariance (Hartikainen & Särkkä 2007):

$$\boldsymbol{K}_k = \boldsymbol{C}_k \boldsymbol{S}_k^{-1} \tag{13}$$

$$\hat{\boldsymbol{x}}_{k|k} = \hat{\boldsymbol{x}}_{k|k-1} + \boldsymbol{K}_k [z_k - \hat{z}_{k|k-1}]. \tag{14}$$

$$\boldsymbol{P}_{k|k} = \boldsymbol{P}_{k|k-1} - \boldsymbol{K}_k \boldsymbol{S}_k \boldsymbol{K}_k^T. \tag{15}$$

2.2. Modeling a Meteoroid Trajectory Using a UKF

UKF parameters used here are the same as those used by Sansom et al. (2015) to allow a comparison of the methodologies. Values used in the process noise covariance matrix $\boldsymbol{Q}_c$ (16) reflect the uncertainties introduced by the dynamic model being used. For example, uncertainty in position and velocity is introduced through noise in acceleration. The changes in mass and velocity as a function of time are also dependent on unmodeled factors such as fragmentation and variations in assumed constants and are influenced by the precision of atmospheric densities:

$$\boldsymbol{Q}_c = \begin{pmatrix} (3.75\ \mathrm{m\ s^{-1}})^2 & 0 & 0 \\ 0 & (0.2\ \mathrm{kg\ s^{-1}})^2 & 0 \\ 0 & 0 & (75\ \mathrm{m\ s^{-2}})^2 \end{pmatrix}. \tag{16}$$

All observed positions of the meteoroid are assigned the same covariance $\boldsymbol{R}_k$ in this simulation:

$$\boldsymbol{R}_k = (100\ \mathrm{m})^2. \tag{17}$$

As for the scaling parameters required for Equations (4) and (5), given that there are three states used in the meteoroid problem, $L = 3$. To ensure a reasonable spread of sample points, $\kappa = 0$ and $\alpha = 1$ is used, following Särkkä & Sarmavuori (2013).

2.3. Results of the UKF

Once again the Bunburra-Rockhole data set is used to test the model. Observation measurements are taken from Table 2 of Spurný et al. (2012) and include all values after the first recorded dash. As the constants σ and κ in (1) are unknown, a prior assumption of their values, along with the initial state values, must be made. As with the EKF presented by Sansom et al. (2015), we must precede this estimator with the dynamic optimization step described in that paper. To allow a direct comparison between the two filters, we will use the same initial conditions as determined by these authors for the Bunburra Rockhole fireball: $m_0 = 30.12$ kg, $v_0 = 13198\ \mathrm{m\ s^{-1}}$, κ (SI) $=$ 0.0124 and $\sigma = 0.0371\ \mathrm{s^2\ km^{-2}}$. A drag coefficient of 1 is used. The state values after each measurement update step are represented in Figure 1. This appears similar to Figure 3 in Sansom et al. (2015); however standard deviation values are lower and the final mass and velocity estimates using this more robust form of filtering are $m_f = 2.88 \pm 1.04$ kg and $v_f = 6095 \pm 203\ \mathrm{m\ s^{-1}}$.

The lower error values here show that the use of a UKF gives us an improved state estimate compared to an EKF (see the summary Table 1).

The incorporation of sudden significant mass loss, however, is still not fully represented. Fragmentation events that occur within the error ranges are allowed to be incorporated due to

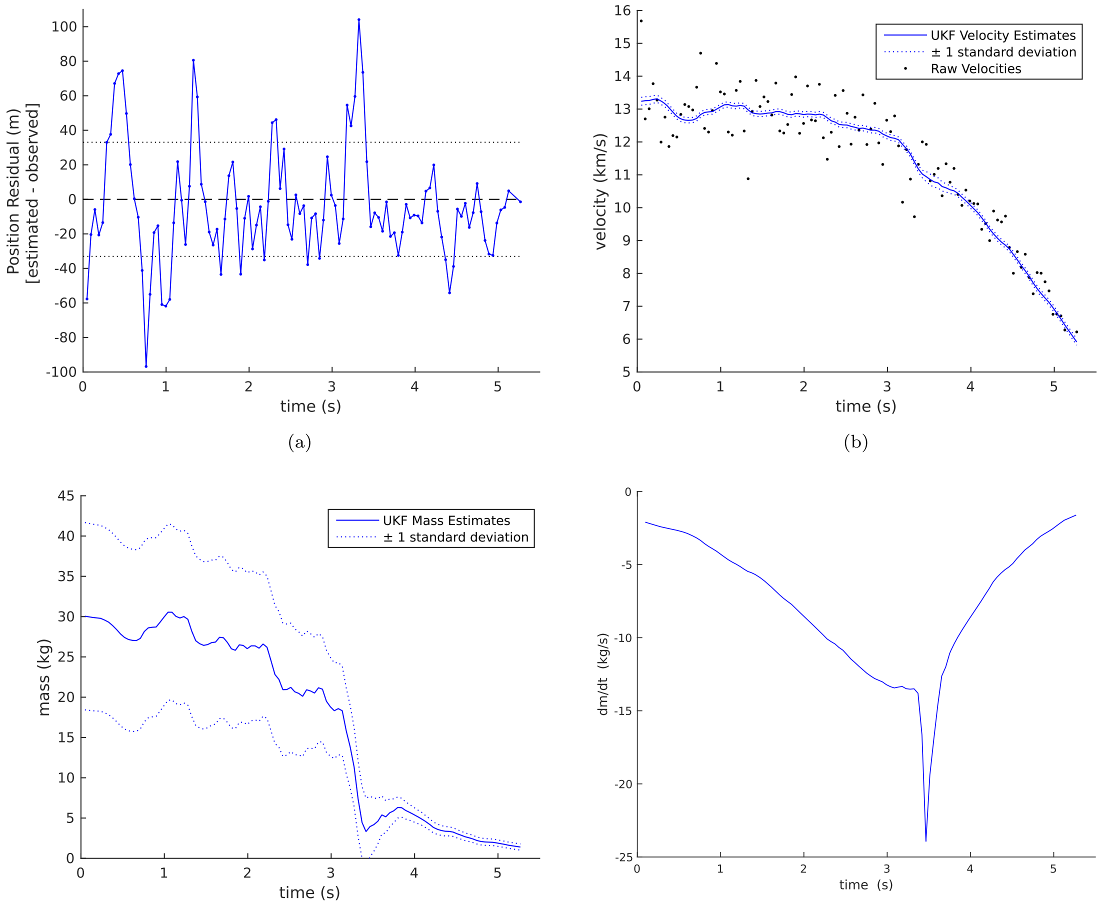

(a) (b)

(c) (d)

Figure 1. Unscented Kalman filter results for an initial mass of 30.12 kg. (a) Residual plot of observed position data subtracted from the UKF position estimate. Dotted lines represent one standard deviation (33.05 m). (b) The blue curve shows UKF velocity estimates with blue dotted curves representing ± one standard deviation, calculated from the $\boldsymbol{P}_k$ matrix. Black points represent velocity values calculated from observations using $v = dl/dt$. (c) UKF mass estimates with the dotted curve representing ± one standard deviation, taken from $\boldsymbol{P}_k$ matrix. Slight increases in velocity and mass are within error ranges and are due to the constant updating as part of the filtering process. (d) Rate of mass loss calculated by change in state mass estimates over the difference in observation times.

the observation update but the timing of their occurrence is not directly examinable. As discussed by Sansom et al. (2015), the minima in the dm/dt plot (Figure 1) may indicate fragmentation event locations. A more robust way of modeling fragmentation events and fully incorporating them may be achieved with an IMM.

3. INTERACTING MULTIPLE MODEL

The IMM algorithm is an effective and efficient hybrid model for state estimation (Blom & Bar-Shalom 1988; Mazor et al. 1998). The adaptive approach of an IMM enables the inclusion of discrete changes to the meteoroid flight model that would be difficult to handle in a single UKF. Model changes such as instantaneous gross fragmentation may therefore be explicitly included. This is achieved by running two UKFs simultaneously with different values for mass uncertainty within the process noise covariance, Q_c. Equation 18*(a)* allows typical error ranges for ablation. Equation 18*(b)* has larger errors in order to include gross fragmentation events:

$$\boldsymbol{Q}_c^1 = \begin{pmatrix} (3.75\ \mathrm{m\ s^{-1}})^2 & 0 & 0 \\ 0 & (0.05\ \mathrm{kg\ s^{-1}})^2 & 0 \\ 0 & 0 & (75\ \mathrm{m\ s^{-2}})^2 \end{pmatrix} \tag{18a}$$

$$\boldsymbol{Q}_c^2 = \begin{pmatrix} (3.75\ \mathrm{m\ s^{-1}})^2 & 0 & 0 \\ 0 & (2\ \mathrm{kg\ s^{-1}})^2 & 0 \\ 0 & 0 & (75\ \mathrm{m\ s^{-2}})^2 \end{pmatrix}. \tag{18b}$$

Different initial uncertainties in mass are also set to vary by model, allowing the confidence in the initial mass value to also be tested:

$$\boldsymbol{P}_0^1 = \begin{pmatrix} (10\ \mathrm{m})^2 & 0 & 0 \\ 0 & (2\ \mathrm{kg})^2 & 0 \\ 0 & 0 & (1500\ \mathrm{m\ s^{-1}})^2 \end{pmatrix} \tag{19a}$$

$$\boldsymbol{P}_0^2 = \begin{pmatrix} (10\ \mathrm{m})^2 & 0 & 0 \\ 0 & (5\ \mathrm{kg})^2 & 0 \\ 0 & 0 & (1500\ \mathrm{m\ s^{-1}})^2 \end{pmatrix}. \tag{19b}$$

For each model, M^i, we assign a prior probability,

$$\mu_0 = [P\{M_0^1\} \quad P\{M_0^2\}] = [\mu_0^1 \quad \mu_0^2]. \tag{20}$$

For the meteoroid problem, an equal weighting is given to both models initially; $\mu_0 = [0.5 \quad 0.5]$.

The probability of changing between model j from time $k-1$ to model i at time k is written as $p_{ij} = P\{M_k^i | M_{k-1}^j\}$ (Hartikainen & Särkkä 2007). These can be combined into a two-model transition probability matrix

$$\boldsymbol{\Phi} = \begin{bmatrix} P\{M_k^1|M_{k-1}^1\} & P\{M_k^1|M_{k-1}^2\} \\ P\{M_k^2|M_{k-1}^1\} & P\{M_k^2|M_{k-1}^2\} \end{bmatrix}. \tag{21}$$

Here we assume an 80% probability that an ablating meteoroid will not suddenly fragment at any point in time, and a body that is in the process of fragmenting is 40% likely to carry on doing so (Equation (22)). These likelihood values are based on the results of this analysis with the Bunburra Rockhole fireball. Further examination will be required to determine the general suitability of these values for other fireball events:

$$\boldsymbol{\Phi} = \begin{bmatrix} 0.8 & 0.2 \\ 0.6 & 0.4 \end{bmatrix}. \tag{22}$$

Three stages of the IMM filter are performed at each time step (Mazor et al. 1998; Hartikainen & Särkkä 2007; equations described in these stages are after these works). First, an interaction between all the model states based on the mixing probabilities, $\mu_k^{i|j}$; then filtering using a UKF on each model; finally a recombination of states, based on the weightings of each model estimates, to produce a final state and covariance estimate.

3.1. Interaction:

The mixing probability for each model with a prior probability μ_{k-1}^i is calculated using a normalization factor, c_j:

$$\mu_k^{i|j} = \frac{1}{c_j} p_{ij}\, \mu_{k-1}^i \tag{23a}$$

$$c_j = \sum_i p_{ij}\, \mu_{k-1}^i. \tag{23b}$$

The "mixed" mean and covariance that will be used as the a priori inputs to the filtering step are calculated as

$$\hat{\boldsymbol{x}}_{k-1|k-1}^{0i} = \sum_i \mu_k^{i|j} \hat{\boldsymbol{x}}_{k-1|k-1}^i \tag{24a}$$

$$\boldsymbol{P}_{k-1|k-1} = \sum_i \mu_k^{i|j} \times (\boldsymbol{P}_{k-1|k-1}^i + [\hat{\boldsymbol{x}}_{k-1|k-1}^i - \hat{\boldsymbol{x}}_{k-1|k-1}^{0j}] \times [\hat{\boldsymbol{x}}_{k-1|k-1}^i - \hat{\boldsymbol{x}}_{k-1|k-1}^{0j}]^T). \tag{24b}$$

3.2. Applying the Filter:

The filtering step uses the UKF as described in Section 2.1. Both the prediction and measurement update of the mean and covariance are calculated for each model. The likelihood, Λ_k^i, of the predicted position measurement is calculated for each model as the Gaussian probability of the position residual with zero mean and covariance $\boldsymbol{S}_k$ (from (11)) (Equation (25)). This is then used to determine the overall probability of that model (Equation (27)), where c is another normalization factor:

$$\Lambda_k^i \approx \mathcal{N}([z_k - \hat{z}_{k|k-1}];\, 0,\, \boldsymbol{S_k}) \tag{25}$$

$$c = \sum_i \Lambda_k^i c_i \tag{26}$$

$$\mu_k^i = \frac{1}{c} \Lambda_k^i c_i. \tag{27}$$

3.3. Combination:

Finally, to calculate a single state and covariance estimate, the updated estimates, Equations (14) and (15), from each model are weighted using the probabilities from Equation (27):

$$\hat{\boldsymbol{x}}_{k|k} = \sum_i \mu_k^i \hat{\boldsymbol{x}}_{k|k}^i \tag{28}$$

$$\boldsymbol{P}_{k|k} = \sum_i \mu_k^i \times (\boldsymbol{P}_{k|k}^i + [\hat{\boldsymbol{x}}_{k|k} - \hat{\boldsymbol{x}}_k][\hat{\boldsymbol{x}}_{k|k} - \hat{\boldsymbol{x}}_k]^T). \tag{29}$$

The state estimates at each time step are continuously updated based on the past data; future observations are not included. This means only the state estimate for the end of the trajectory is the result of processing all observations. This is how any filter works and is necessary if data are acquired in real time. If the full data set is available, however, it is more logical to include all the known data (both past and future) by the process known in this field as smoothing. To incorporate all the data, we can apply an IMM smoother to the data.

3.4. IMM Smoother

In the context of filtering, smoothing does not relate to any form of averaging, rather to the method of determining estimates based on all (past and future) measurements (Särkkä 2008). An IMM smoother will therefore incorporate all the observations of the fireball data set into each estimate. To do so, the IMM filter is run forwards as described in Section 3, then subsequently in reverse. A backwards (b) filtering probability, $\mu_k^{i(b)}$ is calculated, along with the mixed backwards mean and covariance ($\hat{\boldsymbol{x}}_k^{(b)}$ and $\hat{\boldsymbol{P}}_k^{(b)}$). Together with the forward probabilities and estimates, the smoothed estimates for each time step can be determined. The smoothed state and covariance estimates are calculated following the equations outlined in Hartikainen & Särkkä (2007) where the smoothed model probabilities are calculated by

$$\mu_k^{i(s)} = \frac{1}{d} \mu_k^i \boldsymbol{d}_j \tag{30}$$

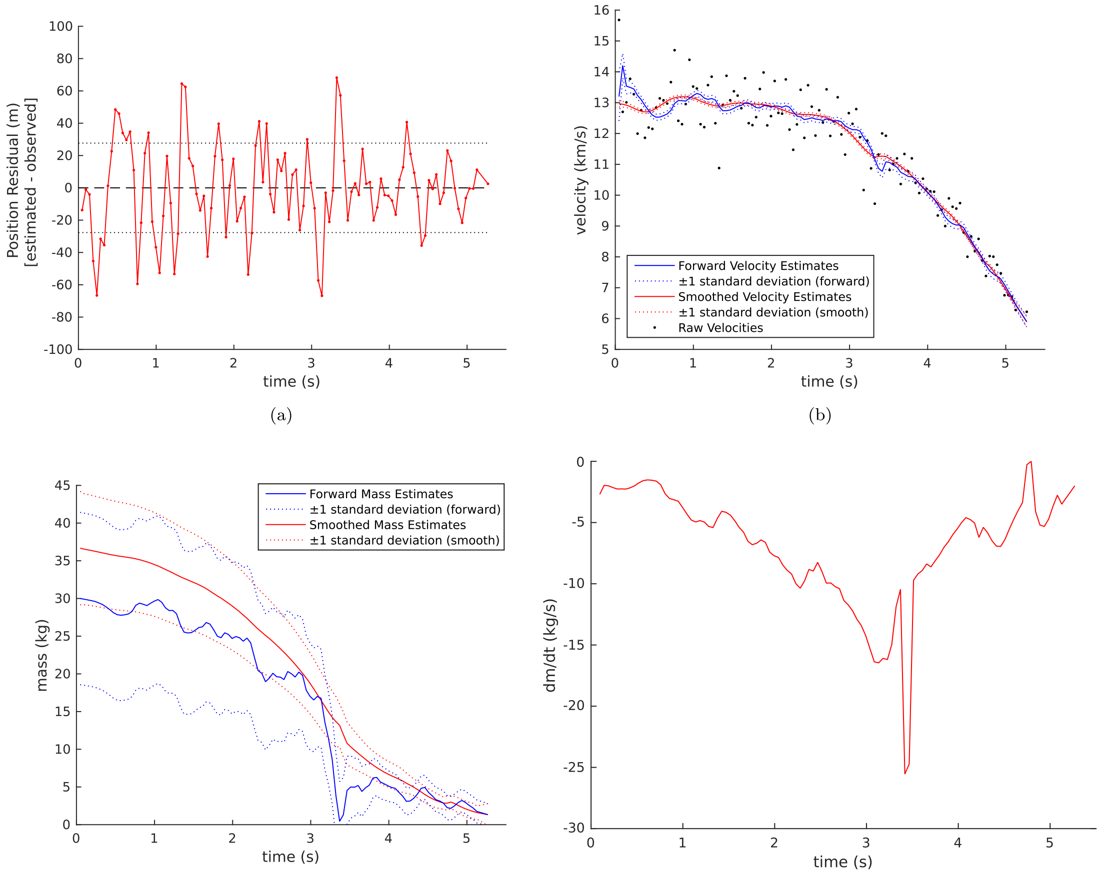

(a) (b)

(c) (d)

Figure 2. UKF IMM results for forward pass (blue) and smoother (red). (a) Residual plot of position data subtracted from IMM smoother position estimate—dotted lines represent one standard deviation (28 m). (b) Velocity estimates with standard deviation values taken from $\boldsymbol{P}_k$ matrix. Black points represent velocity values calculated from observations using $v = dl/dt$. (c) Mass estimates with standard deviation values taken from $\boldsymbol{P}_k$ matrix. (d) Rate of mass loss calculated by change in state mass estimates over the difference in observation times.

where

$$\boldsymbol{d}_j = \sum_i p_{ij} \Lambda_k^{i(s)} \tag{31}$$

$$d = \sum_i d_j \mu_k^i \tag{32}$$

and for our two-model problem, the smoothed likelihoods of each model, $\Lambda_k^{i(s)}$, are calculated as a Gaussian distribution and can be written as

$$\Lambda_k^{i(s)} = \begin{bmatrix} \mathcal{N}(\hat{\boldsymbol{x}}_k^{1(b)} - \hat{\boldsymbol{x}}_k^1 \mid 0, \boldsymbol{P}_k^{1(b)} - \boldsymbol{P}_k^1) & \mathcal{N}(\hat{\boldsymbol{x}}_k^{2(b)} - \hat{\boldsymbol{x}}_k^1 \mid 0, \boldsymbol{P}_k^{2(b)} - \boldsymbol{P}_k^1) \\ \mathcal{N}(\hat{\boldsymbol{x}}_k^{1(b)} - \hat{\boldsymbol{x}}_k^2 \mid 0, \boldsymbol{P}_k^{1(b)} - \boldsymbol{P}_k^2) & \mathcal{N}(\hat{\boldsymbol{x}}_k^{2(b)} - \hat{\boldsymbol{x}}_k^2 \mid 0, \boldsymbol{P}_k^{2(b)} - \boldsymbol{P}_k^2) \end{bmatrix}. \tag{33}$$

By taking into account the entire data set at each observation time, this allows for a full analysis of the trajectory based on all observations, and a comprehensive understanding of all the errors throughout the bright flight.

4. RESULTS OF IMM AND SMOOTHER

The same initial parameters as used in Section 2.3 are used for both UKF models. The mixed state mean estimates shown in Figure 2 are represented by prior data only and therefore display an overall higher covariance. The smoothed estimates are more consistent and are a truer representation of the overall covariance at each time step.

The smoothed model probabilities (Equation (30)) are shown in Figure 3(a). Likely fragmentation events may be attributed to periods when the higher mass covariance allocated to model 2 is of greater probability.

The incorporation of fragmentation by way of the IMM significantly decreases the errors attributed to the final state estimates as seen in Table 1.

Using a Rauch–Tung–Striebel smoother with the EKF, Sansom et al. (2015) estimated the initial mass to be 30.20 ± 6.53 kg. The use of the UKF IMM smoother allows for a better estimate of the initial states resulting in lower covariance values; $m_0 = 36.68 \pm 3.81$ kg and $v_0 = 12963 \pm 35$ m s^{-1}.

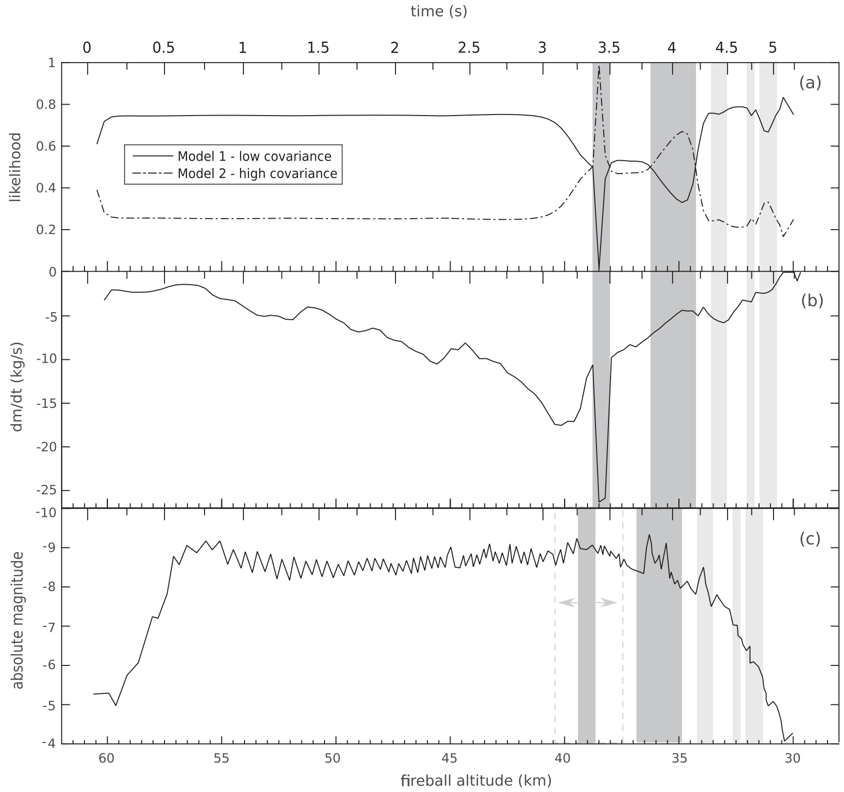

Figure 3. The primary *x*-axis displays altitude in kilometers (below). The secondary *x*-axis displays time in seconds from the start of the second measured dash (above)—note the nonlinearity of the secondary axis. (a) Smoothed model probabilities. Model 1 (solid) has a low mass covariance and mass loss is dominated by ablation. Model 2 (dashed) has a high mass covariance and likely indicates fragmentation events when likelihood increases. Dark gray areas show where $\mu_k^{M2(s)} > \mu_k^{M1(s)}$ and light gray areas show where there are local maxima in $\mu_k^{M2(s)}$. (b) Rate of mass loss calculated by change in state mass estimates over difference in observation times. (c) Light curve for the Bunburra Rockhole fireball replicated from Spurný et al. (2012). Highlighted areas are duplicated from (a) but offset by 530 m altitude. Dashes outline the extent of a "hump" in the light curve.

Table 1
Comparison of Final State Values Using Different Filtering Methods

	Final Position Estimate With Error $(\sqrt{\sigma_l^2})$	Final Mass Estimate With Error $(\sqrt{\sigma_m^2})$	Final Velocity Estimate With Error $(\sqrt{\sigma_v^2})$
EKF[a]	60032 ± 62 m	2.30 ± 1.63 kg	6052 ± 241 m s^{-1}
UKF	60040 ± 58 m	2.88 ± 1.04 kg	6095 ± 203 m s^{-1}
IMM	60011 ± 7 m	1.32 ± 0.49 kg	5896 ± 59 m s^{-1}

Note.
[a] Sansom et al. (2015).

5. DISCUSSION

In our model, we use all measurements from the second recorded dash onward of the Bunburra Rockhole fireball (published in Table 2 of Spurný et al. 2012) and therefore $t_0 = 0.1899$ s. All model time values are therefore shifted by 0.1899 s from those published in Spurný et al. (2012). Comparisons will therefore be made in altitude. The same filter parameters ($\boldsymbol{P}_0$, $\boldsymbol{Q}_c$, $\boldsymbol{R}_k$) used by Sansom et al. (2015) for the EKF were used here in the UKF. From Table 1, there is a small overall decrease in the errors of the state estimates for the UKF in comparison to the EKF results of Sansom et al. (2015). This shows that the nonlinear dynamics of fireball trajectories are better estimated by the Gaussian distribution of sample points of the UKF. The application of this estimator in an IMM allows the possibility of sudden large changes in mass that would not be allowable within the normal error range of simple ablation dynamics modeled by a single EKF or UKF. The similarity in the final covariance values of all estimators used (Table 1) shows that the final state estimates remain consistent with the observed positions.

The IMM smoothed model probabilities plotted in Figure 3(a) show the relative likelihoods of a given model compared to the observation data. When low error ranges are able to fit the data (Model 1 (M1)—(18*a*)) mass loss is most likely via steady ablation. When higher error ranges are needed to produce a good fit to the data, Model 2 (M2)—(18*b*) is more probable and gross fragmentation is likely contributing to a sudden increase in mass loss. Figure 3(a) highlights two regions where M2 has a higher likelihood than M1: from 38.8to

38.0 km and from 36.2 to 34.2 km. There are also features highlighted at ~33.2, ~31.9, ~31.1 km where the probability of M2 shows a slight increase. Figure 3(c) is a reproduction of the corrected radiometric light curve for Bunburra Rockhole produced by Spurný et al. (2012). The highlighted regions from Figure 3(a) have been replicated on the light curve (Figure 3(c)) with an offset of 530 m. The initial spike in Figure 3(a) at 38.8–38.0 km appears at the center of a hump in the light curve (width of "hump" outlined in 3(c)). A hump in the light curve according to Borovička et al. (2013) is caused by an eroding fragment; a larger chunk that itself holds together and ablates gradually. This coincides well with the large decrease in mass loss at this time (Figure 3(b)). The sharper spike in the light curve seen from 36.5 to 35.4 km on the other hand would correspond to release of dust (Borovička et al. 2013) and not necessarily to a large mass loss, which indeed is not a feature in Figure 3(b). The other three lightly highlighted features in Figure 3(a) also appear to correspond to relative spikes in the light curve (Figure 3(c)) as well as roughly correlating with local minima in the rate of mass loss (Figure 3(b)).

As the IMM smoothed model probabilities include all the observed data, the offset between Figures 3(a) and (c) is not due to any lag in model response time. A 530 m offset in altitude at the end of the trajectory roughly corresponds to 2–3 shutter iterations (2–3 observations). This offset could be due to a physical delay between the emission of light recorded by the light curve and the time taken for the meteoroid to decelerate. It is also possible that it is a ramification of the light curve processing itself. In order to convert the highly accurate photometric light curve into a function of altitude (no calibrated light curve with time published), it is compared to the photographic record and errors in the fit may introduce uncertainties in altitude values.

The first half of the changing mass profile seen in Figure 2(c) does not resemble that given in Figure 13 of Spurný et al. (2012). This is likely due to Spurný et al. (2012) excluding all points between 62.4 and 58.2 km; 51.9 and 51.6 km; and 42.8 to 39.1 km altitude. Spurný et al. (2012) acknowledge that the points around 40 km altitude are most likely caused by large fragments "forming the head." This corresponds to our analysis of an eroding fragment, albeit modeled to begin at 38.8 km; however, Spurný et al. (2012) also do not illustrate any significant mass loss in their Figure 13 at an altitude of 40 km. The large amount of fragmentation surmized by Spurný et al. (2012) to cause the anomalies at the start of the trajectory (altitude above 58.2 km) cannot be substantiated. The scatter within the first 0.38 s (altitude above 58.2 km) is not dissimilar to that of the first 2.5 s (altitude above 44 km). The UKF/IMM smoother constrains the error of the state for the full trajectory by including all observation errors and issues caused by the single body Equation (1) simplifying the fireball process. There is no need for a drastic change in initial mass for the model to fit the observed data. The final decreases in mass in Figure 13 of Spurný et al. (2012) are at approximately 38 km and 36 km, as well as smaller steps at 34.6, 33.6, 32.3, 31.2, corresponding well to the shaded regions in Figure 3(a).

The incorporation of the UKF within an IMM smoother provides likely occurrences of fragmentation as well as providing a statistical analysis of the state uncertainties. This is a fully automated method of obtaining a likely fragmentation pattern of a meteoroid trajectory from position observations alone.

6. CONCLUSION

The use of an unscented Kalman filter within an interactive multiple model smoother allows a set of dynamic equations alone to model a fireball trajectory. A UKF enables an estimation of the state using a more robust approach to the nonlinear equations for the dynamics of this system. The application of this estimator in an IMM smoother allows the incorporation of gross fragmentation events and identifies their approximate time of occurrence. Different shapes in the light curve can also be said to correspond to local minima in the rate of mass loss. This method can handle highly noisy data in the Bunburra Rockhole example, indicating that the method is robust enough to be applied to other raw fireball data sets, including all observations with no need for prior smoothing. The use of a UKF/IMM filter, however, still requires assumptions to be made for the initial entry parameters and unknown equation constants. The initial state covariance matrix allows for flexibility in the initial state values, and some uncertainty in the unknown constants will be included in the model noise covariance, although it must be remembered that the state estimates and their covariance remain dependent on the initial assumptions used. To remove this dependency, a statistical analysis should be made for the selection of these parameters.

The authors would like to thank the reviewer for their outstanding and thorough review of this paper. This work was funded by the Australian Research Council as part of the Australian Laureate Fellowship scheme.

REFERENCES

Bland, P. A., Spurný, P., Bevan, A. R., et al. 2012, AuJES, 59, 117
Blom, H. a. P., & Bar-Shalom, Y. 1988, ITAC, 33, 780
Borovička, J., Tóth, J., Igaz, A., et al. 2013, M&PS, 48, 1757
Bronshten, V. A. 1983, Physics of Meteoric Phenomena (Dordrecht: Reidel)
Ceplecha, Z., Borovička, J., Elford, W. G., et al. 1998, SSRv, 84, 327
Ceplecha, Z., & Revelle, D. O. 2005, M&PS, 40, 35
Ceplecha, Z., Spalding, R. E., Jacobs, C. F., & Tagliaferri, E. 1996, Proc. SPIE, 2813, 46
Ceplecha, Z., Spurný, P., Borovička, J., & Keclikova, J. 1993, A&A, 279, 615
Grewal, M. S., & Andrews, A. P. 1993, Kalman Filtering: Theory and Practice (Englewood Cliffs, NJ: Prentice-Hall)
Halliday, I., Griffin, A. a., & Blackwell, A. T. 1996, M&PS, 31, 185
Hartikainen, J., & Särkkä, S. 2007, Journal of Interprofessional Care, 25, 1
Julier, S. J. 2002, in Proc. 2002 American Control Conf. (IEEE Cat. No. CH37301) 6, The Scaled Unscented Transformation (Piscataway, NJ: IEEE), 4555
Julier, S. J., & Uhlmann, J. K. 1997, in Int Symp. AerospaceDefense Sensing Simul and Controls 3, A New Extension of the Kalman Filter to Nonlinear Systems (Orlando, FL: SPIE), 26
Julier, S. J., & Uhlmann, J. K. 2004, IEEEP, 92, 401
Mazor, E., Averbuch, A., Bar-Shalom, Y., & Dayan, J. 1998, ITAES, 34, 103
McCrosky, R. E., & Posen, A. 1968, SAOSR, #273
Ning, X., & Fang, J. 2007, Aerospace Science and Technology, 11, 222
Picone, J. M., Hedin, A. E., Drob, D. P., & Aikin, A. C. 2002, JGRA, 107, 1468
Sansom, E. K., Bland, P., Paxman, J., & Towner, M. 2015, M&PS, 50, 1423
Särkkä, S. 2007, ITAC, 52, 1631
Särkkä, S. 2008, ITAC, 53, 845
Särkkä, S., & Sarmavuori, J. 2013, SigPr, 93, 500
Spurný, P., Bland, P., Shrbený, L., et al. 2012, M&PS, 47, 163
Thrun, S., Montemerlo, M., Dahlkamp, H., et al. 2006, Journal of Field Robotics, 23, 661
Wan, E. A., & Merwe, R. V. D. 2000, in Adaptive Systems for Signal Processing, Communications and Control Symp. 2000 AS-SPCC. The IEEE 2000, The Unscented Kalman Filter for Nonlinear Estimation (Piscataway, NJ: IEEE), 153
Wan, E. A., & Merwe, R. V. D. 2001, Kalman Filtering and Neural Networks (New York, NY: Wiley)

PAPER 3 – ANALYSING METEOROID FLIGHTS USING PARTICLE FILTERS

The Astronomical Journal (2017), Volume 153, Issue 2, pp. 87-95

Sansom, E. K., Rutten, M. G., Bland, P. A.

STATEMENT OF AUTHORSHIP

TITLE OF PAPER: Analysing Meteoroid Flights Using Particle Filters

PUBLICATION STATUS: Published.

AUTHOR CONTRIBUTIONS

By signing the Statement of Authorship, each author certifies that their stated contribution to the publication is accurate and that permission is granted for the publication to be included in the candidate's thesis.

Name of Principal Author: Eleanor K. Sansom

Contribution to the Paper: Led all aspects of this research, drafted and revised the manuscript of this publication.

Overall Percentage: 90%

Signature: ***Date:*** 01 / 12 / 16

Name of Co-Author: Mark G. Rutten

Contribution to the Paper: Helped with initial model formulation and reformatting background sections 2-4 of the manuscript.

Overall Percentage: 8%

Signature: ***Date:*** 5 / 12 / 16

Name of Co-Author: Phillip A. Bland

Contribution to the Paper: Helped in the final review of the manuscript.

Overall Percentage: 2%

Signature: ***Date:*** 4 / 12 / 16

DRAFT VERSION NOVEMBER 30, 2016
Preprint typeset using LaTeX style AASTeX6 v. 1.0

ANALYSING METEOROID FLIGHTS USING PARTICLE FILTERS

E. K. SANSOM[1], M. G. RUTTEN[2], P. A. BLAND[1]

[1]Applied Geology, Curtin University, Western Australia
[2]Defence Science and Technology Group, Edinburgh, South Australia

ABSTRACT

Fireball observations from camera networks provide position and time information along the trajectory of a meteoroid that is transiting our atmosphere. The complete dynamical state of the meteoroid at each measured time can be estimated using Bayesian filtering techniques. A particle filter is a novel approach to modelling the uncertainty in meteoroid trajectories and incorporates errors in initial parameters, the dynamical model used and observed position measurements. Unlike other stochastic approaches, a particle filter does not require predefined values for initial conditions or unobservable trajectory parameters. The Bunburra Rockhole fireball (Spurný et al. 2012), observed by the Australian Desert Fireball Network (DFN) in 2007, is used to determine the effectiveness of a particle filter for use in fireball trajectory modelling. The final mass is determined to be $2.16 \pm 1.33\,kg$ with a final velocity of $6030 \pm 216\,m\,s^{-1}$, similar to previously calculated values. The full automatability of this approach will allow an unbiased evaluation of all events observed by the DFN and lead to a better understanding of the dynamical state and size frequency distribution of asteroid and cometary debris in the inner solar system.

1. INTRODUCTION

A meteoroid is a small object moving in interplanetary space. When one enters the Earth's atmosphere, it creates a bright phenomenon called a meteor, fireball or bolide (depending on brightness). The interaction of this material with our atmosphere provides us with an opportunity to observe and study a portion of interplanetary material that would otherwise be inaccessible to us. Telescopes cannot image mm-m sized objects, and discoveries of 10s m sized asteroids constitute a tiny fraction of the predicted population (Harris 2012). Determining the physical state of this material in our atmosphere its strength and mass distribution, and its velocity frequency distribution, provides a unique window on cometary and asteroidal material in the inner solar system. In order to derive that data, we need to model the meteoroid-atmosphere interaction.

A set of idealised equations govern how a single meteoroid body will respond in terms of velocity and mass loss. The amount of deceleration experienced by a meteoroid is related to its shape and bulk density via a *shape-density parameter*, $\kappa = \frac{c_d A}{2\rho_m^{2/3}}$, where c_d is the aerodynamic drag coefficient [1], A the shape parameter as described by Bronshten (1983) and the bulk density of the meteoroid- ρ_m. Both ablation and gross fragmentation of the meteoroid is responsible for loss of mass. Gross fragmentation is hard to predict and is linked to the strength of the object. Ablation can be quantified through the *ablation parameter* - σ, which is defined as $\sigma = \frac{c_h}{H^* c_d}$ [1] (where c_h is the coefficient of heat and H^* the enthalpy of vaporisation).

If the meteoroid survives this luminous trajectory or *bright flight*, there is the possibility of recovering a meteorite on the ground. Dedicated fireball camera networks such as the Desert Fireball Network (DFN) in Australia (Bland et al. 2012) allow triangulated trajectories of larger meteoroid bodies to be observed. Special shutters are used (in the case of the DFN, a liquid crystal shutter using modulated sequences (Howie et al. in review)) to encode timing throughout the trajectory. Being able to predict the final state of the meteoroid is paramount to determining if there is any recoverable material, and is a necessary input to so-called *dark flight* modelling (the process by which data from the luminous trajectory is converted into a fall line on the ground using atmospheric wind models), enabling likely search areas to be defined (Ceplecha 1987). Accurately calculating a trajectory also allows the orbit for that body to be determined. Meteorites with orbits are rare; less than 0.05 % of all meteorites. Knowing a meteorite's pre-atmospheric orbit gives

---

[1] Γ is referred to as the drag factor in many meteoroid trajectory works, including (Ceplecha and Revelle 2005). The aerodynamic drag coefficient, $c_d = 2\Gamma$ (Bronshten 1983; Borovička et al. 2015).

contextual information to the picture they provide on early Solar System formation. Over time, the statistical analysis of calculated orbits may also assist in planetary defence of asteroidal debris streams.

Determining the state of a physical system based on a set of noisy measurements is known as filtering. The *state* describes what a system is 'doing' at any given time. The flight path of an aircraft for example may be represented by its position, velocity and heading; position observations can be made in real time to estimate the velocity and heading of the aircraft. Bayesian state-space estimation methods, such as the Kalman filter and its variants, address the filtering problem with the aim of estimating the true state of a system. The adaptive approach predicts future states through a model of system equations and updates with respect to an observation. Links between state variables defined in model equations allows unobserved state values to also be updated.

This stochastic filtering approach suits the modelling of meteoroid trajectories using noisy and uncertain measurements. Typical meteoroid models mostly rely on measurements of the meteor/fireball brightness (Kikwaya et al. 2011; Murray et al. 2000; Ceplecha and Revelle 2005), though light curves tend to be variable and do not represent typical values predicted by single-body ablation models (Campbell-Brown and Koschny 2004). The meteoroid problem is complicated not only by unpredictable gross fragmentation in the atmosphere, but the majority of initial state parameters are entirely unknown (m_0, σ, κ). Multiple approaches have been taken to handle these unknowns in fireball trajectory analysis. The manually intensive method of Revelle (2007) is based on the brute force least squares approach of Ceplecha and Revelle (2005). It does include the luminosity of the fireball (derived from manual interpretation of a light curve) as a proxy for mass loss and solves for fragmentation as well as σ and κ. As it is still based on a least squares optimisation, model and observation errors are not rigorously examined, rather overall errors are given as the standard deviation of residuals. The amount of manual input required also limits the number of fireballs that may be analysed. The DFN observed over 300 fireball events in 2015 over its 2.5 million km^2 double station viewing area. This continental scale deployment of > 50 automated observatories has been possible by the low cost of each system. At this time, there is no expensive, high voltage photomultiplier tube to measure fireball brightnesses. A trajectory analysis approach that is able to determine meteoroid parameters without a light curve, and which can be automated, will allow an unbiased evaluation of all events.

Very few models exist that enable the reduction of fireball data without a light curve. The method of Gritsevich (2009) solves for two dimensionless parameters rather than multiple unknown trajectory parameters. This still requires an initial accurate velocity and struggles with highly scattered datasets (Sansom et al. 2015). The various Kalman filtering methods used by Sansom et al. (2015) and Sansom et al. (2016) are fully automated techniques of determining the statistical likelihood of meteoroid state throughout bright flight, and allow a robust analysis of observation and model errors. As with previous dynamical approaches to fireball modelling, these require a pre-determined initial parameter set, withholding a general solution. To remove this limitation and fully analyse the statistical likelihood of the final state of a meteoroid given a range of likely initial states, we can use a method that combines a Monte Carlo (MC) approach to the filtering problem- a particle filter (Gordon et al. 1993). Simply, a 'cloud' of particles are initiated with state values determined by a probability function. The 'cloud' will be denser where probabilities are higher. Particles are propagated forward in time according to the state equations and weighted according to an observation. A new generation of particles are *resampled* from the existing pool, based on their weighting, and particles that are of low probability are preferentially removed.

The Bunburra Rockhole fireball was observed over the Australian outback by the DFN in 2007, and produced the network's first recovered meteorite (Spurný et al. 2012). An extended Kalman filter (Sansom et al. 2015) and an unscented Kalman filter (Sansom et al. 2016) have been used to model the Bunburra Rockhole fireball given a set of starting parameters. Neither filters explicitly include gross fragmentation, however Sansom et al. (2016) applied two Unscented Kalman filters in an Interactive Multiple Model to determine likely periods of fragmentation. Here we will examine the suitability of this sequential Monte Carlo technique for modelling fireball meteoroid trajectories using the Bunburra Rockhole fireball dataset.

2. BAYESIAN STATE-SPACE ESTIMATION

The technique used in this paper for estimating meteoroid parameters is one of a broader class of techniques known as Bayesian state-space methods. These methods involve encapsulating the knowledge of a system based on its *state*, given by the vector $\mathbf{x}$. The state of an object could be its position and velocity, for example. The probability of the object being in state $\mathbf{x}$ at time instant t_k is represented as the conditional probability density function

$$p(\mathbf{x}_k|\mathbf{z}_{1:k}), \tag{1}$$

where $\mathbf{z}_k$ is the observation of the system made at time t_k and $\mathbf{z}_{1:k}$ is the history of all observations up until time t_k.

The calculation of (1) is achieved recursively through the application of Bayes' rule

$$p(\mathbf{x}_k|\mathbf{z}_{1:k}) = \frac{p(\mathbf{z}_k|\mathbf{x}_k)p(\mathbf{x}_k|\mathbf{z}_{1:k-1})}{p(\mathbf{z}_k|\mathbf{z}_{1:k-1})}. \tag{2}$$

The terms in the numerator of (2) are defined through the *state-space equations*, while the denominator can simply be considered as a normalising constant.

There are three state-space equations. The state *prior* initialises the recursion and encapsulates all prior information about the state of the system

$$p(\mathbf{x}_0). \tag{3}$$

The *measurement equation* relates the observations (e.g. position) to the state of the system (e.g. position and velocity)

$$\mathbf{z}_k = h(\mathbf{x}_k, \mathbf{w}_k), \tag{4}$$

where $\mathbf{w}_k$ is a stochastic noise process with known distribution. Equation (4) defines the *likelihood function*, $p(\mathbf{z}_k|\mathbf{x}_k)$, which is the first term in the numerator of (2). The *process equation* models how the state evolves in discrete time

$$\mathbf{x}_{k+1} = f(\mathbf{x}_k, \mathbf{u}_k), \tag{5}$$

where $\mathbf{u}_k$ is another noise process with known distribution. Equation (5) defines the transition density $p(\mathbf{x}_{k+1}|\mathbf{x}_k)$, which is incorporated into the second term in the numerator of (2) through the Chapman-Kolmogorov equation (Jazwinski 1970)

$$p(\mathbf{x}_k|\mathbf{z}_{1:k-1}) = \int p(\mathbf{x}_k|\mathbf{x}_{k-1})p(\mathbf{x}_{k-1}|\mathbf{z}_{1:k-1})d\mathbf{x}_{k-1}. \tag{6}$$

3. METEOROID STATE-SPACE EQUATIONS

This section outlines the state-space and the state-space equations chosen to model the motion and measurement of a meteoroid process for the purposes of this paper. The specific parameters used in the model to estimate the trajectory characteristics of the Bunburra Rockhole data-set are given in Section 5.

The state that defines the meteoroid system includes the physical parameters of motion, as well as trajectory parameters σ and κ;

$$\mathbf{x}_k = \begin{bmatrix} l_k \\ v_k \\ m_k \\ \sigma_k \\ \kappa_k \end{bmatrix} \begin{matrix} \text{position} \\ \text{velocity} \\ \text{mass} \\ \text{ablation parameter} \\ \text{shape-density parameter,} \end{matrix} \tag{7}$$

where the position is measured along a pre-defined path produced by triangulating observations from several imaging sensors.

The measurement equation (4) is given by

$$\mathbf{z}_k = H\mathbf{x}_k + \mathbf{w}_k, \tag{8}$$

where the measurement matrix is

$$H = \begin{bmatrix} 1 & 0 & 0 & 0 & 0 \end{bmatrix} \tag{9}$$

and the measurement noise process, $\mathbf{w}_k$, is Gaussian with zero mean and variance R_k.

As a meteoroid passes through the atmosphere, its behaviour can be modelled by the aerodynamic equations from the single body theory of meteoroid entry (Hoppe 1937; Baldwin and Sheaffer 1971) (11), which uses atmospheric densities, ρ_a, acquired using the NRLMSISE-00 atmospheric model (Picone et al. 2002), local acceleration due to gravity, g, and entry angle from horizontal, γ_e. It is natural to model the change of meteoroid state as a continuous-time differential equation

$$\dot{\mathbf{x}} = f_c(\mathbf{x}) + \mathbf{u}_c, \tag{10}$$

where $f_c(\mathbf{x})$ is defined using

$$\begin{aligned}
\frac{dl}{dt} &= v && && \text{(11a)}\\
\frac{dv}{dt} &= -\frac{1}{2}\frac{c_d A\rho_a}{\rho_m^{2/3}}v^2 m^{(\mu-1)} + g\sin\gamma_e && = -\kappa\rho_a v^2 m^{(\mu-1)} + g\sin\gamma_e && \text{(11b)}\\
\frac{dm}{dt} &= -\frac{1}{2}\frac{c_h A\rho_a}{H^*}v^3 m^{\mu} && = -\sigma\kappa\rho_a v^3 m^{\mu} && \text{(11c)}\\
\frac{d\sigma}{dt} &= 0 && && \text{(11d)}\\
\frac{d\kappa}{dt} &= 0, && && \text{(11e)}
\end{aligned}$$

and the continuous-time process noise, $\mathbf{u}_c$, is Gaussian with zero mean and covariance $\mathbf{Q}_c$. Time integration of (10) is needed to arrive at the form required by the filtering state-space equation (5). In this case

$$\mathbf{x}_{k+1} = \int_{t_k}^{t_{k+1}} f_c(\mathbf{x})\,dt + \mathbf{u}_k. \tag{12}$$

Due to the non-linearities of (11) the discrete-time process noise, $\mathbf{u}_k$, is not Gaussian, but can be closely approximated by Gaussian noise with zero mean and covariance

$$\mathbf{Q}_k = \int_{t_k}^{t_{k+1}} e^{Ft}\,\mathbf{Q}_c\,e^{F^T t}\,dt \tag{13}$$

(Grewal and Andrews 1993), where the matrix F is the linearised form of the process equation

$$F = \frac{\partial f_c(\mathbf{x})}{\partial \mathbf{x}}. \tag{14}$$

Due to the form of the nonlinear functions (11), the integrations required by (12) and (13) cannot be found analytically. Numerical methods are used to calculate the integrals.

4. PARTICLE FILTER

There are a range of methods for finding the distribution of $\mathbf{x}_k$ by solving (2). The applicability of the method depends on the form of the state-space equations. If the measurement function and process function are linear and all the noise and prior distributions are Gaussian, then the solution to (2) can be found analytically. This solution is known as the Kalman Filter (Grewal and Andrews 1993). In the case where the equations are non-linear or the distributions are non-Gaussian, such as the single body equations for modelling meteoroid trajectory (11), there are no exact solutions and approximations are required.

The Extended Kalman Filter (EKF) (Sansom et al. 2015) approximates the noise distributions as Gaussian and finds a linear approximation to the process equations. The Unscented Kalman Filter (Sansom et al. 2016) approximates the posterior distribution as a Gaussian, but avoids approximating the measurement or process equations through a method of statistical linearisation (Särkkä 2007).

A particle filter does not require any assumptions about the form of the state equations or have any limitations on the noise distributions. This flexibility is achieved by representing the posterior density (2) as a set of N_s weighted particles, which are simply points in the state space (Gordon et al. 1993; Arulampalam et al. 2002). The ith random particle at time t_k is represented by its state, $\mathbf{x}_k^i$, and weight, w_k^i

$$\{\mathbf{x}_k^i, w_k^i\} \quad i = 1, ..., N_s. \tag{15}$$

Weights are normalised so that

$$\sum_i^{N_s} w_k^i = 1. \tag{16}$$

The probability distribution of the state is approximated by this set of weighted particles

$$p(\mathbf{x}_k|\mathbf{z}_{1:k}) \approx \sum_i^{N_s} \delta(\mathbf{x}_k - \mathbf{x}_k^i)w_k^i, \tag{17}$$

where $\delta(\mathbf{y})$ is the Dirac delta function, defined such that

$$\delta(\mathbf{y}) = \begin{cases} 1 & \mathbf{y} = 0 \\ 0 & \text{otherwise.} \end{cases} \tag{18}$$

Statistics can be computed on this set of particles, for example the mean of the distribution at any time t_k is approximated by

$$\hat{\mathbf{x}}_k = \sum_i^{N_s} w_k^i \mathbf{x}_k^i, \tag{19}$$

with the state covariance calculated as

$$Cov(\mathbf{x}_k) = \sum_i^{N_s} w_k^i (\mathbf{x}_k^i - \hat{\mathbf{x}}_k)(\mathbf{x}_k^i - \hat{\mathbf{x}}_k)^T. \tag{20}$$

There are strong similarities between the implementation of a particle filter and the simpler Kalman filter. Both follow the three steps

1. Initialisation: start the filter with a known prior distribution, $p(\mathbf{x}_0)$
2. Prediction: propagate the distribution from time $k-1$ to time k using the process equation (5)
3. Update: use the measurement equation (4) to update the predicted distribution with the measurement information, producing the posterior distribution at time k, $p(\mathbf{x}_k|\mathbf{z}_{1:k})$

The Kalman filter achieves these steps by exact analytic equations which manipulate the mean and covariance of the distribution at each step. On the other hand the particle filter proceeds through calculation on each of the particles individually.

To initialise the particle filter, a set of particles are randomly sampled from the prior distribution, $p(\mathbf{x}_0)$, and weighted equally as $w_0^i = \frac{1}{N_s}$.

In the prediction step each particle is propagated forward in time via the process equation (12). To incorporate the uncertainty of the system, a sample from the process noise, u_k, is randomly generated for each particle. Using the process equation to propagate the particles results in the simplest form of the filter. The particle filter literature generalises this through importance sampling, where an arbitrary proposal distribution can be used, instead of the process equation (Arulampalam et al. 2002). Sophisticated proposal distributions can make a particle filter implementation more efficient (require fewer particles), but they have not been investigated for this application.

The update step adjusts the weight of each particle. The weight is obtained by evaluating the likelihood function for each particle

$$\tilde{w}_k^i = p(\mathbf{z}_k|\mathbf{x}_k^i) w_{k-1}^i. \tag{21}$$

The weights are then normalised to satisfy (16)

$$w_k^i = \frac{\tilde{w}_k^i}{\sum_i^{N_s} \tilde{w}_k^i}. \tag{22}$$

Over time the particle weights can transfer to a few select particles, thereby updating insignificant particles at the expense of computing power (Arulampalam et al. 2002). This is known as the degeneracy problem and equation (23) gives an approximate measure of particle effectiveness that can be used to assess the severity of the issue (Arulampalam et al. 2002).

$$\hat{N}_{\text{eff}} = \left(\sum_i^{N_s} (w_k^i)^2 \right)^{-1} \tag{23}$$

The degeneracy problem can be addressed by resampling the data after weights have been calculated. A new population of particles are generated from the current sample pool based on given weightings; the objective being to preferentially remove samples of lower weights. The probability of resampling any given particle i is w_k^i. The optional resampling step is taken if the number of effective particles drops below some threshold. After resampling all of the particle weights are set to $1/N_s$.

5. PARTICLE FILTER PARAMETERS FOR A METEOROID TRAJECTORY

Dedicated fireball networks, such as the DFN, capture fireball events from multiple locations, providing triangulated position observations with time. This also enables a rough calculation of velocities throughout the trajectory.

5.1. *Initialisation*

When initialising the state prior for the set of N_s particles at the start of the luminous trajectory (t_0), the initial position and, to an extent, the initial velocity[2] can be reasonably well constrained. The other state parameters, m, σ, κ, however are not directly observable. To explore the data space and determine likely values for m_0, as well as constants σ and κ, each particle is initiated with a random value within a given range. The state prior for each particle is initialised according to Table 1, with m_0^{min} in all cases set to 0.5 kg.

Table 1. Describes the method used by the particle filter to initialise state parameters for each particle. A random selection is made for each value using either a Gaussian probability density function (PDF) (mean and standard deviation given), a uniform PDF within a given value range or a multi-modal distribution in the case of bulk density.

parameter to be initiated	**method used**
l_0	random choice based on Gaussian $\mathcal{N}(0, 10\,m)$ (from triangulation errors)
v_0	random choice based on Gaussian $\mathcal{N}(v_0, 500\,m\,s^{-1})$ (from triangulation errors)
m_0	random choice from 0 to m_0^{max} (kg)
σ	random choice between 0.001 to 0.05 $s^2\,km^{-2}$ (from Ceplecha et al. (1998) for asteroidal material)
κ	c_d - random choice based on Gaussian $\mathcal{N}(1.3, 0.3)$ (based on aerodynamic drag values from Zhdan et al. (2007))
	A - random choice based on Gaussian $\mathcal{N}(1.4, 0.33)$ (close to spherical values)
	ρ_m - the PDF representing meteorite bulk densities is multi-modal. To fully represent this distribution, initialisation is performed in two stages. First, a random choice of meteorite type is made based on recovered percentages (80 % chondrites, 11 % achondrites, 2 % stony-iron, 5 % iron, 2% cometary (Grady 2000)). Second, a random choice of bulk density is made based on the Gaussian PDF representing chosen meteorite type;
	chondrites - $\mathcal{N}(2700, 420)$ (after Britt and Consolmagno (2003));
	achondrites - $\mathcal{N}(3100, 133)$ (after Britt and Consolmagno (2003));
	stony-iron - $\mathcal{N}(4500, 133)$ (after Britt and Consolmagno (2003));
	iron - $\mathcal{N}(7500, 167)$ (after Consolmagno S.J. and Britt (1998)) ;
	cometary - $\mathcal{N}(850, 117)$ (after Weissman and Lowry (2008)).

5.2. *Prediction*

At every observation time, t_k, the state of each particle is evaluated using the system model (10). $\mathbf{Q}_c$ values used here to represent the continuous process noise in the given model for meteoroid trajectories are given by (24). The diagonal elements of $\mathbf{Q}_c$ in (24) are the variance values for dl/dt, dv/dt, dm/dt, $d\sigma/dt$, $d\kappa/dt$ respectively. The uncertainty in

---

[2] Determining v_{inf} - or the velocity with which a body entered the Earth's atmosphere, as opposed to the 'initial' velocity that it has when its luminous trajectory is first observed, can be determined using reverse integration methods from the start of the luminous trajectory back to beyond the Earth's sphere of influence (e.g. Trigo-Rodriguez et al. (2015)). This is done by the DFN data reduction process as part of orbital modelling. For the larger objects that generate fireballs (and that are the focus of this work) the difference between v_{inf} and v_0 is likely to be small, however a detailed discussion is outside the scope of this paper as the method described in this work (in accordance with others in the literature) model meteoroid bright flight only.

position and velocity are introduced through noise in the acceleration model 11b, and the variance for dl/dt for this process model is therefore set to $0\,m\,s^{-1}$. The other model equations however are not able to represent the system in its entirety; complications, such as fragmentation, affect all other state process models. At this stage, we assume that the shape density and ablation parameters will not change dramatically over the meteoroid flight and are attributed small process noise values. There is a high uncertainty in the mass loss for the single-body ablation model 11c and so a large range of masses are allowed to be explored by the particles. The process noise in mass is a multiple of the mass in order to keep it within a consistent order of magnitude. The discrete process noise, $\mathbf{Q}_k$, is calculated at every time step following (13).

$$\mathbf{Q}_c = \begin{bmatrix} (0\,m\,s^{-1})^2 & 0 & 0 & 0 & 0 \\ 0 & (75\,m\,s^{-2})^2 & 0 & 0 & 0 \\ 0 & 0 & (0.2 \times m_k\ kg\,s^{-1})^2 & 0 & 0 \\ 0 & 0 & 0 & (10^{-4}\,s\,km^{-2})^2 & 0 \\ 0 & 0 & 0 & 0 & (10^{-5}(SI)\,s^{-1})^2 \end{bmatrix} \tag{24}$$

To improve compute time of this method, the non-linear integration (12) of all N_s particles, and their associated $\mathbf{Q}_k$, is performed simultaneously using parallel multiprocessing.

5.3. *Update*

The triangulated position of the meteoroid along the trajectory at time k is the observation measurement $\mathbf{z}_k$. The weight ($\tilde{w}_k^i$) for each particle, $\mathbf{x}_k^i$ is calculated using a one dimension Gaussian probability distribution function

$$p(\mathbf{z}_k|\mathbf{x}_k^i) = \frac{1}{\sqrt{2R_k\pi}} e^{-\frac{(\mathbf{z}_k - \mathbf{H}\mathbf{x}_k^i)^2}{2R_k}} \tag{25}$$

in (21), with the observation noise having a variance $R_k = (100\,m)^2$. This is based on errors in timing and triangulated position, reflecting the accuracy of the data set being used.

In order to avoid degeneracy in the particle set, we have use the stratified resampling method described by Arulampalam et al. (2002) after each update step.

6. USING A PARTICLE FILTER TO PREDICT A METEOROID TRAJECTORY

The data acquired by Spurný et al. (2012) for the Bunburra Rockhole fireball is used to test the suitability of the particle filter in estimating the state of a meteoroid during atmospheric entry. The Bunburra Rockhole dataset consists of 113 published observations of position with time along the trajectory. Note that no observation data were published between $t = 0.0\,s$ and $t = 0.1899\,s$ or from $t = 5.3165\,s$ to $t = 5.4589\,s$. Our modelling will use times relative to $t_0 = 0.1899\,s$ along the trajectory. A particle filter is run using set of 10,000 particles ($N_s = 10,000$). Particles are initiated according to Table 1 with m_0^{max} set to 2,000 kg.

Figure 1 shows all the resulting particle masses with weights > 0 from t_0 to t_{end}. The range of σ and κ values used to initiate each particle results in a variety of predicted trajectory 'paths'.

To aid in understanding the different trajectories predicted by the particle filter, five particles at t_0 have been selected to discuss ($\mathbf{x}_0^j$ given in Table 2). Figure 2 highlights these particles, $\mathbf{x}_0^{a-e}$, along with all particles that are generated from them at later time steps (either by propagation from t_{k-1} or resampling at t_k).

The variation in σ (Figure 2b) and κ (Figure 2c) values with time is due to the addition of process noise, $\mathbf{u}_k$, in (10). As this noise is random Gaussian, it allows small variations between identical resampled particles that would have originally shared equal values. Areas of greater particle density are characteristic of higher probability states.

Orange particles in Figure 2 originate from $\mathbf{x}_0^e$. The steep change in mass with time (Figure 2(a) is due to the high σ (Figure 2(b)) and κ (Figure 2(c) values with which they were initiated. Particles that no longer fit the observed data are preferentially removed by the resampling process and their 'path' discontinues in Figure 2. Although particles originating from $\mathbf{x}_0^{c-e}$ were initiated with diverse σ (Figure 2b) and κ (Figure 2c) values, they, along with all other particles with $m_0^i > 27\,kg$ have insignificant weight past 5.0 seconds. A visual comparison of predicted particle velocities with velocities calculated from position measurements is shown in Figure 2d. The 'survival' of $\mathbf{x}_0^{a,b}$ to t_{end} is due to their higher w_k^i values indicating superior fits to the observations (and visually noticeable in Figure 2d).

The final trajectory parameters of the Bunburra Rockhole meteoroid have been previously determined by Spurný et al. (2012) using the dynamic gross fragmentation model (GFM) of Ceplecha et al. (1993) and the meteoroid fragmentation

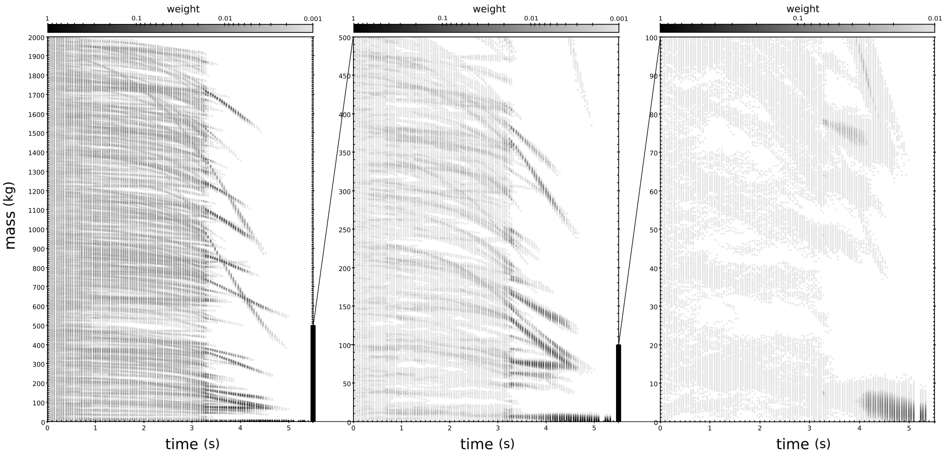

Figure 1. Mass estimates for particles, with $w_k^i > 0$, produced by the particle filter where $N_s = 10,000$, $m_0^{max} = 2000\,kg$ were used and $\mathbf{Q}_c$ given by (24). Colour scale is additive; weights of particles plotted in the same location are summed. Note the change in colour scale in the third frame to highlight t_{end} weightings. At $t = 4.9\,s$ all particles with a weight greater than zero have a mass of 11 kg or lower. Times correspond to the seconds since the 2nd recorded dash of the Bunburra Rockhole fireball; $t_0 = 0.1899\,s$ into the trajectory. It is noticeable at $t_k = 3.32\,s$ that there is a drastic reduction in the number of particle 'paths' that fit the observational data.

Table 2. The state of five particles at t_0 are shown. All future particles resampled from these are highlighted in Figure 2 according to the colour given here.

$\mathbf{x}_0^j$	l_0 (m)	v_0 $(km\,s^{-1})$	m_0 (kg)	σ_0 $(s^2\,km^{-2})$	κ_0 (SI)	reference colour in Figure 2
$\mathbf{x}_0^a$	-1.57	12.80	10.1	0.022	0.0083	blue
$\mathbf{x}_0^b$	-18.60	12.88	14.3	0.020	0.0058	green
$\mathbf{x}_0^c$	5.00	12.48	176.2	0.021	0.0039	red
$\mathbf{x}_0^d$	-17.19	12.96	212.1	0.037	0.0083	dark orange
$\mathbf{x}_0^e$	12.41	13.10	234.0	0.041	0.0133	light orange

model (MFM) of Ceplecha and Revelle (2005) which integrates fireball brightness with the dynamics (Table 3). Both the GFM and MFM require initial assumptions including the entry mass and a manually pre-defined fragmentation pattern based on the light curve (Ceplecha and Revelle 2005). Errors given by these models relate to the standard deviation of the residuals between modelled and measured observations; observational uncertainties, assumptions made in the model and model parameters are not propagated. The Kalman filter methods applied by Sansom et al. (2015) and Sansom et al. (2016) to meteoroid trajectory modelling perform a comprehensive analysis of the errors of both model and observations but share the limitations of previous models in requiring a single set of initial entry parameters to be pre-determined.

The statistical approach of the particle filter is not limited to any one set of input parameters. It encapsulates all prior knowledge of the parameter space by exploring the full range of plausible parameter values to produce an unbiased analysis. Given that model and observation uncertainties are incorporated and propagated, this method provides a statistically robust final state estimate which is no longer dependent on any single set of assumed input parameters, providing a more realistic understanding of real-world variability. The independence of the particle filter and lack of manual input enables full automation of this method.

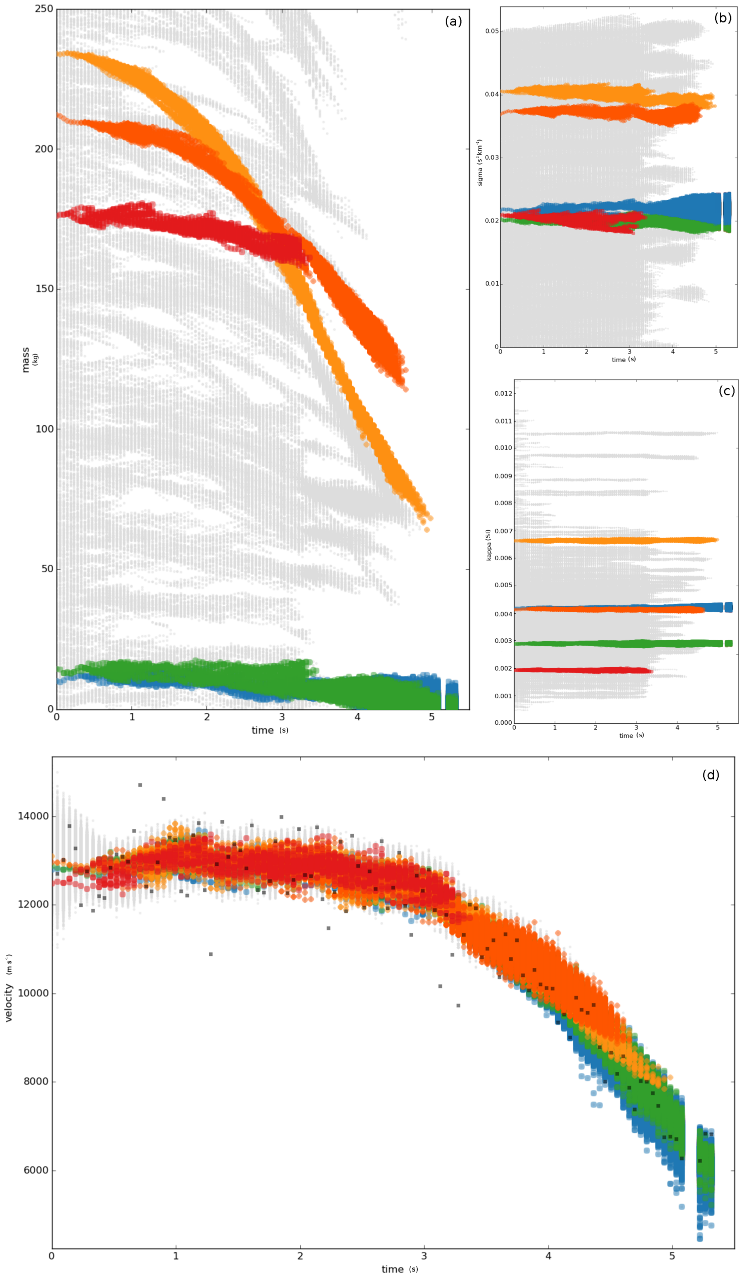

Figure 2. Particle states estimated by the particle filter. (a) Predicted mass with time. (b) Predicted ablation parameter,σ with time. (c) Predicted shape density, κ, with time. (d) Predicted velocity with time. Particles originating from $\mathbf{x}_0^{a-e}$ (Table 2) are highlighted with reference colours given in Table 2). Note times correspond to seconds since the 2nd recorded dash of the Bunburra Rockhole fireball; $t_0 = 0.1899\,s$ into the trajectory. It is noticeable at $t_k = 3.32\,s$ that there is a drastic reduction in the number of particle 'paths' that fit the observational data. The parameter space after this time is much more constrained.

Table 3. Mean final state values estimated by the particle filter (19), alongside published values. Errors given by all previous methods reflect only model errors within the given initial input assumptions given. The GFM and MFM methods do not consider observation uncertainties (Ceplecha and Revelle 2005). The particle filter errors are calculated as $\sqrt{Var(\hat{\mathbf{x}}_k)}$ given by (20), and alone gives a fully inclusive analysis of trajectory model and observation uncertainties to provide a more realistic understanding of real-world variability.

	l_{end} (km)	v_{end} $(km\,s^{-1})$	m_{end} (kg)	σ_{end} $(s^2\,km^{-2})$	κ_{end} (SI)
GFM [1]			1.5 ± 0.2	0.0331 ± 0.0007 (apparent)	
MFM [1]		5.77 ± 0.04	1.1	$0.002 \pm 0.001/0.004$ (intrinsic)	0.0035
Dynamic [2] optimisation	60.07	6.109	2.36	0.0371 (apparent)	0.0062
EKF [2]	60.03 ± 0.062	6.05 ± 0.24	2.30 ± 1.63		
UKF [3]	60.04 ± 0.058	6.10 ± 0.20	2.88 ± 1.04		
IMM [3]	60.01 ± 0.007	5.90 ± 0.06	1.32 ± 0.49		
Particle filter	59.89 ± 0.038	6.03 ± 0.22	2.16 ± 1.33	0.0219 ± 0.0007 (apparent)	0.0042 $\pm$0.000

[1] Spurný et al. (2012); GFM = gross fragmentation model; MFM = meteoroid fragmentation model.

[2] Sansom et al. (2015); κ value determined using $c_d = 1.3$; EKF = extended Kalman filter.

[3] Sansom et al. (2016); UKF = unscented Kalman filter; IMM = interactive multiple model.

The spread of final particle states at t_{end} can be summarised by the weighted mean (19) in Table 3. Errors are calculated as the square root of the covariance diagonal elements given by Equation (20). The ablation parameter is an interesting result. Although the particle filter does not explicitly model fragmentation, Q_c allows for a certain amount of variation in state parameters due to un-modelled processes and inherently includes fragmentation to some extent, without the need for a pre-defined fragmentation pattern (required by MFM (Ceplecha and Revelle 2005)). As discussed by Ceplecha and Revelle (2005), the intrinsic value of the ablation parameter remains constant throughout the trajectory regardless of fragmentation. When fragmentation is not modelled explicitly, variations in the ablation parameter appear to occur and must therefore be expressed as the *apparent* ablation parameter. The GFM produces an *apparent* σ whereas the MFM, as it incorporates the light curve, is able to define the *intrinsic* σ. The value determined using the particle filter is slightly lower than the apparent σ of the GFM and it is therefore plausible that we can use this difference to quantify the extent to which fragmentation is included in the final state estimate.

Using a particle filter the state estimates at each time step are iteratively updated based on the past data; future observations are not included. The final states alone result from processing all observations. As a predicted particle becomes inconsistent with the observations, it becomes an unlikely scenario for future times but it does not mean this original path can be discounted. It is noticeable at $t_k = 3.32\,s$ that there is a drastic reduction in the number of particle 'paths' that fit the observational data. The parameter space after this time is much more constrained. All particles at t_{end} originate from particles with $\mathbf{x}_0 < 27\,kg$; these particles are consistent with both parts of the trajectory displaying no dramatic change in mass. It is possible that particles of initially higher mass are discontinued in favour of lower mass scenarios as a result of gross fragmentation reflected in the observation data. Without including all the data at every time-step, the most likely state 'path' for the entire trajectory cannot be constrained; we cannot distinguish the full particle history.

In order to distinguish likely initial masses, we need to be able to explore drastic changes in mass. The interactive multiple model (IMM) smoother as described by Sansom et al. (2016) has this capability and uses all observational data at each time step. It however requires a single pre-defined set of initial parameters. This is a well suited complementary method to our current implementation of a particle filter. The particle filter framework however is flexible enough to incorporate dynamic models that explicitly capture gross fragmentation events. Future work will explore more sophisticated dynamic models as well as particle filter smoothing to reconstruct the full meteoroid trajectory.

Including brightness as a state in trajectory modelling would also provide an additional observation with which to weight particles. As brightness is linked to mass, its addition would not only improve state estimates, but would inherently include information on fragmentation.

7. CONCLUSION

The use of a particle filter to approximate fireball trajectories provides a statistical analysis of the meteoroid state, including unobservable trajectory parameters. This is the first approach of its kind in this field. Other non-linear filtering algorithms such as the Extended Kalman filter (Sansom et al. 2015) and the Unscented Kalman filter (Sansom et al. 2016), as well as other least-squares approaches (Ceplecha et al. 1993; Ceplecha and Revelle 2005), require a predetermined set of initial parameters to statistically analyse the trajectory of a meteoroid. The iterative Monte Carlo simulations of a particle filter is not only capable of automating the analysis of fireball trajectories, but is able to do so without the need for limiting input parameters to single assumed values, rather it encapsulates all prior knowledge of the parameter space, to produce an unbiased analysis. The adaptive filter approach uses the observations of the meteoroid's position as it travels through the Earth's atmosphere to update state estimates. Predicted positions similar to those observed are given a higher weighting and are preferentially resampled at the next time step. This gives a final state estimate (Table 3) with robust error propagation of uncertainties in the initial parameters, observations and the dynamic model (e.g. unpredictable gross fragmentation events). Even though trajectory parameters σ and κ are not currently set to vary systematically with time (noise is added to create diversity between resampled particles to avoid degeneracy only), a stochastic approach to their determination has not previously been conducted. Incorporating brightness as an additional state will provide supplementary data and improve estimates. This method currently allows an automated dynamic analysis of fireball trajectories.

ACKNOWLEDGEMENTS

This work was funded by the Australian Research Council as part of the Australian Laureate Fellowship scheme.

REFERENCES

M. S. Arulampalam, S. Maskell, N. Gordon, and T. Clapp. A tutorial on particle filters for online nonlinear/non-Gaussian Bayesian tracking. *IEEE Transactions on Signal Processing*, 50(2):174–188, 2002. ISSN 1053587X. doi:10.1109/78.978374.

B. Baldwin and Y. Sheaffer. Ablation and breakup of large meteoroids during atmospheric entry. *Journal of Geophysical Research*, 76(19):4653–4668, 1971.

P. Bland, P. Spurnỳ, A. Bevan, K. Howard, M. Towner, G. Benedix, R. Greenwood, L. Shrbenỳ, I. Franchi, G. Deacon, et al. The australian desert fireball network: a new era for planetary science. *Australian Journal of Earth Sciences*, 59 (2):177–187, 2012.

J. Borovička, P. Spurnỳ, and P. Brown. Small near-earth asteroids as a source of meteorites. *Asteroids IV*, page 257, 2015.

D. Britt and G. Consolmagno. Stony meteorite porosities and densities: A review of the data through 2001. *Meteoritics & Planetary Science*, 38(8):1161–1180, 2003. ISSN 10869379. doi:10.1111/j.1945-5100.2003.tb00305.x.

V. A. Bronshten. *Physics of Meteoric Phenomena*. Geophysics and Astrophysics Monographs. Reidel, Dordrecht, Netherlands, 1983. ISBN 9789027716545.

M. D. Campbell-Brown and D. Koschny. Model of the ablation of faint meteors. *Astronomy and Astrophysics*, 418(2): 751–758, 2004. ISSN 0004-6361. doi:10.1051/0004-6361:20041001-1.

Z. Ceplecha. Geometric, dynamic, orbital and photometric data on meteoroids from photographic fireball networks. *Bulletin of the Astronomical Institutes of Czechoslovakia*, 38:222–234, 1987.

Z. Ceplecha and D. O. Revelle. Fragmentation model of meteoroid motion, mass loss, and radiation in the atmosphere. *Meteoritics & Planetary Science*, 40(1):35–54, 2005. doi:10.1111/j.1945-5100.2005.tb00363.x.

Z. Ceplecha, P. Spurný, J. Borovička, and J. Keclikova. Atmospheric fragmentation of meteoriods. *Astronomy and Astrophysics*, 279:615–626, 1993.

Z. Ceplecha, J. Borovička, W. G. Elford, D. O. ReVelle, R. L. Hawkes, V. Porubčan, and M. Šimek. Meteor Phenomena and Bodies. *Space Science Reviews*, 84(3):327–471, 1998. doi:10.1023/A:1005069928850.

G. J. Consolmagno S.J. and D. T. Britt. The density and porosity of meteorites from the vatican collection. *Meteoritics & Planetary Science*, 33(6):1231–1241, 1998. ISSN 1945-5100. doi:10.1111/j.1945-5100.1998.tb01308.x.

N. Gordon, D. Salmond, and A. Smith. Novel approach to nonlinear/non-Gaussian Bayesian state estimation. *IEE Proceedings F -Radar and Signal Processing*, 140(2):107, 1993. ISSN 0956375X. doi:10.1049/ip-f-2.1993.0015.

M. M. Grady. *Catalogue of Meteorites*, volume 1. Cambridge University Press, 5 edition, 2000.

M. S. Grewal and A. P. Andrews. *Kalman filtering: theory and practice.* Prentice-Hall Inc., New Jersey, 1993.

M. I. Gritsevich. Determination of parameters of meteor bodies based on flight observational data. *Advances in Space Research*, 44(3):323–334, 2009. ISSN 02731177. doi:10.1016/j.asr.2009.03.030.

A. W. Harris. The value of enhanced neo surveys. In *AAS/Division for Planetary Sciences Meeting Abstracts*, volume 44, 2012.

J. Hoppe. Die physikalischen Vorgänge beim Eindringen meteoritischer Körper in die Erdatmosphäre. *Astronomische Nachrichten*, 262(10):169–198, 1937. URL `http://onlinelibrary.wiley.com/doi/10.1002/asna.19372621002/abstract`.

R. Howie, J. Paxman, P. Bland, M. Towner, E. Sansom, and H. Devillepoix. Sub-millisecond fireball timing for precise heliocentric orbits using de Bruijn timecodes. *Meteoritic and Planetary Science*, in review.

A. H. Jazwinski. *Stochastic Processes and Filtering Theory*. Academic Press, New York, 1970.

J.-B. Kikwaya, M. D. Campbell-Brown, and P. G. Brown. Bulk density of small meteoroids. *Astronomy & Astrophysics*, 530: A113, 2011. ISSN 0004-6361. doi:10.1051/0004-6361/201116431.

I. S. Murray, M. Beech, M. J. Taylor, P. Jenniskens, and R. L. Hawkes. Comparison of 1998 and 1999 leonid light curve morphology and meteoroid structure. *Earth, Moon, and Planets*, 82(0):351–367, 2000. ISSN 1573-0794. doi:10.1023/A:1017003019448.

J. M. Picone, A. E. Hedin, D. P. Drob, and A. C. Aikin. NRLMSISE-00 empirical model of the atmosphere: Statistical comparisons and scientific issues. *Journal of Geophysical Research: Space Physics (1978–2012)*, 107(A12):1468, 2002.

D. O. Revelle. *NEO fireball diversity: energetics-based entry modeling and analysis techniques.* Proceedings of the International Astronomical Union S236. Cambridge University Press, 2007.

E. K. Sansom, P. Bland, J. Paxman, and M. Towner. A novel approach to fireball modeling: The observable and the calculated. *Meteoritics & Planetary Science*, 50(8):1423–1435, 2015. doi:10.1111/maps.12478.

E. K. Sansom, P. A. Bland, M. G. Rutten, J. Paxman, and M. C. Towner. Filtering meteoroid flights using multiple unscented kalman filters. *The Astronomical Journal*, 152(5): 148, 2016. doi:10.3847/0004-6256/152/5/148. URL `http://stacks.iop.org/1538-3881/152/i=5/a=148`.

S. Särkkä. On unscented Kalman filtering for state estimation of continuous-time nonlinear systems. *IEEE Transactions on Automatic Control*, 52(9):1631–1641, 2007. doi:10.1109/TAC.2007.904453.

P. Spurný, P. Bland, L. Shrbený, J. Borovička, Z. Ceplecha, A. Singelton, A. W. R. Bevan, D. Vaughan, M. C. Towner, T. P. Mcclafferty, R. Toumi, and G. Deacon. The Bunburra Rockhole meteorite fall in SW Australia: Fireball trajectory, luminosity, dynamics, orbit, and impact position from photographic and photoelectric records. *Meteoritics and Planetary Science*, 47(2):163–185, feb 2012. doi:10.1111/j.1945-5100.2011.01321.x.

J. M. Trigo-Rodriguez, E. Lyytinen, M. Gritsevich, M. Moreno-Ibáñez, W. F. Bottke, I. Williams, V. Lupovka, V. Dmitriev, T. Kohout, and V. Grokhovsky. Orbit and dynamic origin of the recently recovered annama's h5 chondrite. *Monthly Notices of the Royal Astronomical Society*, 449(2):2119–2127, 2015.

P. R. Weissman and S. C. Lowry. Structure and density of cometary nuclei. *Meteoritics & Planetary Science*, 43(6): 1033–1047, 2008. ISSN 1945-5100. doi:10.1111/j.1945-5100.2008.tb00691.x. URL `http://dx.doi.org/10.1111/j.1945-5100.2008.tb00691.x`.

I. A. Zhdan, V. P. Stulov, P. V. Stulov, and L. I. Turchak. Drag coefficients for bodies of meteorite-like shapes. *Solar System Research*, 41(6):505–508, dec 2007. ISSN 0038-0946. doi:10.1134/S0038094607060068. URL `http://link.springer.com/10.1134/S0038094607060068`.

MANUSCRIPT – MODELLING FIREBALL NETWORK DATA IN THREE DIMENSIONS

Sansom, E. K., Jansen-Sturgeon, T., Rutten, M. G.

THIS CHAPTER IS LAID OUT AS A MANUSCRIPT TO BE SUBMITTED TO ICARUS

STATEMENT OF AUTHORSHIP

TITLE OF MANUSCRIPT: Modelling Fireball Network Data in Three Dimensions

PUBLICATION STATUS: In preparation; publication style.

AUTHOR CONTRIBUTIONS

By signing the Statement of Authorship, each author certifies that their stated contribution to the manuscript is accurate and that permission is granted for the manuscript to be included in the candidate's thesis.

Name of Principal Author: Eleanor K. Sansom

Contribution to the Paper: Led all aspects of this research and drafted this manuscript.

Overall Percentage: 90%

Signature: ***Date:*** 01 / 12 / 16

Name of Co-Author: Trent Jansen-Sturgeon

Contribution to the Paper: Contributed straight-line least squares data and provided content for Sections 5.2.1 and 5.2.3.

Overall Percentage: 7%

Signature: ***Date:*** 5 / 12 / 16

Name of Co-Author: Mark G. Rutten

Contribution to the Paper: Helped in the editing and final review of the manuscript.

Overall Percentage: 3%

Signature: ***Date:*** 5 / 12 / 16

APPENDIX B

ADDITIONAL PUBLICATIONS

CONFERENCE ABSTRACT A — AUTOMATED DYNAMIC MODELLING OF FIREBALLS FOR THE AUSTRALIAN DESERT FIREBALL NETWORK

Sansom, E. K., Bland, P. A. and Paxman, J.
Presented at the 45th Lunar Planetary Science Conference, March 2014, Woodlands, TX.

Abstract published in proceedings of the Lunar and Planetary Science Conference p.1591.

Reason for inclusion — This work was presented as a poster at an international conference and outlined the work in paper 1.

STATEMENT OF AUTHORSHIP

TITLE OF ABSTRACT: Automated Dynamic Modelling Of Fireballs For The Australian Desert Fireball Network

PUBLICATION STATUS: Published

AUTHOR CONTRIBUTIONS

By signing the Statement of Authorship, each author certifies that their stated contribution to the publication is accurate and that permission is granted for the publication to be included in the candidate's thesis.

Name of Principal Author: Eleanor K. Sansom

Contribution to the Abstract: Led all aspects of the research, drafted the manuscript and presented the research at the 45th Lunar Planetary Science Conference in Texas, USA.

Overall Percentage: 90%

Signature: ***Date:*** 01 / 12 / 16

Name of Co-Author: Phillip A. Bland

Contribution to the Abstract: Assisted in revising and editing the manuscript.

Overall Percentage: 5%

Signature: ***Date:*** 4 / 12 / 16

Name of Co-Author: Jonathan Paxman

Contribution to the Abstract: Assisted in revising and editing the manuscript.

Overall Percentage: 5%

Signature: ***Date:*** 5/12/16

45th Lunar and Planetary Science Conference (2014) **1591.pdf**

Automated Dynamic Modelling Of Fireballs For The Australian Desert Fireball Network. E. K. Sansom[1], P. A. Bland[2] and J. Paxman[3], [1]Department of Applied Geology, Curtin University, GPO Box U1987, Perth, WA 6845, Australia, eleanor.sansom@curtin.edu.au, [2]Department of Applied Geology, Curtin University, GPO Box U1987, Perth, WA 6845, Australia, p.a.bland@curtin.edu.au, [3]Department of Mechanical Engineering, Curtin University, GPO Box U1987, Perth, WA 6845, Australia, j.paxman@curtin.edu.au.

Introduction: Fireball observations from five dedicated camera networks have led to the recovery of 10 meteorites. Although this is a relatively small dataset, several methods have been applied to derive an initial and final mass from fireball data. Two principal concepts have been used to estimate the mass of a meteoroid during its path through the atmosphere, the photometric and dynamic methods. Öpik [1] was one of the pioneers of the photometric method which uses the luminosity of the fireball to determine the incoming 'photometric' mass, and a corresponding luminous efficiency as a proxy for mass loss. Although analyses were conducted on the best data available, these datasets are limited in number and detail. It is therefore difficult to justify having "established a fully calibrated luminous efficiency parameter" [2]. The dynamic method uses the deceleration of the fireball to estimate mass. The accuracy to which deceleration could be measured from photographic plates was a limitation of this method [3, 4]. In recent years, Stulov [5] has combined unknown parameters in the dynamic equations into two dimensionless parameters to enable an easier analytical solution. This method was applied by Gritsevich [6, 7] to data sets which led to recovered meteorites. Although both methods have their limitations, a new approach to the dynamic method is presented here with the aim of completely automating the process of calculating the terminal bright flight mass. This calculation will form part of an automated workflow from fireball detection and triangulation through to orbit and fall calculation as part of the Australian Desert Fireball Network. The network will soon be expanding to a coverage area of 1.5-2 million km^2 with 50-60 camera stations. The data generated will exceed 100TB per year, and therefore automating the data pipeline – from event detection, image processing of the fireball track, triangulation, calculating terminal bright-flight mass, to darkflight and climate modelling – is a priority. The result will be automation of meteorite fall position estimates, with uncertainties, to facilitate rapid recovery of samples which may provide invaluable data for cosmo-chemists (particularly when combined with orbital data). This approach will also allow confirmation and refinement of mass and fragmentation models.

Model: The dynamic equations used for the entry of meteoroids through the atmosphere after [5] are

$$m\frac{dV}{dt} = -\frac{1}{2}c_d\rho_a V^2 S \qquad (1)$$

$$H^*\frac{dm}{dt} = -\frac{1}{2}c_h\rho_a V^3 S, \qquad (2)$$

where m is meteoroid mass, V is velocity, c_d and c_h the drag and heat coefficients respectively. H^* is the enthalpy of sublimation, ρ_a the atmospheric density and S the cross sectional area of the body which can also be written as

$$S = A\left(\frac{m}{\rho_m}\right)^{\mu}. \qquad (3)$$

Here A is the shape parameter, ρ_m is the meteoroid density and μ the spin parameter.

Combining equation (3) with (1)-(2), the equations become

$$\frac{dV}{dt} = -\frac{1}{2}\frac{c_d\rho_a A}{\rho_m}V^2 m_m^{(\mu-1)} \qquad (4)$$

$$\frac{dM}{dt} = -\frac{1}{2}\frac{c_h\rho_a}{H^*\rho_m}V^3 m_m^{\mu}. \qquad (5)$$

The method proposed in this research takes a two-step approach. Initially a constrained dynamic optimisation is carried out to estimate the set of unknown parameters ($\frac{c_h}{H^*}$, A, ρ_m and μ) and the initial states (m_0, V_0). These parameters are then used to perform an extended Kalman filter estimation of the dynamic states (position, velocity and mass) from a sequence of position observations. Errors associated with the terminal mass and position are also calculated and are extremely valuable in estimating fall probabilities on the ground, which previous methods have not explicitly quantified.

Extended Kalman Filter. The objective of the Kalman filter is to estimate the states of a dynamic model based on a two-step process of "predict" and "update" [8]. In the meteoroid estimation problem, the states include the position along the line of trajectory, the velocity and mass of the meteoroid in the atmosphere. The prediction step involves estimating the state at an extrapolated time using the given dynamic model, including a covariance estimate for the estimated state vector. The update step refines the state estimate and covariance by taking an observation into account. An optimal "Kalman" gain is applied which takes into account both the uncertainty of the state estimate, and the uncertainty of the observation model.

Results: Ten data sets from the Australian Desert Fireball Network have been analysed in this way. The most complete, and therefore most reliable, being that of Bunburra Rockhole [9]. After the dynamic optimisation step, the optimal initial parameters are determined to be: m_{0}=19.9 *kg*, V_0=13184 m/s, ρ_m=2000 kg/m^3, A=1.58, μ=2/3 and c_h/H^*=4.76x10^{-8} KJ/Kg. These were used in the subsequent extended Kalman filter to produce final states of m_{mf}= 0.909±0. 47 kg and V_f= 5792±309 m/s (with a larger assumed observation variance of 10000, top figure) and m_{mf}=1.08±0.47kg and V_f=5970±485 m/s (with a smaller assumed observation variance of 1000, bottom figure).

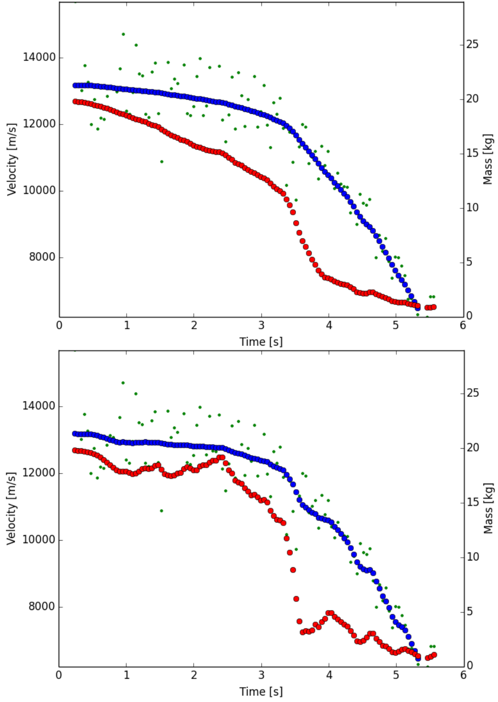

Figure: Results of Kalman filter step for Bunburra Rockhole. Blue shows velocity estimates as calculated by the extended Kalman filter over the raw velocity data (green). Red shows mass estimates along the trajectory. The two simulations apply different observation models.

Discussion: The Bunburra Rockhole data set, although very complete contains a very high initial scatter of ±3800 m/s in velocity. The Kalman filter is capable of producing optimal state estimates in the context of a noisy observation model.

The figure shows the velocities and masses estimated at each time step, considering the prior data. The locations where mass is greater than the previous timestep is a result of the values being updated by the present observation. The final state estimates and the corresponding covariance matrix will be used in subsequent dark flight calculations.

The Q_4 least-squares minimisation method produced by [10] was applied to this same data set. Smoothing was required before a result could be achieved due to the high scatter. All previous datasets analysed by this method have used fewer than 9 data points and are inherently smoothed. The results of this typical dynamic method using the same initial velocity and meteoroid spin as above gave α=27.434 and β=1.3221. When used in the following equation

$$m_f = exp\left(-\beta\,\frac{1-v_f^2}{1-\mu}\right) \qquad \text{(eqn. 6 [10])}$$

a final mass of 2.23 kg is achieved. An initial mass of 19.32 kg was also calculated (eqn. 12 [10]). Both this method and the proposed method give similar results to initial and final bright-flight masses published by [9] (22.0±1.3 kg and 1.1 kg respectively). The Q_4 least-squares minimisation method however requires ad-hoc prior smoothing of noisy data and does not produce explicit error estimates.

Conclusion: The two-step approach proposed here provides a rigorous method for determining the terminal bright-flight mass for use in the automation of the Australian Desert Fireball Network. The extended Kalman filter is applied to raw input data with high variance to estimate the state of a fireball at each time step and give optimal estimate of the terminal bright-flight position, mass and velocity with error estimates. This coupled with the dynamic optimisation for determining unknown input parameters makes it a good method of analysing fireball bright flight trajectories. Currently the approach is limited by the absence of a fragmentation model, and there is also work to be done in refining the parameterization of the dynamic model, but our preliminary results are encouraging. The goal is that future iterations of the model will constrain fragmentation.

Acknowledgements: This work was funded by the Australian Research Council as part of an Australian Laureate Fellowship grant.

References: [1] Öpik, E. (1933) *Acta et Comm. Universitatis Tartu, 26*, 2. [2] Ceplecha, Z. and Revelle, D.O. (2005) *MAPS 40*, 35–54. [3] Ceplecha, Z. (1961) *Bull. Astron. Inst. Czech. 12*, 21 [4] McCrosky, R., Posen, A., Schwartz, G. & Shao, C.-Y. (1971) *JGR 76*, 4090–4108. [5] Stulov, V., Mirskii, V. and Vislyi, A. (1995) *Moscow: Science. Fizmatlit*. [6] Gritsevich, M. (2008) *SSR 42*, 372–390. [7] Gritsevich, M. *Doklady Phys. 53*, 588–594 (2008). [8] Wishner, R., Tabaczynski, J. and Athans, M. A (1969) *Automatica 5*, 487–496. [9] Spurný, P. et al. (2012) *MAPS 47*, 163–185. [10] Gritsevich, M. (2008) *Doklady Phys. 53*, 97–102.

CONFERENCE ABSTRACT B – CHARACTERISING FIREBALLS FOR MASS DETERMINATION: STEPS TOWARD AUTOMATING THE AUSTRALIAN DESERT FIREBALL NETWORK

Sansom, E. K., Bland, P.A , Paxman, J. and Towner, M. C.
Presented at the 31st URSI General Assembly and Scientific Symposium, August 2014, Beijing, China.

Abstract published in proceedings of the General Assembly and Scientific Symposium (URSI GASS), 2014 XXXIth URSI. DOI: 10.1109/URSIGASS.2014.6929860.

Reason for inclusion – This work was presented as an oral presentation at an international conference and outlined the work in paper 1 as well as the Desert Fireball Network pipeline.

STATEMENT OF AUTHORSHIP

TITLE OF ABSTRACT: Characterising Fireballs for Mass Determination: Steps Toward Automating the Australian Desert Fireball Network

PUBLICATION STATUS: Published

AUTHOR CONTRIBUTIONS

By signing the Statement of Authorship, each author certifies that their stated contribution to the publication is accurate and that permission is granted for the publication to be included in the candidate's thesis.

Name of Principal Author: Eleanor K. Sansom

Contribution to the Abstract: Led all aspects of the research, drafted the manuscript and presented the research as an oral presentation at the 31st URSI General Assembly and Scientific Symposium in Beijing, China.

Overall Percentage: 88%

Signature: ***Date:*** 01 / 12 / 16

Name of Co-Author: Phillip A. Bland

Contribution to the Abstract: Assisted in revising and editing the manuscript.

Overall Percentage: 5%

Signature: ***Date:*** 4 / 12 / 16

Name of Co-Author: Jonathan Paxman

Contribution to the Abstract: Assisted in revising and editing the manuscript.

Overall Percentage: 5%

Signature: ***Date:*** 5/12/16

Name of Co-Author: Martin C. Towner

Contribution to the Abstract: Assisted in revising and editing the manuscript.

Overall Percentage: 2%

Signature: M Tow ***Date:*** 05/12/16

Characterising Fireballs for Mass Determination: Steps Toward Automating the Australian Desert Fireball Network

***E. K. Sansom*[1]*, P. A. Bland*[1]*, J. Paxman*[2]*, M. C. Towner*[1]**

[1]Department of Applied Geology, Curtin University, GPO Box U1987, Perth, WA 6845, Australia.
eleanor.sansom@postgraduate.curtin.edu.au; p.a.bland@curtin.edu.au; m. towner@curtin.edu.au

[2]Department of Mechanical Engineering, Curtin University, GPO Box U1987, Perth, WA 6845, Australia.
j.paxman@curtin.edu.au.

Abstract

Determining the mass of a meteoroid passing through the Earth's atmoshphere is essential to determining potential meteorite fall positions. This is only possible if the characteristics of these meteoroids, such as density and shape are in some way constrained. When a meteoroid falls through the atmosphere, it produces a bright fireball. Dedicated camera networks have been established to record these events with the objectives of calculating orbits and recovering meteorites. The Desert Fireball Network (DFN) is one of these programs and will eventually cover ~2 million km^2. Automated observatories take high-resolution optical images throughout the night with the aim of tracking and recovering meteorites. From these optical images, the position, mass and velocity of the meteoroid at the end of it's visible trajectory is required to predict the path to the ground. The method proposed here is a new aproach which aims to automate the process of mass determination for application to any trajectory dataset, be it optical or radio. Two stages are involved, beginning with a dynamic optimisation of unknown meteoroid characteristics followed by an extended Kalman filter. This second stage estimates meteoroid states (including position, velocity and mass) by applying a prediction and update approach to the raw data and making use of uncertainty models. This method has been applied to the Bunburra Rockhole dataset, and the terminal bright flight mass was determined to be 0.412 ±0.256 kg, which is close to the recovered mass of 338.9 g [1]. The optimal entry mass using this proposed method is 24.36 kg, which is consistent with other work based on the estabished photometric method and with cosmic ray analysis. The new method incorporates the scatter of the raw data as well as any potential fragmentation events and can form the basis for a fully automated method for characterising mass and velocity.

1. Introduction

Analysis of meteorites can lead to valuable insights into the formation of the proto-planetary disk within which their parent asteroids were created. Without a constraint on a meteorite's origin in the Solar System, interpreting its unique geological record can be extremely difficult. The recording of fireball phenomena can enable the reconstruction of orbits and has the potential to lead to the recovery of fresh meteorites. This objective has been the driver for a number of dedicated fireball camera network projects dating back to the late 1950s [2]. Such camera networks optically photograph fireballs with the aim of extracting orbital information and estimating potential fall locations. These camera networks have led to the recovery of 10 meteorites, including two by the Desert Fireball Network (DFN) in Australia during its trial phase [3][1]. Over the next few months, the DFN will establish over 50 new camera stations to expand its coverage to an area in excess of 2 million km^2. This will make it the largest fireball network in history, and consequently there is a need for automated systems of data analysis. Determining meteorite fall sites from networked observations relies on characterising meteoroids as they pass through the atmosphere. This process is complicated by a significant number of unknown variables. In addition, in the case of the DFN, very large data volumes will need to be reduced. The current work addresses both of these issues.

There have been two previous approaches to analysing optical image data for mass determination: the photometric method and the dynamic method. The photometric method uses the luminosity of the fireball as a proxy for ablated mass. Since this concept was established by Öpik in 1933 [4] , it has become recognised as the preferred method. This approach however gives unreliable meteoroid entry masses in many cases [5] and is based on ideas of hypersonic aerodynamics that are now out-of-date [5].

The dynamic method uses ballistic equations of flight through the atmosphere to calculate mass from deceleration. In the past this approach was limited by the accuracy of measurements that could be interpreted from photographic plates [2]. Difficulties with this method are also due to the unknown characteristics of the meteoroid such as density and shape that are required for the dynamic calculation. Recent work by [6] has enabled the application of an analytical solution by

978-1-4673-5225-3/14/$31.00

combining these unknown parameters into two dimensionless constants. This has been applied by Gritsevich [7][8] to the Canadian MORP network datasets. This enables a good model fit to the data but later requires assumptions of these same meteoroid characteristics in order to determine mass.

Given the limitations of these established techniques, a new method is presented here. It involves a multi-step approach and is based on the dynamic method; using the same equations. An initial dynamic optimisation stage determines the combination of meteoroid characteristics that will allow a fit to the data. This is then followed by an extended Kalman filter to incorporate the data into the model. The final goal will be to enable the automation of meteoroid mass determination for the DFN to enable the rapid recovery of meteorites.

2. Model

The dynamic equations used for ballistic entry through the atmosphere from [6] are:

$$m\frac{dV}{dt} = -\frac{1}{2}c_d\rho_a V^2 S\ , \tag{1}$$

$$H^*\frac{dm}{dt} = -\frac{1}{2}c_h\rho_a V^3 S, \tag{2}$$

where m is meteoroid mass, V is velocity, c_d the drag coefficient, c_h the heat coefficient, ρ_a atmospheric density, H^* is the enthalpy of sublimation and S the cross sectional area of the body which can also be written in terms of the initial shape parameter A_0 (3) or the rotation of the meteoroid, μ (4)[9]. S_0 and m_0 are the initial mass and cross-sectional area respectively and ρ_{m0} is the initial meteoroid density.

$$S = A\left(\frac{m}{\rho_m}\right)^{\frac{2}{3}}. \tag{3}$$

$$\frac{S}{S_0} = \left(\frac{m}{m_0}\right)^{\mu}. \tag{4}$$

Combining equation (3)-(4) with (1)-(2) and neglecting the effects of gravity, the dynamic equations become

$$\frac{dV}{dt} = -\frac{1}{2}\frac{c_d\rho_a A_0}{{\rho_{m_0}}^{2/3}} m_0^{\left(2/3-\mu\right)} V^2 m^{(\mu-1)}, \tag{5}$$

$$\frac{dm}{dt} = -\frac{1}{2}\frac{c_h\rho_a A_0}{H^*{\rho_{m_0}}^{2/3}} m_0^{\left(2/3-\mu\right)} V^3 m^{\mu}. \tag{6}$$

2.1 Dynamic Optimisation

A specialised shutter in the DFN camera lenses chops the path of an incoming fireball into roughly 0.05 second-long segments on the resultant long exposure image. After fireball recognition software has identified a fireball on more than one camera, triangulation of the two events gives a time, altitude, latitude and longitude for the start of each segment. This enables the calculation of distance from the start of the trajectory and velocity of the meteoroid. This raw velocity has a high uncertainty as the errors associated with determining distance propagate through.

A dynamic optimisation is performed using equations (5)-(6) to determine possible values for the unknown parameters A, μ, ρ_m and c_h/H^*, as well as the initial mass, m_0, and velocity, V_0. A least-squares cost function is used to compare models using different input parameter values with the raw velocity data and cost values can range from 0 to 1. The costs closest to 1 are the best model fits and are plotted for a visual comparison. Due to the large number of degrees of freedom, many combinations are possible. The lowest cost solutions are presented to the extended Kalman filter at the next stage of the mass determination method.

2.2 Extended Kalman Filter

An extended Kalman filter is a method of statistically optimising estimates of an instantaneous state of nonlinear dynamic systems [10]. An accompanying covariance matrix allows the uncertainties in the state estimations to be determined and propagated. The extended Kalman filter state variables for fireball analysis are distance along the fireball path, mass and velocity. The dynamic equations (4)-(5) at a time, t_k, in the fireball trajectory to 'predict' a future state at

t_{k+1} based on all previous data. An observation is made at t_{k+1} and an 'update' takes place using an optimal 'Kalman gain'. This improves the original estimate incorporating the uncertainties of both the observation and the dynamic model.

An extended Kalman filter is performed on the data using initial parameters defined by the dynamic optimisation. The initial mass error remains large but as the extended Kalman filter takes the raw data into consideration, the errors are updated throughout.

3. Results

Of the multiple DFN datasets which were analysed using this method, that of Bunburra Rockhole (BR) is the most reliable: a meteorite was recovered, which gives constraints on final mass [1]. Figure 1 shows the graphical output of the dynamic optimisation step. The fit of all models to the BR raw velocity data, with costs above 0.898, is near identical (Figure 1a). Multiple initial masses (at t=0 in Figure 1b) are able to fit the data closely due to the degrees of freedom in meteoroid characteristics, however the final masses consistently converge to a narrow range at the end of the fireball flight (Figure 1b). The smallest initial mass, m_0=16.19 *kg*, with ρ_m=1492 kg/m^3 and A=1.15, gives a final mass of 0.505 kg. For the largest initial mass, m_0=33.62, with ρ_m=3660 kg/m^3 and A=2.67, a final mass of 1.04 kg results. This gives a final mass range 535 g which results in a well constrained initial estimate of the terminal bright flight mass. Within this range of extremes, the models with the lowest cost favour initial masses of around 24 kg and are used to initialise a number of extended Kalman filters which incorporate uncertainty models to determine a more rigorous final mass estimate, and to quantify the errors.

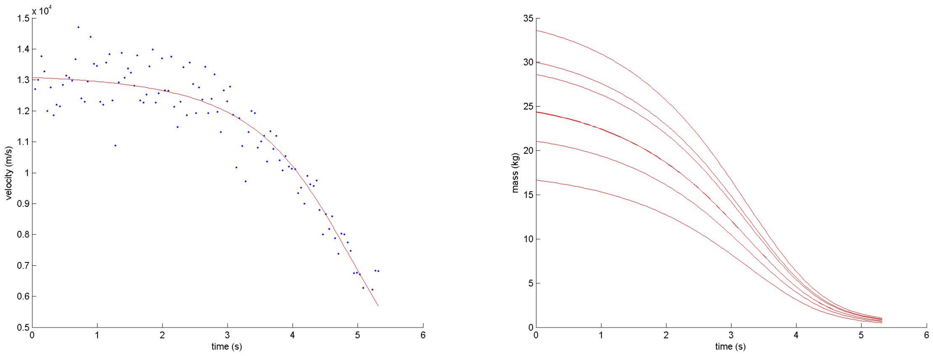

Figure 1- The visual outputs of the dynamic optimisation step. a) raw velocity data shown in blue- note the high scatter. multiple model fits to the raw data are shown by red lines. b) the change in mass throughout the trajectory for multiple initial starting masses.

The updating mass and velocity states obtained by the extended Kalman filter, using the Bunburra Rockhole dataset, show initially large errors which decrease throughout the descent. The final mass for an m_0 of 24.36 kg (using ρ_m=2075 kg/m^3 and A=1.64) is 0.412 kg and the covariance gives the error as ± 0.1 g. Using the minimum and maximum low cost initial masses described previously (16.19 kg and 33.62 kg), the extended Kalman filter calculates the terminal mass range as between 0.156 kg and 0.668 kg. This is a narrower range of 512 g compared to that obtained by the dynamic modelling exclusively and as this is based on the data it is the more robust final mass.

4. Discussion

The initial 3 seconds of the Bunburra Rockhole velocity data has a high scatter of around ±2000 m/s which is handled extremely well by the extended Kalman filter. The covariance incorporates both measurement uncertainty and scatter to give a comprehensive understanding of the errors associated with each state. Despite the variation in initial masses used, the final masses are very similar and their range constrains the final bright flight mass. The final mass of 0.412 ±0.256 kg is less than the 1.1 kg published by [1]. It is however closer to the total mass of meteorite collected 338.9 g [1]. The initial mass determined by these same authors using the typical photometric method is 22.0±1.3 kg. Cosmic ray exposure rates were also analysed for the Bunburra Rockhole meteorite, however the pre-entry radius was determined to be larger than a radius corresponding to a mass of 22 kg [11]. This supports the slightly higher entry mass of 24.36 kg favoured by this method.

Fragmentation is not explicitly taken into account in this method. When a fragmentation event occurs however, the main body mass changes and the resulting changes in dynamics are reflected in the data. The use of the extended Kalman filter allows for these variations in mass and the final mass reflects any such events.

5. Conclusion

The method proposed here gives a more detailed understanding of meteoroid characteristics as they pass through the atmosphere than previous approaches. Although applied to optical images, this same method could easily be applied to radio data of meteoroid entry with little to no alteration. The dynamic optimisation determines the optimum parameters for the meteoroid flight such as density and shape. The extended Kalman filter includes observation and dynamic uncertainty models, which are valuable in understanding the errors in the model states, and which can adapt to fragmentation events or other unexpected dynamic changes. The initial (24.36 kg) and final masses (0.412 ±0.256 kg) calculated from the Bunburra Rockhole dataset is consistent with the previously published values by [1] (22.0 ±1.3 kg and 1.1 kg respectively). This demonstrates that the approach is an acceptable way of calculating the mass of a meteoroid at the end of its bright flight trajectory. It is an automated method which will allow the DFN to calculate multiple fall positions with comprehensive error values to allow for efficient recovery searches. Work still needs to be done on integrating the variability of the heat coefficient as it does not truly remain constant throughout the trajectory as has been assumed so far in this method.

6. Acknowledgements

This work was funded by the Australian Research Council as part of the Australian Laureate Fellowship scheme.

7. References

1. P. Spurný, P. A. Bland, L. Shrbený, J. Borovička, Z. Ceplecha, A. Singelton, A. Bevan, D. Vaughan, M. C. Towner, T. P. McClafferty, R. Toumi, G. Deacon, Geoff, “The Bunburra Rockhole meteorite fall in SW Australia: fireball trajectory, luminosity, dynamics, orbit, and impact position from photographic and photoelectric records,” *Meteoritics & Planetary Science*, vol. 47, no. 2, pp. 163–185, 2012.

2. Z. Ceplecha, “Multiple fall of Pribram meteorites photographed. 1. Double-station photographs of the fireball and their relations to the found meteorites,” *Bulletin of the Astronomical Institutes of Czechoslovakia*, vol. 12, p. 21, 1961.

3. M. Towner P. A. Bland, P. Spurný, G. K. Benedix, K. Dyl, R. C. Greenwood, J. Gibson, I. A. Franchi, L. Shrbený, A. W. R. Bevan, et al., “Mason Gully: The second meteorite recovered by the Desert Fireball Network,” *Meteoritics and Planetary Science Supplement*, vol. 74, p. 5124, 2011.

4. E. J. Öpik, *Atomic collisions and radiation of meteors*. Astronomical Observatory of Harvard College, 1933.

5. I. Brykina and V. Stulov, “The reciprocal role of convective and radiant heat exchange in the meteor-parameter range,” *Doklady Physics*, vol. 57, no. 4, 2012, pp. 164–165.

6. V. Stulov, V. Mirskii, and A. Vislyi. *Aerodynamics of Bolides*. Moscow, Fizmatlit, 1995.

7. M. Gritsevich, “The Pribram, Lost City, Innisfree, and Neuschwanstein falls: An analysis of the atmospheric trajectories,” *Solar System Research*, vol. 42, no. 5, pp. 372–390, 2008.

8. M. Gritsevich, “Estimating the terminal mass of large meteoroids,” *Doklady Physics*, vol. 53, no. 11, 2008, pp. 588–594.

9. V. A. Bronshten. *Physics of meteoric phenomena*. Dordrecht, D. Reidel Publishing, 1983, 372 p. *Translation of: Fizika meteornykh iavlenii*, Moscow, Izdatel’stvo Nauka, 1981.

10. M. Grewal and A. P. Andrews. *Kalman filtering: theory and practice*, New Jersey: Prentice-Hall, 1993.

11. K. C. Welten, M. M. M. Meier, M. W. Caffee, M. Laubenstein, K. Nishizumi, R. Wieler, P. A. Bland, M. C. Towner, P. Spurný, “Cosmic-ray exposure age and preatmospheric size of the Bunburra Rockhole achondrite,” *Meteoritics & Planetary Science*, vol. 47, no. 2, pp. 186–196, 2012.

CONFERENCE ABSTRACT C – INITIAL RESULTS FROM THE EXPANDED DESERT FIREBALL NETWORK

Sansom, E. K. , Bland, P. A., Towner, M. C., Paxman, J. P., Howie, R. M., Cupak, M., Galloway, M. J., Benedix, G. K.

Presented at the 78th Annual Meeting of the Meteoritical Society, July 2015, San Francisco, CA.

Abstract published in LPI contributions, p. 5172.

Reason for inclusion – This work was presented as an oral presentation at an international conference and outlined the first results calculated by the Desert Fireball Network pipeline.

STATEMENT OF AUTHORSHIP

TITLE OF ABSTRACT: Initial Results from the Expanded Desert Fireball Network

PUBLICATION STATUS: Published

AUTHOR CONTRIBUTIONS

By signing the Statement of Authorship, each author certifies that their stated contribution to the publication is accurate and that permission is granted for the publication to be included in the candidate's thesis.

Name of Principal Author: Eleanor K. Sansom

Contribution to the Abstract: Determined masses for 5 fireball events presented, drafted the manuscript and presented the research as an oral presentation at the 78th Annual Meeting of the Meteoritical Society in California, USA.

Overall Percentage: 42%

Signature: ***Date:*** 01 / 12 / 16

Name of Co-Author: Phillip A. Bland

Contribution to the Abstract: Assisted in revising and editing the manuscript.

Overall Percentage: 15%

Signature: ***Date:*** 4 / 12 / 16

Name of Co-Author: Martin C. Towner

Contribution to the Abstract: Calculated strewn fields from dark flight models for events presented and assisted in revising manuscript.

Overall Percentage: 15%

Signature: M T *Date:* 05/12/16

Name of Co-Author: Jonathan Paxman

Contribution to the Abstract: Assisted in revising the manuscript.

Overall Percentage: 2%

Signature: *Date:* 5/12/16

Name of Co-Author: Robert M. Howie

Contribution to the Abstract: Assisted in revising the manuscript.

Overall Percentage: 10%

Signature: Robert Howie *Date:* 5 / 12 / 16

Name of Co-Author: Martin Cupak

Contribution to the Abstract: Calculated wind models for dark flight modelling and assisted in revising the manuscript.

Overall Percentage: 10%

Signature: *Date:* 6/12/2016

Name of Co-Author: Monty J. Galloway

Contribution to the Abstract: Determined fireball position in still images.

Overall Percentage: 3%
Monty Galloway was not contactable at the time of thesis submission and I, Phil Bland, as co-author and supervisor to Eleanor, endorse his level of contribution.

Signature: Phil Bland ***Date:*** 4 / 12 / 16

Name of Co-Author: Gretchen K. Benedix

Contribution to the Abstract: Assisted in revising the manuscript.

Overall Percentage: 3%

Signature: Gretchen Benedix ***Date:*** 1/12/16

78th Annual Meeting of the Meteoritical Society (2015) 5172.pdf

INITIAL RESULTS FROM THE EXPANDED DESERT FIREBALL NETWORK

E. K. Sansom[1], P. A. Bland[1], M. C. Towner[1], J. P. Paxman[2], R. M. Howie[2], M. Cupak[1] , M. J. Galloway[3], G. K. Benedix[1] [1]Dept. Applied Geol., Curtin Univ., GPO Box U1987, Perth, WA 6845, Australia. E-mail: eleanor.sansom@curtin.edu.au. [2]Dept. Mech. Eng., Curtin Univ., Perth, WA 6845, Australia. [3]School Comp. Math., Univ. Western Australia, Perth, WA 6009, Australia.

Introduction: Meteorite falls that are observed with enough accuracy from multiple locations can give orbits and constrain origins of meteorites from within the Solar System. Dedicated camera networks have been established previously around the world for fireball observation (e.g. [1]), each with limited success based on their locations in temperate zones. The Desert Fireball Network (DFN) is well suited to meteorite recovery and the only network in the Southern Hemisphere. In its initial stage of 4 film cameras, two meteorites with orbits were recovered [2][3]. Since 2012, the DFN has been establishing a digital network and, over a short period from September to November 2014, the number of autonomous observatories more than doubled from 15 to 32. This amounts to a current observ-ation area of 1.7 million km^2: the largest network ever built.

Automated Data Reduction: Data is acquired at a rate of ~57.6 TB / month, requiring an automated pipeline for data reduction. With a significant amount of hardware deployed, the autonomous fireball observatories were left to acquire data while this pipeline was established.

Event detection at an observatory is cross-checked for multi station confirmation. Points are picked along the fireballs [4], calibrated to altitude and azimuth and their exact times identified [5] before triangulation for orbit and positions along the trajectory. Velocities are then used to estimate masses [6].

Recent Events: This year 91 double-station fireballs over 2 secs in length have been automatically detected and triangulated. Of these, 17 were over South Australia (SA), 34 across the Nullarbor Plain (NP) and 43 from the Western Australian Wheatbelt (WA). At this stage, we have selected five interesting candidates to reduce and test our pipeline software. DN150417 captured over NP was 10.3 secs long, making it the longest fireball in our dataset. DN141125 (SA) was 9.3 secs and was captured by eight DFN observatories. This is unprecedented. The trajectory is also visibly seen to become two separate trails in one image, confirming fragmentation. DN141215 (WA) was captured by four observatories just after the peak of the Geminid meteor shower and has a consistent radiant. DN150331 (SA) has an incredibly bright trail and is just over 3 secs long but with a visible trajectory continuing past the final bright flare. And finally, DN141129 (WA) was 5.9 secs and captured by one of our school outreach observatories.

We anticipate that a subset of these fireballs - and others yet to be analysed - will have delivered a meteorite to the ground. Search sites and strategies will be discussed in the presentation.

References: [1] Halliday I. et al. 1996. *Meteoritics & Planetary Science* 31:185 [2] Bland P.A. et al. 2009. *Science* 325 :1525-1527. [3] Towner M.C. et al. 2011. Abstract #5124. 74th Meteoritical Society Meeting. [4] Galloway et al. 2015. *(this Conference).* [5] Howie et al. 2015 *(this Conference).* [6] Sansom et al 2015. *Meteoritics & Planetary Science. (accepted).*

CONFERENCE ABSTRACT D — EXPLORING ADVANCED ESTIMATORS FROM GUIDANCE, NAVIGATION AND CONTROL IN FIREBALL MODELLING

Sansom, E. K., Bland, P. A., Rutten, M. G.
Presented at the 47th Lunar Planetary Science Conference, March 2016, Woodlands, TX.

Abstract published in proceedings of the Lunar and Planetary Science Conference p.1892

Reason for inclusion — This work was presented as an oral presentation at an international conference and outlined the work in paper 2 and paper 3.

STATEMENT OF AUTHORSHIP

TITLE OF ABSTRACT: Exploring Advanced Estimators from Guidance, Navigation and Control in Fireball Modelling

PUBLICATION STATUS: Published

AUTHOR CONTRIBUTIONS

By signing the Statement of Authorship, each author certifies that their stated contribution to the publication is accurate and that permission is granted for the publication to be included in the candidate's thesis.

Name of Principal Author: Eleanor K. Sansom

Contribution to the Abstract: Led all aspects of the research, drafted the manuscript and presented the research as an oral presentation at the 47th Lunar Planetary Science ConferenceinTexas, USA.

Overall Percentage: 85%

Signature: ***Date:*** 01 / 12 / 16

Name of Co-Author: Phillip A. Bland

Contribution to the Abstract: Assisted in revising the manuscript.

Overall Percentage: 5%

Signature: Philip Bland ***Date:*** 4 / 12 / 16

Name of Co-Author: Mark G. Rutten

Contribution to the Abstract: Assisted in revising and editing the manuscript.

Overall Percentage: 10%

Signature: ***Date:*** 5 / 12 / 16

47th Lunar and Planetary Science Conference (2016) **1892.pdf**

EXPLORING ADVANCED ESTIMATORS FROM GUIDANCE, NAVIGATION AND CONTROL IN FIREBALL MODELLING.

E. K. Sansom[1], P. A. Bland[2] and M. G. Rutten[3], [1]Department of Applied Geology, Curtin University, GPO Box U1987, Perth, WA 6845, Australia, lpsc@ellie.rocks, [2]Department of Applied Geology, Curtin University (p.a.bland@curtin.edu.au), [3]DST Group Edinburgh, PO Box 1500, Edinburgh SA 5111.

Introduction: Observing bright meteor phenomena from multiple dedicated fireball observatories can lead to the discovery of a meteorite with a calculated orbit. The Desert Fireball Network (DFN) in Australia has 32 autonomous observatories across outback Australia, covering an area of 2.6 million km^2. In order to handle this 60 Tb/month dataset, a digital pipeline is used to reduce the data. Software that has been developed for this pipeline includes event detection, calibration of coordinates, triangulation, mass determination, orbital calculations, wind modeling and the prediction of a fall line for potential surviving masses.

Determining the mass of the meteoroid at the end of the bright flight trajectory is key to finding any potential meteorites. As a meteoroid passes through the atmosphere it loses mass by both ablation and fragmentation. Calculating the changing mass has typically been based on photometric and dynamic modelling [1] which are strongly dependent on an accurate light curve and do not provide a rigorous analysis of the inevitable errors introduced by uncertainties in the observations and the modelling process. No dynamical method alone is currently able to fully characterise a meteoroid during its trajectory. Sansom et al. [2] have previously applied the dynamical equations of meteoroid flight in a method used in guidance, navigation and control (GN&C)- an Extended Kalman Filter (EKF). This was used to estimate the state (position, mass and velocity) of a meteoroid during its bright flight as well as to ascertain a comprehensive understanding of the errors involved. This algorithm however requires the dynamical equations to be linearised and does not specifically include fragmentation events.

More advanced estimators used in the field of GN&C include the Unscented Kalman Filter (UKF), Interacting Multiple Model (IMM) and Sequential Importance Sampling Particle Filter (SIS PF). These approaches are applied here to the trajectory dataset for Bunburra Rockhole [3].

Dynamical equations: The hypersonic aerodynamic equations that are used to model a meteoroid path through the atmosphere are (after [1]):

$$\frac{dv}{dt} = -\frac{1}{2}\mathrm{K}\rho_a v^2 m^{(\mu-1)} + g\sin\gamma_e$$

$$\frac{dm}{dt} = -\frac{1}{2}\sigma K\rho_a v^3 m^{\mu}$$

Where ρ_a is the atmospheric density, v and m the velocity and mass of the meteoroid respectively, g the local acceleration of gravity, γ_e the flight angle from vertical, the ablation parameter σ and the shape density coefficient K. These equations are the base models for all the estimators used here. The position of the meteoroid is observed in time and the velocity inherently calculated. The mass is linked to the velocity through these equations. The constants σ and K however are unknown. These equations are also not a perfect representation of the trajectory; however, this is an advantage of using filters as imperfections in the model are accountable in the process noise.

Unscented Kalman Filter: The UKF is an estimator that allows for a more rigorous approach to handling non-linear equations [4]. Rather than estimating the transformation of the mean and covariances at each time step like the EKF, a UKF represents a Gaussian probability distribution by a set of points. These points are then individually propagated according to the dynamic equations and the mean and covariances are recalculated from these.

As the constants σ and K are unknown, in order to use the UKF, as with the EKF, we must precede this estimator with the dynamical optimisation step described by [2]. For the purposes here, we will use the same entry values as given by these authors for the Bunburra Rockhole meteor. The fit of velocities predicted by the UKF to those calculated from observations may be seen in Figure 1. A comparison between the final covariances estimated using a UKF to those calculated by [2] using an EKF can be seen in Table 1.

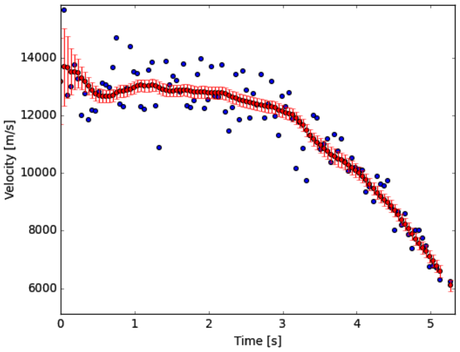

Fig. 1. Velocities calculated from observations (blue) show variable scatter. Velocities estimated by the UKF (red), with covariance as errors, show a good fit.

Interacting Multiple Model: To incorporate instantaneous massive mass loss due to fragmentation, two UKFs may be run simultaneously [5] with different process noise matrices:

1) model parameters with typical error ranges for ablation,
2) model parameters with large errors to include massive fragmentation events.

By using an Interacting Multiple Model (IMM) to weight the likelihood of each model according to the observations, fragmentation events may be handled. This significantly increases the ability to estimate states of the meteoroid proximal to the observations. Figure 2 shows the model 1 is most likely and mass loss is dominated by ablation apart from a brief period at 4.4 seconds where there is most likely a fragmentation event. This can be seen as a spike in the light curve at 34 km altitude on Figure 10 in [3].

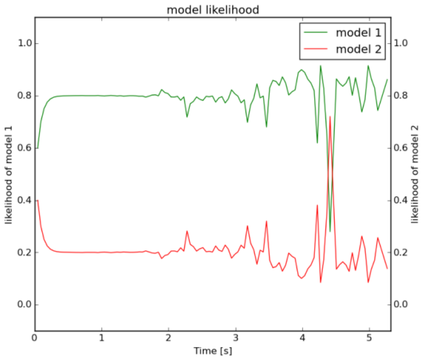

Fig. 2. Model 1 (green) has a low mass covariance and mass loss is dominated by ablation. Model 2 (red) has a high mass covariance and likely indicates fragmentation events when likelihood increases.

Table 1. Comparison of covariance values determined by different estimators for final states.

	Position covariance	Mass covariance	Velocity covariance
EKF	62 m	1.63 kg	241 m/s
UKF	58 m	1.04 kg	203 m/s
UKF IMM	8 m	0.33 kg	61 m/s

SIS Particle Filter: Particle filters apply a Monte-Carlo approach to the filtering problem [6]. This method not only is able to estimate the changing position, mass and velocity of the incoming meteoroid, but also the unknown constants of its flight (σ and K). It is also inherently able to handle fragmentation events, although not explicitly identify their location during the trajectory.

A set of 10,000 particles are initiated with a range of starting parameters that satisfy typical meteoroid characteristics for density, shape, ablation etc. and starting masses ranging from 100g to 5,000 kg. After the prediction of state at t_{k+1} is made for each particle, the resulting state is compared to the observations at that time and assigned a weighting. A new generation of particles is then sampled from this pool based on the weightings. The resulting values of the state (position, mass, velocity, σ and K) are accompanied by an uncertainty matrix.

Discussion and Conclusions: Nonlinear tracking methods may be applied to fireball trajectory modelling to allow a comprehensive understanding of the errors associated with the dynamic equations of this phenomenon. Both Kalman Filters require a single pre-determined set of starting parameters to estimate the states of a meteoroid during its trajectory. The SIS PF does not require a preliminary step to determine starting parameters and takes a Monte Carlo approach to determine the final states based on a broad input range. This approach also means that fragmentation is also accounted for to a certain extent within the covariance ranges.

A powerful tool comes by combining these methods. The use of either Kalman Filter within an IMM allows fragmentation events to be analysed and their timing identified (Fig. 2). We may then run a SIS PF where noise covariances are set to increase at these times. The final values determined by the SIS PF for σ in particular are interesting when this is done as [1] and [3] state that only the apparent value of σ may be determined when fragmentation is not considered. The apparent value determined by [3] for the Bunburra Rockhole meteoroid was an order of magnitude higher than the intrinsic value also calculated by these authors when incorporating brightness (using the MFM method). The value determined by the SIS PF adapted for fragmentation gives the same as intrinsic values in [3]. This indicates that fragmentation is taken into account in the final state estimates. Without brightness data, it has previously been difficult to incorporate fragmentation and determine intrinsic values of σ. Fragmentation events therefore may be incorporated into models without the use of brightness data with a great deal of success.

References: [1] Ceplecha Z. and ReVelle D. O. (2005) *MAPS, 40,* 35-54. [2] Sansom E. K. et al. (2015) *MAPS, 50,* 1423-1435. [3] Spurný P. et al. (2012) *MAPS, 47,* 163-185. [4] Julier S., Uhlmann J. (2004) *Proc. IEEE, 92,* 401-422 [5] Mazor E. et al. (1998) *IEE T Aero Elec Sys, 34,* 103-123 [6] Arulampalam M.S. et al. (2002) *IEEE T Signal Proces., 50,* 174-188.

CONFERENCE ABSTRACT E — FATE OF METEOROID IMPACTS ON MARS DETECTABLE BY THE INSIGHT MISSION

Miljković, K.; Sansom, E. K.; Daubar, I. J.; Karakostas, F.; Lognonné, P.,
Presented at the 47th Lunar Planetary Science Conference, March 2016, Woodlands, TX.

Abstract published in proceedings of the Lunar and Planetary Science Conference p. 1768

Reason for inclusion — This work was presented as a poster presentation at an international conference and was work done as part of a collaboration. Methods described in paper 1 were used to determine effect of ablation on meteoroids entering the Martian atmosphere.

STATEMENT OF AUTHORSHIP

TITLE OF ABSTRACT: Fate of Meteoroid Impacts on Mars Detectable by the InSight Mission

PUBLICATION STATUS: Published

AUTHOR CONTRIBUTIONS

I, Eleanor K. Sansom, as a co-author, contributed the following data to the abstract entitled *"Fate of Meteoroid Impacts on Mars Detectable by the InSight Mission"*, totalling 35% of the total work.

Signature: ***Date:*** 01 / 12 / 16

Meteoroid flight through the Martian atmosphere follows the same principal equations for aerodynamic flight:

$$\frac{dv}{dt} = -\frac{1}{2} c_d S \rho_a v^2 m^{(\mu-1)} + g \sin\gamma \tag{B.1a}$$

$$\frac{dm}{dt} = -\frac{1}{2} \frac{c_h S}{H*} \rho_a v^3 m^{\mu} \tag{B.1b}$$

where v is the velocity along the path of the meteoroid trajectory, with time t, mass m, flight angle from local horizontal γ, the local acceleration of gravity g, spin factor μ, the cross sectional area normal to flight S, the enthalpy of sublimation H^*, and c_d and c_h are the drag and heat coefficients respectively.

The substitution of the relationship

$$\frac{dz}{dt} = -v sin\gamma, \tag{B.2}$$

along with the exponential atmosphere approximation

$$\rho_a(z) = h_0 e^{-z/H} \tag{B.3}$$

and spherical assumptions, gives the differential equations in (B.1) with respect to height, z:

$$\frac{dv}{dz} = -\frac{3}{8}\frac{c_d h_0 e^{-z/H}}{\rho_m sin\gamma}\frac{v}{r} - \frac{g}{v} \tag{B.4a}$$

$$\frac{dr}{dt} = -\frac{1}{8}\frac{c_h h_0 e^{-z/H}}{H^* \rho_m sin\gamma}v^2 \tag{B.4b}$$

where $h_0 = 0.02\,\mathrm{kg\,m^{-3}}$ is the surface atmospheric density on Mars and $H = 11.1\,\mathrm{km}$ is the Mars scale height (Collins et al., 2005). ρ_m is the meteoroid density with spherical radius r.

For my models, I used a drag value of 1.3, a $\frac{c_h}{H^*}$ value of $0.025\,\mathrm{s^2\,km^{-2}}$ and a range of radii, entry angles and densities to determine relative effects of ablation and drag. Cometary meteoroids were modelled with a density of $1000\,\mathrm{kg\,m^{-3}}$, carbonaceous meteoroids with a density of $2200\,\mathrm{kg\,m^{-3}}$, stony meteoroids with a density of $3500\,\mathrm{kg\,m^{-3}}$ and iron meteoroids with a density of $7900\,\mathrm{kg\,m^{-3}}$. For a 45° entry angle, the breakup altitude (z^*) when both drag and ablation are considered for a cometary and carbonaceous meteoroid body are shown in Figure B.1. The difference in breakup altitudes between this model and one that neglects ablation (drag only; Figure B.2) is shown in Figure B.3 and highlights the contribution of the ablation effect. This analysis also contributed to validating results obtained independently by the first author, Katarina Miljković.

I, as first author, endorse that the level of contribution indicated above is accurate.

Signature: Miljković K. ***Date:*** 02/12/2016

REFERENCES

Collins, G. S., Melosh, H. J., and Marcus, R. A., 2005. Earth impact effects program: A web-based computer program for calculating the regional environmental consequences of a meteoroid impact on earth. *Meteoritics & Planetary science*, 40(6):817–840.

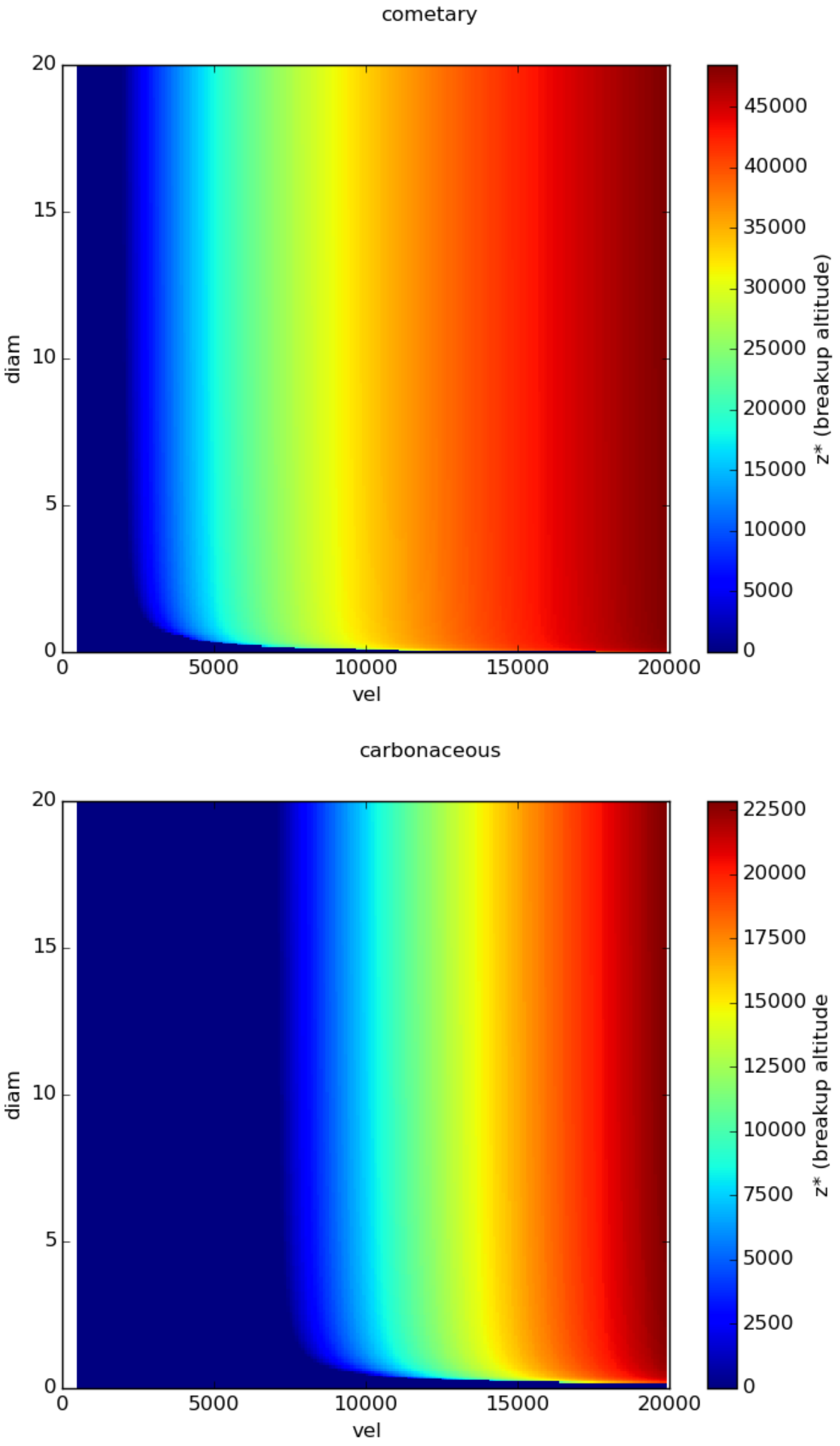

FIGURE B.1: Breakup altitudes for (a) cometary and (b) carbonaceous meteoroid bodies entering at $\gamma = 45^\circ$ and modelled using both drag and ablation effects.

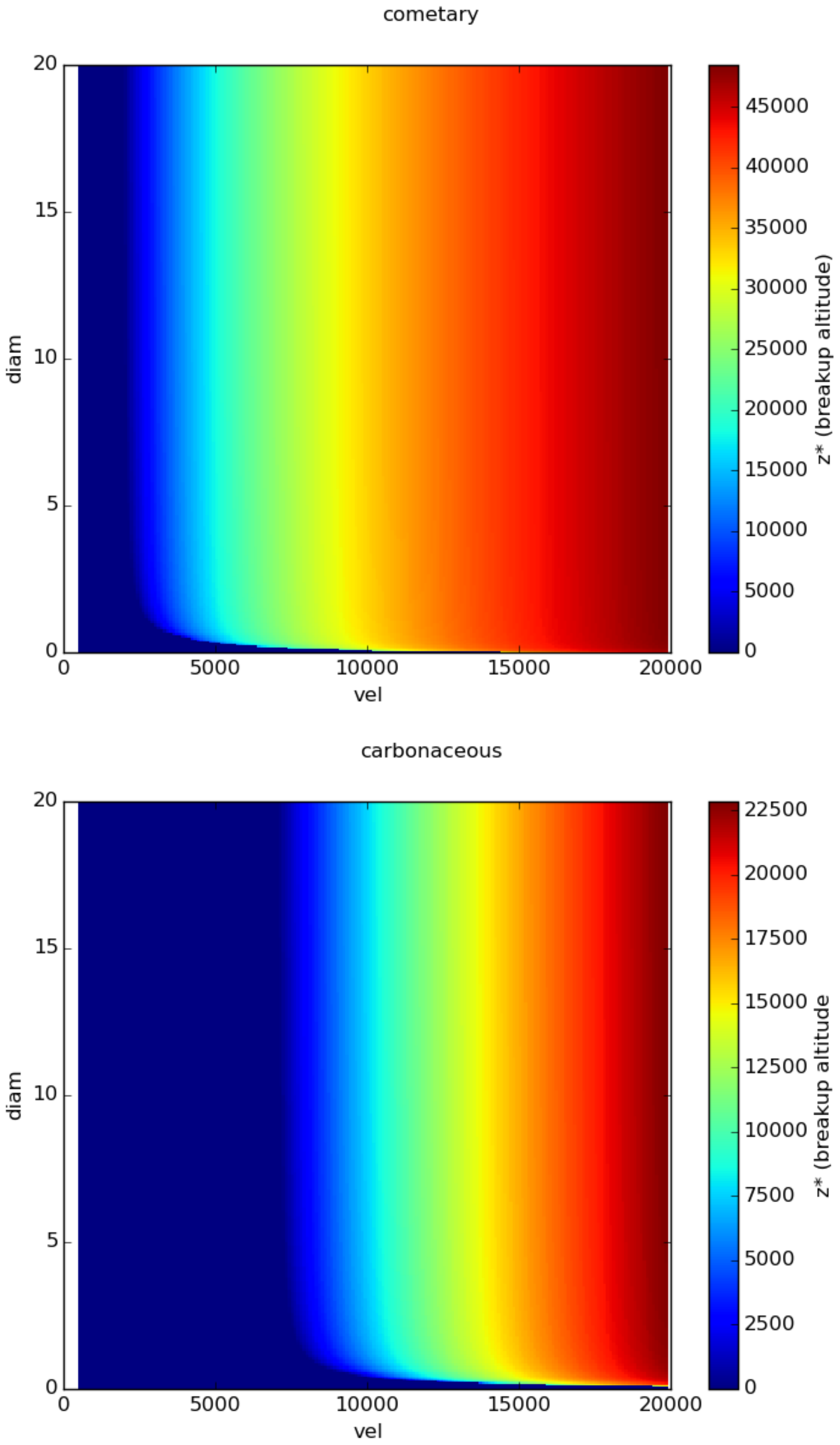

FIGURE B.2: Breakup altitudes for (a) cometary and (b) carbonaceous meteoroid bodies entering at $\gamma = 45^{\circ}$ and modelled only drag effects.

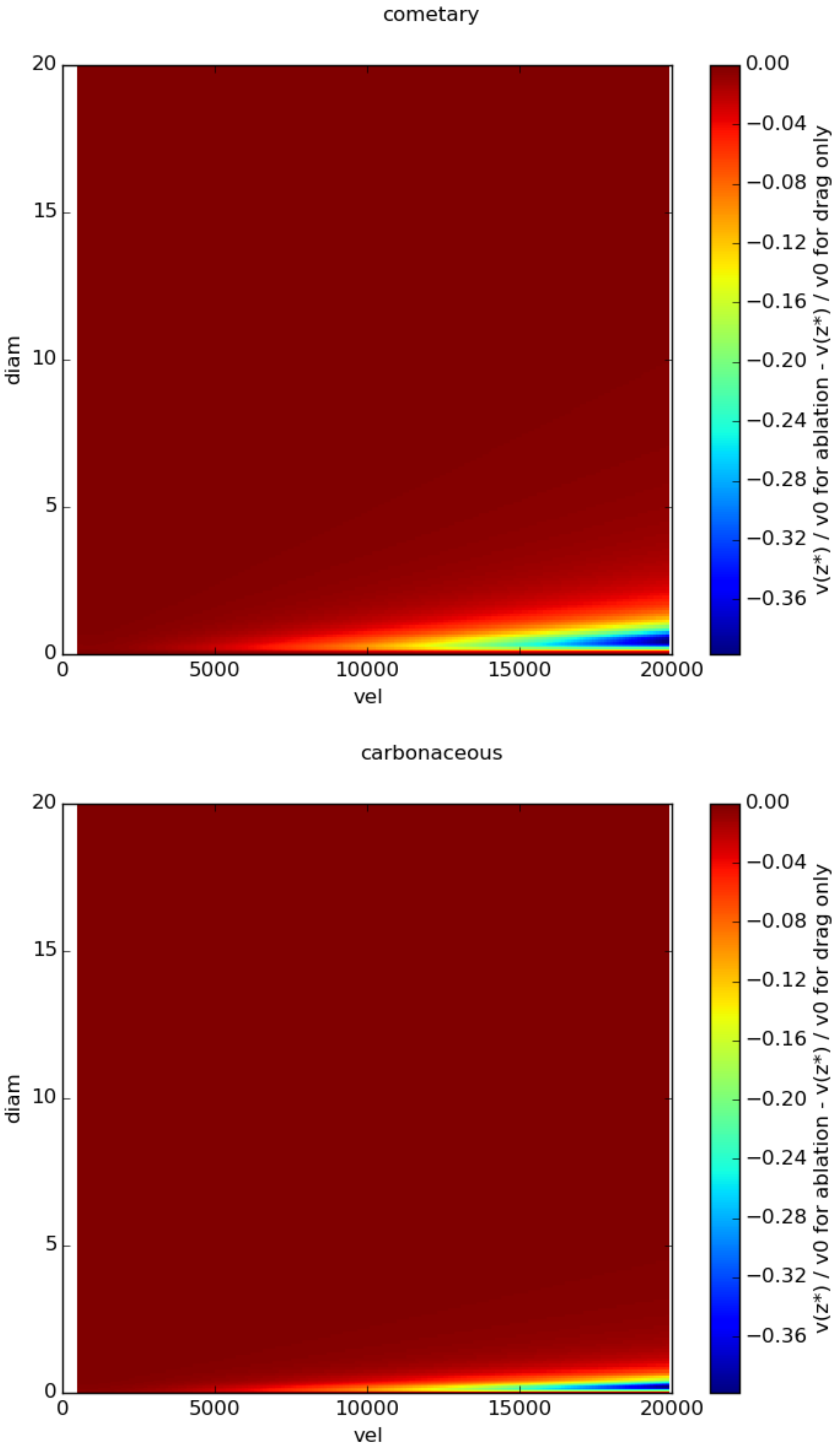

FIGURE B.3: Difference in breakup altitudes from Figures B.1 and B.2 for (a) cometary and (b) carbonaceous meteoroid bodies entering at $\gamma = 45^\circ$, highlighting the relative contribution of ablation effects.

47th Lunar and Planetary Science Conference (2016) 1768.pdf

FATE OF METEOROID IMPACTS ON MARS DETECTABLE BY THE INSIGHT MISSION.

K. Miljković[1], E. K. Sansom[1], I. J. Daubar[2], F. Karakostas[3], P. Lognonné[3]. [1]Dept. of Applied Geology, Curtin University, Australia (Katarina.Miljkovic@curtin.edu.au), [2]Jet Propulsion Laboratory, California Institute of Technology, Pasadena CA 91109, [3]Institut de Physique du Globe de Paris, France.

Introduction: This work investigates the impact conditions required for Martian meteoroids to be capable of making seismic signatures recordable by the SEIS (Seismic Experiment for Interior Structure) instrument during the lifetime of the InSight mission on Mars. Considering that lifetime of a space mission is short on a geologic timescale, only small, more frequent meteoroids are expected to impact Mars during this period [1,2].

Depending on the fate meteoroids experience while passing through the Martian atmosphere, they can be grouped into three classes: a) Meteoroids that survive the entire trajectory through the atmosphere and make a single impact in the ground (no breakup); b) Meteoroids that burst and fragment in the atmosphere, but those fragments predominantly burn up in the atmosphere (airburst); c) Meteoroids that burst and fragment in the atmosphere, but the fragments do not completely burn up in the atmosphere; rather they make an impact in the ground in the form of a cluster of multiple craters.

Break-up altitudes: Basic description of atmospheric entry [3] includes an atmospheric drag (we use C_d=1.3), where the dynamic break-up at altitude z is approximated by comparing the meteoroid crushing strength and stagnation pressure: $Y=\rho(z)V^2(z)$, where Y is the impactor crushing strength, ρ and V are the atmospheric density and impactor velocity at z. To calculate the break-up altitudes, we used a modified model from [3] applied to the current Martian atmosphere. Martian atmosphere was assumed to have an exponentially changing density ($\rho(z)=\rho_0 e^{-z/H}$, where H=11.1 km is the scale height and ρ_0=0.02 kg/m^3 surface atmospheric density).

In this simplified model, the threshold for atmospheric break-up depends largely on impactor properties (density, crushing strength and speed). The break-up threshold for stronger impactors is at higher speeds and, in this model, cometary impactors (Y=0.1 MPa, ρ=1000 kg/m^3) break at speeds larger than 2.5 km/s and carbonaceous impactors (Y=1 MPa, ρ=2200 kg/m^3) at speeds larger than 7.5 km/s. For impactors smaller than 20 m, moving at speeds lower than 20 km/s, the break-up is not strongly dependent on the impactor size (Figures 1 and 2). We also investigated stony (Y=10 MPa, ρ=3500 kg/m^3) and iron meteoroids (Y =100 MPa, ρ=7900 kg/m^3 [4]), and in this model, such impactors could only form single impacts on Mars without breaking up in the atmosphere.

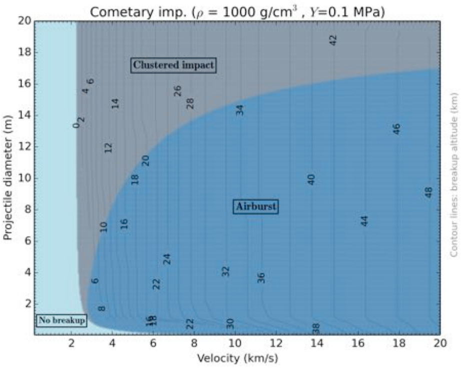

Figure 1. Contour lines show the break-up altitudes for cometary impactors. Dark blue regions denote parameter space in which impactors burn up in the atmosphere (labeled "Airburst"); Grey regions denote the parameter space in which impactors fragment in the atmosphere but survive to form a cluster of craters on the surface of Mars.

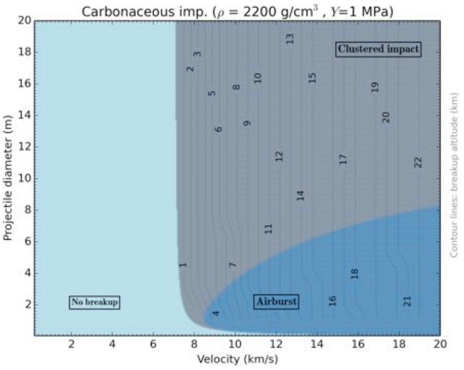

Figure 2. Similarly to Figure 1, but showing fate for carbonaceous impactors.

Velocity and projectile size marked on axes in Figures 1 and 2 are given at atmospheric entry. For impactors that are ~1-20 m in diameter, moving at speeds lower than 20 km/s, the impactor size and speed do not change markedly by the time meteoroids reach their break-up altitudes. In this parameter space and Martian atmosphere, this model estimates less than 10% diameter loss due to ablation for impactors larger than 5 m in diameter. However, for smaller impactors, with a decrease in impactor size and increase in entry speeds above 6 km/s, the ablation becomes increasingly important. There is no change in velocity due to drag for carbonaceous impactors with entry diameter larger than 1 m or larger than 0.5 m for cometary impactors, which is in agreement with [5], where detailed effects of ablation and drag are investigated for smaller and faster impactors.

Clustered craters: After break-up, the dispersion of fragments could be simplified by a so-called pancake model, in which fragments disperse under the differential pressure between front and back surfaces [4,6]. We adopted the analytical approximation from [3].

In this model, the threshold for a clustered crater depends largely on the impactor size, density and strength, and to some extent on impactor speed range. Figure 3 shows a ground spread of fragmented impactors of up to 120 m for cometary impactors, assuming a vertical impact. The dispersion area for oblique impact angles (α) should scale as $L(\alpha) = L(90^{o})/\sin(\alpha)$ in a simplified approximation.

The HiRISE observations of clustered craters on Mars show that the dispersion in clustered craters varies greatly, from a few tens to a few hundreds of meters [1], which loosely corresponds to our results shown in Figure 3.

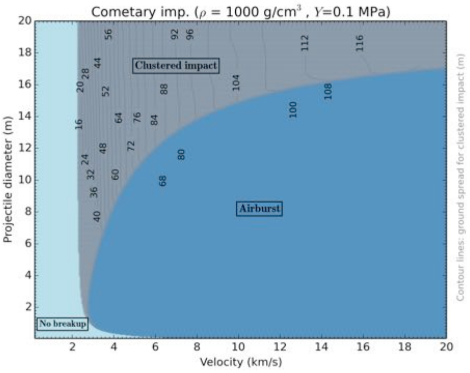

Figure 3. Contour lines show dispersion of fragmented impactors assuming a pancake model for cometary (low strength, low density) impactors.

Strength-dominated impact-scaling: During the two years of the InSight primary mission, the largest impacts on Mars expected during that time will likely be smaller than approximately 50 m in effective diameter [2]. Also, HiRISE data analyses of single and clustered crater diameters indicated that those craters have small effective diameters (for clusters, this is the reconstructed diameter, summed as if the projectile had not broken up in the atmosphere), ranging from less than a meter to approximately up to 40 m, from over a ~decade of observations [1]. The final crater size for such small simple craters largely depend on the target properties (namely, target strength).

We applied the crater-scaling laws for the strength-dominated regime [7] for four different target strengths and densities (simulants for lunar soil, dry sand, soft and hard rock [5]), and considering four types of impactors (cometary, carbonaceous, stony and iron [4]) that also differ in strength and density. We determined that an impactor should be of the order of a meter up to a maximum of a few meters to form craters smaller than 50 m.

Impact-scaling laws estimate the size of an impactor as it reaches the ground, not its size at atmospheric entry. Considering that HiRISE observations include many clustered craters with a small effective diameter, it is possible that impactors have extremely low strengths. However, another possibility is that the modeled crushing strength may not be the most relevant parameter that determines the break-up process, and that the fragmentation process is complex. In the case of the Chelyabinsk impactor, the tensile strength of the incoming impactor was estimated to ~1 MPa, with stronger stony components estimated to ~15 MPa that survived initial atmospheric entry, but later clustered over the ground suggesting that the entry impactor was composed of different components and likely pre-existing fractures [8].

Conclusion: This work separates meteoroid bombardment on Mars into three classes that would greatly differ in terms of their seismic signature in the Martian atmosphere and ground. Further investigations will feed into modeling of different seismic signatures associated with these impact classes [9,10].

References: [1] Daubar, I.J. et al. (2013) *Icarus* 225, 506-516. [2] Daubar, I.J. et al. (2015) 46^{th} *LPSC*, Abstract #2468. [3] Collins, G.S. et al. (2005) *MAPS* 40, 817-840. [4] Chyba C. F. et al. (1993) *Nature* 361, 40–44. [5] Williams, J.-P. et al. (2014) *Icarus* 235, 23-36. [6] Melosh H.J. (1981) In *Multi-ring basins*, New York: Pergamon Press. pp. 29–35. [7] Holsapple, K.A. and Housen, K.R. (2007) *Icarus* 191, 586-597. [8] Borovička, J. et al. (2013) *Nature*, 503, 235–237. [9] Lognonné P., and Johnson C.L. (2015) *Planetary Treatise on Geophysics*, 2^{nd} ed. 10, 65–120. [10] Lognonné et al. (2015) J. Acoust. Soc. Am, submitted.

CONFERENCE ABSTRACT F – EXPLORING UNCERTAINTIES IN FIREBALL MODELLING USING ESTIMATORS

Sansom, E. K. , Bland, P. A., Rutten, M. G., Paxman, J., Towner, M. C.,
Presented at Meteoroids2016, June 2016, Noordwijk, Netherlands.

Abstract is available on the conference website:
http://www.cosmos.esa.int/web/meteoroids2016/conference-programme.

Reason for inclusion – This work was presented as a poster at an international conference and outlined the work in paper 3. ”Meteoroids 2016 was the ninth international conference in a series of meetings on meteors, meteoroids, meteorites, interplanetary dust, and related topics, which have been held since 1992.”

STATEMENT OF AUTHORSHIP

TITLE OF ABSTRACT: Exploring uncertainties in fireball modelling using estimators

PUBLICATION STATUS: Online access

AUTHOR CONTRIBUTIONS

By signing the Statement of Authorship, each author certifies that their stated contribution to the publication is accurate and that permission is granted for the publication to be included in the candidate's thesis.

Name of Principal Author: Eleanor K. Sansom

Contribution to the Abstract: Led all aspects of the research, drafted the manuscript and presented the research as an oral presentation at the Meteoroids2016 conference in Noordwijk, Netherlands.

Overall Percentage: 85%

Signature: ***Date:*** 01 / 12 / 16

Name of Co-Author: Phillip A. Bland

Contribution to the Abstract: Assisted in revising and editing the manuscript.

Overall Percentage: 3%

Signature: Phillip Bland ***Date:*** 4 / 12 / 16

Name of Co-Author: Mark G. Rutten

Contribution to the Abstract: Assisted in revising and editing the manuscript.

Overall Percentage: 10%

Signature: *Date:* 5 / 12 / 16

Name of Co-Author: Jonathan Paxman

Contribution to the Abstract: Assisted in revising the manuscript.

Overall Percentage: 1%

Signature: *Date:* 5/12/16

Name of Co-Author: Martin C. Towner

Contribution to the Abstract: Assisted in revising the manuscript.

Overall Percentage: 1%

Signature: M Tow *Date:* 05/12/16

Exploring uncertainties in fireball modelling using estimators

E. K. Sansom (1), P. A. Bland (1), M. G. Rutten (2), J. Paxman (1), M. Towner (1)
(1) Curtin University, Western Australia, (2) DST Group, South Australia. (meteoroids@ellie.rocks).

Introduction

Camera networks dedicated to observing fireball phenomena allow the bright flight trajectory of meteoroids to be triangulated. The evolution of a meteoroid throughout its flight can be modelled by a set of simple dynamic equations (after [1]):

$$\begin{aligned}\frac{dm}{dt} &= -\frac{1}{2}\kappa\sigma\rho_a v^3 m^{2/3}\\ \frac{dv}{dt} &= -\frac{1}{2}\frac{\kappa\rho_a v^2}{m^{1/3}} + g\sin\gamma_e\end{aligned} \tag{1}$$

where ρ_a, g and γ_e are the local atmospheric density, gravity and flight angle from horizontal respectively, the shape density coefficient $\kappa = \frac{c_d A_0}{\rho_m^{2/3}}$ (c_d being the drag coefficient and A_0 the shape parameter) and the ablation coefficient $\sigma = \frac{c_h}{H^* c_d}$ (c_h is the coefficient of heat and H^* the enthalpy of vaporisation).

In order to gain an understanding of the unknown variables, typical methods perform a least squares analysis and residuals are used as an indicator of overall model errors (eg. [1]). A more robust understanding of errors introduced by the model itself (1) as well as errors in observations can be examined by using tracking algorithms. The estimators to be discussed include the Extended Kalman Filter (EKF) as originally proposed by Sansom et al. [2]; the Unscented Kalman filter (UKF) and its inclusion in an Interactive Multiple Model estimator (IMM); and Sequential Importance Sampling Particle Filter (SISPF).

Tracking Algorithms

The state of a meteoroid at any discrete time step, k, may be represented by a state vector $\mathbf{x}_k = [position\ (l),\ velocity\ (v),\ mass\ (m)]$ and an associated covariance matrix, $\mathbf{P_k}$. Although brightness has not been incorporated at this stage, it can simply be included as an additional state parameter.

Tracking algorithms typically perform a *prediction* at time k using the system equations and includes a process noise $\mathbf{w}_k \sim \mathcal{N}(0, \mathbf{Q}_k)$. This is followed by an *update* where the observations (including observation noise $\mathbf{n}_k \sim \mathcal{N}(0, \mathbf{R}_k)$) are compared to the model prediction.

The non-linear system (1) requires non-linear estimations algorithms. An EKF predicts the future state covariance, $\mathbf{P}_{k+1}$, by using an approximate, linearised form of (1) for the state transition matrix [2]. An UKF uses a set of sample points to represent the mean state and covariance of a Gaussian distribution. These are individually propagated through (1) and the mean state and covariance recalculated. Although fragmentation is not explicitly included in the model, sudden increases in mass loss are incorporated by the process noise covariance, $\mathbf{Q_k}$, to a certain degree. By running two simultaneous UKFs in an IMM, with different values for mass in $\mathbf{Q_k}$, fragmentation events can be identified. All Kalman Filters require initial values for state parameters, κ and σ. This requires a preceding optimisation step using the least squares method (eg. [2]).

A statistical analysis that includes determination of likely starting parameters can be performed using the iterative Monte Carlo approach of a SISPF. A set of particles are initiated with a range of values for mass and velocity as well as for κ and σ (which are included as state parameters in $\mathbf{x}_k$). Each particle is propagated using (1) and its likelihood calculated based on observation values. A new set of particles are resampled from this pool resulting in a robust final estimate.

Conclusion

This presentation will outline the contrasting results of these different tracking methodologies using the flight trajectory of the Bunburra Rockhole meteoroid and assess the advantages and disadvantages of each.

References

[1] Ceplecha, Z. and ReVelle, D. O., MAPS, Vol. 40, pp. 35-54, 2005.
[2] Sansom, E. K., Bland, P. A., Paxman, J., Towner, M., MAPS, Vol 50, pp. 1423-1435, 2015.

BIBLIOGRAPHY

Artemieva, N. and Pierazzo, E., 2009. The canyon diablo impact event: Projectile motion through the atmosphere. *Meteoritics & Planetary Science*, 44(1):25–42. doi: 10.1111/j.1945-5100.2009.tb00715.x.

Artemieva, N. A. and Shuvalov, V. V., 2016. From Tunguska to Chelyabinsk via Jupiter. *Annual Review of Earth and Planetary Sciences*, 44:37–56. doi: 10.1146/annurev-earth-060115-012218.

Arulampalam, M. S., Maskell, S., Gordon, N., and Clapp, T., 2002. A tutorial on particle filters for online nonlinear/non-Gaussian Bayesian tracking. *IEEE Transactions on Signal Processing*, 50(2):174–188. doi: 10.1109/78.978374.

Baldwin, B. and Sheaffer, Y., 1971. Ablation and breakup of large meteoroids during atmospheric entry. *Journal of Geophysical Research*, 76(19):4653–4668.

Barrat, J., Yamaguchi, A., Greenwood, R., Bohn, M., Cotten, J., Benoit, M., and Franchi, I., 2007. The stannern trend eucrites: Contamination of main group eucritic magmas by crustal partial melts. *Geochimica et Cosmochimica Acta*, 71 (16):4108–4124.

Bland, P., Smith, T., Jull, A. T., Berry, F., Bevan, A., Cloudt, S., and Pillinger, C., 1996. The flux of meteorites to the earth over the last 50 000 years. *Monthly Notices of the Royal Astronomical Society*, 283(2):551–565.

Bland, P., Spurný, P., Bevan, A., Howard, K., Towner, M., Benedix, G., Greenwood, R., Shrbený, L., Franchi, I., Deacon, G., et al., 2012. The australian desert fireball network: a new era for planetary science. *Australian Journal of Earth Sciences*, 59(2):177–187.

Bland, P. A. and Artemieva, N. A., 2006. The rate of small impacts on earth. *Meteoritics & Planetary Science*, 41(4):607–631. doi: 10.1111/j.1945-5100.2006.tb00485.x.

Bland, P. A., Spurný, P., Towner, M. C., Bevan, A. W. R., Singleton, A. T., Bottke, W. F., Greenwood, R. C., Chesley, S. R., Shrbený, L., Borovička, J., Ceplecha, Z., McClafferty, T. P., Vaughan, D., Benedix, G. K., Deacon, G., Howard, K. T., Franchi, I. a., and Hough, R. M., 2009. An anomalous basaltic meteorite from the innermost main belt. *Science (New York, N.Y.)*, 325(5947):1525–1527. doi: 10.1126/science.1174787.

Bland, P. A., Towner, M. C., Sansom, E. K., Devillepoix, H., Howie, R. M., Paxman, J. P., Cupak, M., Benedix, G. K., Cox, M. A., Jansen-Sturgeon, T., Stuart, D., and Strangway, D., 2016. Fall and Recovery of the Murrili Meteorite, and an Update on the Desert Fireball Network. *LPI Contributions*, 1921:6265.

Blom, H. A. P. and Bar-Shalom, Y., 1988. Interacting multiple model algorithm for systems with Markovian switching coefficients. *IEEE Transactions on Automatic Control*, 33(8):780–783. doi: 10.1109/9.1299.

Borovička, J., 1990. The comparison of two methods of determining meteor trajectories from photographs. *Bulletin of the Astronomical Institutes of Czechoslovakia*, 41:391–396.

Borovička, J., 1993. A fireball spectrum analysis. *Astronomy and Astrophysics*, 279:627–645.

Borovička, J., Popova, O., Nemtchinov, I. V., Spurný, P., and Ceplecha, Z., 1998. Bolides produced by impacts of large meteoroids into the Earth's atmosphere: comparison of theory with observations. I. Benesov bolide dynamics and fragmentation. *Astronomy and Astrophysics*, 334:713.

Borovička, J., Spurný, P., Kalenda, P., and Tagliaferri, E., 2003. The Morávka meteorite fall: 1. Description of the events and determination of the fireball trajectory and orbit from video records. *Meteoritics & Planetary Science*, 38(7): 975–987.

Borovička, J., Tóth, J., Igaz, A., Spurný, P., Kalenda, P., Haloda, J., Svoreň, J., Kornoš, L., Silber, E., Brown, P., et al., 2013. The Košice meteorite fall:

Atmospheric trajectory, fragmentation, and orbit. *Meteoritics & Planetary Science*, 48(10):1757–1779.

Borovička, J., Spurný, P., and Brown, P., 2015a. Small near-earth asteroids as a source of meteorites. *Asteroids IV*, page 257.

Borovička, J., Spurný, P., Šegon, D., Andreić, Ž., Kac, J., Korlević, K., Atanackov, J., Kladnik, G., Mucke, H., Vida, D., and Novoselnik, F., 2015b. The instrumentally recorded fall of the Kri{ž}evci meteorite, Croatia, February 4, 2011. *Meteoritics & Planetary Science*, 16(7). doi: 10.1111/maps.12469.

Bottke, W. F., Nesvorný, D., Grimm, R. E., Morbidelli, A., and O'Brien, D. P., 2006. Iron meteorites as remnants of planetesimals formed in the terrestrial planet region. *Nature*, 439(7078):821–824.

Britt, D. and Consolmagno, G., 2003. Stony meteorite porosities and densities: A review of the data through 2001. *Meteoritics & Planetary Science*, 38(8): 1161–1180. doi: 10.1111/j.1945-5100.2003.tb00305.x.

Bronshten, V. A., 1983. *Physics of Meteoric Phenomena*. Geophysics and Astrophysics Monographs. Reidel, Dordrecht, Netherlands.

Brown, P., Marchenko, V., Moser, D. E., Weryk, R., and Cooke, W., 2013. Meteorites from meteor showers: A case study of the taurids. *Meteoritics & Planetary Science*, 48(2):270–288.

Brown, P. G., Ceplecha, Z., Hawkes, R. L., Wetherill, G., Beech, M., and Mossman, K., 1994. The orbit and atmospheric trajectory of the Peekskill meteorite from video records. *Nature*, 367(6464):624–626. doi: 10.1038/367624a0.

Brownlee, D. E., Tsou, P., Burnett, D., Clark, B., Hanner, M., Horz, F., Kissel, J., McDonnell, J., Newburn, R., Sandford, S., et al., 1997. The stardust mission: returning comet samples to earth. *Meteoritics and Planetary Science Supplement*, 32.

Brykina, I. G. and Stulov, V. P., 2012. The reciprocal role of convective and radiant heat exchange in the meteor-parameter range. *Doklady Physics*, 57(4): 164–165. doi: 10.1134/S1028335812040039.

Burbine, T. H., McCoy, T. J., Meibom, A., Gladman, B., and Keil, K., 2002. Meteoritic parent bodies: Their number and identification. *Asteroids III*, 653.

Campbell-Brown, M. D. and Koschny, D., 2004. Model of the ablation of faint meteors. *Astronomy and Astrophysics*, 418(2):751–758. doi: 10.1051/0004-6361:20041001-1.

Ceplecha, Z., 1957. Photographic geminids 1955. *Bulletin of the Astronomical Institutes of Czechoslovakia*, 8:51.

Ceplecha, Z., 1961. Multiple fall of Přibram meteorites photographed. 1. Double-station photographs of the fireball and their relations to the found meteorites. *Bulletin of the Astronomical Institutes of Czechoslovakia*, 12:21–47.

Ceplecha, Z., 1977. Fireballs photographed in central europe. *Bulletin of the Astronomical Institutes of Czechoslovakia*, 28:328–340.

Ceplecha, Z., 1987. Geometric, dynamic, orbital and photometric data on meteoroids from photographic fireball networks. *Bulletin of the Astronomical Institutes of Czechoslovakia*, 38:222–234.

Ceplecha, Z. and Rajchl, J., 1965. Programme of fireball photography in czechoslovakia. *Bulletin of the Astronomical Institutes of Czechoslovakia*, 16: 15.

Ceplecha, Z. and Revelle, D. O., 2005. Fragmentation model of meteoroid motion, mass loss, and radiation in the atmosphere. *Meteoritics & Planetary Science*, 40(1):35–54. doi: 10.1111/j.1945-5100.2005.tb00363.x.

Ceplecha, Z., Rajchl, J., and Sehnal, L., 1959. New czechoslovak meteorite" luhy". *Bulletin of the Astronomical Institutes of Czechoslovakia*, 10:147.

Ceplecha, Z., Spurný, P., Borovička, J., and Keclikova, J., 1993. Atmospheric fragmentation of meteoriods. *Astronomy and Astrophysics*, 279:615–626.

Ceplecha, Z., Spalding, R. E., Jacobs, C. F., and Tagliaferri, E., 1996. Luminous efficiencies of bolides. In *SPIE's 1996 International Symposium on Optical Science, Engineering, and Instrumentation*, volume 2813, pages 46–56. International Society for Optics and Photonics. doi: 10.1117/12.256072.

Ceplecha, Z., Borovička, J., Elford, W. G., ReVelle, D. O., Hawkes, R. L., Porubčan, V., and Šimek, M., 1998. Meteor Phenomena and Bodies. *Space Science Reviews*, 84(3):327–471. doi: 10.1023/A:1005069928850.

Collins, G. S., Melosh, H. J., and Marcus, R. A., 2005. Earth impact effects program: A web-based computer program for calculating the regional environmental consequences of a meteoroid impact on earth. *Meteoritics & Planetary science*, 40(6):817–840.

Consolmagno S.J., G. J. and Britt, D. T., 1998. The density and porosity of meteorites from the vatican collection. *Meteoritics & Planetary Science*, 33(6): 1231–1241. doi: 10.1111/j.1945-5100.1998.tb01308.x.

Decker, B. L., 1986. World geodetic system 1984. Technical report, DTIC Document.

DeMeo, F., Alexander, C., Walsh, K., Chapman, C., and Binzel, R., 2015. The compositional structure of the asteroid belt. *Asteroids IV*, pages 13–41.

Devillepoix, H. and Sokolowski, M., in prep. Astrometric calibration of all-sky cameras.

Drummond, J. D., 2000. The D discriminant and near-Earth asteroid streams. *Icarus*, 146(2):453–475.

Gordon, N., Salmond, D., and Smith, A., 1993. Novel approach to nonlinear/non-Gaussian Bayesian state estimation. *IEE Proceedings F -Radar and Signal Processing*, 140(2):107. doi: 10.1049/ip-f-2.1993.0015.

Gounelle, M., Morbidelli, A., Bland, P. A., Spurný, P., Young, E. D., and Sephton, M., 2008. Meteorites from the Outer Solar System. *The Solar System Beyond Neptune*, pages 525–541.

Grady, M. M., 2000. *Catalogue of Meteorites*, volume 1. Cambridge University Press, 5 edition.

Grewal, M. S. and Andrews, A. P., 1993. *Kalman filtering: theory and practice*. Prentice-Hall Inc., New Jersey.

Gritsevich, M. I., 2008a. The Pribram, Lost City, Innisfree, and Neuschwanstein falls: An analysis of the atmospheric trajectories. *Solar System Research*, 42(5): 372–390. doi: 10.1134/S003809460805002X.

Gritsevich, M. I., 2008b. Validity of the photometric formula for estimating the mass of a fireball projectile. *Doklady Physics*, 53(2):97–102. doi: 10.1007/s11446-008-2011-x.

Gritsevich, M. I., 2008c. Estimating the terminal mass of large meteoroids. *Doklady Physics*, 53(11):588–594. doi: 10.1134/S1028335808110098.

Gritsevich, M. I., 2009. Determination of parameters of meteor bodies based on flight observational data. *Advances in Space Research*, 44(3):323–334. doi: 10.1016/j.asr.2009.03.030.

Gritsevich, M. I. and Stulov, V. P., 2007. Entry mass for bolides of the Canadian network. *Doklady Physics*, 52(4):219–224. doi: 10.1134/S102833580704012X.

Gupta, G. and Sahijpal, S., 2010. Differentiation of vesta and the parent bodies of other achondrites. *Journal of Geophysical Research: Planets (1991–2012)*, 115 (E8). doi: 10.1029/2009JE003525.

Haider, A. and Levenspiel, O., 1989. Drag coefficient and terminal velocity of spherical and nonspherical particles. *Powder Technology*, 58(1):63–70. doi: 10.1016/0032-5910(89)80008-7.

Halliday, I., 1973. Photographic fireball networks. *NASA Special Publication*, 319: 1.

Halliday, I., Blackwell, A. T., and Griffin, A. A., 1978. The innisfree meteorite and the canadian camera network. *Journal of the Royal Astronomical Society of Canada*, 72:15–39.

Halliday, I., Blackwell, A. T., and Griffin, A. a., 1989. The flux of meteorites on the earth's surface. *Meteoritics & Planetary Science*.

Halliday, I., Griffin, A. a., and Blackwell, A. T., 1996. Detailed data for 259 fireballs from the Canadian camera network and inferences concerning the influx of large meteoroids. *Meteoritics & Planetary Science*, 31(2):185–217. doi: 10.1111/j.1945-5100.1996.tb02014.x.

Harris, A. W., 2012. The value of enhanced neo surveys. In *AAS/Division for Planetary Sciences Meeting Abstracts*, volume 44.

Hartikainen, J. and Särkkä, S., 2007. Optimal filtering with Kalman filters and smoothers a Manual for Matlab toolbox EKF / UKF. *Journal of Interprofessional Care*, 25:1–57. doi: 10.3109/13561820.2010.500445.

Hayes, W. D. and Probstein, R. F., 1959. *Hypersonic Flow Theory*. Academic Press, New York.

Hildebrand, A. R., McCausland, P. J. A., Brown, P. G., Longstaffe, F. J., Russell, S. D. J., Tagliaferri, E., Wacker, J. F., and Mazur, M. J., 2006. The fall and recovery of the tagish lake meteorite. *Meteoritics & Planetary Science*, 41(3):407–431. doi: 10.1111/j.1945-5100.2006.tb00471.x.

Hofmann-Wellenhof, B., Lichtenegger, H., and Collins, J., 2012. *Global positioning system: theory and practice*. Springer Science & Business Media.

Hoppe, J., 1937. Die physikalischen Vorgänge beim Eindringen meteoritischer Körper in die Erdatmosphäre. *Astronomische Nachrichten*, 262(10):169–198.

Howie, R., Paxman, J., Bland, P., Towner, M., Sansom, E., and Devillepoix, H., in review. Sub-millisecond fireball timing for precise heliocentric orbits using de Bruijn timecodes. *Meteoritic & Planetary Science*.

Hunter, T., 2016. Curtin fireball chasers recover Halloween meteorite from WA farm. *www.fireballsinthesky.com.au, http://news.curtin.edu.au/media-releases/curtin-fireball-chasers-recover-halloween-meteorite-wa-farm*, Accessed: 2016-11-21.

Jacchia, L. G. and Whipple, F. L., 1956. The harvard photographic meteor programme. *Vistas in Astronomy*, 2:982–994.

Jazwinski, A. H., 1970. *Stochastic Processes and Filtering Theory*. Academic Press, New York.

Jenniskens, P., Shaddad, M. H., Numan, D., Elsir, S., Kudoda, A. M., Zolensky, M. E., Le, L., Robinson, G. A., Friedrich, J. M., Rumble, D., Steele, A., Chesley, S. R., Fitzsimmons, A., Duddy, S., Hsieh, H. H., Ramsay, G., Brown, P. G., Edwards, W. N., Tagliaferri, E., Boslough, M. B., Spalding, R. E., Dantowitz, R., Kozubal, M., Pravec, P., Borovička, J., Charvat, Z., Vaubaillon, J., Kuiper, J., Albers, J., Bishop, J. L., Mancinelli, R. L., Sandford, S. A., Milam, S. N., Nuevo, M., and Worden, S. P., 2009. The impact and recovery of asteroid 2008 TC(3). *Nature*, 458(7237):485–488. doi: 10.1038/nature07920.

Jenniskens, P., Nénon, Q., Gural, P., Albers, J., Haberman, B., Johnson, B., Morales, R., Grigsby, B., Samuels, D., and Johannink, C., 2016. Cams newly detected meteor showers and the sporadic background. *Icarus*, 266:384–409.

Julier, S. J., 2002. The scaled unscented transformation. *Proceedings of the 2002 American Control Conference (IEEE Cat. No.CH37301)*, 6(2):4555–4559. doi: 10.1109/ACC.2002.1025369.

Julier, S. J. and Uhlmann, J. K., 1997. A New Extension of the Kalman Filter to Nonlinear Systems. *Int Symp AerospaceDefense Sensing Simul and Controls*, 3 (2):26. doi: 10.1117/12.280797.

Julier, S. J. and Uhlmann, J. K., 2004. Unscented filtering and nonlinear estimation. *Proceedings of the IEEE*, 92(3):401–422. doi: 10.1109/JPROC.2003.823141.

Khanukaeva, D. Y., 2005. Calculation of variable drag and heat-transfer coefficients in meteoric physics equations. In *Modern Meteor Science An Interdisciplinary View*, pages 433–439. Springer.

Kikwaya, J.-B., Campbell-Brown, M. D., and Brown, P. G., 2011. Bulk density of small meteoroids. *Astronomy & Astrophysics*, 530:A113. doi: 10.1051/0004-6361/201116431.

Kulakov, A. and Stulov, V., 1992. Determination of meteor body parameters from observational data. *Astronomicheskii Vestnik*, 26:67–75.

MacPherson, G. J., 2014. Calcium–Aluminum-Rich Inclusions in Chondritic Meteorites. In Davis, A. M., editor, *Meteorites and Cosmochemical Processes*, pages 139–179.

Masson, D. J., Morris, D. N., and Bloxsom, D. E., 1960. *Measurements of Sphere Drag From Hypersonic Continuum to Free-Molecular Flow*. Rand Corporation, Santa Monica, CA.

Mazor, E., Averbuch, a., Bar-Shalom, Y., and Dayan, J., 1998. Interacting multiple model methods in target tracking: A survey. *IEEE Transactions on Aerospace and Electronic Systems*, 34(1):103–123. doi: 10.1109/7.640267.

McCrosky, R., Posen, A., Schwartz, G., and Shao, C.-Y., 1971. Lost city meteorite - its recovery and a comparison with other fireballs. *Journal of Geophysical Research*, 76(17):4090–4108. doi: 10.1029/JB076i017p04090.

McCrosky, R. E. and Boeschenstein, H., 1965. The prairie meteorite network. *Optical Engineering*, 3(4):304127–304127.

McCrosky, R. E. and Posen, A., 1968. Special Data-Reduction Procedures for Prairie Network Meteor Photographs. *SAO Special Report*, 273.

Meteoritical Society, 2015. Creston. volume 104.

Morbidelli, A., Lunine, J. I., O'Brien, D. P., Raymond, S. N., and Walsh, K. J., 2012. Building Terrestrial Planets. *Annual Review of Earth and Planetary Sciences*, 40: 251–275. doi: 10.1146/annurev-earth-042711-105319.

Mueller, M., Delbo, M., Hora, J., Trilling, D. E., Bhattacharya, B., Bottke, W., Chesley, S., Emery, J., Fazio, G., Harris, A., et al., 2011. Exploreneos. iii. physical characterization of 65 potential spacecraft target asteroids. *The Astronomical Journal*, 141(4):109.

Murray, I. S., Beech, M., Taylor, M. J., Jenniskens, P., and Hawkes, R. L., 2000. Comparison of 1998 and 1999 leonid light curve morphology and meteoroid structure. *Earth, Moon, and Planets*, 82(0):351–367. doi: 10.1023/A:1017003019448.

Ning, X. and Fang, J., 2007. An autonomous celestial navigation method for leo satellite based on unscented kalman filter and information fusion. *Aerospace Science and Technology*, 11(2):222–228.

Palme, H. and Jones, A., 2003. Solar system abundances of the elements. In Davis, A. M., Holland, H. D., and Turekian, K. K., editors, *Meteorites, Comets and Planets: Treatise on Geochemistry*, volume 1, pages 41–61, Amsterdam, The Netherlands. Elsevier.

Picone, J. M., Hedin, A. E., Drob, D. P., and Aikin, A. C., 2002. NRLMSISE-00 empirical model of the atmosphere: Statistical comparisons and scientific issues. *Journal of Geophysical Research: Space Physics (1978–2012)*, 107(A12): 1468.

Ray, S. and Fröhlich, J., 2015. An analytic solution to the equations of the motion of a point mass with quadratic resistance and generalizations. *Archive of Applied Mechanics*, 85(4):395–414.

ReVelle, D. O., 1976. *Dynamics and thermodynamics of large meteor entry: a quasi-simple ablation model.* Herzberg Institute of Astrophysics, National Research Council Canada.

Revelle, D. O., 2007. NEO fireball diversity: energetics-based entry modeling and analysis techniques. In Milani, A., Valsecchi, G. B., and Vokrouhlicky, D., editors, *Near Earth Objects, Our Celestial Neighbors: Opportunity and Risk*, Proceedings of the International Astronomical Union S236, pages 95–106. Cambridge University Press.

Righter, K., Harvey, R., McCoy, T., and Corrigan, C., 2014. *35 Seasons of US Antarctic Meteorites (1976–2010)*. Wiley Online Library.

Ristic, B., Arulampalam, S., and Gordon, N., 2004. *Beyond the Kalman filter: Particle filters for tracking applications*, volume 685. Artech house Boston.

Sansom, E. K., Bland, P. A., Paxman, J., and Towner, M. C., 2015. A novel approach to fireball modeling: The observable and the calculated. *Meteoritics & Planetary Science*, 50(8):1423–1435. doi: 10.1111/maps.12478.

Sansom, E. K., Bland, P. A., Rutten, M. G., Paxman, J., and Towner, M. C., 2016. Filtering meteoroid flights using multiple unscented kalman filters. *The Astronomical Journal*, 152(5):148. doi: 10.3847/0004-6256/152/5/148.

Sansom, E. K., Rutten, M. G., and Bland, P. A., in press. Analysing Meteoroid Flights Using Particle Filters. *The Astronomical Journal*.

Särkkä, S., 2007. On unscented Kalman filtering for state estimation of continuous-time nonlinear systems. *IEEE Transactions on Automatic Control*, 52(9):1631–1641. doi: 10.1109/TAC.2007.904453.

Särkkä, S., 2008. Unscented Rauch-Tung-Striebel Smoother. *Automatic Control, IEEE Transactions on*, 53(3):845–849.

Särkkä, S. and Sarmavuori, J., 2013. Gaussian filtering and smoothing for continuous-discrete dynamic systems. *Signal Processing*, 93(2):500–510. doi: 10.1016/j.sigpro.2012.09.002.

Schlichting, H. and Gersten, K., 2000. *Boundary Layer Theory*. Springer, New York, 8th edition.

Scott, E. and Krot, A., 2003. Chondrites and their components. In Davis, A. M., Holland, H. D., and Turekian, K. K., editors, *Meteorites, Comets and Planets: Treatise on Geochemistry*, volume 1, pages 143–200, Amsterdam, The Netherlands. Elsevier.

Seckel, S., 2016. Tracking down the Arizona fireball. *https://asunow.asu.edu/20160628-discoveries-tracking-down-arizona-fireball*, Accessed: 2016-11-21.

Shuvalov, V., 1999. Multi-dimensional hydrodynamic code sova for interfacial flows: Application to the thermal layer effect. *Shock Waves*, 9(6):381–390. doi: 10.1007/s001930050168.

Shuvalov, V. V. and Artemieva, N. a., 2002. Numerical modeling of Tunguska-like impacts. *Planetary and Space Science*, 50(2):181–192. doi: 10.1016/S0032-0633(01)00079-4.

Spurný, P., Oberst, J., and Heinlein, D., 2003. Photographic observations of neuschwanstein, a second meteorite from the orbit of the příbram chondrite. *Nature*, 423(6936):151–153.

Spurný, P., Borovička, J., and Shrbený, L., 2006. Automation of the Czech part of the European fireball network: equipment, methods and first results. *Proceedings of the International Astronomical Union*, 2(S236):121. doi: 10.1017/S1743921307003146.

Spurný, P., Borovička, J., Kac, J., Kalenda, P., Atanackov, J., Kladnik, G., Heinlein, D., and Grau, T., 2010. Analysis of instrumental observations of the jesenice meteorite fall on april 9, 2009. *Meteoritics & Planetary Science*, 45(8):1392–1407. doi: 10.1111/j.1945-5100.2010.01121.x.

Spurný, P., Bland, P., Shrbený, L., Borovička, J., Ceplecha, Z., Singelton, A., Bevan, A. W. R., Vaughan, D., Towner, M. C., Mcclafferty, T. P., Toumi, R., and Deacon, G., 2012. The Bunburra Rockhole meteorite fall in SW Australia: Fireball trajectory, luminosity, dynamics, orbit, and impact position from photographic and photoelectric records. *Meteoritics & Planetary Science*, 47(2): 163–185. doi: 10.1111/j.1945-5100.2011.01321.x.

Spurný, P., Boroviŭka, J., Haloda, J., and Shrbený, L., 2016. Two Very Precisely Instrumentally Documented Meteorite Falls: Žd'ár nad Sázavou and Stubenburg - Prediction and Reality. In *79th Annual Meteoritical Society Meeting (2016)*, volume 1921, page 6221.

Stulov, V. P., Mirsky, V. N., and Visly, A. I., 1995. Aerodynamics of Bolides. *Nauka*.

Thrun, S., Montemerlo, M., Dahlkamp, H., Stavens, D., Aron, A., Diebel, J., Fong, P., Gale, J., Halpenny, M., Hoffmann, G., Lau, K., Oakley, C., Palatucci, M., Pratt, V., Stang, P., Strohband, S., Dupont, C., Jendrossek, L.-e., Koelen, C., Markey, C., Rummel, C., Niekerk, J. V., Jensen, E., Alessandrini, P., Bradski, G., Davies, B., Ettinger, S., Kaehler, A., Nefian, A., Mahoney, P., van Niekerk, J., Jensen, E., Alessandrini, P., Bradski, G., Davies, B., Ettinger, S., Kaehler, A., Nefian, A., and Mahoney, P., 2006. Stanley: The robot that won the DARPA Grand Challenge. *Journal of Field Robotics*, 23(9):661–692. doi: 10.1002/rob.20147.

Towner, M. C., Bland, P. A., Spurný, P., Benedix, G. K., Dyl, K., Greenwood, R. C., Gibson, J., Franchi, I. A., Shrbený, L., Bevan, A. W. R., and Vaughan, D., 2011. Mason Gully: The Second Meteorite Recovered by the Desert Fireball Network. In *74th Annual Meteoritical Society Meeting (2011)*, volume 74, pages 53124–53124.

Trigo-Rodríguez, J. M., Llorca, J., Lyytinen, E., Ortiz, J. L., Caso, A. S., Pineda, C., and Torrell, S., 2004. 2002 leonid storm fluxes and related orbital elements. *Icarus*, 171(1):219–228.

Trigo-Rodriguez, J. M., Lyytinen, E., Gritsevich, M., Moreno-Ibáñez, M., Bottke, W. F., Williams, I., Lupovka, V., Dmitriev, V., Kohout, T., and Grokhovsky, V., 2015. Orbit and dynamic origin of the recently recovered Annama's H5 chondrite. *Monthly Notices of the Royal Astronomical Society*, 449(2):2119–2127.

Truitt, R. W., 1959. *Hypersonic aerodynamics*. Ronald Press, New York.

Wan, E. A. and Merwe, R. V. D., 2000. The unscented kalman filter for nonlinear estimation. In *Adaptive Systems for Signal Processing, Communications, and Control Symposium 2000. AS-SPCC. The IEEE 2000*, pages 153–158. doi: 10.1109/ASSPCC.2000.882463.

Wan, E. A. and Merwe, R. V. D., 2001. The Unscented Kalman Filter. In Hayki, S., editor, *Kalman Filtering and Neural Networks*, chapter Chapter 7, page 62 pages. Wiley Publishing.

Weissman, P. R. and Lowry, S. C., 2008. Structure and density of cometary nuclei. *Meteoritics & Planetary Science*, 43(6):1033–1047. doi: 10.1111/j.1945-5100.2008.tb00691.x.

Welten, K. C., Meier, M. M. M., Caffee, M. W., Laubenstein, M., Nishizumi, K., Wieler, R., Bland, P. a., Towner, M. C., and Spurný, P., 2012. Cosmic-ray exposure age and preatmospheric size of the Bunburra Rockhole achondrite. *Meteoritics & Planetary Science*, 47(2):186–196. doi: 10.1111/j.1945-5100.2011.01262.x.

Whipple, F. L., 1952. Meteoritic phenomena and meteorites. *Physics and Medicine of the Upper Atmosphere*, 137:149–153.

Zhdan, I. A., Stulov, V. P., Stulov, P. V., and Turchak, L. I., 2007. Drag coefficients for bodies of meteorite-like shapes. *Solar System Research*, 41(6):505–508. doi: 10.1134/S0038094607060068.